



**US Army Corps
of Engineers**
Hydrologic Engineering Center

HEC-RAS Verification and Validation Tests

April 2018

REPORT DOCUMENTATION PAGE

Form Approved OMB No. 0704-0188

The public reporting burden for this collection of information is estimated to average 1 hour per response, including the time for reviewing instructions, searching existing data sources, gathering and maintaining the data needed, and completing and reviewing the collection of information. Send comments regarding this burden estimate or any other aspect of this collection of information, including suggestions for reducing this burden, to the Department of Defense, Executive Services and Communications Directorate (0704-0188). Respondents should be aware that notwithstanding any other provision of law, no person shall be subject to any penalty for failing to comply with a collection of information if it does not display a currently valid OMB control number.

PLEASE DO NOT RETURN YOUR FORM TO THE ABOVE ORGANIZATION.

1. REPORT DATE (DD-MM-YYYY) April 2018			2. REPORT TYPE Research Document		3. DATES COVERED (From - To)	
4. TITLE AND SUBTITLE HEC-RAS Verification and Validation Tests			5a. CONTRACT NUMBER			
			5b. GRANT NUMBER			
			5c. PROGRAM ELEMENT NUMBER			
6. AUTHOR(S) Gary W. Brunner, CEIWR-HEC-HHT Dr. Alejandro Sanchez, CEIWR-HEC-HHT Dr. Tom Molls, David Ford Consulting Engineers Dr. David A. Parr, University of Kansas			5d. PROJECT NUMBER			
			5e. TASK NUMBER			
			5f. WORK UNIT NUMBER			
7. PERFORMING ORGANIZATION NAME(S) AND ADDRESS(ES) U.S .Army Corps of Engineers Institute for Water Resources Hydrologic Engineering Center (CEIWR-HEC) 609 Second Street Davis, CA 95616-4687			8. PERFORMING ORGANIZATION REPORT NUMBER			
9. SPONSORING/MONITORING AGENCY NAME(S) AND ADDRESS(ES)			10. SPONSOR/ MONITOR'S ACRONYM(S)			
			11. SPONSOR/ MONITOR'S REPORT NUMBER(S)			
12. DISTRIBUTION / AVAILABILITY STATEMENT Approved for public release; distribution is unlimited.						
13. SUPPLEMENTARY NOTES						
14. ABSTRACT This research document summarizes all of the test cases performed in order to verify and validate the HEC-RAS one-dimensional Steady and Unsteady Flow computational code, as well as the two-dimensional Unsteady Flow Computational code. The purpose of performing these tests with HEC-RAS is to demonstrate that the HEC-RAS computational code is working correctly, as well as to demonstrate how well the software performs against analytical, text book, laboratory, and real world (field) datasets with measured data. Test datasets include: Analytical solutions to a range of problems; tests from well known hydraulic text books; comparisons with well known laboratory datasets; and comparisons with well gaged real world datasets.						
15. SUBJECT TERMS HEC-RAS; River Analysis System; HEC; Hydrologic Engineering Center; two-dimensional; R&D; research & development; United Kingdom; research project; models; hydraulic; benchmarking; test; grid cell sizes; grid; bathymetry; cell face; terrain; elevation; flow solver; time steps; result; water surface; velocities; computational interval						
16. SECURITY CLASSIFICATION OF:			17. LIMITATION OF ABSTRACT UU	18. NUMBER OF PAGES 154	19a. NAME OF RESPONSIBLE PERSON	
a. REPORT U	b. ABSTRACT U	c. THIS PAGE UU			19b. TELEPHONE NUMBER	

HEC-RAS

Verification and Validation Tests

April 2018

U.S. Army Corps of Engineers
Institute for Water Resources
Hydrologic Engineering Center
609 Second Street
Davis, CA 95616

(530) 756-1104
(530) 756-8250 FAX
www.hec.usace.army.mil

Table of Contents

Table of Contents	<i>i</i>
List of Figures	<i>iii</i>
List of Tables	<i>vii</i>
Abbreviations	<i>ix</i>
Chapter	Page
1 Introduction	
1.1 Overview	1
1.2 Acknowledgements	1
2 One-Dimensional Steady Flow	
2.1 Overview	3
2.2 Analytical and Text Book Datasets	3
2.2.1 Standard Step Backwater Test.....	3
2.2.2 One-Dimensional Transcritical Flow over a Bump without Friction.....	5
2.3 Laboratory Datasets	7
2.3.1 Flow over a Drop Structure	7
2.4 Field Datasets	11
2.4.1 Beaver Creek Bridge	11
3 One-Dimensional Unsteady Flow	
3.1 Overview	17
3.2 Analytical and Text Book Datasets	17
3.2.1 Standard Step Backwater Test.....	17
3.3 Laboratory Datasets	19
3.4 Field Datasets	19
3.4.1 San Joaquin Canal Test	19
3.4.2 Lower Columbia River System Test	22
4 Two-Dimensional Unsteady Flow	
4.1 Overview	31
4.2 Analytical and Text Book Datasets	31
4.2.1 Standard Step Backwater Test.....	31
4.2.2 Subcritical Flow over a Variable Sloping Bed.....	33
4.2.3 Flow over a Bump without Friction	36
4.2.4 Flood Wave Propagation over a Flat Bed.....	39
4.2.5 Dam Break over a Flat Frictionless Bed.....	44
4.2.6 Sloshing in a Rectangular Basin.....	48
4.2.7 Long-wave Run-up on a Planar Slope.....	52
4.2.8 Surface Runoff on a Plane.....	55
4.2.9 Rectangular Basin with Coriolis.....	59
4.3 Laboratory Datasets	62
4.3.1 Flow in a Compound Channel.....	62
4.3.2 Flow in a Rectangular Channel with a Sudden Expansion.....	65
4.3.3 Two-Dimensional Surface Runoff	79
4.3.4 Rectangular Channel with a 180-Degree Bend	83
4.3.5 Sudden Dam Break in a Rectangular Flume	88

Table of Contents

Chapter	Page
4.3.6 Flow in a Channel Contraction.....	91
4.3.7 Dam Break in a Channel with a 180-Degree Bend	94
4.3.8 Flow around a Spur-Dike	99
4.3.9 Flow through a Bridge.....	106
4.4 Field Datasets	117
4.4.1 Malpasset Dam Break	117
4.4.2 New Madrid Floodway Levee Breaching.....	124

List of Figures

Figure	Page No.
2-1. HEC-RAS Cross Section Editor - Upstream most Cross Section.....	4
2-2. HEC-RAS Computed versus Hand Calculations from Chow (1959)	5
2-3. HEC-RAS Cross Section Editor - Downstream most Cross Section.....	6
2-4. Computed and Analytical Solution of a Mixed Flow Regime Problem	7
2-5. WES Report Plate 13 (USACE, 1994).....	8
2-6. Plan View of the Drop Structure's Geometric Layout from the HEC-RAS Geometry Editor.....	9
2-7. Comparison between Flume Data and HEC-RAS for a Drop Structure	10
2-8. HEC-RAS Bridge Culvert Editor with Beaver Creek Bridge Data Entered	12
2-9. Bridge Modeling Approach Editor with Beaver Creek Data	12
2-10. HEC-RAS Computed Versus Observed Water Surface at for Beaver Creek	13
3-1. HEC-RAS Cross Section Editor - Upstream most Cross Section.....	18
3-2. HEC-RAS Computed versus Hand Calculations from Chow (1959)	19
3-3. HEC-RAS Cross Section Editor - Downstream Cross Section, just above Gated Structure	20
3-4. HEC-RAS Computed versus Observed Water Surface at Downstream Station 0.0.....	21
3-5. HEC-RAS Computed versus Observed Water Surface at Upstream Station 29335.....	21
3-6. Overview map of Lower Columbia River System.....	22
3-7. HEC-RAS Schematic of the Lower Columbia River System.....	25
3-8. Example of Storage Areas and Lateral Structures used to Model Protected Areas	26
3-9. Computed Profile Plot of Columbia River with Observed High Water Marks for 1996 Flood....	28
4-1. Computational Grid and Terrain for the Step Backwater Test Case.....	32
4-2. RAS Mapper Velocity Plot with Profile Lines at Locations of Velocity Measurements	33
4-3. Example Comparison of Computed and Analytic Water Depths for MacDonald One-Dimensional Test Case with a Four-Meter Grid Resolution	35
4-4. Grid Convergence for the MacDonald One-Dimensional Test Case	36
4-5. Computational Grid for the Two-Dimensional Bump Test Dataset	37
4-6. Two-Dimensional Computed and Analytical Solution of the Bump Test	38
4-7. Comparison of Analytical and Computed Water Depth Profiles at Different Times using the HEC-RAS Diffusion Wave Equation (DWE) Solver	41
4-8. Comparison of Analytical and Computed Water Depth Profiles at Different Times using the HEC-RAS Shallow Water Equation (SWE) Solver.....	41
4-9. Comparison of Analytical and Computed Current Velocity Profiles at Different Times using the HEC-RAS Diffusion Wave Equation (DWE) Solver	42
4-10. Comparison of Analytical and Computed Current Velocity Profiles at Different Times using the HEC-RAS Shallow Wave Equation (SWE) Solver	42
4-11. Comparison of Analytical and Computed Water Depth Time-Series at Three Stations using the HEC-RAS Diffusion Wave Equation (DWE) Solver	43
4-12. Comparison of Analytical and Computed Water Depth Time-series at Three Stations using the HEC-RAS Shallow Water Equation (SWE) Solver.....	43
4-13. Computed and Analytical Water Depths for the Idealized Dam Break Test Case	46
4-14. Computed and Analytical Current Velocities for the Idealized Dam Break Test Case	47
4-15. Computational Grid for the Sloshing Test Case	49
4-16. Water Surface Elevation (WSEL) Profiles at Different Times for the Sloshing Test Case. Calculated with the first and second order temporal schemes. Time step equals 0.5 seconds; Implicit weighting factor equals 0.6.	50

List of Figures

Figure	Page No.
4-17. Water Surface Elevation (WSEL) Time Series Calculated at $x = \Delta x/2$ for Time Steps of 0.5 and 5 seconds and an Implicit Weighting Factor (Theta) set to 0.6	51
4-18. Water Surface Elevation (WSEL) Time Series Calculated at $x = \Delta x/2$ for the Implicit Weighting Factors (Theta) Set to 0.6 and 1.0 with a Time Step of 0.5 seconds.....	52
4-19. Water Surface Elevation (WSEL) Time Series Calculated at $x = \Delta x/2$ for the Implicit Weighting Factors (Theta) Set to 0.6 and 1.0 with a Time Step of 5 seconds.....	52
4-20. Initial Water Surface Elevation (WSEL) for the Long-Wave Run-Up Test Case	53
4-21. Close-Up View of Computation Grid where Grid Resolution Transition Occurs	53
4-22. Comparison of Analytical and Computed WSEL at Different Time Steps for the Long-Wave....	54
4-23. Comparison of Analytical and Computed Shoreline Position for the Long-Wave Run-Up Test Case.....	55
4-24. Schematic of One-Dimensional Surface Runoff Case (Therrien, 2003).....	56
4-25. Normalized Hydrograph for Test Case 1 with $F_0 = 0.5$ and $K = 10$	58
4-26. Normalized hydrograph for Case 2 with $F_0 = 1.5$ and $K = 3$	58
4-27. Flow Hydrograph for the Coriolis Test Case	60
4-28. Steady-State Water Surface Elevation (A), and Current Velocity (B) Fields.....	61
4-29. Cross Section of Flume for Compound Channel Test Case.....	62
4-30. Computational Grid for the Compound Channel Experiments.....	63
4-31. RAS Mapper Velocity Plot with Profile Line at Location of Velocity Measurements.....	64
4-32. Observed and Computed Velocities for Compound Channel Test Case	64
4-33. Computational Mesh for the Sudden Expansion Test Case (zoomed near the expansion).....	66
4-34. Computed Velocity Magnitude Plot with Particle Traces (for $Q=0.01815$ cms),.....	67
4-35. Velocity Profile (computed and experimental), at $X = 0$ in Figure 4-34	68
4-36. Velocity Profile (computed and experimental), at $X = 1$ in Figure 4-34 (one meter downstream of the expansion) for $Q = 0.01815$ cms	68
4-37. Velocity Profile (computed and experimental), at $X = 2$ in Figure 4-34 (two meters downstream of the expansion) for $Q = 0.01815$ cms.....	69
4-38. Velocity Profile (computed and experimental), at $X = 3$ in Figure 4-34 (three meters downstream of the expansion) for $Q = 0.01815$ cms.....	70
4-39. Velocity Profile (computed and experimental), at $X = 4$ in Figure 4-34 (four meters downstream of the expansion) for $Q = 0.01815$ cms.....	71
4-40. Velocity Profile (computed and experimental), at $X = 5$ in Figure 4-34 (five meters downstream of the expansion) for $Q = 0.01815$ cms.....	72
4-41. Velocity Profile (computed and experimental), at $X = 0$ (just upstream of the expansion) for $Q = 0.03854$ cms	73
4-42. Velocity Profile (computed and experimental), at $X = 1$ (one meter downstream of the expansion) for $Q = 0.03854$ cms	74
4-43. Velocity Profile (computed and experimental), at $X = 2$ (two meters downstream of the expansion) for $Q = 0.03854$ cms	75
4-44. Velocity Profile (computed and experimental), at $X = 3$ (three meters downstream of the expansion) for $Q = 0.03854$ cms.....	76
4-45. Velocity Profile (computed and experimental), at $X = 4$ (four meters downstream of the expansion) for $Q = 0.03854$ cms.....	77
4-46. Velocity Profile (computed and experimental), at $X = 5$ (five meters downstream of the expansion) for $Q = 0.03854$ cms.....	78
4-47. Physical Model Geometry for the Cea (2008) Test Cases	79

List of Figures

Figure	Page No.
4-48. Computational Mesh and Terrain for the Cea (2008) Test Cases.....	80
4-49. Comparison of Measured and Computed Discharge for Test Case C1 (Coe, 2008)	81
4-50. Comparison of Measured and Computed Discharge for Test Case 2B (Coe, 2008)	81
4-51. Comparison of Measured and Computed Discharge for Test Case 2C (Coe, 2008)	82
4-52. Example Current Velocity Field for Test Case 2C at 55 seconds.....	82
4-53. Rectangular Channel with a 180-degree Bend (Rozovskii, 1957).....	83
4-54. Curvilinear Computational Mesh for the 180-degree Bend Test Case	84
4-55. Velocity Magnitude (computed by HEC-RAS), with Faster Velocity along inside of Bend	85
4-56. Velocity Profile (computed and experimental), at Section A-B in Figure 4-55	86
4-57. Velocity Profile (computed and experimental), at Section C-D in Figure 4-55	86
4-58. Velocity Profile (computed and experimental), at Section E-F in Figure 4-55	87
4-59. Depth (computed by HEC-RAS), with Deeper Depths along.....	87
4-60. Sidewall Depth (computed and experimental) Showing Super-Elevation.....	88
4-61. Schematic Diagram of the Test Flume.....	89
4-62. Measured Water Surface Elevations for the Instantaneous Dam Break Flume Experiment	90
4-63. Computational Grid for the Instantaneous Dam Break Experiments.....	90
4-64. HEC-RAS Computed Results versus the Measured Water Surface Elevations.....	91
4-65. Computational Mesh for the Channel Contraction Test Case.....	92
4-66. Depth Contour Plot (experimental and computed)	93
4-67. Channel centerline depth profile plot (experimental and computed), with computed flow rates shown in boxes. Solid and dashed lines are based on upstream depths of 0.55 and 0.58 feet, respectively.....	94
4-68. Test Facility Schematic: Dam Break in a Channel with a 180-degree Bend (Bell, 1989).....	95
4-69. Depth Hydrograph (computed and experimental), at Station 2 in Figure 4-68 (bend entrance)....	97
4-70. Depth Hydrograph (computed and experimental), at Station 4 in Figure 4-68 (midway through bend, 90-degrees).....	97
4-71. Depth Hydrograph (computed and experimental), at Station 6 in Figure 4-68 (bend exit)	98
4-72. Depth Hydrograph (computed and experimental), at Station 8 in Figure 4-68 (7.5 feet downstream of bend exit).....	98
4-73. Computational Mesh for the Spur-Dike (zoomed-in near the spur-dike)	100
4-74. Computed Velocity Magnitude Plot with Particle Traces, the Blue Shaded Eddy Zone is Clearly Evident Downstream of the Spur-Dike	101
4-75. Longitudinal Velocity Profile (computed and experimental), at $y/b=1.5$ in Figure 4-74 (where $U_0=0.242$ m/s is the average upstream channel velocity)	102
4-76. Longitudinal Velocity Profile (computed and experimental), at $y/b=2$ in Figure 4-74 (where $U_0=0.242$ m/s is the average upstream channel velocity)	103
4-77. Longitudinal Velocity Profile (computed and experimental), at $y/b=3$ in Figure 4-74 (where $U_0=0.242$ m/s is the average upstream channel velocity).	104
4-78. Longitudinal Velocity Profile (computed and experimental), at $y/b=4$ in Figure 4-74 (where $U_0=0.242$ m/s is the average upstream channel velocity).	105
4-79. Plan View of Laboratory Flume (20-scale HEC-RAS model Dimensions in parenthesis)	106
4-80. Piezometer Locations.....	106
4-81. Piezometer Surface for an Experiment	107
4-82. Section A-A in 20-scale Model Dimensions.....	107
4-83. Section B-B in 20-scale Model Dimensions for Labatory and Model.....	108
4-84. Section C-C in 20-scale Model Dimensions	108

List of Figures

Figure	Page No.
4-85. Plan View Showing the HEC-RAS 2D Model Domain.....	110
4-86. Three-Dimensional Shapefiles used to create 0.1-foot Land Raster	111
4-87. Creating a Pier Raster	111
4-88. Pier 0.1-foot Raster used in this Study.....	112
4-89. ArcScene® Illustration of Combining Land and Pier Rasters to Create the HEC-RAS Two-Dimensional Terrain	112
4-90. Plan View of the Entire HEC-RAS 2D Mesh and Terrain.....	113
4-91. Zoomed in View of the HEC-RAS Two-Dimensional Mesh near Bridge Piers and Abutments	113
4-92. Example Upstream Boundary Condition Flow Hydrograph.....	115
4-93. Computed and Observed Profiles for Runs 1 to 3	116
4-94. Computed and Observed Profiles for Runs 4 and 5.....	116
4-95. Computed and Observed Profiles for Runs 7 to 9	117
4-96. Malpasset Dam, France after having Failed on 2 December 1959 (source http://ecolo.org/documents/documents_in_french/malpasset/malpasset.htm).....	118
4-97. Malpasset Dam Area Showing Location of Measurement Stations and Terrain	119
4-98. Computation Domain and Model Terrain.....	119
4-99. Measured and Computed Maximum Water Surface Elevations (WSEL) for the High-Water Marks Collected by the Police after the Malpasset Dam Break.....	120
4-100. Measured and Computed Flood Wave Arrival Times for the Malpasset Dam Break at Three Locations where Electric Transformers were Damaged	121
4-101. Computed Water Surface Elevation Maps for the real-life Malpasset Dam Break Simulation...	122
4-102. Measured and Computed Maximum Water Surface Elevations (WSEL) as Estimated by a Physical Model of the Malpasset Dam Break.....	123
4-103. Measured and Computed Arrival Times (minutes) as Estimated by a Physical	123
4-104. Location Map of the New Madrid Floodway and Levee Breach Locations (USGS, 2013)	125
4-105. Combined One- and Two-Dimensional HEC-RAS Model of the Mississippi, Ohio, and New Madrid Floodway.....	126
4-106. Manning's n versus Land Cover Data for the New Madrid Floodway Area.....	127
4-107. Computed versus Observed Water Surface Elevations for Location H1	129
4-108. Computed versus Observed Water Surface Elevations for Location H7	130
4-109. Computed versus Observed Water Surface Elevations for Location H8	130
4-110. Computed versus Observed Water Surface Elevations for Location H10.....	131
4-111. Computed versus Observed Water Surface Elevations for Location H12	131
4-112. Computed versus Observed Water Surface Elevations for Location H17	132
4-113. Computed versus Observed Water Surface Elevations for Location H20.....	132
4-114. Computed versus Observed Water Surface Elevations for Location H24.....	133
4-115. Computed versus Observed Water Surface Elevations for Location H26.....	134
4-116. Computed versus Observed Water Surface Elevations for Location H33	134

List of Tables

Tables	Page No.
2-1. Specifications for the One-Dimensional Backwater Test Case	3
2-2. Specifications for the One-Dimensional Transcritical Flow.....	6
2-3. Cross Section Spacing for the HEC-RAS Model.....	8
2-4. Computed and Observed Water Surface Elevations at the Approach Section for each Model	14
2-5. Average Absolute Error in Water Surface Elevation Based on Three Locations	14
3-1. Specifications for the Simple Trapezoidal Channel Test Case	17
3-2. Specifications for the San Joaquin Canal Test Case	20
3-3. Model Parameters for the HEC-RAS Unsteady Flow Analysis Simulation	21
3-4. Description of GIS Layers Created to Extract Information for Hydraulic Modeling	24
3-5. Manning's n Value Ranges for Main Channels and Overbank Areas	25
3-6. Summary of Model Calibration Results.....	27
3-7. Summary of Model Verification Results	28
4-1. Specifications for the One-Dimensional Backwater Test Case	31
4-2. Model Setup Parameters for the Step Backwater Test Case	32
4-3. Model Setup Parameters for the MacDonald One-Dimensional Test Case	34
4-4. Water Depth Goodness-of-Fit Statistics for the MacDonald One-Dimensional Test Case	35
4-5. Model Setup Parameters for the MacDonald Bump Test Case.....	37
4-6. Model Setup Parameters for the Two-Dimensional Bump Test Case	38
4-7. Convergence Criteria Analyzed after each Outer Loop Iteration	40
4-8. Model Setup Parameters for the Dam Break Test Cases	46
4-9. Water Depth Goodness-of-Fit Statistics for the Idealized Dam Break Case	47
4-10. Current Velocity Goodness-of-Fit Statistics for the Idealized Dam Break Case	48
4-11. Summary of the Model Setup for the Sloshing Test Case	49
4-12. WSEL Profile Goodness-of-Fit Statistics for Sloshing Test Case	50
4-13. WSEL Time -Series Goodness-of-Fit Statistics for Sloshing Test Case	51
4-14. Model Setup Parameters for the Long-Wave Run-Up on a Planar Slope Test Case	53
4-15. Goodness-of-Fit Statistics for the Long-Wave Run-Up Test Case	54
4-16. General HEC-RAS Parameters and Boundary Conditions	57
4-17. Summary of Test Case 1 Conditions and Parameters	57
4-18. Summary of Test Case 2 Conditions and Parameters	57
4-19. General HEC-RAS Parameters and Boundary Conditions for the Coriolis Test Cases.....	60
4-20. General HEC-RAS Parameters and Boundary Conditions	61
4-21. Specification for Compound Channel Experiment	63
4-22. Model Parameters for Compound Channel Experiment	63
4-23. Specifications of the Sudden Expansion Flume Experiment	65
4-24. Model Specifications for the Sudden Expansion Test Case.....	66
4-25. Model Setup Parameters for the Cea (2008) Test Cases.....	80
4-26. Goodness-of-Fit Statistics for the Cea (2008) Test Cases	82
4-27. Specifications of the 180-degree Bend Flume Experiment.....	84
4-28. Model Specifications for the 180-degree Bend Test Case	85
4-29. Model Data for Sudden Dam Break Flume Experiment.....	90
4-30. Specifications of the Channel Contraction Flume Experiment.....	92
4-31. Model Specifications for the Channel Contraction Test Case	93
4-32. Specifications of the Dam Break Experiment.....	96

List of Tables

Table	Page No.
4-33. Model Specifications for the Dam Break Test Case	96
4-34. Specifications of the Spur-Dike Experiment	99
4-35. Model Specifications for the Spur-Dike Test Case.....	100
4-36. Cross Section and Bridge Station-Elevation Data for Sections A-A and B-B.....	108
4-37. Laboratory Results	109
4-38. Model Parameters for the Malpasset Dam Break Validation Test Case	120
4-39. Model parameters for the New Madrid Floodway Breaching Validation Test Case	127
4-40. Measured and Computed Peak Water Surface Elevations (WSEL)	128

Abbreviations

1D	One-Dimensional
2D	Two-Dimensional
3D	Three-Dimensional
B	Bias
BSI	Brier Skill Index
BSS	Brier Skill Score
CEIWR	USACE, Institute for Water Resources
CENWP	USACE, Portland District
cfs	cubic feet per second
cms	cubic meter per second
DEM	Digital Elevation Model
D _T	Eddy Viscosity Mixing Coefficient
DWE	Diffusion Wave Equations
E	Nash-Sutcliffe Coefficient
ERDC	USACE, Engineering Research and Design Center
ES	Nash-Sutcliffe Score
ESRI	Environmental Systems Research Institute
FEMA	Federal Emergency Management Agency
GIS	Geographic Information System
HEC	USACE, Hydrologic Engineering Center
HEC-GeoRAS	HEC GIS Tools for Support of HEC-RAS using ESRI ArcGIS®
HEC-RAS	HEC River Analysis System software

HGL	hydraulic grade line
IA	Index of Agreement
KU	University of Kansas
L_e	Edy Zone Length
LiDAR	Light Detection and Ranging
MAE	Mean Absolute Error
ME	Mean Error
MPI	Model Performance Index
MPS	Model Performance Score
NAD	North American Datum
NAVD	North American Vertical Datum
NOAA	National Oceanic and Atmospheric Administration
OPI	Operational Performance Index
PS	Performance Scores
Q	flow
R	Correlation Coefficient
RMSD	Root Mean Squared Deviation
RMSE	Root Mean Squared Error
SDR	Standard Deviation of Residuals
SI	Scattered Index
SWASHES	Shallow Water Analytic Solutions for Hydraulic and Environmental Studies
SWE	Shallow Water Equations
USACE	U.S. Army Corps of Engineers
USGS	U.S. Geological Survey

WES USACE, Waterways Experiment Station

WSEL Water Surface Elevation

Chapter 1

Introduction

1.1 Overview

This research document summarizes a series of test cases performed in order to verify and validate the HEC-RAS (Hydrologic Engineering Center's (HEC) River Analysis System software) one-dimensional (1D) Steady and Unsteady Flow computational code, as well as the two-dimensional (2D) Unsteady Flow computational code.

The purpose of performing these tests with HEC-RAS is to demonstrate that the HEC-RAS computational code is working correctly, as well as to demonstrate how well the software performs against analytical, text book, laboratory, and real world (field) datasets with measured data. Test datasets include: analytical solutions to a range of problems; tests from well-known hydraulic text books (e.g., Chow, 1959); comparisons with well known laboratory datasets; and comparisons with well gaged real world datasets.

This document verifies and validates that the algorithms in the HEC-RAS software correctly solve the 1D energy equation (Chapter 2); the 1D unsteady flow equations (continuity and momentum; Chapter 3); as well as the 2D unsteady flow equations (continuity and momentum, plus options for turbulence and Coriolis forces; Chapter 4). The document also validates the use of HEC-RAS for a wide range of hydraulic situations.

1.2 Acknowledgements

The datasets, model development, and documentation for this research work were put together by Mr. Gary W. Brunner and Dr. Alejandro Sanchez at HEC. Dr. Tom Molls, David Ford Consulting Engineers, developed and documented four of the 2D Laboratory test sections (4.3.2, 4.3.4, 4.3.6, and 4.3.8). Section 4.3.9 (2D Bridge Hydraulics) is from the research work of Dr. David A. Parr, Professor; Mr. Evan Deal, Research Assistant; and Mr. Bryan C. Young, Associate Professor, Civil, Environmental and Architectural Engineering Department at the University of Kansas.

Chapter 2

One-Dimensional Steady Flow

2.1 Overview

The objective of this chapter is to verify and validate the HEC-RAS steady flow hydraulic computations. This is accomplished by applying HEC-RAS steady flow hydraulics to a wide range of analytical, text book, laboratory, and real world field datasets.

2.2 Analytical and Text Book Datasets

There are several analytical and well documented text book datasets that were used to verify that the HEC-RAS 1D Steady Flow hydraulics was working correctly. This verification shows that the 1D Steady Flow equations were derived correctly and then programmed correctly. The following 1D Steady Flow tests are offered as verification of the software.

2.2.1 Standard Step Backwater Test

Overview

An early test was to compare hand calculations from backwater profiles listed in Chow's "Open Channel Hydraulics" book (Example 10.1, page 250) with HEC-RAS model results. This comparison shows the basic capability of the HEC-RAS program to reproduce results for a simple trapezoidal channel under the influence of a backwater condition. The test verifies the solution of the energy equation solved by the Standard Step Backwater method, which includes friction losses, but no contraction and expansion losses (contraction and expansion coefficients were set to zero).

Problem and Data Description

The test is a trapezoidal channel with a downstream boundary condition of a lake at elevation 5.0 feet. Table 2-1 describes the physical properties of the channel and flow event:

Table 2-1. Specifications for the One-Dimensional Backwater Test Case

Parameter	Value
Bottom width, b (feet)	20
Side slopes, z	2:1 H:V
Bed slope, S	0.0016
Roughness, n	0.025
Flow rate, Q cfs (cubic feet per second)	400
Downstream Boundary Condition, WS (feet)	5.0

Model Setup

A simple 1D river reach was used for this example. A cross section was entered for River Station 0.0 and River Station 3000. Cross sections were then interpolated on a 25.0-foot spacing. Figure 2-1 displays a cross section plot in the HEC-RAS Cross Section Editor.

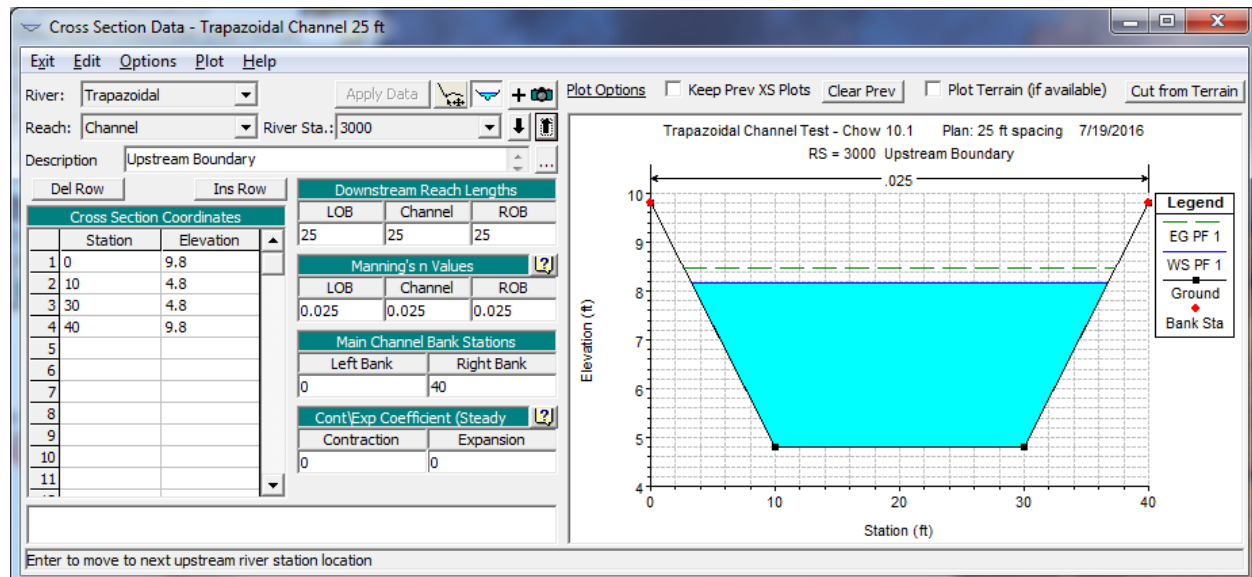


Figure 2-1. HEC-RAS Cross Section Editor - Upstream most Cross Section

Flow data and boundary conditions were entered into the HEC-RAS Steady Flow Data Editor. Additionally the results from Chow's book (Chow, 1959) were entered as "Observed" data into the HEC-RAS Steady Flow Data Editor for results comparisons. An HEC-RAS Steady Flow Analysis plan was developed and the model was run in Subcritical flow mode.

Results and Discussion

The results from the Steady Flow Analysis were compared to the documented results in Chow's book (Table 10.1, page 250). Figure 2-2 displays a plot of the computed water surface profile versus documented results from Chow's book (Chow, 1959). Differences in water surface elevations (WSEL) are less than 0.01 feet at all locations.

The test verifies the 1D steady flow analysis computations can reproduce a backwater profile for a trapezoidal channel with friction losses. The test verifies that the solution of the Energy equation, based on the standard step method, as well as the friction loss calculations, are working correctly.

References

1. Chow, 1959. Chow, Ven Te. *Open-Channel Hydraulics*. McGraw-Hill Civil Engineering Series, McGraw-Hill Book Company. New York, New York.

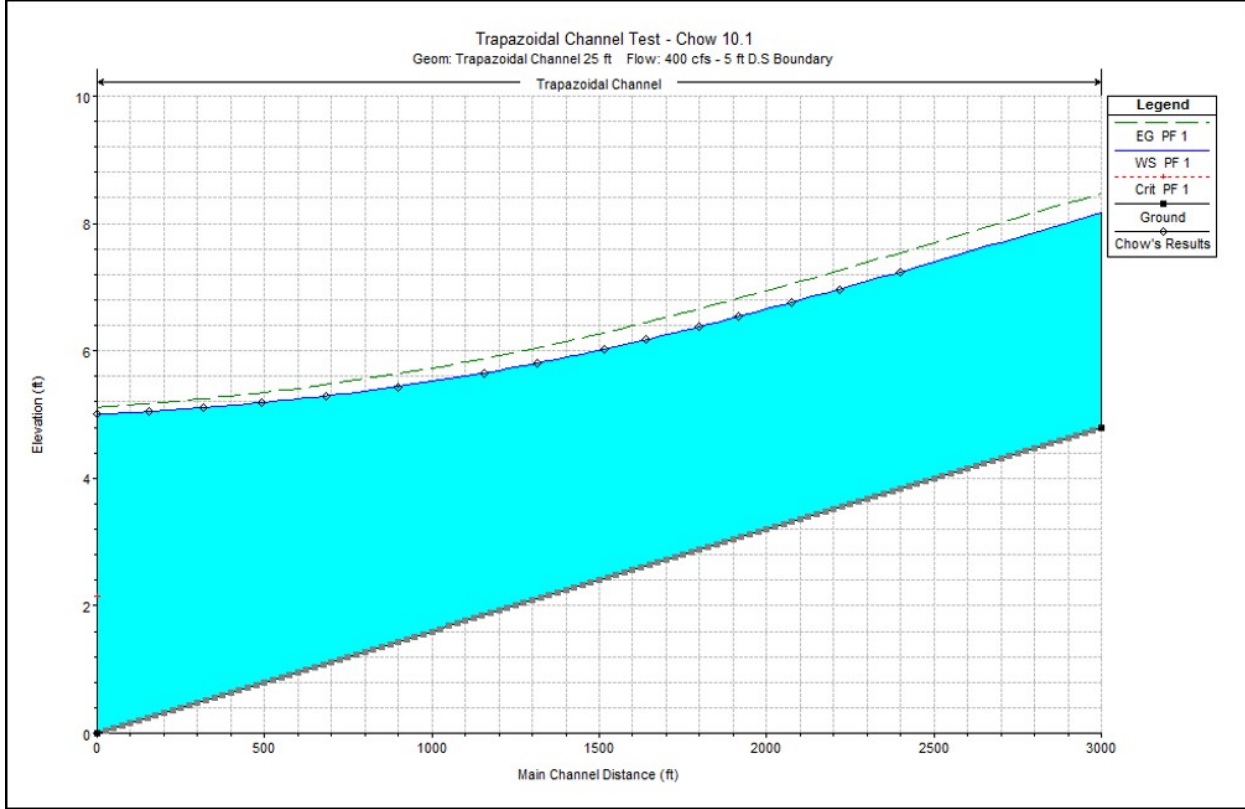


Figure 2-2. HEC-RAS Computed versus Hand Calculations from Chow (1959)

2.2.2 One-Dimensional Transcritical Flow over a Bump without Friction

Overview

This test case is used to evaluate HEC-RAS's ability to simulate flow transitioning from subcritical to supercritical flow (transcritical flow), and then through a hydraulic jump. The analytical solution was done assuming a frictionless surface in order to simplify the solution. This test case will validate several terms in the computational equations, except the friction loss term.

Problem and Data Description

The test is a 0.3-meter wide rectangular channel for a reach that is approximately 20-meters long. The bed slope is flat and the surface is assumed to be frictionless. The bump has a peak elevation of 0.2-meters, and is centered at River Station 10.0. The bump shape is described in Equation 2-1 (Caleffi, 2003):

$$z_b = \begin{cases} 0, & \text{for } x < 8 \\ 0.2 - 0.05(x-10)^2, & \text{for } 8 \leq x < 12 \\ 0, & \text{for } 12 \leq x \end{cases} \quad (2-1)$$

where z_b is the bed elevation with respect to the still water level, and x is the horizontal distance. The analytical solution is obtained with Bernoulli's equation for the transition from subcritical flow, through critical depth, and then supercritical flow down the bump. The location of the jump is obtained with the specific force equation (momentum with no friction or gravitational force). Table 2-2 provides details about the additional data required for this dataset.

Table 2-2. Specifications for the One-Dimensional Transcritical Flow over a Bump without Friction Test Case

Parameter	Value
Bottom width, b (meter)	0.3
Side slopes, z	0.0
Bed slope, S	0.0
Roughness, frictionless, n	0.0001
Flow rate, Q cms (cubic meter per second)	0.054
Downstream Boundary Condition, WS (meter)	0.33

Model Setup

A simple 1D river reach was used for this example. A cross section was entered for River Station 0.0 and River Station 20.6. Cross sections were then interpolated on a 0.2-meter spacing. Figure 2-3 displays a cross section plot in the HEC-RAS Cross Section Editor.

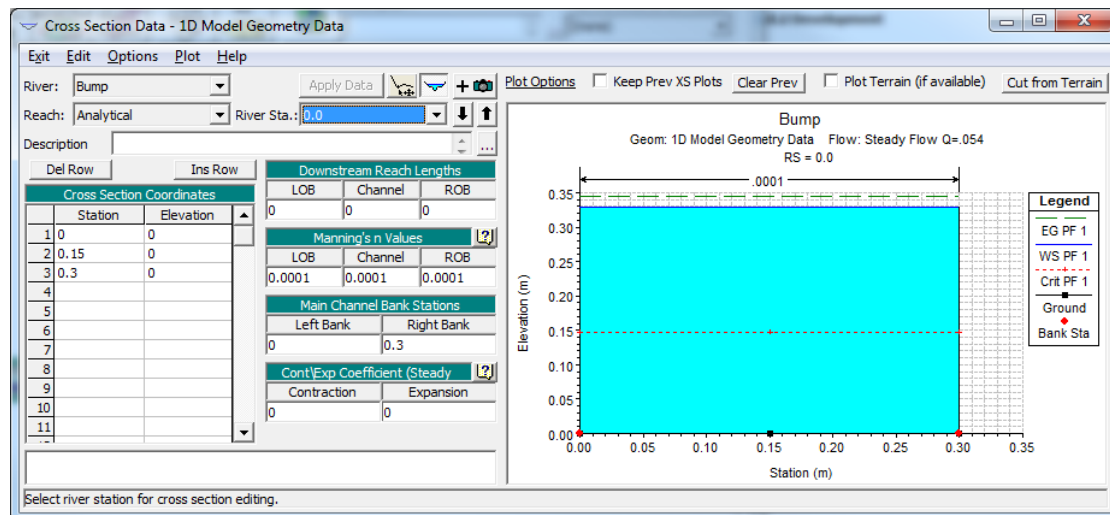


Figure 2-3. HEC-RAS Cross Section Editor - Downstream most Cross Section

Flow data and boundary conditions were entered into the HEC-RAS Steady Flow Data Editor. An HEC-RAS steady flow analysis plan was developed and the model was run in mixed flow regime mode.

Results and Discussion

The results from the Steady Flow Analysis were compared to the analytical solution to this problem. Figure 2-4 displays a plot of the computed water surface profile versus the analytical solution results. The difference in computed and analytical solution results is less than 0.01-meters throughout the reach.

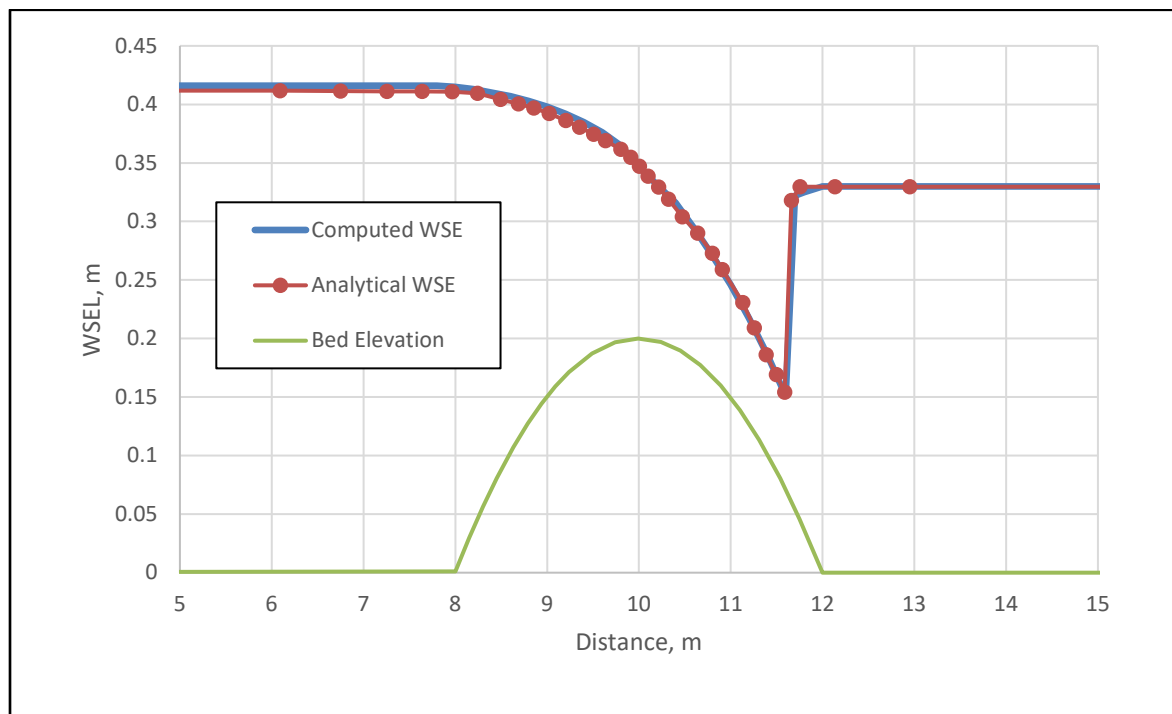


Figure 2-4. Computed and Analytical Solution of a Mixed Flow Regime Problem

The test verifies the 1D steady flow analysis computations can reproduce a flow transitioning from subcritical to supercritical, and then through a hydraulic jump for a channel with no friction losses. The test verifies that the solution of the energy equation and the momentum equations (within the HEC-RAS mixed flow regime analysis) are working correctly.

References

1. Caleffi, 2003. Caleffi, Valerio, Valiani, Alessandro and Zanni, Andrea. *Finite volume method for simulating extreme floods in natural channels*. Journal of Hydraulic Research, Vol. 41, No. 2, pp 167-177. 2003.

2.3 Laboratory Datasets

2.3.1 Flow over a Drop Structure

Overview

In order to evaluate the use of HEC-RAS for modeling drop structures, a comparison was made between a physical model study and an HEC-RAS model of the drop structure. During the design phase of improvements to the Santa Ana River, the United States Army Corps of Engineers (USACE) Waterways Experiment Station (WES), now referred to as the Engineering Research and Design Center (ERDC), was contracted to study the drop structures and make recommendations. The results of this study were reported in "General Design for Replacement of or Modifications to the Lower Santa Ana River Drop Structures, Orange County, California" (USACE, 1994). Over fifty different designs were tested in 1:25 scale flume models and 1:40

scale full width models. The designs evaluated existing structures, modifying original structures, and, replacing the existing structures with entirely new designs. The drop structure design used in the Santa Ana River is similar to one referred to as Type 10 in the report (USACE, 1994). An HEC-RAS model was developed to model the Type 10 drop structure and the model results were compared to the flume results, scaled up to prototype dimensions.

Problem and Data Description

The geometry for the HEC-RAS model was developed from the following design diagram (Figure 2-5) in the WES report (USACE, 1994). All of the data for modeling this drop structure was taken from Technical Report HL-94-4 (USACE, 1994).

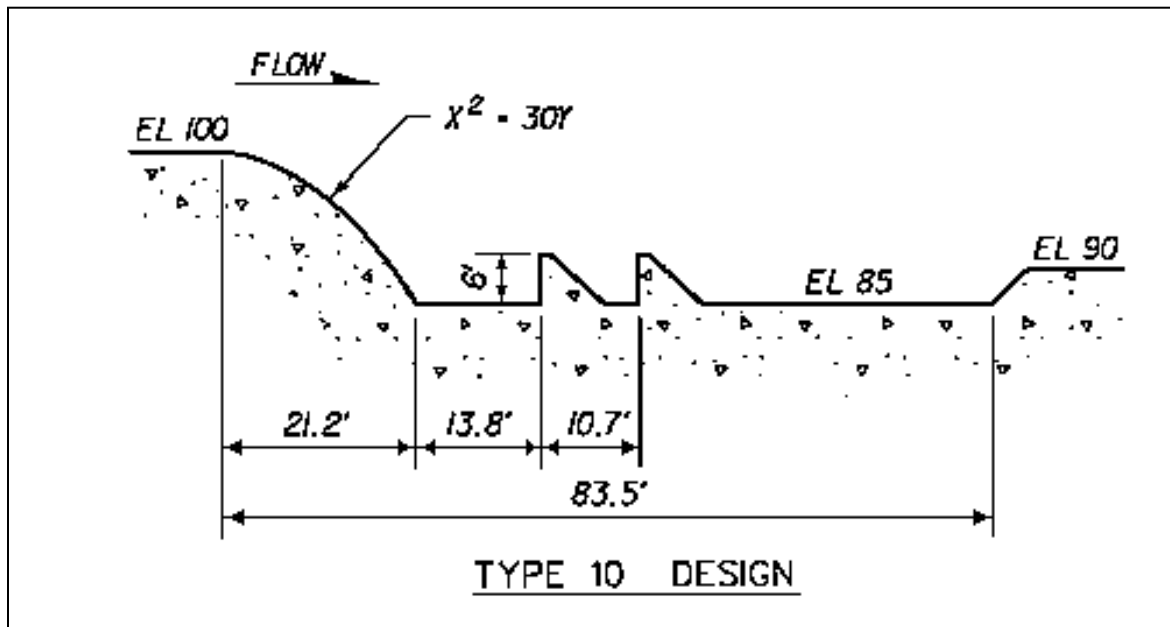


Figure 2-5. WES Report Plate 13 (USACE, 1994)

Model Setup

A 1D steady flow HEC-RAS model was developed to model this structure. The total reach in the model was 350 feet, 150 feet upstream of the crest of the drop structure and 200 feet below the crest. Figure 2-6 displays the plan view of the HEC-RAS model layout from the HEC-RAS Geometry Editor. The cross sections were rectangular, Table 2-3 details the spacing used in the HEC-RAS model:

Table 2-3. Cross Section Spacing for the HEC-RAS Model

Location	Reach Lengths (feet)
Upstream of drop structure	10
Over the drop	2
Inside the stilling basin	10
Downstream of structure	10

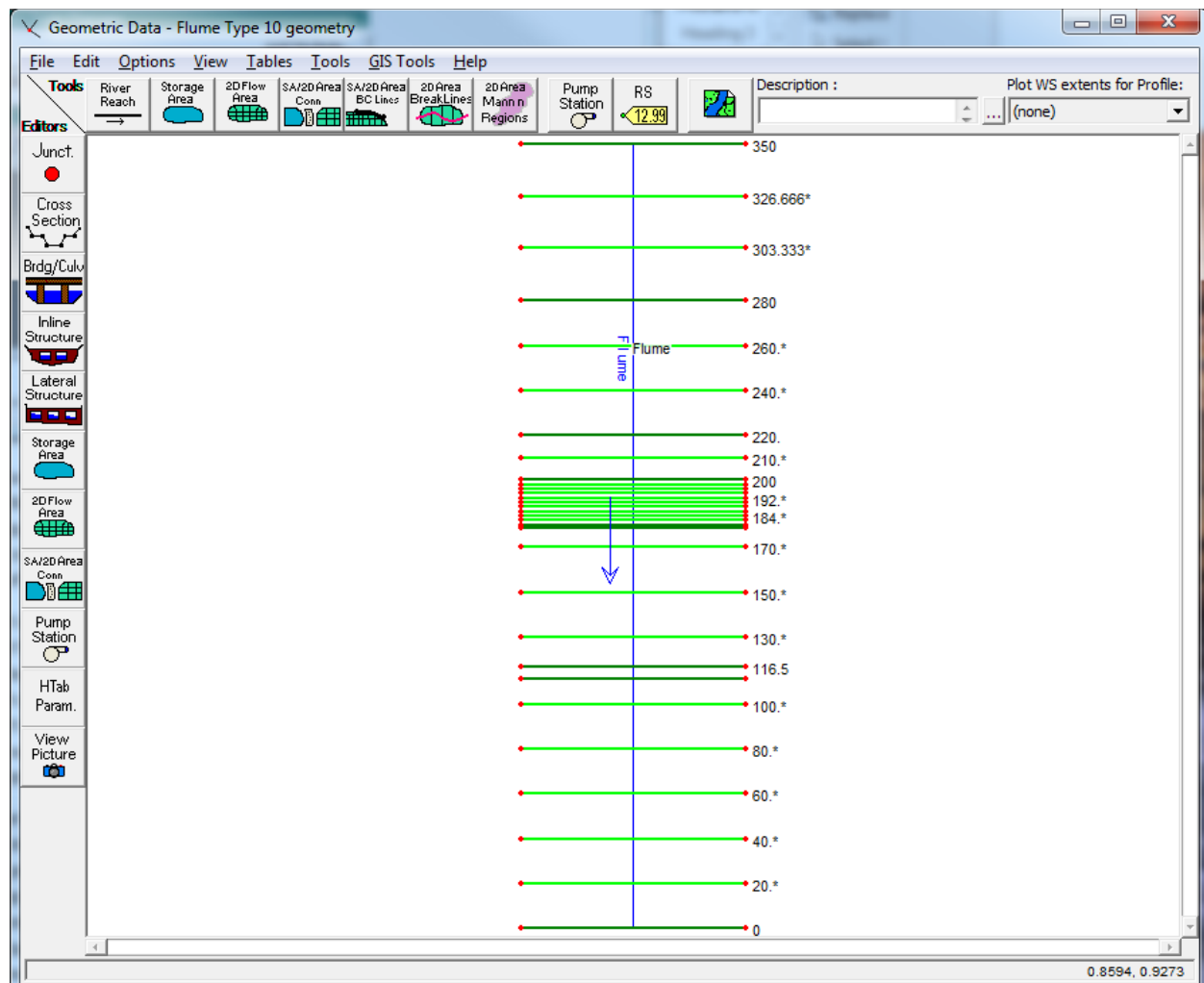


Figure 2-6. Plan View of the Drop Structure's Geometric Layout from the HEC-RAS Geometry Editor

The expansion and contraction coefficients were set to 0.3 and 0.1, respectively. Two Manning's n values were used in the HEC-RAS model of the flume. Inside the stilling basin where the bottom elevation was 85 feet, the Manning's n values were set to 0.05. In all other cross sections the Manning's n values were set to 0.03. The higher Manning's n value was used in the stilling basin to account for the additional energy loss due to the rows of baffles that exist in the flume but were not added into the cross sections data of HEC-RAS.

The original data from the flume experiments were obtained from the WES report (USACE, 1994) and entered in HEC-RAS as "observed" data. The flow rate for this experiment was 25,000 cfs. The downstream boundary condition was setup as a known water surface elevation, by entering in the measured water surface from the flume study.

Results and Discussion

The results of the HEC-RAS model are compared in profile to the observed water surface elevations from the flume study in Figure 2-7. These results show that HEC-RAS was able to adequately model the drop structure, both upstream and downstream of the crest.

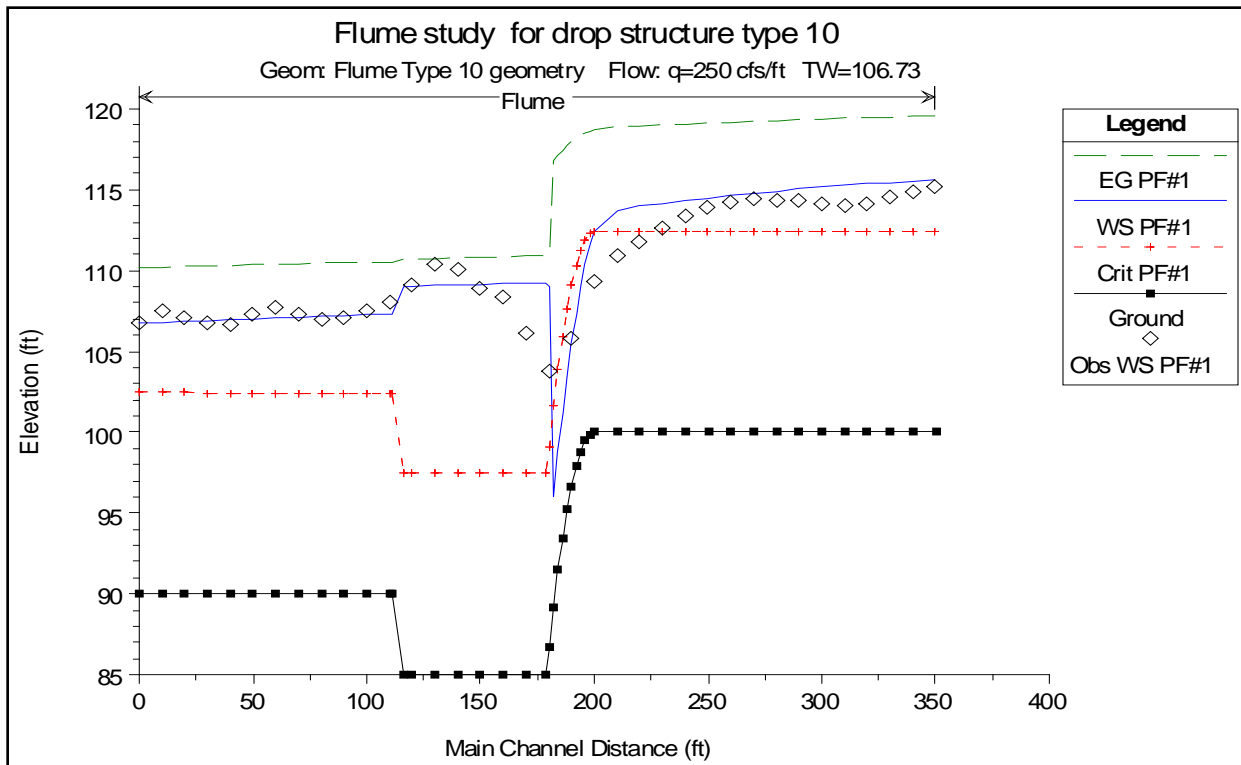


Figure 2-7. Comparison between Flume Data and HEC-RAS for a Drop Structure

Some differences occur right at the crest and through the hydraulic jump. The differences at the crest are due to the fact that the energy equation will always show the flow passing through critical depth at the top of the crest. Whereas, in the field it has been shown that the flow passes through critical depth at a distance upstream of three to four time's critical depth. However, as shown in Figure 2-7, a short distance upstream of the crest HEC-RAS converges to the same depth as the observed data. HEC-RAS correctly obtained the maximum upstream water surface.

Downstream of the drop, the flow is supercritical and then goes through a hydraulic jump. The flume data shows the jump occurring over a distance of fifty to sixty feet with a lot of turbulence. The HEC-RAS 1D model cannot predict how long of a distance it will take for the jump to occur, but it can predict where the jump will begin. The HEC-RAS model will always show the jump occurring between two adjacent cross sections. The HEC-RAS model shows the higher water surface inside of the stilling basin and then going down below the stilling basin. The model shows all of this as a fairly smooth transition, whereas it is actually a turbulent transition with the water surface bouncing up and down. In general, the results from the HEC-RAS model are very good at predicting the stages upstream, inside, and downstream of the drop structure.

References

1. USACE, 1994. George, John F., Pickering, Glenn A., and Turner, Herman O., Jr. *General Design for Replacement of or Modifications to the Lower Santa Ana River Drop Structures, Orange County, California*. U.S. Army Corps of Engineers, Waterways Experimentation Station (WES), Vicksburg, MS. Technical Report HL-94-4. April 1994.

2.4 Field Datasets

2.4.1 Beaver Creek Bridge Hydraulics

Overview

HEC-RAS has been tested against many real world datasets, especially for bridge hydraulics. This test is one of several bridge datasets with real world data that were performed for an earlier research study, "A Comparison of the One-Dimensional Bridge Hydraulic Routines from: HEC-RAS, HEC-2, and WSPRO" (HEC, 1995), Research Document 41 (HEC, 1995). This test of the HEC-RAS bridge routines against observed data measured by the U.S. Geological Survey (USGS) was performed for thirteen different bridge locations. The USGS collected extensive data for bridge crossings over wide, densely vegetated floodplains between 1969 and 1974. The USGS data has been published in the form of Hydrologic Investigation Atlases, which are available to the public. The HEC-RAS software compared very well with the observed data for these bridge sites. The mean absolute error in computed versus observed water surface elevations was 0.24 feet for this test. The Beaver Creek dataset represents just one of these bridge model studies that were performed and documented in RD-41.

Problem and Data Description

The USGS Hydrologic Investigation Atlases provided extensive information about the terrain (cross section data), the details of the bridge, and observed data from historic events that occurred at each of the sites. Cross section data was based on surveyed cross sections by the USGS. Manning's n values were estimated from land use information. Manning's n values were calibrated by raising or lowering Manning's n values of the entire model by the same percentage. This was done to not bias the model results at any one cross section. Detailed bridge data was provided within the USGS atlases. Ineffective flow areas were entered around the bridge (upstream and downstream), and contraction and expansion coefficients were estimated from the guidance in the HEC-RAS Hydraulic Reference Manual (HEC, 2016).

Model Setup

A simple 1D river reach was used for this example. Cross section data was entered from surveyed information provided by the USGS. Nine surveyed cross sections were entered for the Beaver Creek dataset. Additional cross sections were deemed as necessary, so five additional cross sections were interpolated. In Figure 2-8, the HEC-RAS Bridge Culvert Data Editor displays the surveyed cross section data, and the detailed bridge information entered for Beaver Creek.

The bridge modeling approach for this bridge was to use the higher answer from the Energy, Momentum, and Yarnell (WES, 1973) methods, for low flow hydraulics. However, because the bridge blocks out a huge amount of the overbank area, and there is a significant rise in the water surface from downstream to upstream, the Pressure and Weir flow method was used for the high flow method approach. For further details on these methods, refer to the HEC-RAS Reference Manual (HEC, 2016). Figure 2-9 displays the selection and data for the bridge modeling approach in the HEC-RAS Bridge Culvert Editor.

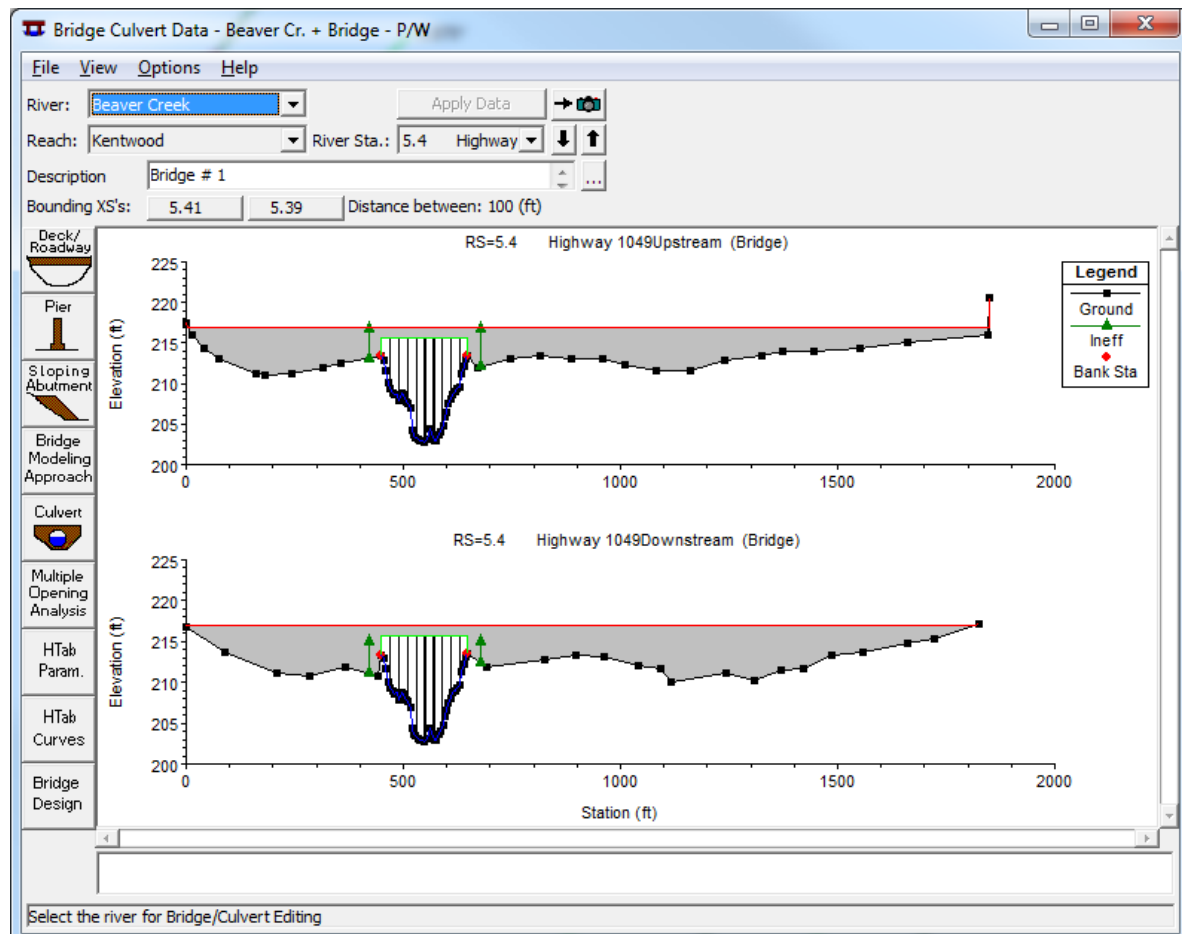


Figure 2-8. HEC-RAS Bridge Culvert Editor with Beaver Creek Bridge Data Entered

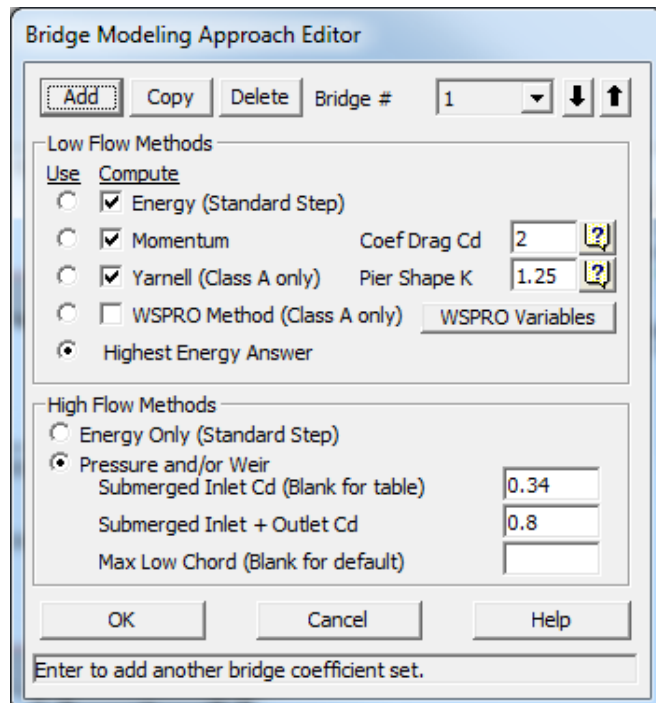


Figure 2-9. Bridge Modeling Approach Editor with Beaver Creek Data

Flow data and boundary conditions were entered into the HEC-RAS Steady Flow Data Editor. There was only one observed event of significance that was documented for this site. This was the May 1974 flood event. The peak flow was estimated from measured velocities that were taken during the flood event. The peak flow of 14,000 cfs was entered into the HEC-RAS Steady Flow Data Editor. A downstream boundary condition of a "Known Water Surface" was used in the model. The USGS measured the maximum water surface at multiple locations after the event. Observed high water marks were used to estimate the known water surface elevation at the most downstream cross section. Other observed data were entered into the Steady Flow Data editor, to be used for comparing computed to observed data on the profile plot.

Results and Discussion

The results from the steady flow analysis were compared to the measured data taken by the USGS. Observed high water marks as well as measured data directly around the bridge were taken during and after the event. Shown in Figure 2-10 is a plot of the computed versus observed water surface elevations during the peak flow of the event. As displayed in Figure 2-10, HEC-RAS matched the downstream observed data very well. The change in water surface elevation from downstream of the bridge to upstream of the bridge is predicted very accurately, based on the bridge hydraulic computations. Additionally, the water surfaces upstream of the bridge are also matched very accurately.

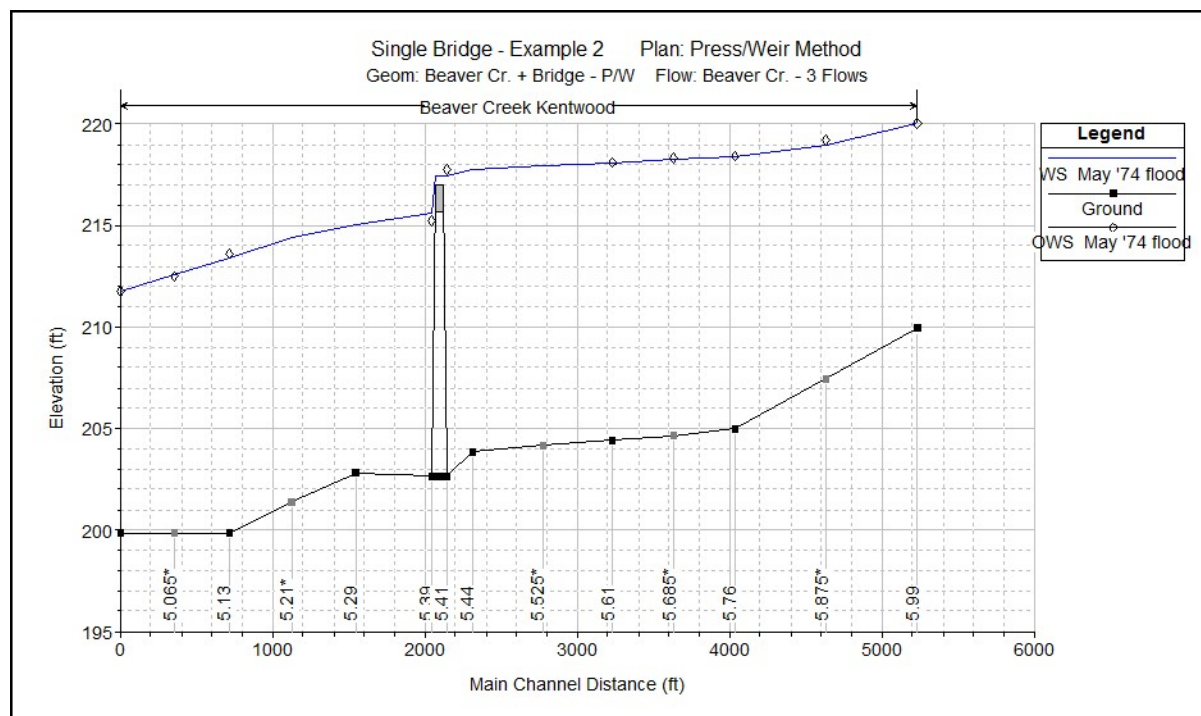


Figure 2-10. HEC-RAS Computed Versus Observed Water Surface at for Beaver Creek

The test verifies the HEC-RAS 1D steady flow analysis computations and bridge hydraulics computations. This test verifies that the solution of the energy equation, as well as the pressure and weir flow computations, are working correctly in HEC-RAS, and are able to reproduce real world bridge hydraulics.

The reader is referred to RD-41 (HEC, 1994), for more detailed information about the bridge hydraulics comparison study that was performed by HEC. A summary of the results of that study are displayed in Table 2-4 and Table 2-5.

Table 2-4. Computed and Observed Water Surface Elevations at the Approach Section for each Model

Study Location	Flow (cfs)	Observed WSEL (feet)	HEC-RAS		HEC-2		WSPRO	
			WSEL (feet)	Error (feet)	WSEL (feet)	Error (feet)	WSEL (feet)	Error (feet)
Alexander Creek	5,508	88.4	88.2	-0.2	88.1	-0.3	88.3	-0.1
Alexander Creek	9,500	90.2	90.1	-0.1	90.0	-0.2	90.1	-0.1
Beaver Creek	14,000	217.8	217.9	0.1	217.8	0.0	217.3	-0.5
Bogue Chitto	25,000	337.3	337.8	0.5	337.5	0.2	337.6	0.3
Bogue Chitto	31,500	338.3	338.9	0.6	338.5	0.2	338.8	0.5
Buckhorn Creek	4,150	322.0	322.1	0.1	322.2	0.0	322.3	0.3
Cypress Creek	1,500	116.1	115.8	-0.3	115.7	-0.4	115.9	-0.2
Flagon Bayou	4,730	76.3	76.2	-0.1	76.2	-0.1	76.9	0.6
Okatama Cr near Magee	16,100	367.2	367.3	0.1	367.1	-0.1	367.3	0.1
Okatama Cr near Magee	12,100	371.9	371.5	-0.4	371.5	-0.4	372.6	0.7
Pea Creek	1,780	359.1	358.9	-0.2	358.8	-0.3	359.4	0.3
Poley Creek	1,900	234.8	234.7	-0.1	234.6	-0.2	235.0	0.2
Poley Creek	4,600	237.2	237.2	0.0	237.2	0.0	237.6	0.4
Tenmile Creek	6,400	110.9	111.0	0.1	111.0	0.1	110.9	0.0
Thompson Creek	3,800	200.3	200.6	0.3	200.6	0.3	200.9	0.6
Yellow River	2,000	234.2	234.2	0.0	234.1	-0.1	234.3	0.1
Yellow River	6,603	237.3	237.7	0.4	237.5	0.2	237.8	0.5
Average Absolute Error				0.21		0.18		0.32

Table 2-5. Average Absolute Error in Water Surface Elevation Based on Three Locations

Study Location	Flow (cfs)	HEC-RAS		HEC-2		WSPRO	
		Rank	Ave Abs Error (feet)	Rank	Ave Abs Error (feet)	Rank	Ave Abs Error (feet)
Alexander Creek	5,508	2	0.20	3	0.30	1	0.17
Alexander Creek	9,500	1	0.10	2	0.13	3	0.23
Beaver Creek	14,000	2	0.07	1	0.03	3	0.50
Bogue Chitto	25,000	1	0.23	3	0.27	1	0.23
Bogue Chitto	31,500	3	0.40	1	0.27	2	0.33
Buckhorn Creek	4,150	1	0.20	1	0.20	3	0.23
Cypress Creek	1,500	2	0.23	3	0.30	1	0.17
Flagon Bayou	4,730	1	0.27	2	0.30	2	0.30
Okatama Cr near Magee	16,100	1	0.17	2	0.20	3	0.23
Okatama Cr near Magee	12,100	1	0.40	2	0.47	3	0.80
Pea Creek	1,780	1	0.37	1	0.37	3	0.50
Poley Creek	1,900	1	0.30	2	0.37	3	0.40
Poley Creek	4,600	1	0.20	2	0.23	3	0.50
Tenmile Creek	6,400	2	0.23	2	0.23	1	0.10
Thompson Creek	3,800	1	0.20	1	0.20	3	0.40
Yellow River	2,000	1	0.17	1	0.17	3	0.23
Yellow River	6,603	2	0.40	1	0.30	3	0.43
Mean Average Absolute Error			0.24		0.26		0.33
Total Number of No. 1 Rankings		11		7		3	
Total Number of No. 2 Rankings		5		7		2	
Total Number of No. 3 Rankings		1		3		12	

Table 2-4 shows summary results for all of the events at all of the bridge sites. This table shows observed and computed water surface elevations at the cross section upstream of the bridge, which is considered the Approach cross section. This is the cross section upstream at the point at which the flow begins to contract to get into the bridge opening.

Table 2-5 shows the average absolute error in water surface elevations based on a comparison of three locations for each dataset. These locations were: just downstream of the bridge; at the bridge approach cross section; and, the cross section just upstream of the approach cross section.

References

1. HEC, 1995. *A Comparison of the One-Dimensional Bridge Hydraulic Routines from: HEC-RAS, HEC-2, and WSPRO*. U.S. Army Corps of Engineers, Hydrologic Engineering Center, Davis CA. September 1995. RD-41.
2. HEC, 2016. *HEC-RAS, Hydraulic Reference Manual*, Version 5.0. U.S. Army Corps of Engineers, Hydrologic Engineering Center, Davis CA. February 2016. CPD-69.
3. WES, 1973. Bridge Pier Losses, Section 010-6, Hydraulic Design Criteria, U.S. Army Corps of Engineers, Waterways Experimentation Station (WES), Vicksburg, MS. 1973.

Chapter 3

One-Dimensional Unsteady Flow

3.1 Overview

The objective of this chapter is to verify and validate the HEC-RAS 1D unsteady flow hydraulic computations. This is accomplished by applying HEC-RAS 1D unsteady flow hydraulics to a wide range of analytical, text book, laboratory, and real world field datasets.

3.2 Analytical and Text Book Datasets

There are several analytical and well documented text book datasets that were used to verify that the HEC-RAS 1D unsteady flow hydraulics was working correctly. This verification shows that the 1D unsteady flow equations were derived correctly and then programmed correctly. The following 1D unsteady flow tests are offered as verification of the software.

3.2.1 Standard Step Backwater Test

Overview

An early test was to compare hand calculations from backwater profiles listed in "*Open Channel Hydraulics*" (Chow, 1959; Example 10.1, page 250) with HEC-RAS model results. This comparison shows the basic capability of the HEC-RAS program to reproduce results for a simple trapezoidal channel under the influence of a backwater condition. The test verifies the solution of the momentum equation, which includes gravity, friction losses, pressure forces, and convective acceleration forces.

Problem and Data Description

Table 3-1 provides the specifications for the trapezoidal channel test case.

Table 3-1. Specifications for the Simple Trapezoidal Channel Test Case

Parameter	Value
Bottom width, b (feet)	20
Side slopes, z (H:V)	2:1
Bed slope, S	0.0016
Roughness, n	0.025
Flow rate, Q cfs	400
Downstream Boundary Condition, WS (feet)	5.0

Model Setup

A simple 1D river reach was used for this example. A cross section was entered for River Station 0.0 and River Station 3000. Cross sections were then interpolated on a 25.0-foot spacing. Figure 3-1 displays a cross section plot in the HEC-RAS Cross Section Editor.

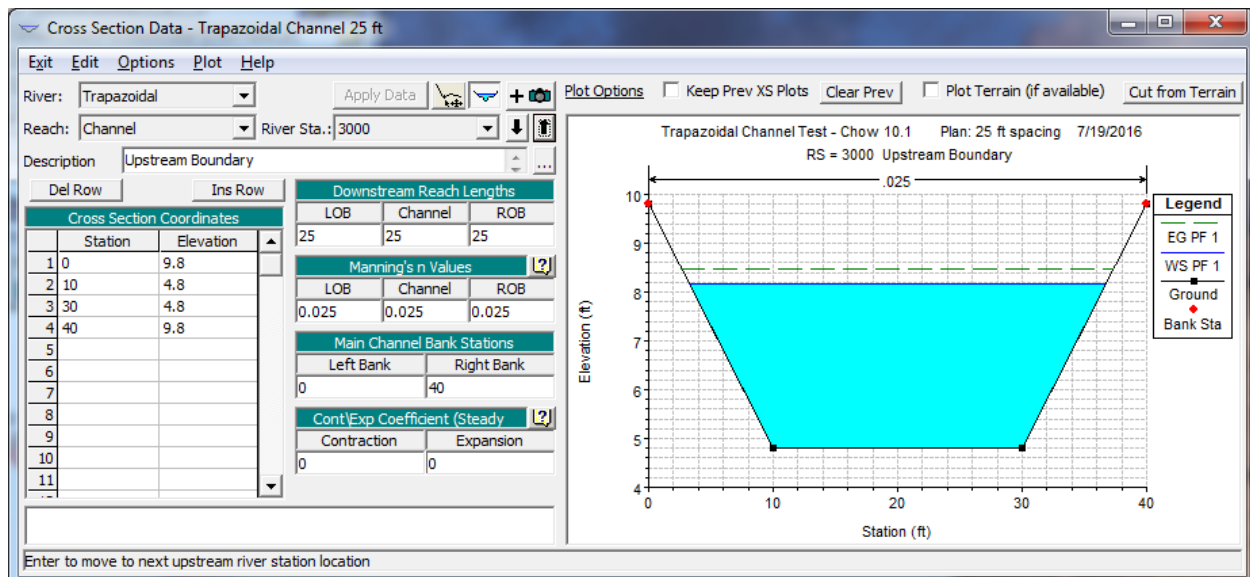


Figure 3-1. HEC-RAS Cross Section Editor - Upstream most Cross Section

Flow data and boundary conditions were entered into the HEC-RAS Unsteady Flow Data Editor. Additionally, the results from Chow (Table 10-1, page 250; 1959) were entered as "observed" data into the HEC-RAS Unsteady Flow Data Editor for results comparisons. An HEC-RAS unsteady flow analysis plan was developed and the model was run in subcritical flow mode.

Results and Discussion

The results from the unsteady flow analysis were compared to the documented results in Chow (Table 10.1, page 250; 1959). Figure 3-2 displays a plot of the computed water surface profile versus Chow (1959) documented results. The maximum difference in water levels are less than 0.01 feet.

The test verifies the HEC-RAS 1D unsteady flow analysis computations can reproduce a backwater profile for a trapezoidal channel with friction losses. The test verifies that the solution of the momentum equation, as well as the friction loss calculations, are working correctly.

References

- Chow, 1959. Chow, Ven Te. *Open-Channel Hydraulics*. McGraw-Hill Civil Engineering Series, McGraw-Hill Book Company. New York, New York.

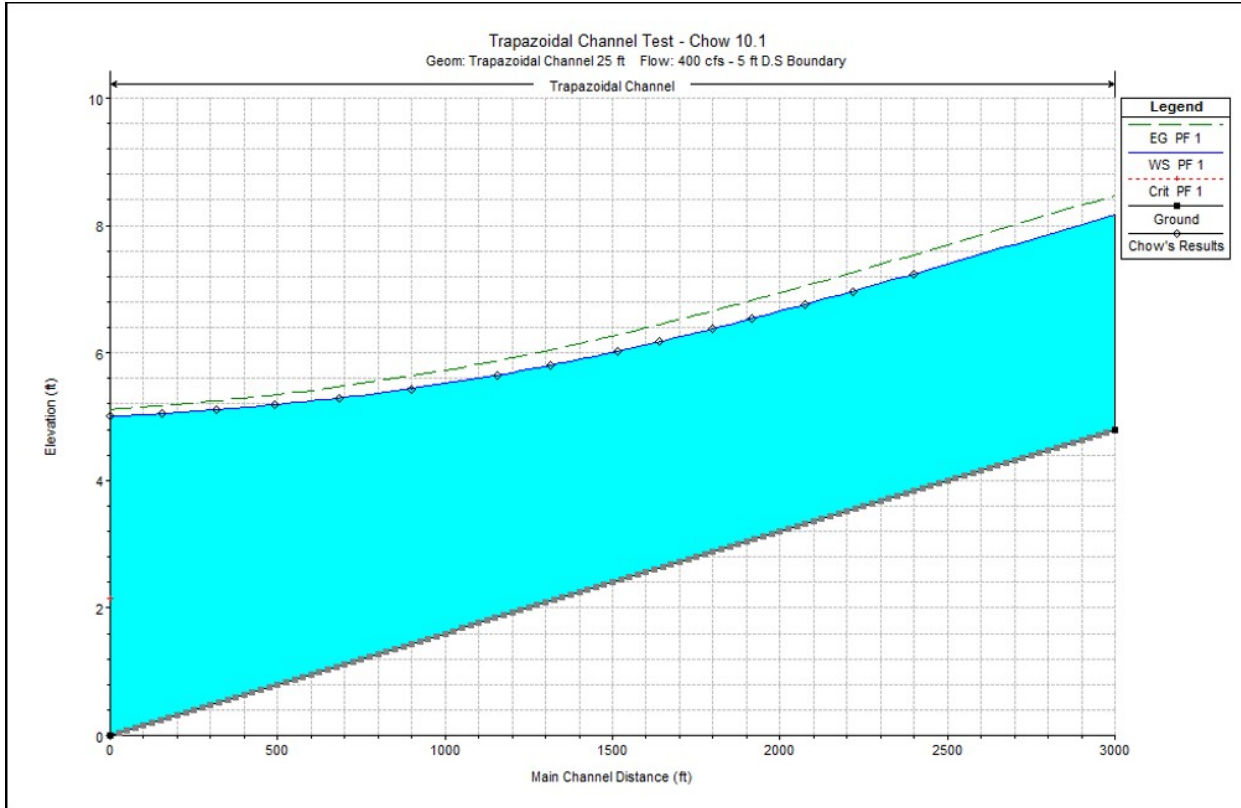


Figure 3-2. HEC-RAS Computed versus Hand Calculations from Chow (1959)

3.3 Laboratory Datasets

This section is a place holder for future 1D unsteady flow datasets that are based on laboratory studies.

3.4 Field Datasets

3.4.1 San Joaquin Canal Test

Overview

Another example of testing HEC-RAS against "observed" data is a comparison against "observed" water level data from the San Joaquin Canal system in Central California. In this comparison, the HEC-RAS unsteady flow algorithm was compared against measured stages from within the San Joaquin canal for a test that consisted of closing the gates at the upper and lower end of a reach of the canal, and measuring the resulting wave action. This test can be used to ensure that the 1D unsteady flow equations are being solved accurately. The results of this test are shown in Figure 3-3. As shown in Figure 3-3, the HEC-RAS model was able to track the dynamic wave through the canal system very accurately.

Problem and Data Description

Table 3-2 provides the specification for the San Joaquin Canal test case.

Table 3-2. Specifications for the San Joaquin Canal Test Case

Parameter	Value
Bottom width, b (feet)	40
Side slopes, z	1.5:1 H:V
Bed slope, S	0.00005
Roughness, n	0.012
Flow rate, Q cfs	1,700 to 0.0
Downstream Gated Structure, Gate Openings (feet)	2.6 to 0.0
Downstream Boundary Condition, WS (feet)	219.8

Model Setup

A simple 1D river reach was used for this example. A cross section was entered for River Station 0.0 and River Station 29335. Cross sections were then interpolated on a 50.0-foot spacing. Figure 3-3 displays a cross section plot in the HEC-RAS Cross Section Editor.

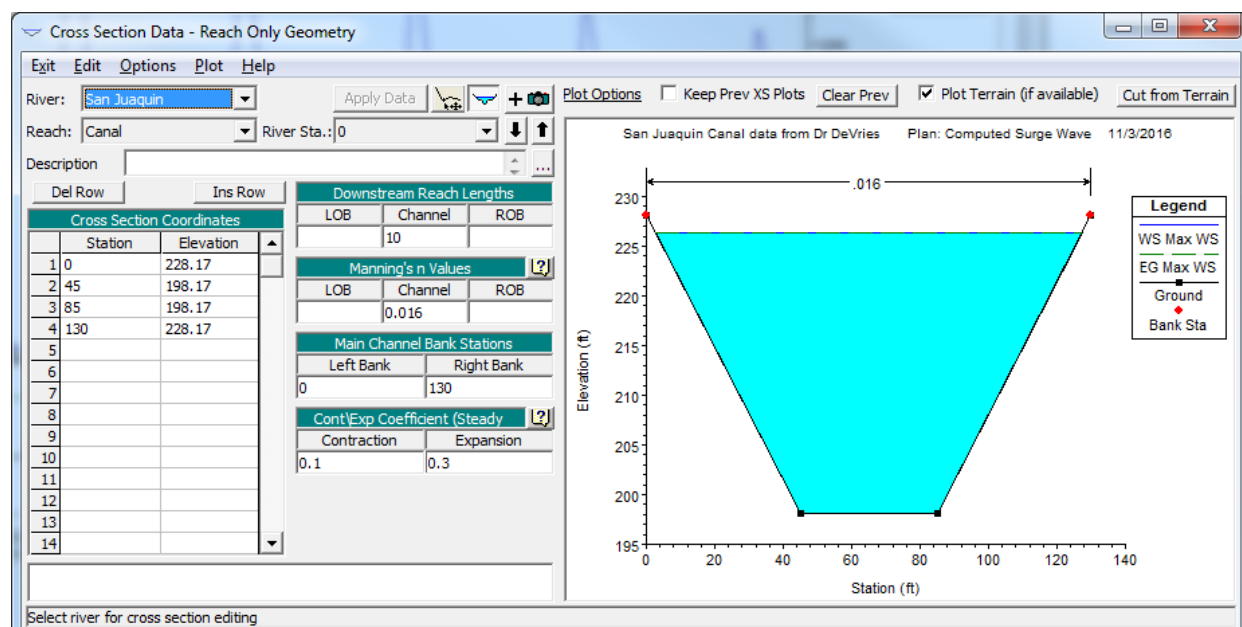


Figure 3-3. HEC-RAS Cross Section Editor - Downstream Cross Section, just above Gated Structure

Flow data and boundary conditions were entered into the HEC-RAS Unsteady Flow Data Editor. An upstream inflow hydrograph was used to represent the flow coming out of the upstream gates. The inflow hydrograph started at a flow of 1,700 cfs, then went to 1.0 cfs in a time span of one minute. The downstream boundary is a stage hydrograph with a constant stage of 219.8 feet. Upstream of the downstream boundary is an inline gated structure. A time series of gate openings was used to simulate the gate being open to 2.6 feet at first, then being closed to 0.0 feet in a time span of four minutes.

An HEC-RAS unsteady flow analysis plan was developed and the model was run in subcritical flow mode. Table 3-3 provides the HEC-RAS model parameters that were used for the unsteady flow analysis simulation:

Table 3-3. Model Parameters for the HEC-RAS Unsteady Flow Analysis Simulation

Parameter	Value
Computational Interval (second)	5
Theta Weighting Factor	0.6
Water Surface Tolerance (feet)	0.01

Results and Discussion

The results from the unsteady flow analysis were compared to the measured data taken during the testing of San Joaquin canal system. Water surface elevations were measured at the upstream end of the canal (just below the upstream gated structure, River Station 29335) and the downstream end of the canal (just above the downstream gated structure, River Station 0.0). Figure 3-4 and Figure 3-5 provide plots of the computed versus observed water surface elevations over time.

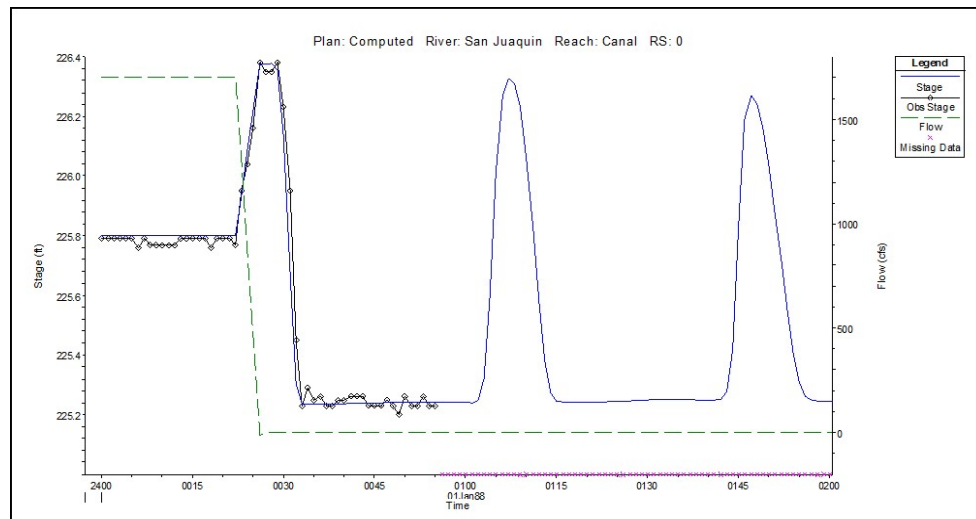


Figure 3-4. HEC-RAS Computed versus Observed Water Surface at Downstream Station 0.0

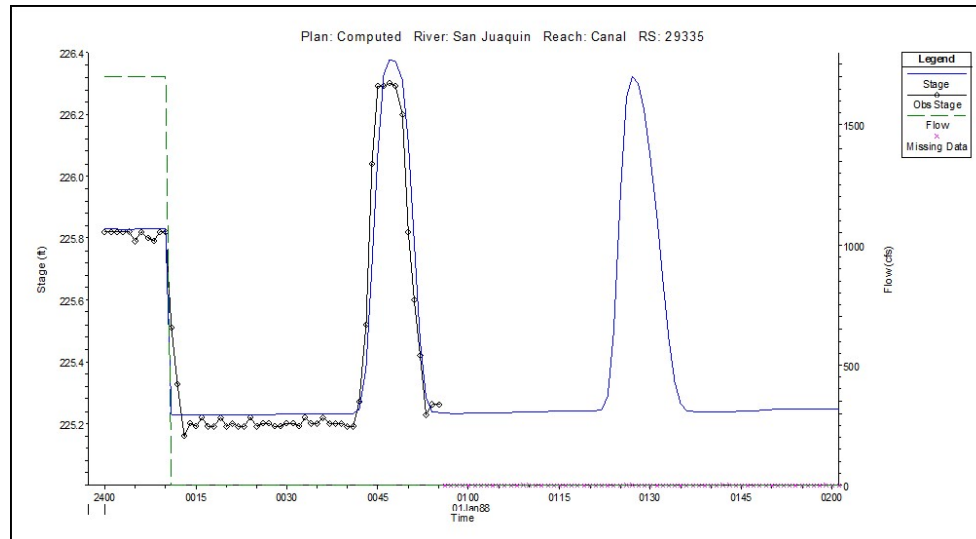


Figure 3-5. HEC-RAS Computed versus Observed Water Surface at Upstream Station 29335

The test verifies the 1D unsteady flow analysis computations can reproduce a transient wave due to a quick closer of a gate. This test verifies that the solution of the momentum equation, as well as the friction loss calculations, are working correctly.

3.4.2 Lower Columbia River System Test

Overview

HEC on behalf of the USACE, Portland District (CENWP), Hydrology and Hydraulics Branch, completed an HEC-RAS unsteady-flow hydraulic model of the Lower Columbia River System from the outflow of Bonneville Dam to the Pacific Ocean (Columbia River miles 146.1 to 0.0). The model includes a portion of all of the major tributaries that flow into the Columbia River below Bonneville Dam (Figure 3-6). The modeled tributaries are: Willamette, Cowlitz, Lewis, Multnomah channel, Columbia Slough, Youngs, Westport, West-Kerry, Will-Ross, Wallooskee, Skipanon, Lewis and Clark, Lake, Klaskanine, Johnson, John Day, Grays, Deer, and Coal rivers.

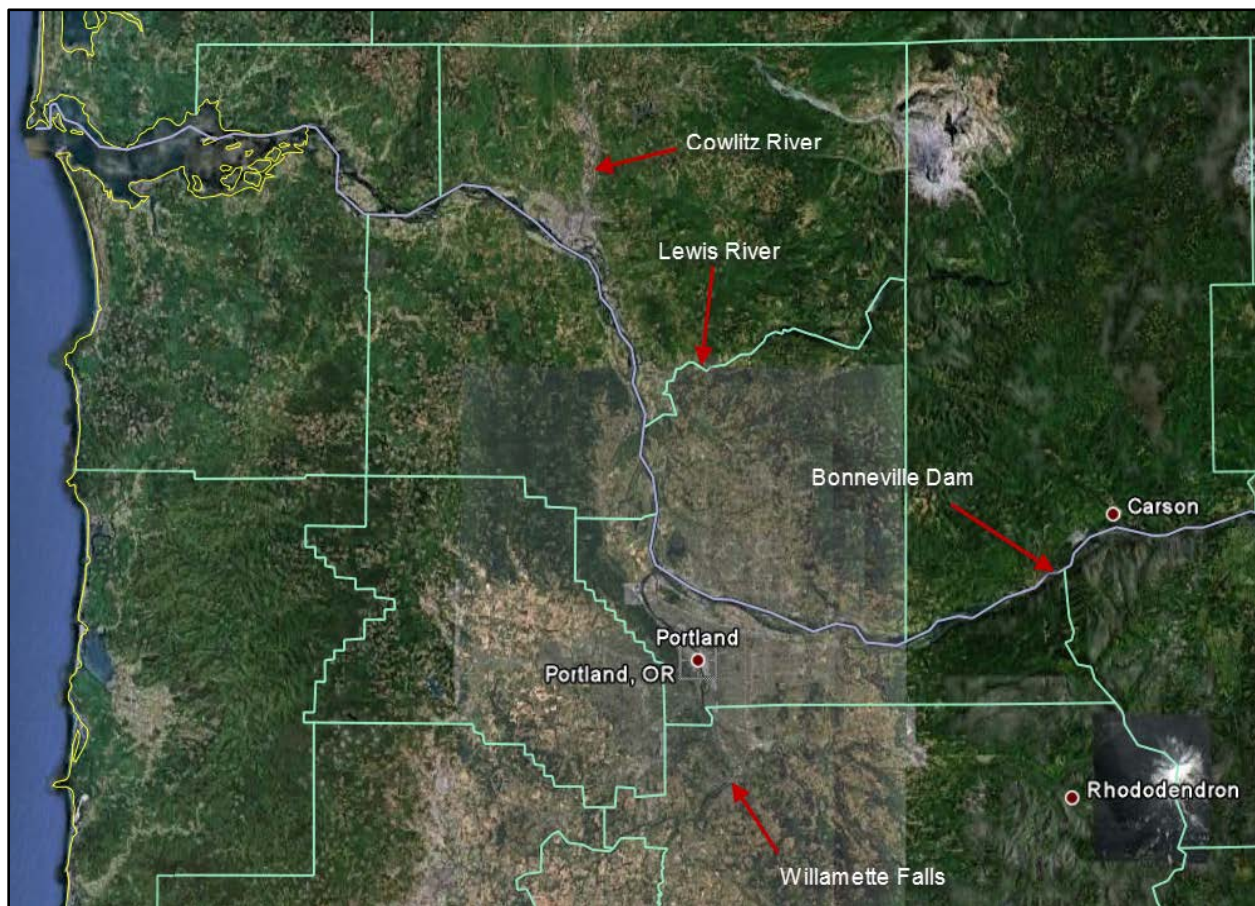


Figure 3-6. Overview map of Lower Columbia River System

The purpose of this hydraulic model is to predict water levels that will occur under low probability exceedance events, from the zero-damage event up to the 0.2 percent annual exceedance event (500 year). The HEC-RAS model uses the outflow from Bonneville Dam as its main upstream boundary condition, as well as flow hydrographs computed for each of the major tributaries modeled. The downstream boundary condition is a tidal stage hydrograph.

HEC-RAS in conjunction with RAS Mapper (a tool available from the HEC-RAS software) produces water surface profiles, hydrographs, stage-discharge curves, and inundation grids.

Problem and Data Description

The hydraulic model described in this section was developed to support the evaluation of flood risks under existing and future conditions in the Columbia River and tributaries as they are influenced by alternative reservoir operation scenarios in the Columbia River basin.

Hydrology

Flood runoff on the Lower Columbia River Basin is primarily the result of the spring snowmelt rather than specific storm events. However, weather conditions during the critical snowmelt period, such as below normal spring temperatures, rain-on-snow, or above normal temperature, may slow or increase the melting process and the runoff rates. Historical high flows have come from the upper Columbia River Basin, but on occasion large flows have also come out of the Willamette Basin. For example, the flood in February of 1996 was predominately a large flow event from the Willamette River, with a peak flow in the 420,000 to 460,000 cfs range, combined with a flow over 400,000 cfs coming down the Columbia River.

Model Geometry Data

Terrain data was obtained using LiDAR (Light Detection and Ranging) topographic data for much of the Columbia River Basin with extents equal to or greater than the FEMA (Federal Emergency Management Agency) Q3 500-year floodplain coverage (Watershed Sciences, 2010).

The one-meter LiDAR was converted to feet and modified to an ESRI (Environmental Systems Research Institute) grid format with a spatial reference of NAD (North American Datum) 1983 Albers. Bathymetric data was also surveyed during 2010, for the Columbia River and the Willamette River. Both data sources were combined together to develop a terrain model with a grid resolution of one meter. Bathymetric data was not acquired for all of the tributaries modeled. Channel cross section hydro survey data was obtained from previously developed hydraulic models for the Cowlitz and Lewis River systems. Channel data for all of the other tributaries was estimated by measuring channel top widths from Google Earth® and then cutting a reasonable trapezoidal channel into the section using the HEC-RAS channel modification tools.

Channel and floodplain geometry needed by the HEC-RAS model were extracted from a one-meter DEM (Digital Elevation Model) and aerial imagery data using HEC-GeoRAS (HEC, 2011). Additional data not extracted by HEC-GeoRAS was defined in the HEC-RAS model, such as detailed channel data for areas where no bathymetric data were available. HEC-GeoRAS utilizes user-defined GIS (Geographic Information System) layers to extract information from the terrain data. For example, a GIS layer of cross-section cut lines is needed so that HEC-GeoRAS knows where to extract cross-section information from the terrain data. Table 3-4 contains a list of the GIS layers that were created, by digitizing lines and polygons, as well as a brief description of importance.

Table 3-4. Description of GIS Layers Created to Extract Information for Hydraulic Modeling

GIS Layer	Description
Stream Centerline	The stream network is comprised of stream centerlines for the Main Columbia River and all major tributaries. Stream centerlines identify the connectivity between different streams for flood routing and are used to establish the river and reach name for cross sections and hydraulic structures within HEC-RAS.
Main Channel Bank Lines	Main channel bank lines establish the separation of the main low flow channel and the overbank areas (floodplain areas).
Flow Path Centerlines	Flow path centerlines define the center-of-mass of flow in the left overbank, channel, and right overbank areas. Flow path centerlines are used to compute the lengths between adjacent cross sections.
Cross-Section Cut Lines	Cross-section cut lines establish the location and extent for extracting station-elevation data from the terrain model for the channel cross-sections. Cross-sections were added at locations in order to capture changes in the channel and floodplain geometry as well as define an adequate floodplain boundary for mapping purposes.
Bridges/Culverts	Bridge and culvert cut lines establish the location and extent for extracting station-elevation data from the terrain model for describing the top-of-deck profile of the bridge or culvert. For this model bridges were not modeled as they were deemed high enough to not affect the water surface profiles.
Ineffective Flow Areas	Polygons were created defining areas in the floodplain that do not actively convey water. HEC-GeoRAS overlays the ineffective flow areas with the cross-section cut lines to determine the portion of the cross-section that does not actively convey water.
Lateral Structures	Lateral structure cut lines define the location and extent of natural and man-made structures (levees) where water can flow out into overbank areas, or areas protected by levees. The majority of the levees in this system were modeled as Lateral Structures. Station-elevation data was extracted from the terrain model for the top of the lateral structure.
Storage Areas	Storage areas were used to model areas behind levees, as well as storage for tributaries, that were not specifically modeled as separate routing reaches. Polygons were created defining the extents of all storage areas and used to extract the elevation-storage data from the terrain model. Lateral structures and storage area connections were used to connect the storage areas to the main channel.
Storage Area Connections	Storage Area Connections are used to define a hydraulic structure between two storage areas. Storage Area Connections are often used to model interior levees, significant roads, or natural high ground that will prevent water from going from one area to another.

The geometric data generated by HEC-GeoRAS was imported into HEC-RAS. This data included the river system schematic (main Columbia River and all tributaries), station-elevation points for cross-sections, reach lengths between cross-sections, ineffective flow areas in the floodplain, station-elevation location and station-elevation information for lateral and inline structures, and elevation-storage information for storage areas. Additional data was entered into the HEC-RAS model based on information provided by CENWP. Geospatial data was extracted from aerial photography, and other data from standard engineering equations to estimate model parameters. The model schematic, as depicted in HEC-RAS, is shown in Figure 3-7. This model has 34 different rivers with eighty different river reaches defined within the system.

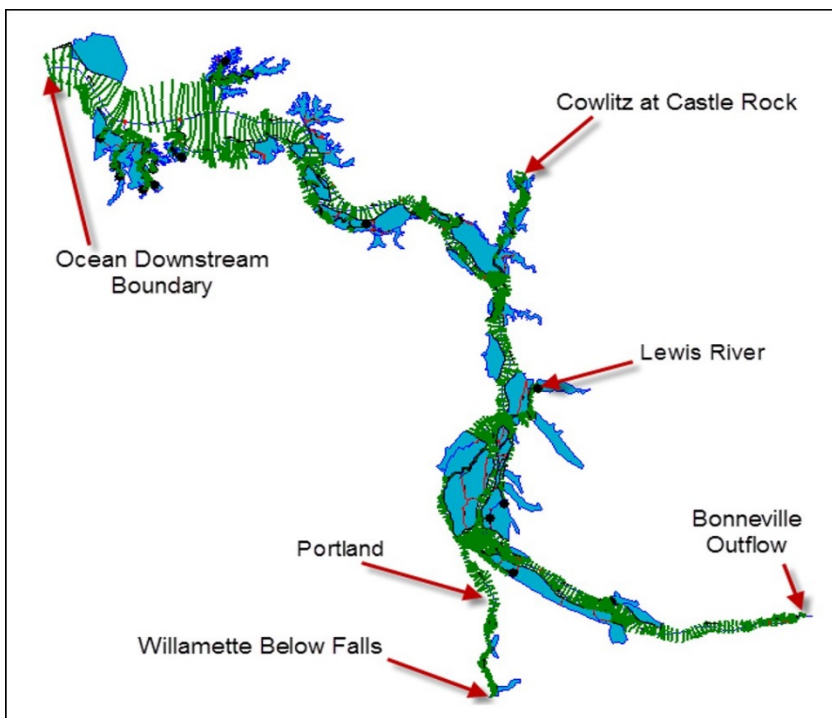


Figure 3-7. HEC-RAS Schematic of the Lower Columbia River System

Model Setup

Initial estimates of Manning's n values for the main channels were estimated from previously developed HEC-RAS models, visualization of the river using Google Earth®, and hydraulic modeling experience gained from other studies. Main channel Manning's n values were estimated for the channel as a whole, rather than separate values for the channel bottom and the channel banks. A large portion of the river corridor has extensive and thick brush and trees on the banks of the main channel. Channel Manning's n values were estimated by weighting the base Manning's n value of the bottom with a larger n values for the channel banks. Overbank

Manning's n values were estimated by using aerial images to define areas of similar land use, then assigning an n value for that land use type. For example, thick forested areas were assigned a Manning's n value of 0.10; urban areas with high densities of building were assigned a value of 0.15; and open fields with grass was assigned values of 0.05. After all of the cross sections were assigned initial Manning's n value estimates, further refinement of the Manning's n values was made during the model calibration process. Model calibration is described below. Table 3-5 displays the range of Manning's n values for the major rivers.

Table 3-5. Manning's n Value Ranges for Main Channels and Overbank Areas

River Name	Main Channel Manning's n Coefficient	Overbank Manning's n Coefficient
Columbia River	0.028 - 0.035	0.05 - 0.10
Willamette River	0.03 - 0.039	0.05 - 0.15
Cowlitz River	0.025 - 0.031	0.05 - 0.10
Lewis River	0.032	0.05 - 0.10
All Other Channels	0.03	0.05 - 0.15

Lateral structures were used to model all of the levees that go directly along any of the modeled rivers. Lateral structures are connected from a river reach, to an area behind the levee (which were modeled as storage areas). In the HEC-RAS model, 208 separate lateral structures (levees) were defined and entered into the HEC-RAS model to represent reaches of levee systems. The lateral structures were laid out in HEC-GeoRAS either by hand drawing them, or by following existing levee shapefiles. The terrain data for the lateral structures (levees) were originally extracted from the one-meter DEM and imported into HEC-RAS. However, detailed surveys were made of most of the levees (those that protected property and human life).

Also, included in the HEC-RAS model were 160 storage areas that were used to model protected areas behind levees, as well as available storage in smaller tributaries that would incur backwater from the Columbia River. The lateral structure feature in HEC-RAS was used to connect the main channel to each storage area. Figure 3-8 shows the use of several lateral structures, along multiple river reaches, and storage areas to model the typical situation of levees protecting a valued property. Figure 3-8 displays the levees protecting the Longview area along the Columbia River, Cowlitz River, and Coal Creek.

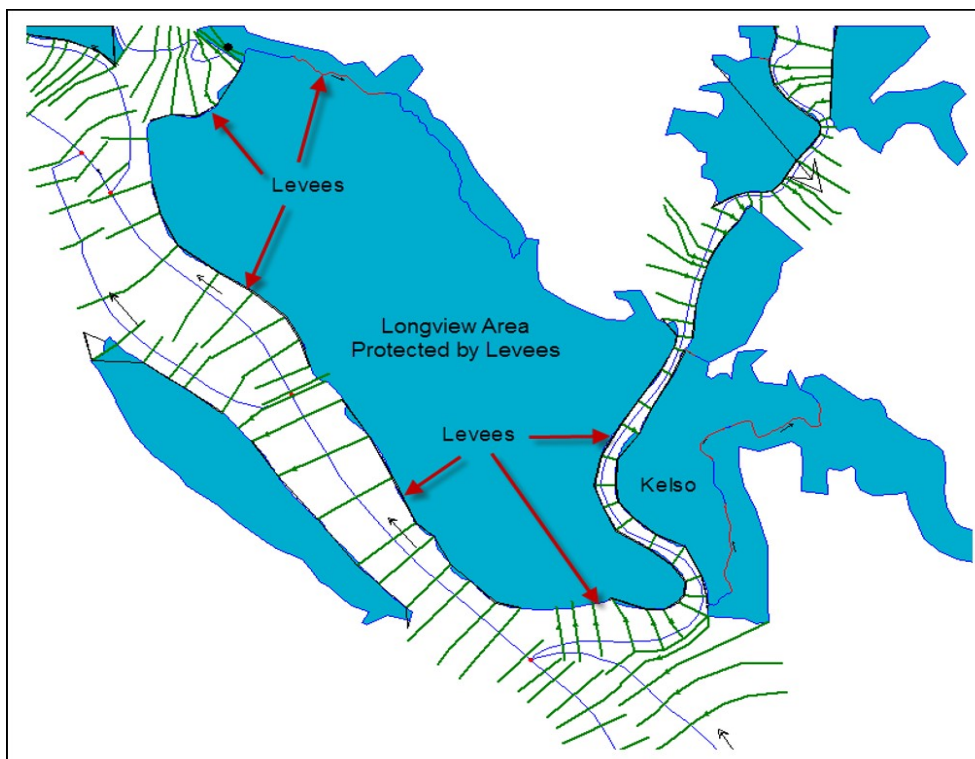


Figure 3-8. Example of Storage Areas and Lateral Structures used to Model Protected Areas

Model Calibration and Validation

Calibration and validation of flow and stage data were obtained from CENPP. This data consisted of USGS gages, NOAA (National Oceanic and Atmospheric Administration) gages, and CENWP owned and operated gages. Three events were used for calibration and two events were used for model validation. The calibration events were the 1996 flood event (record gaged flow on the Willamette River), the Spring 1997 flood (big flow on the Columbia River mainstem), and the May 2008 to February 2009 event (typical flow on the Columbia River, but a large flow on the Cowlitz River). In addition to gaged data, an extensive set of high water marks

and a flood inundation boundary shapefile was available for the 1996 flood event. The high water marks and the flood inundation boundary were used to calibrate the model between gages and in areas where there was no gaged data. Validation events were the 2006 and 2010 runoff periods.

Results and Discussion

Calibration results shown in Table 3-6 are the computed peak stages, observed peak stages, differences in computed minus observed stages, and the timing differences of when the peak stages occurred (computed time minus observed time). Locations shown in the table are all gaged locations. Note gaged data was not available at all locations for the 1996 and 1997 events.

Table 3-6. Summary of Model Calibration Results

Location	Flood Event	Computed Peak Stage NAVD (feet)	Observed Peak Stage NAVD (feet)	Stage Difference (feet)	Time Difference (hours)
Columbia River @ Bonneville	1996	37.4	38.3	-0.9	0.0
	1997	37.8	38.0	-0.2	-1.0
	2008	32.2	32.4	-0.2	+1.0
Columbia River @ Vancouver	2008	20.3	20.1	+0.2	+1.0
Columbia River @ Saint Helens	2008	17.5	17.6	-0.1	-1.0
Columbia River @ Longview	2008	14.5	15.7	-1.2	-0.75
Columbia River @ Beaver Army Terminal	1996	17.3	16.4	+0.9	0.0
	1997	15.4	15.0	+0.4	0.0
	2008	13.0	13.3	-0.3	0.0
Columbia River @ Astoria	1996	11.8	12.1	-0.3	0.0
	1997	11.9	12.1	-0.2	-1.0
	2008	11.1	11.4	-0.3	+1.0
Willamette River Below Falls	1996	46.2	*49.2	-3.0	N/A
	1997	39.0	40.0	-1.0	+1.0
	2008	30.7	29.6	+1.1	-3.0
Willamette Reiver @ Portland	1996	33.0	32.7	+0.3	-1.0
	1997	28.3	28.0	+0.3	+3.0
	2008	19.9	19.6	+0.3	-1.0
Cowlitz River @ Castle Rock	1996	55.8	55.9	-0.1	-2.0
	1997	46.6	47.0	-0.4	-1.0
	2008	54.7	54.6	+.1	+0.75
Cowlitz River @ Lexington	2008	37.8	37.8	0.0	-1.0
Cowlitz River @ Ostrander	2008	30.6	30.6	0.0	+1.0
Cowlitz River @ Gearhart	2008	17.9	18.0	-0.1	0.75

*Note: Data value estimated from high water marks. This could actually be the energy gradeline instead of the true average water surface elevation.

Figure 3-9 displays a profile plot comparing computed water surface elevations versus high water marks for the 1996 flood event on the Columbia River. The calibrated model was validated using flow and stage from the 2006 and 2010 flood events. Shown in Table 3-7 are the computed peak stages, observed peak stages, differences in computed minus observed stages, and the timing differences of when the peak stages occurred (computed time minus observed time). Locations shown in the table are all at the gaged locations.

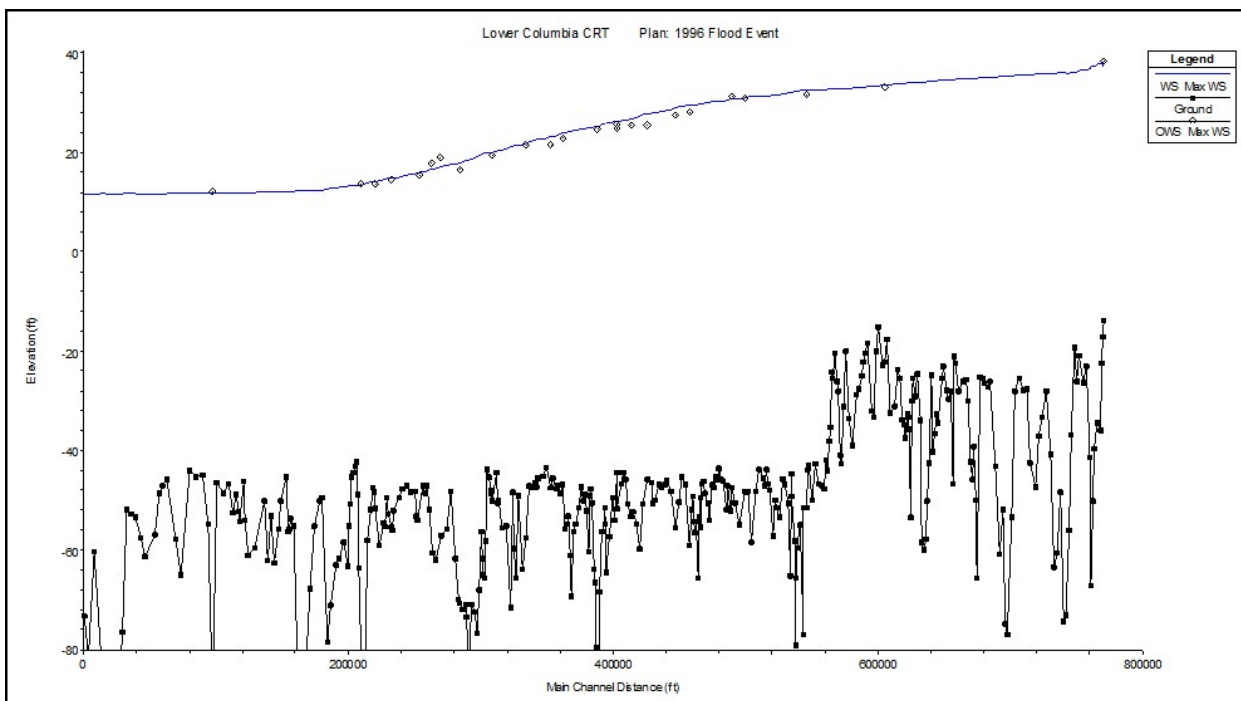


Figure 3-9. Computed Profile Plot of Columbia River with Observed High Water Marks for 1996 Flood

Table 3-7. Summary of Model Verification Results

Location	Flood Event	Computed Peak Stage NAVD (feet)	Observed Peak Stage NAVD (feet)	Stage Difference (feet)	Time Difference (hours)
Columbia River @ Bonneville	2006	31.1	31.1	0.0	-2.0
	2010	31.2	31.9	-0.7	+1.0
Columbia River @ Vancouver	2006	20.1	20.4	-0.3	-4.0
	2010	19.8	20.0	-0.2	-2.0
Columbia River @ Saint Helens	2006	17.9	18.3	-0.4	-1.0
	2010	16.9	17.4	-0.5	0.0
Columbia River @ Longview	2006	14.9	15.5	-0.6	0.0
	2010	13.7	14.2	-0.5	0.0
Columbia River @ Beaver Army Terminal	2006	14.0	14.2	-0.2	0.0
	2010	12.0	12.0	0.0	0.0
Columbia River @ Astoria	2006	12.4	12.5	-0.1	0.0
	2010	10.3	10.8	-0.5	0.0
Willamette River Below Falls	2006	32.1	31.8	+0.3	+2.0
	2010	25.0	24.5	+0.5	+2.0
Willamette River @ Portland	2006	20.8	20.4	+0.4	+3.0
	2010	19.4	19.5	-0.1	-2.0
Cowlitz River @ Castle Rock	2006	46.6	45.7	+0.9	-1.0
	2010	37.8	38.0	-0.2	0.0

Calibration results came out very well for the entire model except the upper end of the Willamette River, just below the Falls, and at Longview on the Columbia River. The model results differed from the observed in this area by more than a foot. The validation runs were also very good, with almost all locations showing results within 0.5 feet of the observed

measurements, except for two locations, which still showed differences less than 1.0 feet. Hydrograph shape, timing, and magnitude of the stages and flows agreed very well throughout the entire model. In general it is believed that this model is capable of reproducing hydrographs from low to high events, and is very well suited for predicting future flood event stages and flows (given good boundary conditions for inflows).

This test case shows that the HEC-RAS 1D unsteady flow computations are capable of modeling complex hydraulic systems, and provide accurate answers to past flood events as well as future predictions.

References

1. HEC, 2011. *HEC-GeoRAS, GIS Tools for Support of HEC-RAS using ArcGIS®*, Version 4.3.92. U.S. Army Corps of Engineers, Hydrologic Engineering Center, Davis CA. February 2011. CPD-83.

Chapter 4

Two-Dimensional Unsteady Flow

4.1 Overview

The objective of this chapter is to verify and validate the HEC-RAS 2D unsteady flow hydraulic computations. This is accomplished by applying HEC-RAS 2D unsteady flow hydraulics to a wide range of analytical, text book, laboratory, and field datasets.

4.2 Analytical and Text Book Datasets

There are several analytical and well documented text book datasets that were used to verify that the HEC-RAS 2D unsteady flow hydraulics code was working correctly. Results from this verification shows that the 2D unsteady flow equations were derived correctly and then programmed correctly. The following 2D unsteady flow tests are offered as verification of the software.

4.2.1 Standard Step Backwater Test

Overview

Earlier tests within the 1D steady flow and 1D unsteady flow chapters were to compare hand calculations from backwater profiles listed in "*Open Channel Hydraulics*" (Chow, 1959; Example 10.1, page 250) with HEC-RAS model results. This comparison provides details that the basic capability of the 2D unsteady flow option in HEC-RAS can reproduce results for a simple trapezoidal channel under the influence of a backwater condition. The test verifies the solution of the 2D Shallow Water Equations (SWE) equations for a 1D channel flow situation, which includes friction losses. The test case is also useful for verifying the implementation of the flow hydrograph and stage hydrograph boundary conditions.

Problem and Data Description

The test is a trapezoidal channel with the following properties. A summary of the important model setup parameters are described in Table 4-1. The test conditions are the same as those utilized in Section 2.2.1 for verifying the 1D steady flow model.

Table 4-1. Specifications for the One-Dimensional Backwater Test Case

Parameter	Value
Bottom width, b (feet)	20
Side slopes, z	2:1 H:V
Bed slope, S	0.0016
Roughness, n	0.025
Flow rate, Q cfs (cubic feet per second)	400
Downstream Boundary Condition, WS (feet)	5.0

Model Setup

A 2D model was developed for this dataset with a computational domain of 3,000 feet long and 40 feet wide. A constant grid resolution of 40 x 40 foot cells was used. Therefore, the mesh was only one computational wide. A flow boundary condition was specified at the upstream end of the system and a stage boundary condition with a constant water level at the downstream end. Figure 4-1 displays the 2D mesh and terrain for this test case.



Figure 4-1. Computational Grid and Terrain for the Step Backwater Test Case

Manning's n values were set up as a constant $n = 0.025$ for the entire domain. Turbulence modeling was turned off for this test case, as it is 1D flow with no significant mixing. A summary of the important model setup parameters is provided in Table 4-2.

Table 4-2. Model Setup Parameters for the Step Backwater Test Case

Parameter	Value
Governing equations	SWE
Manning's n roughness coefficient ($s/m^{1/3}$)	0.025
Turbulence	Off
Time step (second)	2
Simulation duration (hour)	1
Implicit weighting factor	1
Water surface tolerance (meter)	0.0001
Volume tolerance (meter)	0.0001

Results and Discussion

The results from the 2D computations analysis were compared to the results from Chow (Example 10.1; 1959). Figure 4-2 displays the computed results from the 2D model versus the results documented in Chow (1959). The 2D model is able to reproduce the results for this 1D channel flow. Results show that the 2D unsteady flow option in HEC-RAS is accurately computing friction losses, pressure differential forces, and advective acceleration forces for this type of test case. The Mean Error (ME), Mean Absolute Error (MAE), and Root Mean Squared Error (RMSE) of the water levels are -0.0074 feet, 0.0136 feet, and 0.0172 feet, respectively. The total water volume error for the simulation was 0.00174 percent which indicates excellent water volume conservation

References

1. Chow, 1959. Chow, Ven Te. *Open-Channel Hydraulics*. McGraw-Hill Civil Engineering Series, McGraw-Hill Book Company. New York, New York.

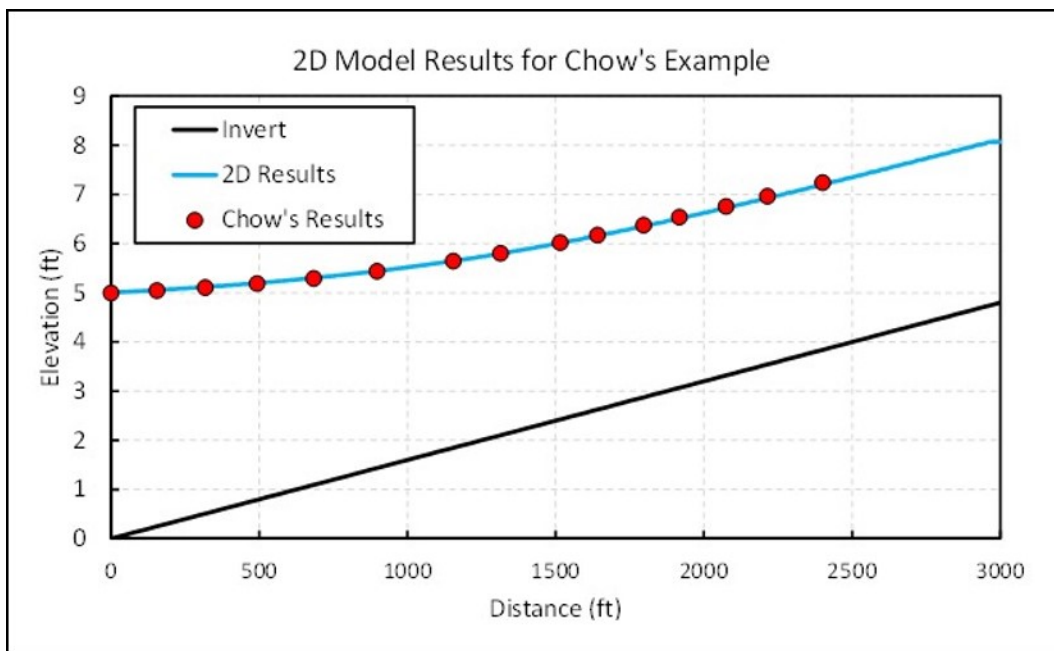


Figure 4-2. Velocity Plot with Profile Lines at Locations of Velocity Measurements

4.2.2 Subcritical Flow over a Variable Sloping Bed

Overview

This test case solves the SWE over a 1D geometry with a variable bed slope. The test case is utilized to perform a grid convergence analysis to evaluate the ordered discretization error of the SWE solver. The analysis involves performing several simulations with different grid resolutions and evaluating the rate of solution error reduction with progressively finer grid resolutions as compared to the analytic solution. The model features which are verified include the upstream flow hydrograph boundary condition and a downstream stage boundary condition. The test case also evaluates the 2D model's ability to preserve a steady-state solution.

Problem and Data Description

The analytic solution is derived by first simplifying the governing equations. Assuming no Coriolis, rain, or horizontal mixing, the steady-state one-dimensional (1D) momentum equation may be written as (MacDonald, 1996; MacDonald, 1997):

$$\frac{\partial z_b}{\partial x} = \left(\frac{q^2}{gh^3} - 1 \right) \frac{\partial h}{\partial x} - S_f \quad (4-1)$$

where:

z_b = bed elevation [L]

$q = hU$ equals unit discharge [L^2/T]

U = current velocity [L/T]

h = water depth [L]

g = gravitational acceleration [L/T²]

$S_f = \frac{n^2 U^2}{h^{4/3}}$ equals friction slope assuming a Manning-Strickler friction law [-]

n = Manning's n roughness coefficient [T/L^{1/3}]

Using Equation 4-1, any number of analytic solutions may be obtained by specifying the discharge (constant throughout the domain) and the water depth profile. Here the analytical solution is obtained with the SWASHES (Shallow Analytic Solutions for Hydraulic and Environmental Studies) software, Version 1.03.00 (Delestre, 2013). The specified water depth profile is given as:

$$h = \left(\frac{4}{g}\right)^{1/3} \left\{ 1 + \frac{1}{2} \exp \left[-16 \left(\frac{x}{1000} - \frac{1}{2} \right)^2 \right] \right\} \text{ for } 0 \leq x \leq 1,000 \text{ meters} \quad (4-2)$$

with $g = 9.81 \text{ m/s}^2$. The unit discharge is specified as $q = 2 \text{ m}^2/\text{s}$ and the Manning's n roughness coefficient as $n = 0.033 \text{ s/m}^{1/3}$. These conditions lead to a subcritical flow over the whole domain with a Froude number between 0.544 and 0.986. The bed elevations were then obtained from SWASHES which integrates the momentum equation using the above water depth profile, unit discharge, and Manning's n roughness coefficient.

Model Setup

A summary of the model setup parameters is shown in Table 4-3. A total of six different grid resolutions were tested, each with a constant grid refinement ratio of two (Table 4-3). The computational grid consists of a rectangular domain two-cells-wide with a constant grid resolution. A constant upstream discharge and downstream water depth are specified. The model domain is initialized dry. The simulation is run well past the steady state condition for forty minutes. Horizontal mixing is not considered in this test case. The implicit weighting factor is set to the default value 1.0. Since the test case is a steady-state problem, the implicit weighting factor is not important as it does not affect the solution once a steady-state condition is reached.

Table 4-3. Model Setup Parameters for the MacDonald One-Dimensional Test Case

Parameter	Value
Manning's n roughness coefficient (s/m ^{1/3})	0.033
Grid resolution (meter)	1, 2, 4, 8, 16, 32
Governing equations	SWE
Courant number	0.5 - 1.0
Implicit weighting factor	1.0
Water surface tolerance (meter)	0.001
Volume tolerance	0.001
Mixing coefficient	0.0
Upstream unit discharge (m ² /s)	2
Downstream water depth (meter)	0.771429
Initial water depth (meter)	0
Simulation duration (minutes)	40

Results and Discussion

As mentioned in the previous section, a total of six simulations were carried out with grid resolutions between one and 32 meters. As an example of the simulation results, Figure 4-3 shows the computed water surface elevation with a four-meter grid resolution compared to the analytic solution. In general the computed water surface elevation compares well with the analytic solution as demonstrated by the goodness-of-fit statistics in Table 4-4 . Definitions of the goodness-of-fit statistics are provided in Appendix A.

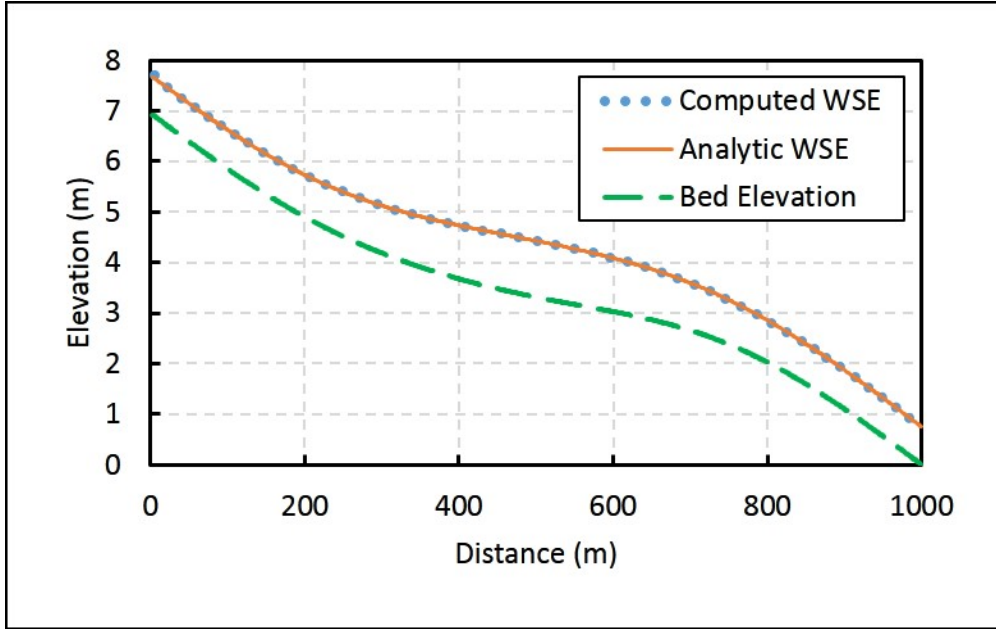


Figure 4-3. Example Comparison of Computed and Analytic Water Depths for MacDonald One-Dimensional Test Case with a Four-Meter Grid Resolution

Table 4-4. Water Depth Goodness-of-Fit Statistics for the MacDonald One-Dimensional Test Case

Statistic	Grid Resolution (meter)					
	1	2	4	8	16	32
ME (meter)	0.00017	0.00023	0.00016	-0.00016	-0.00104	-0.00241
NME (percent)	0.003	0.003	0.002	-0.002	-0.015	-0.035
MAE (meter)	0.00050	0.00062	0.00072	0.00096	0.00150	0.00334
NMAE (percent)	0.007	0.009	0.011	0.014	0.022	0.048
RMSE (meter)	0.00252	0.00337	0.00304	0.00392	0.00855	0.01772
NRMSE (percent)	0.037	0.049	0.044	0.057	0.124	0.257
R ²	0.999994	0.999996	0.999997	0.999995	0.999974	0.999885

The grid convergence is shown in Figure 4-4 using MAE. The order of convergence p is obtained from fitting the curve $MAE = C\Delta x^p$ where C is a coefficient which is constant within the asymptotic range of convergence. In this case, the overall order of convergence is found to be almost around 1.32. Similar results are found when plotting the RMSE. The pressure gradient term is discretized with a second-order central difference scheme. The Eulerian-Lagrangian scheme for the acceleration terms involves two steps. The first is the backward

tracking which is the computation of the Lagrangian trajectory by integrating the velocity backwards from the cell faces. The second step is the interpolation of the cell-face normal component of the current velocity at the end of the Lagrangian trajectory. For Cartesian grids, the current velocity interpolation is second-order. However, the backward tracking is computed with a simple first-order Euler scheme. Therefore, the major contributing error between first and second order grid convergence is the backward tracking.

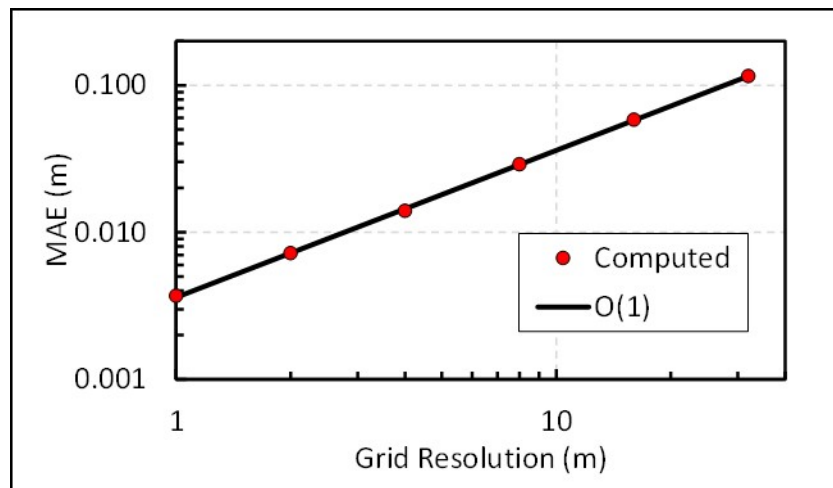


Figure 4-4. Grid Convergence for the MacDonald One-Dimensional Test Case

References

1. Delestre, 2013. Delestre, Olivier, Lucas, C., Ksinant, P.-A., Darboux, F., Laguerre, C., Vo, T.-N.T., James, F., and, Cordier, S. *SWASHES: a compilation of shallow water analytic solutions for hydraulic and environmental studies*. International Journal for Numerical Methods in Fluids, Volume 72, Issue 3, pages 269-300. November 2013.
2. MacDonald, 1996. MacDonald, Ian. *Analysis and computation of steady open channel flow*. PhD Thesis, University of Reading, Department of Mathematics. 219 pages.
3. MacDonald, 1997. MacDonald, I., Baines, M.J., Nichols, N.K., and Samuels, P.G. *Analytic benchmark solutions for open-channel flows*. Journal of Hydraulic Engineering, ASCE, Volume 123, Issue 11, pages 1041–1045. November 1997.

4.2.3 Flow over a Bump without Friction

Overview

This test case is used to evaluate the HEC-RAS's ability to evaluate flow transitioning from subcritical to supercritical flow (transcritical flow), and then through a hydraulic jump. The analytical solution was computed assuming a frictionless surface in order to simplify the solution. This test case will validate several terms in the computational equations, except the friction loss term. The model features which are verified include the upstream hydrograph boundary condition and a downstream stage boundary condition. The test case also evaluates the model's ability to preserve a steady-state solution.

Problem and Data Description

The test is a 0.3 meter wide rectangular channel for a reach that is approximately twenty meters long. The bed slope is flat and the surface is assumed to be frictionless. The bump has a peak elevation of 0.2 meters, and is centered at River Station 10.0. The bump shape is described with the following equation (Goutal, 1997):

$$z_b = \begin{cases} 0, & \text{for } x < 8 \\ 0.2 - 0.05(x-10)^2, & \text{for } 8 \leq x < 12 \\ 0, & \text{for } 12 \leq x \end{cases} \quad (4-3)$$

where z_b is the bed elevation with respect to the still water level, and x is the horizontal distance. The water depth may be computed by solving the Bernoulli's equation before and after the hydraulic jump and the momentum equation at the hydraulic jump (Goutal, 1997; Delestre, 2013). Table 4-5 provide a listing of the additional data used to describe this test case.

Table 4-5. Model Setup Parameters for the MacDonald Bump Test Case

Parameter	Value
Manning's roughness coefficient ($s/m^{1/3}$)	0.00001
Bottom width (meter)	0.3
Side slopes	0.0
Unit discharge (m^2/s)	0.18
Downstream water level (meter)	0.33

Model Setup

A 2D model was developed for this dataset with a computational domain of 21 meters long and 0.3 meters wide. A constant grid resolution 0.05×0.05 meter cells were used. A flow boundary condition was specified at the upstream end of the system and a stage boundary condition with a constant water level of 0.33 meters was used at the downstream end.

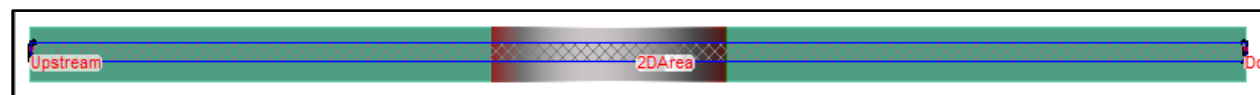


Figure 4-5. Computational Grid for the Two-Dimensional Bump Test Dataset

Results and Discussion

The results from the 2D unsteady flow analysis were compared to the documented analytical solution to this problem. The analytical solution was obtained with Bernoulli's equation for the transition from subcritical flow, through critical depth, and then supercritical flow down the bump. The location of the jump is obtained with the specific force equation (momentum with no friction or gravitational force). Figure 4-6 displays a plot of the computed water surface profile versus the analytical solution results.

Table 4-6. Model Setup Parameters for the Two-Dimensional Bump Test Case

Parameter	Value
Manning's roughness coefficient ($s/m^{1/3}$)	0.00001
Grid resolution (meter)	0.05
Governing equations	SWE
Implicit weighting factor	1.0
Water Surface Elevation Tolerance (meter)	1×10^{-3}
Volume Tolerance	1×10^{-3}
Mixing coefficient	0.0
Upstream discharge (m^3/s)	0.054
Downstream water level (meter)	0.33
Initial water depth (meter)	0.33
Simulation duration (minutes)	5

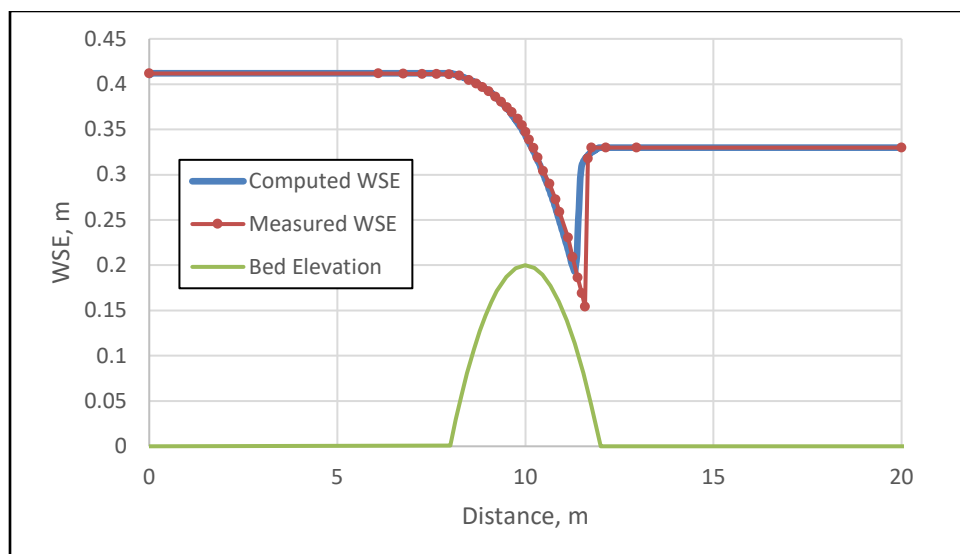


Figure 4-6. Two-Dimensional Computed and Analytical Solution of the Bump Test

The test verifies the 2D unsteady flow analysis computations can reproduce a flow transitioning from subcritical to super critical, and then though a hydraulic jump for a channel with no friction losses. The 2D results show the jump occurring a little sooner than the analytical solution, but the results are still very good. In general this is due to the fact that the solution of the momentum equation is between first and second order accurate, and there is some loss of momentum over the contraction zone. Additionally, HEC-RAS 2D requires a friction loss coefficient greater than zero to be used, so there is still some friction losses being computed.

References

1. Delestre, 2013. Delestre, Olivier, Lucas, C., Ksinant, P.-A., Darboux, F., Laguerre, C., Vo, T.-N.T., James, F., and, Cordier, S. *SWASHES: a compilation of shallow water analytic solutions for hydraulic and environmental studies*. International Journal for Numerical Methods in Fluids, Volume 72, Issue 3, pages 269-300. November 2013.
2. Goutal, 1997. Goutal, N., and Maurel, F. *Proceedings of the 2nd workshop on dam-break wave simulation*. Technical Report HE-43/97/016/B. Electricité de France, Direction des études et recherches. [In French].

4.2.4 Flood Wave Propagation over a Flat Bed

Overview

This test case is useful for evaluating the model wetting capability and the correct implementation of the non-linear SWE and Diffusion Wave Equations (DWE). The test case is based on a simplified 1D geometry with a horizontal bed slope. A clever analytical solution was provided by Hunter (2005) in which the wetting front moves forward while preserving its shape. The model features which are verified include the upstream flow hydrograph boundary condition and water volume conservation and stability during wetting of cells.

Problem and Data Description

For completeness, the derivation of the analytical solution from the governing equations is shown here and is based on Hunter (2005). Assuming no Coriolis or rain, the one-dimensional SWE are:

$$\frac{\partial U}{\partial t} + \frac{\partial(hU)}{\partial x} = 0 \quad (4-4)$$

$$\frac{\partial U}{\partial t} + U \frac{\partial U}{\partial x} = -g \frac{\partial \eta}{\partial x} - \frac{\tau_b}{\rho} \quad (4-5)$$

where:

u = depth-averaged current velocity [L/T]

t = time [T]

$\tau_b = \rho c_d U^2$ equals bed shear stress [M/L/T²]

ρ = water density [M/L³]

$c_d = gn^2 h^{-4/3}$ equals drag coefficient

h = water depth [L]

x = horizontal coordinate [L]

g = gravitational acceleration [L/T²]

η = Manning's roughness coefficient [T/L^{1/3}]

A solution may be found in which the flood wave propagates forward while maintaining its shape (i.e., $h(x,t) = h(x-ut)$) by imposing a constant current velocity and assuming a flatbed (i.e., $\partial h / \partial x = \partial n / \partial x$). With these assumptions the momentum equation simplifies to (Hunter, 2005):

$$g \frac{\partial h}{\partial x} = - \frac{gn^2 U^2}{h^{4/3}} \quad (4-6)$$

which also forms the basis for the DWE. Dividing both sides of the above equation by the square root of their norm, the above equation may be rewritten as:

$$U = - \frac{h^{2/3}}{n} \frac{\nabla h}{|\nabla h|^{1/2}} \quad (4-7)$$

Now inserting the above equation into the continuity equation leads to the one-dimensional DWE:

$$\frac{\partial h}{\partial t} = \frac{\partial}{\partial x} \left(\beta \frac{\partial h}{\partial x} \right) \quad (4-8)$$

where:

$$\beta = \frac{h^{5/3}}{n|\nabla h|^{1/2}} \text{ equals the nonlinear diffusion coefficient}$$

Therefore, the solution to the above problem is a solution to both the SWE and DWE. An analytical solution was obtained by Hunter (2005) by integrating the momentum equation as:

$$h = \left\{ \frac{7}{3} [C - n^2 U^3 (x - Ut)] \right\}^{3/7} \quad (4-9)$$

where C is a constant of integration which is calculated from the problem initial conditions. For the problem analyzed here, the constant of integration is $C = 0$, representing $h(x=0, t=0) = 0$. The other problem parameters are specified as $U = 1$ m/s, and $n = 0.01$ s/m^{1/3}.

Model Setup

HEC-RAS was setup using a simple Cartesian mesh with a constant resolution of 25 meters. Table 4-7 provides a listing of the additional data used to describe this test case.

Table 4-7. Convergence Criteria Analyzed after each Outer Loop Iteration

Parameter	Value
Manning's roughness coefficient, n (s/m ^{1/3})	0.01
Current velocity u (m/s)	1
Grid resolution (meter)	25
Initial water surface elevation (meter)	0
Governing equations	SWE, DWE
Time step (seconds)	10
Implicit weighting factor	1 (default)
Water Surface Tolerance (meter)	0.001 (default)
Volume Tolerance (meter)	0.001 (default)

Results and Discussion

A comparison between the analytical and computed results using the HEC-RAS DWE and SWE solvers is shown in Figure 4-7 and Figure 4-8 , respectively. The HEC-RAS results computed with both the SWE and DWE solvers agree well with the analytical solution. There are small discrepancies near the edge of the moving front, with the DWE solver tracking a little closer to the analytical solution. While the SWE solver is also in very good agreement overall, the front of the flood wave is traveling faster than the analytical solution.

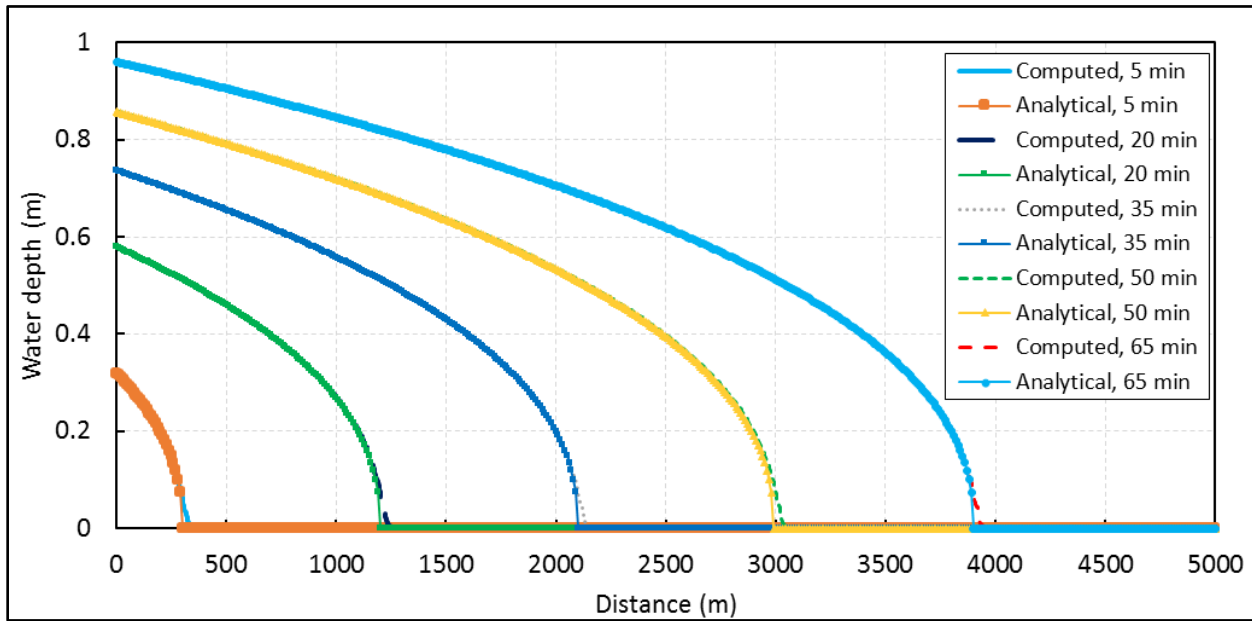


Figure 4-7. Comparison of Analytical and Computed Water Depth Profiles at Different Times using the HEC-RAS Diffusion Wave Equation (DWE) Solver

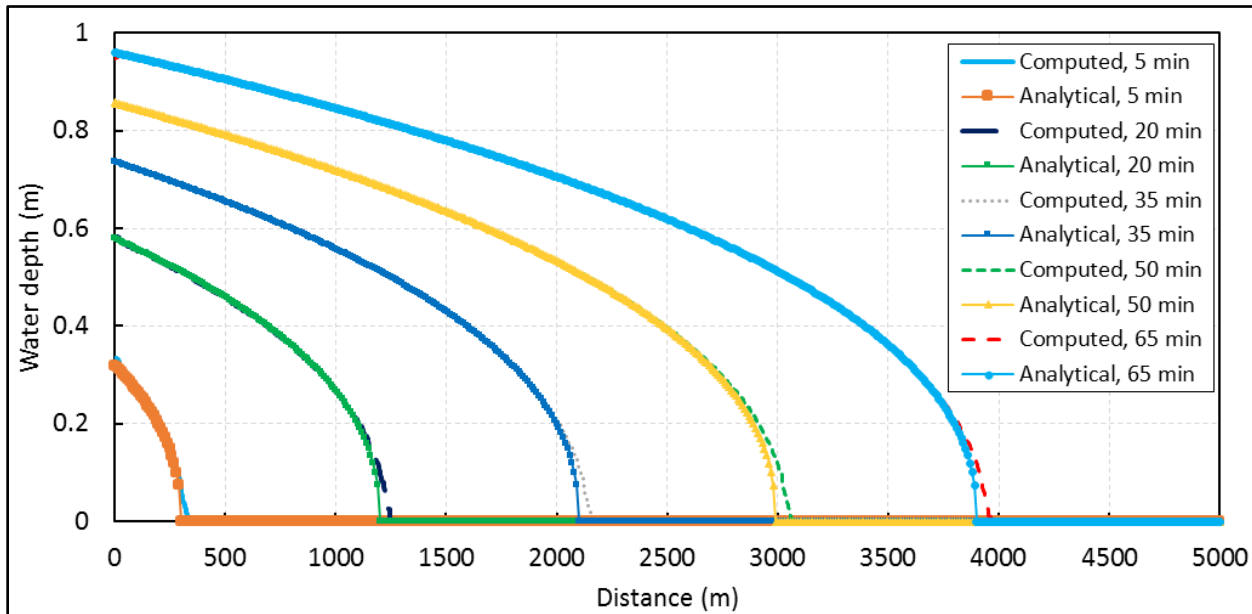


Figure 4-8. Comparison of Analytical and Computed Water Depth Profiles at Different Times using the HEC-RAS Shallow Water Equation (SWE) Solver

Both solvers produced leading edges which advanced slightly faster than the analytical solution's. The face of the wetting front is very steep and is difficult for models to resolve (Hunter, 2005; Leandro, 2014). However, the model results are comparable to those obtained by Hunter (2005) and Leandro (2014). The error in water volume conservation computed for both simulations is less than 1×10^{-6} percent.

A comparison of the analytical and computed current velocity profiles for the DWE and SWE solvers is shown in Figure 4-9 and Figure 4-10, respectively. The slight overshoot of the leading edge of the flood wave is also evident in the current velocity profiles for both solvers similar to the water depth profiles. Both the DWE and the SWE undershoots the peak velocity at the front of the wave in the same region. This is due to the fact that both the DWE and SWE solvers have some slight numerical diffusion of the peak velocity at the wave front. Tests with smaller time steps down to one second did not significantly change the solutions.

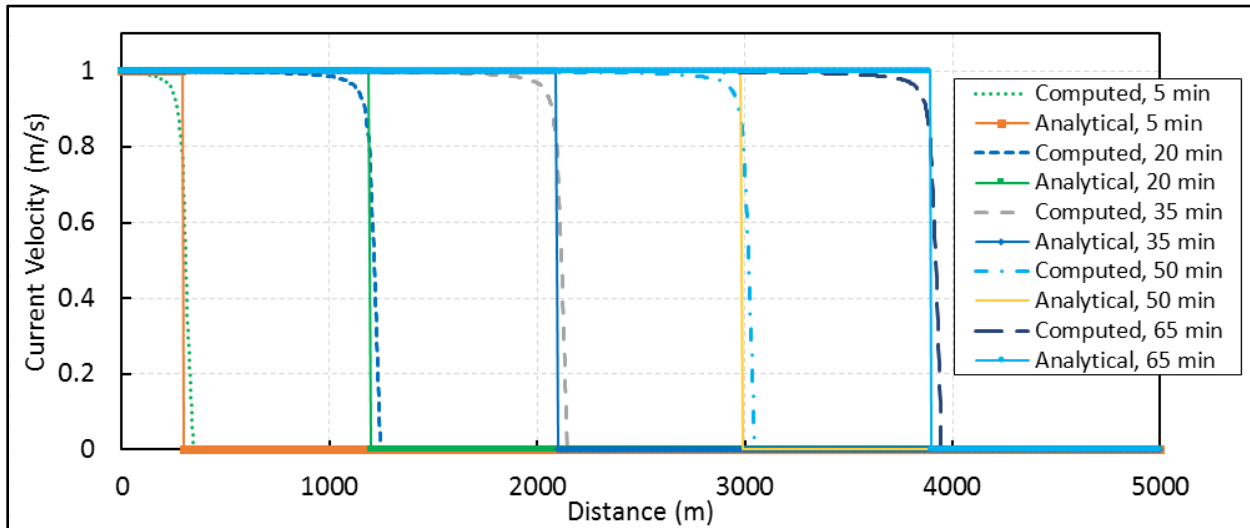


Figure 4-9. Comparison of Analytical and Computed Current Velocity Profiles at Different Times using the HEC-RAS Diffusion Wave Equation (DWE) Solver

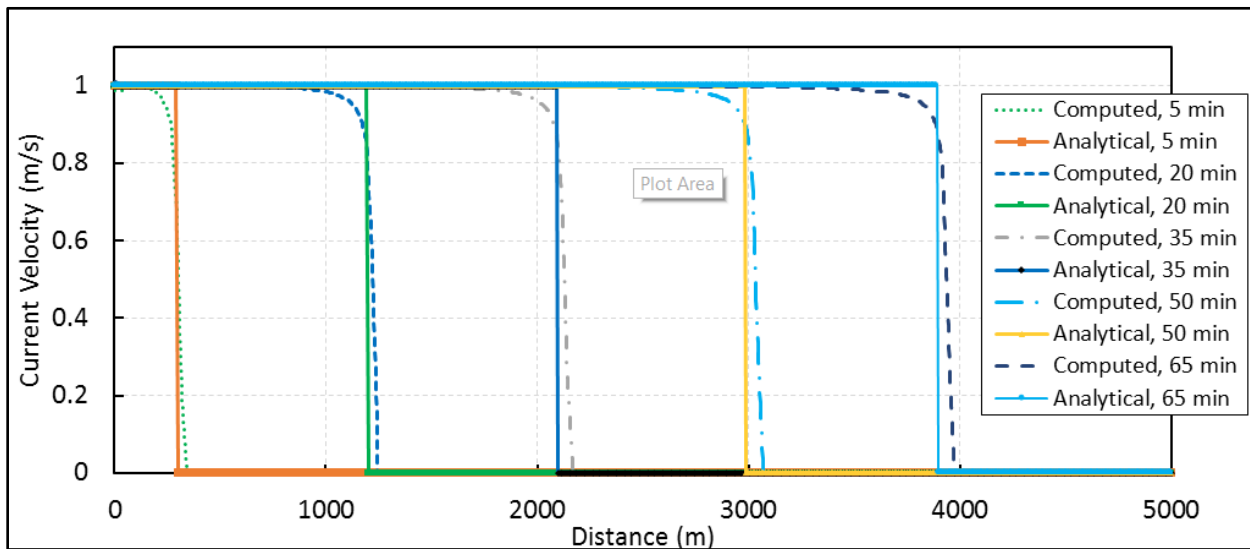


Figure 4-10. Comparison of Analytical and Computed Current Velocity Profiles at Different Times using the HEC-RAS Shallow Wave Equation (SWE) Solver

A comparison of computed water depths time series with the DWE and SWE solvers with the analytical solution are shown in Figure 4-11 and Figure 4-12, respectively. The shape of the water depth time series is the same as the profiles shown in Figure 4-7 and Figure 4-8. Figure 4-11 and Figure 4-12 demonstrate the same behavior of the computed results in which the

leading edge of the flood wave arrives slightly early. However, once the leading edge is passed, say above a depth of 0.2 m, the model results agree very well with the analytical solution.

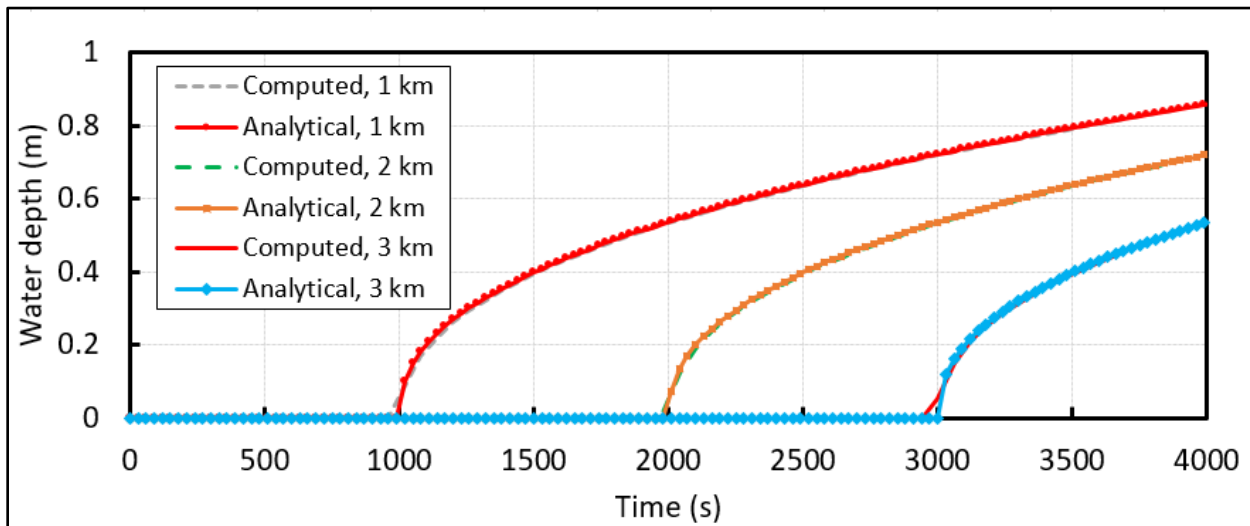


Figure 4-11. Comparison of Analytical and Computed Water Depth Time-Series at Three Stations using the HEC-RAS Diffusion Wave Equation (DWE) Solver

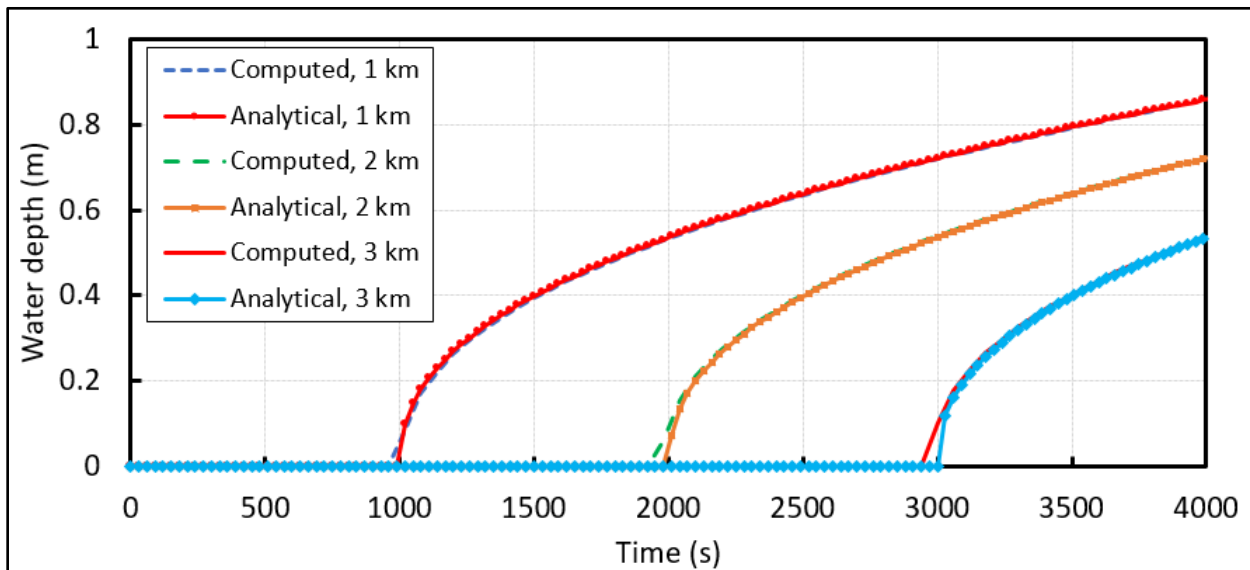


Figure 4-12. Comparison of Analytical and Computed Water Depth Time-series at Three Stations using the HEC-RAS Shallow Water Equation (SWE) Solver

References

1. Leandro, 2014. Leandro, J., Chen, A.S., and Schumann, A. *A 2D parallel diffusive wave model for floodplain inundation with variable time step (P-DWave)*. Journal of Hydrology, Volume 517, pages 250-259. September 2014.
2. Hunter, 2005. Hunter, Neil, .M., Horritt, M.S., Bates, P.D., Wilson, M.D., and, Werner, M.G.F. *An adaptive time step solution for raster-based storage cell modelling of floodplain inundation*. Advances in Water Resource, Volume 28, Issue 9, pages 975–991. September 2005.

4.2.5 Dam Break over a Flat Frictionless Bed

Overview

This test case consists of idealized dam break problems over a flat and frictionless bed. The test case is useful to verify the model implementation of the SWE. The test case has analytical solutions for when the water is initially at rest and with wet and dry conditions adjacent to the dam. The test case may be utilized to analyze the model performance in simulating dam break problems.

Problem and Data Description

Assuming a flat bed and no Coriolis, rain, horizontal mixing, and bottom friction, the 1D St. Venant equations are given by:

$$\frac{\partial h}{\partial t} + \frac{\partial q}{\partial x} = 0 \quad (4-10)$$

$$\frac{\partial q}{\partial t} + \frac{\partial}{\partial x} \left(\frac{q^2}{h} \right) + \frac{g}{2} \frac{\partial h^2}{\partial x} = 0 \quad (4-11)$$

where:

h = water depth [L]

t = time [T]

x = horizontal distance [L]

q = unit discharge [L^2/T]

g = gravitational acceleration [L/T^2]

Stoker (1957) presented an analytical solution to the dam break problem for an initially wet bed. The solution is presented here for the case where the initial condition is given by:

$$h(x, t=0) = \begin{cases} h_L & \text{for } x < x_0 \\ h_R & \text{for } x_0 \geq x \end{cases} \quad (4-12)$$

$$U(x, t=0) = \frac{q}{h} = 0 \quad (4-13)$$

Assuming a flat and frictionless bed, the analytical solution is given by (Stoker, 1957):

$$h = \begin{cases} h_L & \text{for } x \leq x_l \\ h_r & \text{for } x_l < x < x_r \\ h_* & \text{for } x_r \leq x < x_* \\ h_R & \text{for } x \geq x_* \end{cases} \quad (4-14)$$

$$U = \begin{cases} 0 & \text{for } x \leq x_l \\ U_r & \text{for } x_l < x < x_r \\ U_* & \text{for } x_r \leq x < x_* \\ 0 & \text{for } x \geq x_* \end{cases} \quad (4-15)$$

where:

$$h_r = \frac{1}{g} \left(\frac{2}{3} \sqrt{gh_L} - \frac{x-x_0}{3t} \right)^2$$

$$U_r = \frac{2}{3} \left(\sqrt{gh_L} - \frac{x-x_0}{t} \right)$$

h_* = positive wave water depth [L]

U_* = positive wave current velocity [L]

$$x_r = x_0 + t(2\sqrt{gh_L} - 3\sqrt{gh_*})$$

$$x_l = x_0 - t\sqrt{gh_L}$$

$$x_* = x_0 + t\sqrt{gh_R} \sqrt{\frac{h_*}{2h_R} \left(1 + \frac{h_*}{h_R} \right)}$$

The water depth and current velocity for the starred region are computed with an iterative Riemann solver which minimizes the following equation:

$$f(h_*) = f_L(h_*, h_L) + f_R(h_*, h_R) \quad (4-16)$$

where:

$$f_X(h_*, h_X) = \begin{cases} 2(\sqrt{gh_*} - \sqrt{gh_X}) & \text{for } h_* \leq h_X \text{ (rarefaction)} \\ (h_* - h_X) \sqrt{\frac{1}{2} g \left(\frac{h_* + h_X}{h_* h_X} \right)} & \text{for } h_* > h_X \text{ (shock)} \end{cases} \quad \text{with } X=L,R$$

Once h_* is solved, U_* may be calculated as:

$$U_* = \frac{1}{2} [f_R(h_*, h_R) - f_L(h_*, h_L)] \quad (4-17)$$

Model Setup

A summary of the model setup parameters is provided in Table 4-8. The HEC-RAS SWE solver was run for the idealized dam break problem with a simple Cartesian grid consisting of $1,200 \times 2$ cells with a constant resolution of one meter. The analytical solutions are based on zero bottom friction. However, HEC-RAS requires a small Manning's n value, so a Manning's roughness coefficient of $1 \times 10^{-6} \text{ s/m}^{1/3}$ was specified for the model. Two cases were simulated. Both cases had an initial water level of ten meters to the left of the dam, and a water level of zero and five meters to the right of the dam. The initial current velocity was set to zero everywhere in the domain. A small time step of 0.1 seconds specified with an implicit weighting factor of 0.6. Horizontal mixing was disabled by setting the mixing coefficient to zero. The simulation duration was sixty seconds.

Table 4-8. Model Setup Parameters for the Dam Break Test Cases

Parameter	Value
Manning's roughness coefficient ($s/m^{1/3}$)	1×10^{-6}
Grid resolution (meter)	1
Initial left water depth (meter)	10
Initial right water depth (meter)	0, 5
Initial current velocity (meter per second)	0
Governing equations	SWE
Time step (second)	0.05
Implicit weighting factor	0.6
Water Surface Tolerance (meter)	1×10^{-5}
Volume Tolerance (meter)	1×10^{-5}
Mixing coefficient	0.0
Simulation duration (second)	60

Results and Discussion

A comparison of the calculated and analytical water depths are presented in Figure 4-13. In general the computed results agree well with the analytical solution as demonstrated by the goodness-of-fit statistics shown in Table 4-9. The model is able to accurately simulate the propagation of the negative wave (propagation of the change in water surface in the upstream direction). The simulated results do not show any numerical instabilities and the amount numerical diffusion is reasonable. The major discrepancy between simulated and analytical water depths is the propagation velocity of the shock wave which is under-estimated slightly. This results in increasing differences between computed and simulated water depths with time (Table 4-9). The behavior of the computed water depths for the shock wave are consistent with the solution of SWE (Matins, 2016) and are interesting to note. This indicates that the numerical errors are associated with the discretization of the advection term near the leading edge of the shock wave.

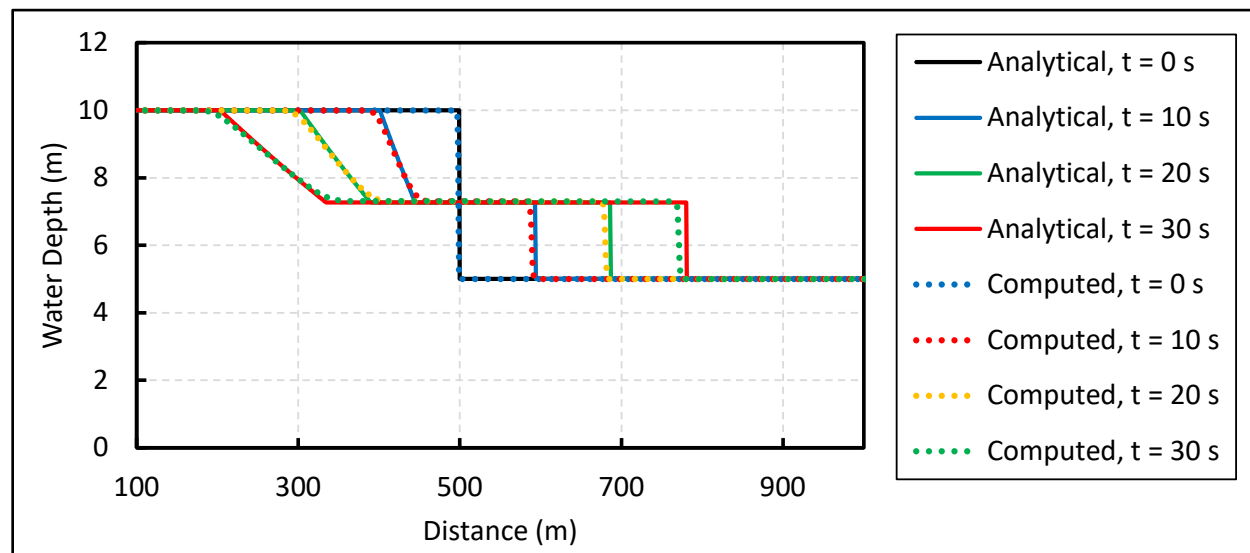


Figure 4-13. Computed and Analytical Water Depths for the Idealized Dam Break Test Case

Table 4-9. Water Depth Goodness-of-Fit Statistics for the Idealized Dam Break Case

Time (seconds)	10	20	30
ME (1×10^{-3} meter)	-6.01	-4.68	-2.97
NME (percent)	-0.06	-0.05	-0.03
MAE (1×10^{-2} meter)	2.00	3.13	4.18
NMAE (percent)	0.20	0.31	0.42
RMSE (meter)	0.128	0.163	0.190
NRMSE (percent)	1.28	1.63	1.90
R ²	0.99683	0.99372	0.98909

A comparison of the computed and analytical current velocities are presented in Figure 4-14. The corresponding goodness-of-fit statistics are shown in Table 4-10. The computed current velocities of the negative (rarefaction) wave compare well with the analytical solution. The current velocities of the positive (shock) wave are slightly under-estimated, which leads to a slight solution divergence with time. As in the case of the computed water depths, the computed current velocities in the shock wave show a similar behavior to the GSE solution (Matins, 2016) again indicating that the errors in the shock wave are possibly related to the discretization of the advection term.

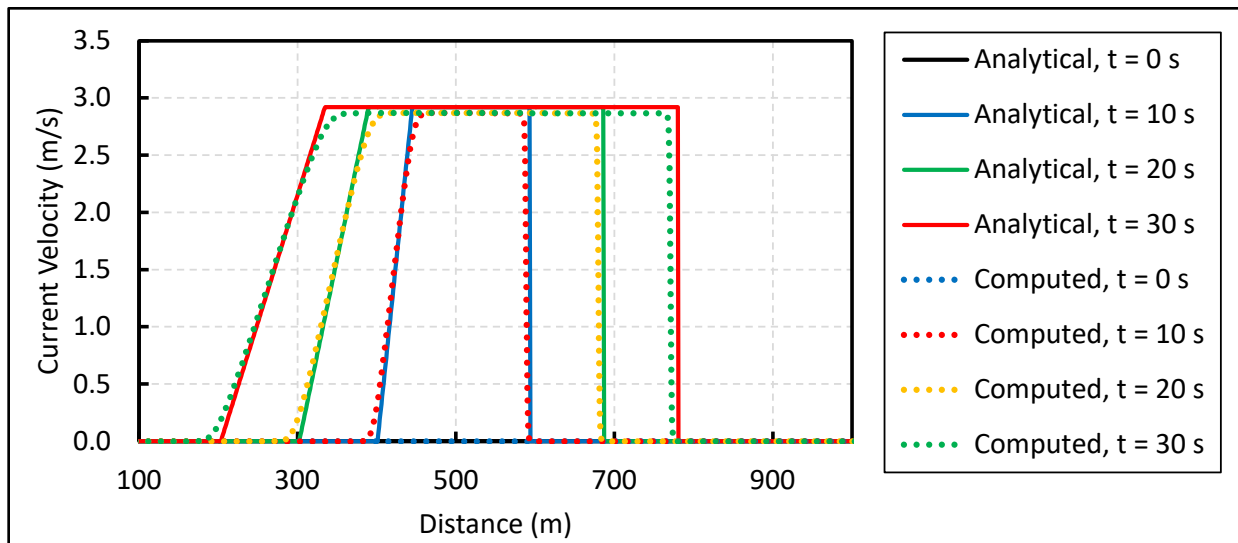


Figure 4-14. Computed and Analytical Current Velocities for the Idealized Dam Break Test Case

References

1. Stoker, 1957. Stoker, Janus J. *Water waves: The mathematical theory with applications*. Institute of Mathematical Sciences, New York University.
2. Matins, et. al., 2016.

Table 4-10. Current Velocity Goodness-of-Fit Statistics for the Idealized Dam Break Case

Time	10 seconds	20 seconds	30 seconds
ME (1×10^{-2} m/s)	-1.11E	-2.08	117.0
NME (percent)	-0.38	-0.71	39.9
MAE (1×10^{-2} meter)	2.24	3.29	122.0
NMAE (percent)	0.77	1.13	41.56
RMSE (meters per second)	0.165	0.209	1.835
NRMSE (percent)	5.64	7.15	62.74
R ²	0.97254	0.97328	0.96964

4.2.6 Sloshing in a Rectangular Basin

Overview

The sloshing test case is useful to verify the temporal scheme implementation and for analyzing the numerical dissipation as a function of time step and numerical scheme.

Problem and Data Description

Assuming no Coriolis, bottom friction, advection, diffusion, and that the water elevation is much smaller than the water depth, the governing equations are given by:

$$\frac{\partial \eta}{\partial t} + h \frac{\partial U}{\partial x} = 0 \quad (4-18)$$

$$\frac{\partial U}{\partial t} = -g \frac{\partial \eta}{\partial x} \quad (4-19)$$

where:

t = time [T]

x = horizontal coordinate [L]

U = current velocity [L/T]

h = water depth [L]

g = gravity [L/T²]

η = water level with respect to the Still Water Level (SWL) [L]

Eliminating the velocity from both equations leads to the classical wave equation:

$$\frac{\partial^2 \eta}{\partial t^2} = g h \frac{\partial^2 \eta}{\partial x^2} \quad (4-20)$$

Given a closed rectangular basin of length L and width W , the following solution can be found for simple harmonic motion (Lamb 1945):

$$\eta(x,t) = A \cos(kx) \exp(iwt) \quad (4-21)$$

where $k = m\pi/L$ is the eigenvalue, with $m = 1, 2, \dots$; and $w = 2\pi/T$ is the wave frequency, with T being the eigen (wave) period given by:

$$T = \frac{2}{\sqrt{gh(m/L)^2}} \quad (4-22)$$

When $m = 1$, the solution is referred to as the fundamental mode. The fundamental mode is the mode analyzed here.

Model Setup

The model domain is 10,000-meters long and 300-meters wide, with a zero slope. The computational grid is shown in Figure 4-15. The grid has a constant resolution of 100 meters.



Figure 4-15. Computational Grid for the Sloshing Test Case

The water surface elevation was initialized with the analytical solution given by Equation 4-18. The model setup is summarized in the Table 4-11.

Table 4-11. Summary of the Model Setup for the Sloshing Test Case

Model Parameter	Value
Water depth (meter)	10
Wave amplitude (cm)	1
Wave length (km)	10
Gravity (m/s^2)	9.780327
Time step (seconds)	0.5, 5
Simulation duration (hours)	10
Grid resolution (meter)	100
Implicit Weighting Factor	0.6, 1.0
Manning's roughness coefficient ($\text{s/m}^{1/3}$)	1×10^{-5}

There is a small inconsistency between the test case's governing equations and the model's governing equations, that should be noted. The numerical model solves the complete shallow water equations including the advection and bottom friction terms. However, since the current velocities are relatively small, the effect of the advection term may be ignored. Although the Manning's roughness coefficient cannot be set to zero in HEC-RAS, it is set to $1 \times 10^{-5} \text{ s/m}^{1/3}$ which is sufficiently small enough that the bottom friction is insignificant. A time step of 5 seconds corresponds to a Courant number of approximately 0.5 based on the long-wave celerity $c = \sqrt{gh}$. The implicit weighting factor is set to the minimum value allowed in HEC-RAS which is 0.6.

Results and Discussion

Figure 4-16 shows a comparison of the analytical and computed water levels after approximately 1, 5, 9, 13, and 17 cycles and at different phases of the standing wave. In general, the computed water levels agree extremely well with the analytical solution as demonstrated by the goodness-

of-fit statistics shown in Table 4-12. The differences between computed analytical water levels increase with time due to numerical dissipation within HEC-RAS. There is a small asymmetry in the water level which gets more pronounced with time. The location of the wave node at the center of the basin and the antinodes at the ends of the basin are maintained throughout the simulation.

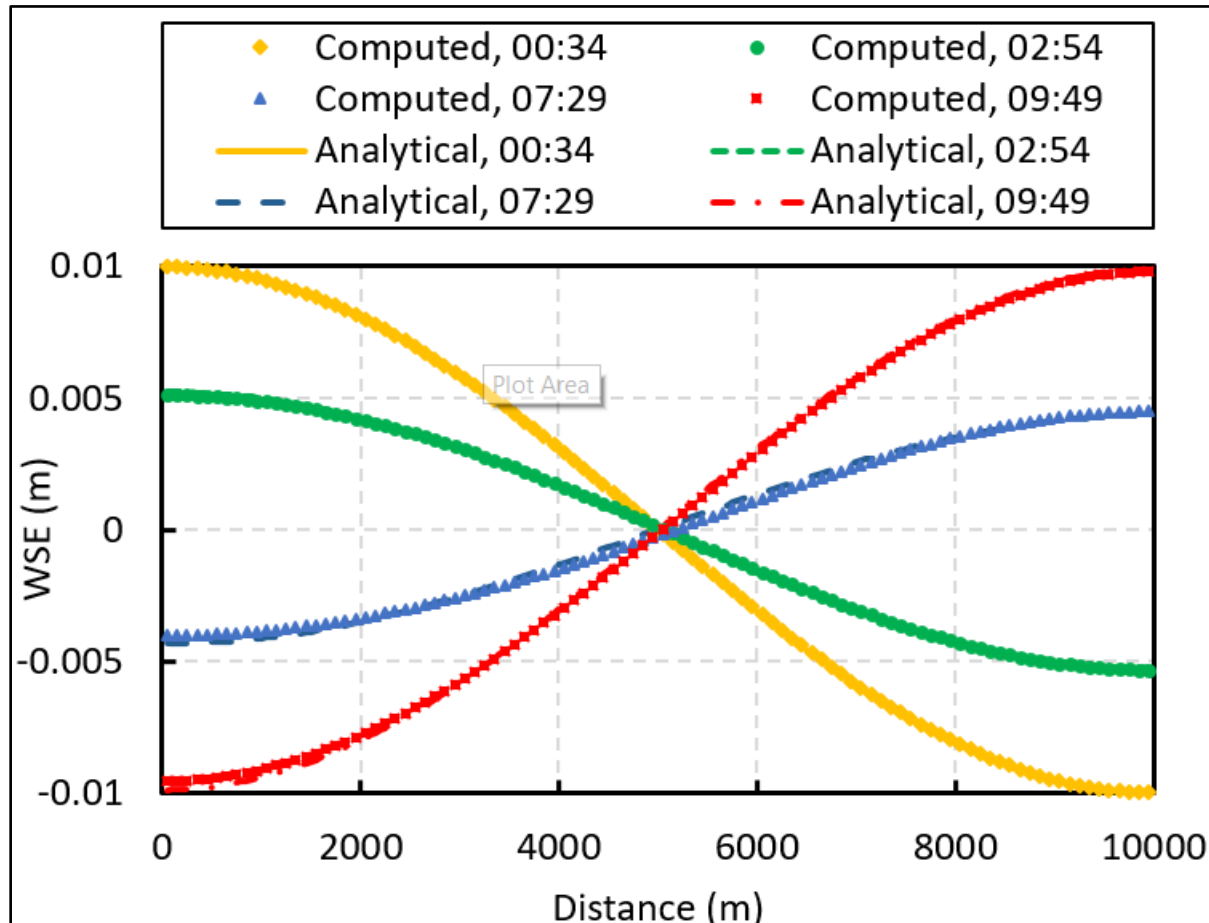


Figure 4-16. Water Surface Elevation (WSEL) Profiles at Different Times for the Sloshing Test Case. Calculated with the first and second order temporal schemes. Time step equals 0.5 seconds; Implicit weighting factor equals 0.6.

Table 4-12. WSEL Profile Goodness-of-Fit Statistics for Sloshing Test Case

Time (hours)	00:34	02:54	7:29	09:49
RMSE (10^{-4} meter)	0.076	0.76	1.77	1.62
NRMSE (percent)	0.076	0.76	1.77	1.62
MAE (10^{-4} meter)	0.066	0.68	1.56	1.39
NMAE (percent)	0.066	0.68	1.56	1.39
R ²	0.999	0.999	0.997	0.999

A time-series of the water level at the first computational cell (i.e., $x = \Delta x/2 = 50$ meters) is presented in Figure 4-17 as a function of two different time steps (0.5 and 5.0 seconds). The goodness-of-fit statistics for the WSEL time series are shown in Table 4-13.

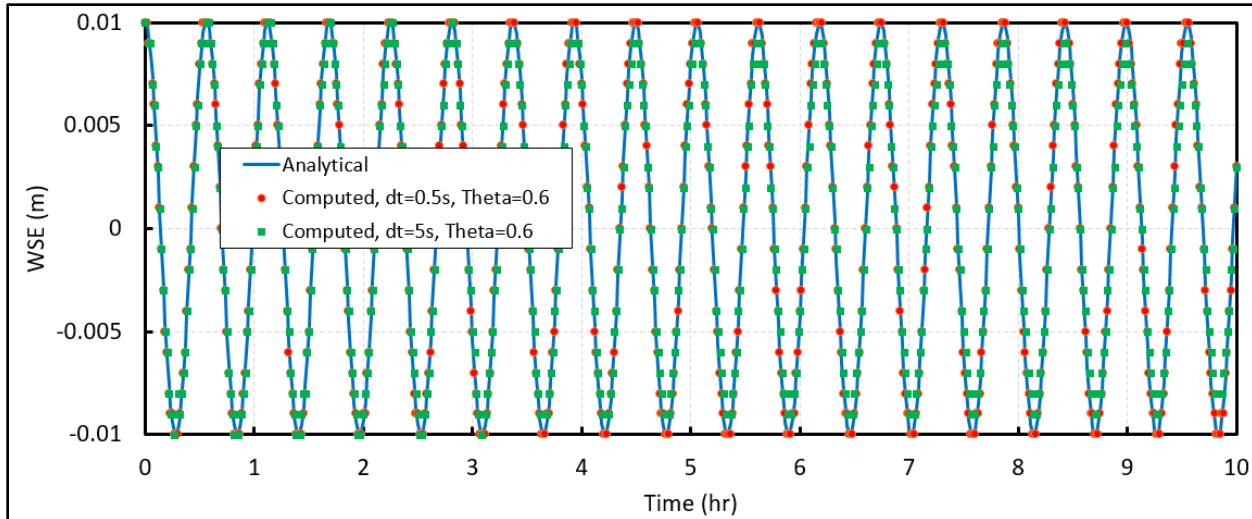


Figure 4-17. Water Surface Elevation (WSEL) Time Series Calculated at $x = \Delta x/2$ for Time Steps of 0.5 and 5 seconds and an Implicit Weighting Factor (Theta) set to 0.6

Table 4-13. WSEL Time-Series Goodness-of-Fit Statistics for Sloshing Test Case

	Case 1	Case 2	Case 3	Case 4
Time step (second)	0.5	5	0.5	5
Theta	0.6	0.6	1.0	1.0
RMSE (1×10^{-4} meter)	1.62	14.00	2.70	21.03
NRMSE (percent)	1.62	14.00	2.70	21.03
MAE (1×10^{-4} meter)	1.18	17.62	3.74	26.16
NMAE (percent)	1.18	17.62	3.74	26.16
R ²	0.9998	0.9778	0.9989	0.9415

As shown in Figure 4-17, the smaller time step produces less numerical dissipation. There is no significant phase difference developed in the computed model results. Figure 4-18 shows a comparison of the computed and analytical water levels at the first computational cell from the left using an implicit weighting factor of 0.6 and one. As expected, the larger value produces more numerical dissipation. However, the differences are relatively minor compared to dissipation produced by using a much larger time step of five seconds as shown in Figure 4-17. The reason for the small differences is because of the relatively small time step used. This illustrates the fact that when small time steps are used, the relative improvement of the solution by using a smaller implicit weighting factor is reduced. In order to illustrate the effect of the implicit weighting factor at a larger time step, a five-second time step was used with implicit weighting factors of 0.6 and 1.0 (Figure 4-19). As shown in the time-series of WSEL, the implicit weighting factor can significantly reduce the numerical dissipation when large time steps are utilized.

References

1. Leandro, 2014. Leandro, J., Chen, A.S., and Schumann, A. *A 2D parallel diffusive wave model for floodplain inundation with variable time step (P-DWave)*. Journal of Hydrology, Volume 517, pages 250-259. September 2014.

2. Hunter, 2005. Hunter, Neil, .M., Horritt, M.S., Bates, P.D., Wilson, M.D., and, Werner, M.G.F. *An adaptive time step solution for raster-based storage cell modelling of floodplain inundation*. Advances in Water Resource, Volume 28, Issue 9, pages 975–991. September 2005.

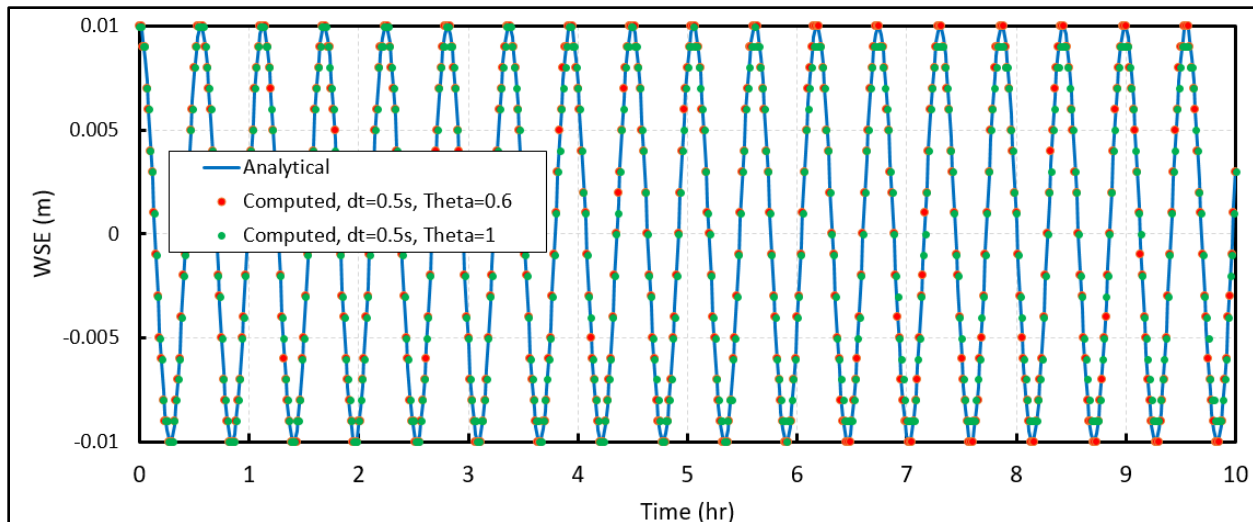


Figure 4-18. Water Surface Elevation (WSEL) Time Series Calculated at $x = \Delta x/2$ for the Implicit Weighting Factors (Theta) Set to 0.6 and 1.0 with a Time Step of 0.5 seconds

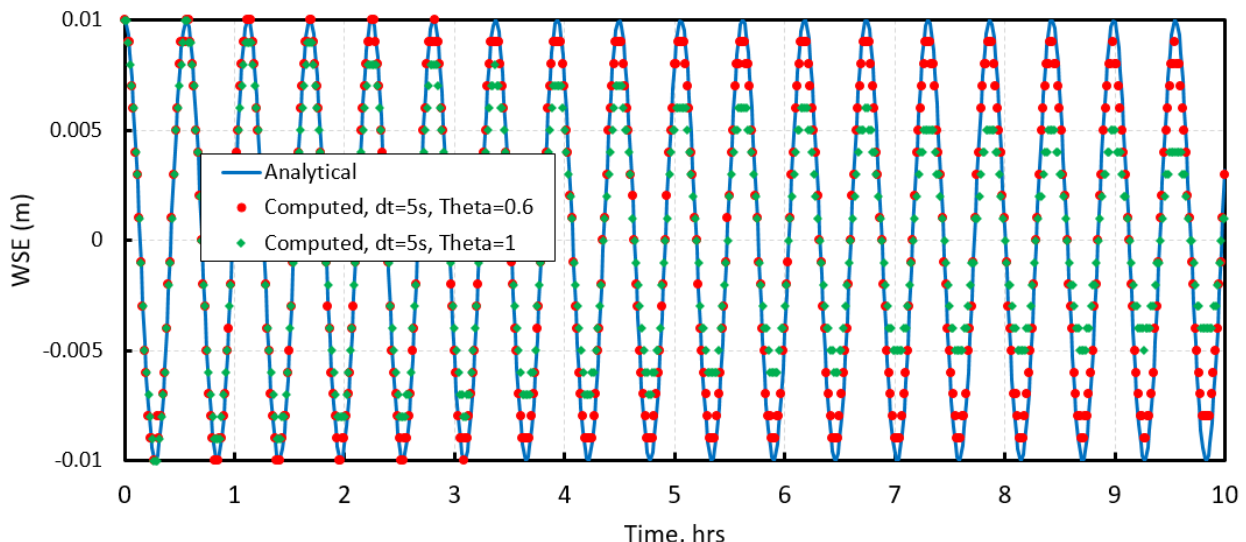


Figure 4-19. Water Surface Elevation (WSEL) Time Series Calculated at $x = \Delta x/2$ for the Implicit Weighting Factors (Theta) Set to 0.6 and 1.0 with a Time Step of 5 seconds

4.2.7 Long-wave Run-up on a Planar Slope

Overview

The performance of HEC-RAS is analyzed for calculating nonlinear long-wave run up over a frictionless planar slope by comparing the computed water levels and shoreline position to an analytical solution presented by Carrier (2003).

Problem and Data Description

The bed has a constant slope of 1/10 with the initial shoreline located at $x = 0$ meters. Figure 4-20 shows the initial water level is given by a leading depression N-wave (characteristic of the waves caused by submarine landslides). The initial current velocity is equal to zero everywhere.

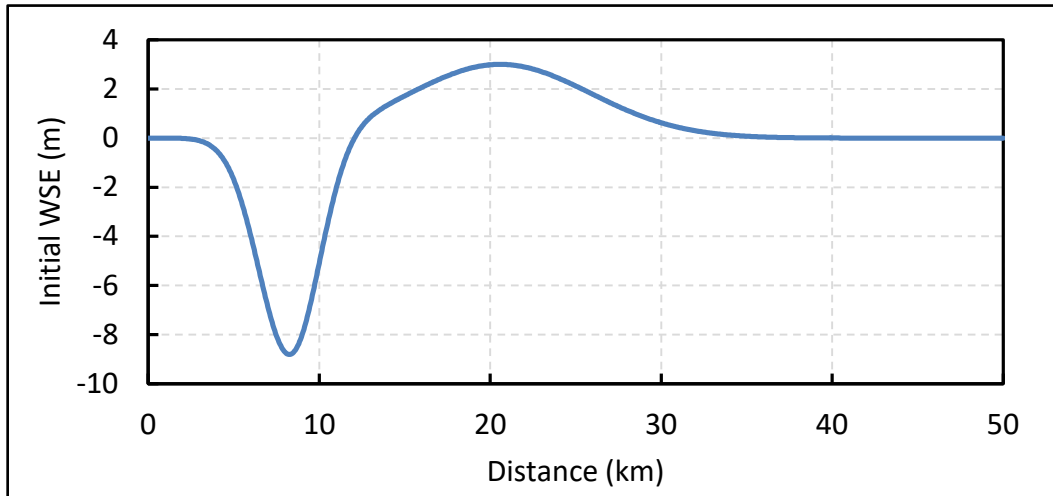


Figure 4-20. Initial Water Surface Elevation (WSEL) for the Long-Wave Run-Up Test Case

Model Setup

The computational grid has a variable grid resolution of three meters for x less than 300 meters and increases to ten meters offshore with an aspect ratio of 1.05. A close-up of the grid resolution where the grid resolution transition occurs is displayed in Figure 4-21. The general model parameters used in the simulation are detailed in Table 4-14. A relatively small time step of 0.1 seconds is required due to the moving wet/dry boundary. Bottom friction and turbulent mixing are set to zero.

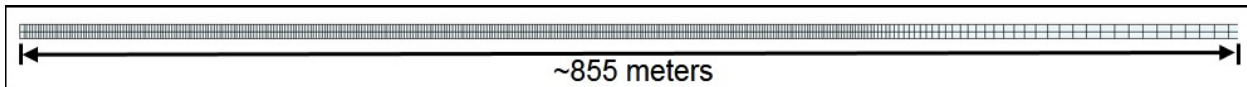


Figure 4-21. Close-Up View of Computation Grid where Grid Resolution Transition Occurs

Table 4-14. Model Setup Parameters for the Long-Wave Run-Up on a Planar Slope Test Case

Parameter	Value
Manning's roughness coefficient ($s/m^{1/3}$)	0.0000001
Grid resolution (meter)	5 (constant)
Governing equations	SWE
Time step (second)	0.1
Implicit weighting factor	1.0
Water Surface Tolerance (meter)	1×10^{-5}
Volume Tolerance(meter)	1×10^{-5}
Mixing coefficient	0.0
Simulation duration (second)	360

Results and Discussion

Figure 4-22 displays the comparison of computed and analytical WSEL near the shoreline at three different time steps. The WSEL variation is characterized by a leading negative wave followed by a rapid run-up event with a steep front. In general, the model performance is good as demonstrated by the goodness-of-fit statistics shown in Table 4-15. However, the model has difficulty capturing the wave run-up with the steep front. A small instability is produced near the leading edge of the wave and decreases the model accuracy from there out.

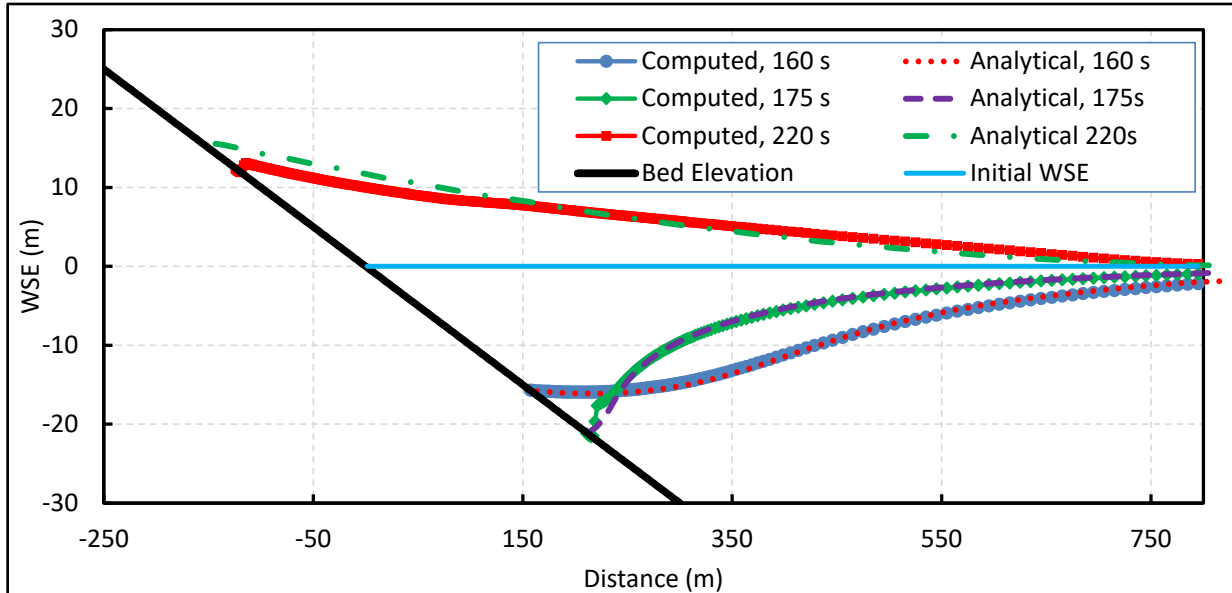


Figure 4-22. Comparison of Analytical and Computed WSEL at Different Time Steps for the Long-Wave Run-Up Test Case

Table 4-15. Goodness-of-Fit Statistics for the Long-Wave Run-Up Test Case

	WSEL Profile (for $x < 800$ meter)			Shoreline Position
	160 (second)	175 (second)	220 (second)	
RMSE (meter)	0.236	0.384	1.016	24.195
NRMSE (percent)	1.68	1.88	6.53	5.96
MAE (meter)	0.211	0.199	0.879	11.160
NMAE (percent)	1.50	0.98	5.65	2.75
R ²	0.9996	0.9956	0.9884	0.9714
ME (meter)	0.042	-0.027	-0.049	2.398
NME (percent)	0.30	-0.13	-0.31	0.59

A comparison of the computed and analytical solution for the shoreline position is displayed in Figure 4-23. The water shoreline position of the leading depression wave is well captured including the peak shoreline position. However the shoreline position during the inundation or advancement of the first wave is slightly under predicted. This is due to the small instability which is shown at the 220 second time step near the shoreline position in Figure 4-22. The small instability is formed during the uprush of water but does not grow significantly and does not cause significant error in the computed water levels. Further tests can be done in the future to investigate if the instability can be reduced by increasing model resolution or reducing the time

step. Once the first wave begins to recede, the calculated shoreline position again agrees well with the analytical solution.

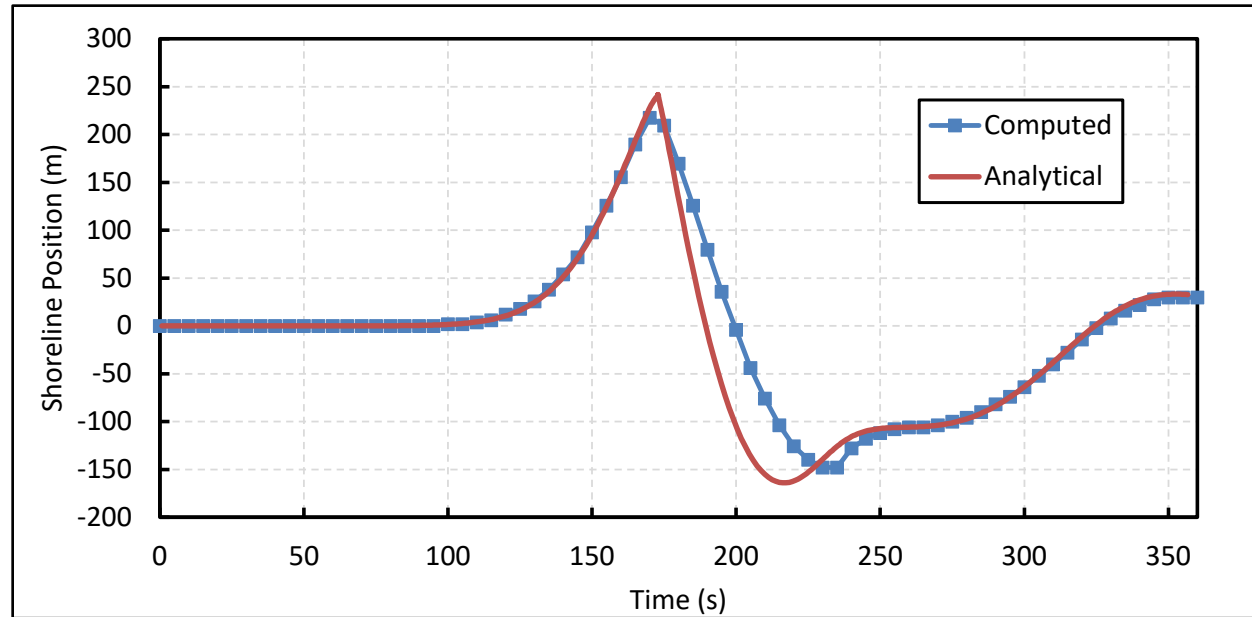


Figure 4-23. Comparison of Analytical and Computed Shoreline Position for the Long-Wave Run-Up Test Case

In practical field applications, it is noted that the bottom is not frictionless or inviscid and that these two will improve the model stability. In general, the model wetting and drying performance is considered satisfactory for the purposes of the model. The implicit solution scheme is designed for practical applications of tidal flow and wind- and wave-induced currents. This verification test provides a good case for testing the model's nonlinear hydrodynamics and wetting and drying algorithm. Due to the small time step necessary for accurately resolving wetting and drying boundaries, the implicit solution scheme is not as efficient when compared to an explicit solution scheme.

References

1. Carrier, 2003. Carrier, George, Tei Wu, T., and Yeh, H. *Tsunami run-up and draw-down on a plane beach*. Journal of Fluid Mechanics, Volume 475, Issue 01, pages 79-99. January 2003.

4.2.8 Surface Runoff on a Plane

Overview

The goal of the 1D surface runoff test case is to verify the implementation of the Diffusion Wave Equation. The test case was also simulated by Therrien (2003); Govindaraju (1988); and, Lai (2006). An approximate series solution is also available from Govindaraju (1988).

Problem and Data Description

The test case consists of a flat plane with a constant slope, constant precipitation, and zero infiltration. A schematic of the test case is provided in Figure 4-24.

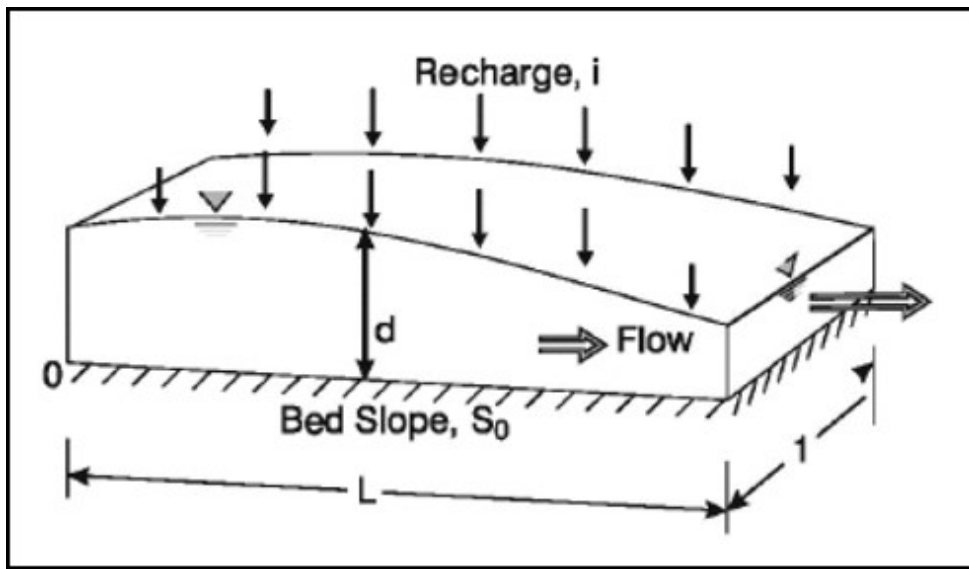


Figure 4-24. Schematic of One-Dimensional Surface Runoff Case (Therrien, 2003)

The problem can be characterized by the following by the Froude number F_0 and kinematic wave number K given by:

$$F_0 = \frac{u_0}{\sqrt{gh_0}} \quad (4-23)$$

$$K = \frac{S_0 L}{h_0 F_0^2} \quad (4-24)$$

where:

u_0 = steady-state final velocity [L/T]

g = gravitational acceleration [L/T²]

h_0 = steady-state final water depth [L/T]

L = length of plane (in downstream direction) [L]

Model Setup

Two cases are simulated with different conditions but with the same basic computational mesh and boundary conditions. A summary of the mesh parameters and boundary conditions are provided in Table 4-16. A longitudinal grid resolution of one meter was specified, except near the downstream boundary where the mesh was modified in order to enforce the downstream boundary within the correct limits. A transverse grid resolution of 0.5 meters was specified, again with the exception of the downstream boundary. The same computational time was used for all runs.

Table 4-16. General HEC-RAS Parameters and Boundary Conditions

Variable	Value
Horizontal length (meter)	100
Horizontal width (meter)	1
Longitudinal grid resolution (meter)	1
Transverse grid resolution (meter)	0.5
Time step (second)	0.1
Downstream boundary condition	Normal depth
Downstream friction slope	0.01

The case specific conditions are summarized in Table 4-17 and Table 4-18. In both cases, the bed was initially dry and the rainfall intensity was constant. The model setup is essentially the same as in Lai (2006); Govindaraju (1988); and, Therrien (2003).

Table 4-17. Summary of Test Case 1 Conditions and Parameters

Variable	Value
Froude number, F_0	0.5
Kinematic wave number K	10
Rainfall intensity (mm/s)	4
Manning's roughness coefficient (s/m ^{1/3})	0.0548

Table 4-18. Summary of Test Case 2 Conditions and Parameters

Variable	Value
Froude number, F_0	1.5
Kinematic wave number, K	3
Rainfall intensity (mm/s)	2.7
Manning's roughness coefficient (s/m ^{1/3})	0.0155

Results and Discussion

The model results for Test Cases 1 and 2 are presented and compared to previous studies in Figure 4-25 and Figure 4-26, respectively. The figures show the downstream discharge normalized by the steady-state discharge. The time is normalized by the steady-state downstream current velocity divided by the length of the domain (Govindaraju, 1988). The HEC-RAS Diffusion Wave Model results are compared to the Diffusion Wave models of Lai (2006) and Therrien (2003). Also, included for comparison in the Figure 4-25 and Figure 4-26 are the kinematic wave solutions of Govindaraju (1988) and the St. Venant equations solutions of Vieira (1983). In general, the computed results agree well with the Diffusion Wave model results of Lai (2006) and Therrien (2003).

References

1. Lai, 2006. Lai, Yong G. *Theory and User Manual for SRH-W Version 1.1: Sedimentation and River Hydraulic – Watershed model*. U.S. Department of the Interior, Bureau of Reclamation, Denver, CO, USA. November 2006.
<https://www.usbr.gov/tsc/techreferences/computer%20software/models/srh2d/downloads/SRH-W%20v1.1%20User%20Manual%20June2007.pdf>

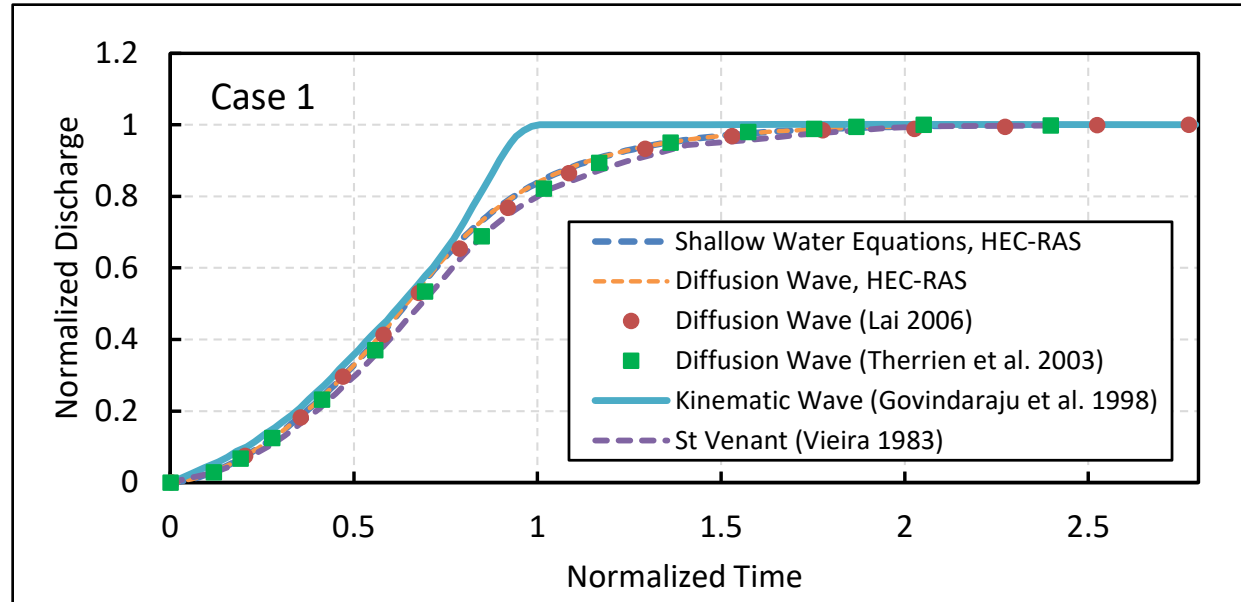


Figure 4-25. Normalized Hydrograph for Test Case 1 with $F_0 = 0.5$ and $K = 10$

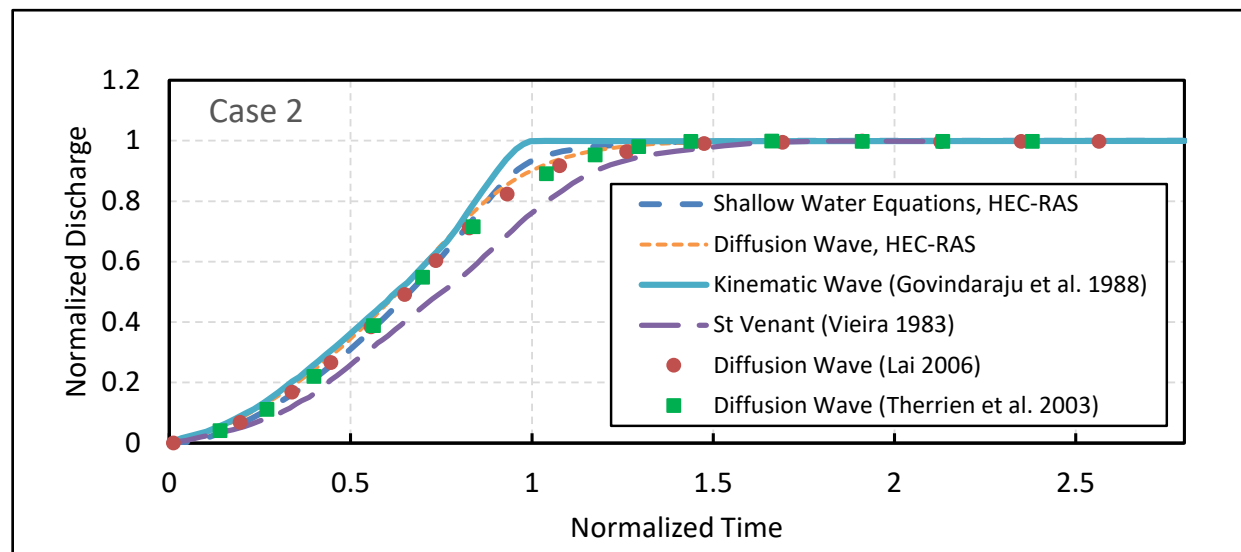


Figure 4-26. Normalized hydrograph for Case 2 with $F_0 = 1.5$ and $K = 3$

2. Govindaraju, 1988. Govindaraju, Rao S., Jones, S.E., and Kavvas, M.L. *On the diffusion wave model for overland flow 1: Solution for steep slopes*. Water Resources Research, AGU Journal, Volume 24, Issue 5, pages 734-744. May 1988.
3. Therrien, 2003. Therrien, R., Panday, S.M., McLaren, R.G., Sudicky, E.A., Demarco, D.T., Matanga, G.B., and Huyakorn, P.S. 2003 *HydroSphere: a three dimensional numerical model describing fully-integrated subsurface and surface flow and solute transport*. User's Manual of HydroSphere, a Draft. 2003.
4. Vieira, 1983. Vieira, J.H.Daluz. *Conditions governing the use of approximations for the Saint Venant equations for shallow surface water flow*. Journal of Hydrology, Volume 60, Issues 1-4, pages 43-58. January 1983.

4.2.9 Rectangular Basin with Coriolis

Overview

The goal of this test case is to verify the implementation of the Coriolis term in the SWE. This test case is also useful for testing the implementation of the flow hydrograph and stage boundary conditions.

Problem and Data Description

Assuming no spatial or temporal accelerations, turbulence, wind, atmospheric pressure gradients, precipitation, or infiltration, the governing equations may be simplified to (Gill, 1982)

$$f\hat{k} \times \dot{\vec{U}} = -g\nabla\eta - \vec{\tau}_b \quad (4-25)$$

where:

$f = 2\Omega\sin\varphi$ equals Coriolis parameter or frequency [1/T]

Ω = earth's rotation rate [rad/T]

φ = latitude [rad]

\hat{k} = unit vector in the vertical direction

$\dot{\vec{U}}$ = current velocity vector [L/T]

x, y = x- and y-coordinates [L]

g = gravitational acceleration [L/T²]

η = water surface elevation [L]

By using an idealized geometry consisting of a flat rectangular basin oriented in either the x- or y-direction, when applying constant boundary conditions, the steady solution to the shallow water equations may be used to verify the geostrophic balance in the direction perpendicular to the flow (i.e., transverse direction). Since the current velocity in the transverse direction is zero, the bottom friction term in that direction becomes zero and the shallow water equation reduces to a geostrophic balance. By setting the basin depth to a large value, the differences in the water surface on the depth and the current velocity are negligible resulting in a nearly constant current velocity field. The exception to the constant velocity field is expected to be region near the downstream water level boundary condition. Unfortunately, a variable water level boundary condition is not available in HEC-RAS nor does it apply corrections to the water level for Coriolis effects, so the downstream current velocity and water level solution is not expected to be accurate.

Model Setup

Four cases were simulated with two different geometries and latitudes but otherwise the same boundary conditions and setup parameters. Both geometries consist of long rectangular basins with constant bed elevations. However, one is oriented in the x-direction, while the other is oriented in the y-direction. Both grids has a constant 200-meter resolution. The mesh has a total of 12,500 cells. A constant Manning's n roughness coefficient of 0.01 s/m^{1/3}. As mentioned previously, because the current velocity is zero in the transverse direction the bottom friction

does not affect the geostrophic balance in this direction. A constant time step of two minutes was used for two cases. A simulation duration of four days was found to be sufficient for the solution to reach steady-state. Because this is a steady-state problem, time is only used as a means to reach a steady-state and the time step and implicit weighting factor do not affect the results once the model has reaches a steady-state condition. The Manning's equation was used to obtain a friction slope of 2.15×10^{-7} , which was applied at the upstream flow hydrograph boundary condition. A constant initial water level of 100 meters was specified. The flow hydrograph was slowly increased with a cosine ramp function over two days to reduce the creation of oscillations in the computational domain (Figure 4-27). Due to the small magnitude of the elevation differences, it is important to lower significantly the water surface elevation and volume tolerances for HEC-RAS. In this study these were both set to 1×10^{-5} meters. A summary of the mesh parameters and boundary conditions are provided in Table 4-19.

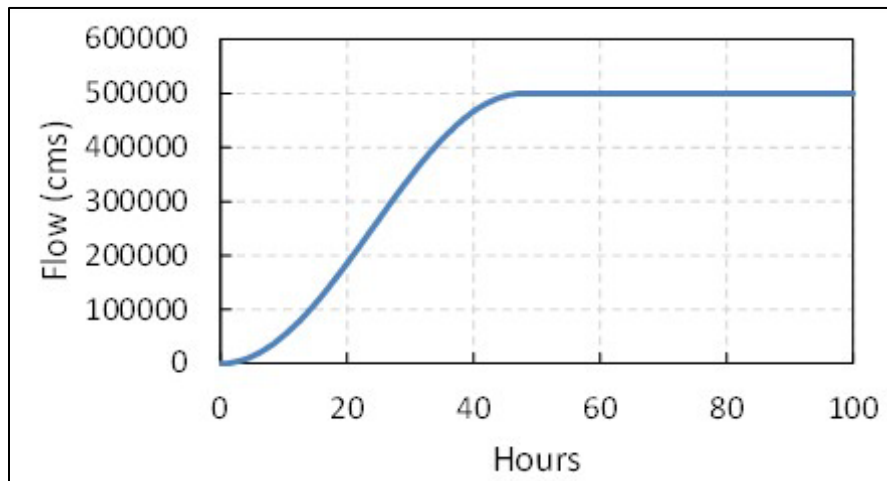


Figure 4-27.Flow Hydrograph for the Coriolis Test Case

Table 4-19. General HEC-RAS Parameters and Boundary Conditions for the Coriolis Test Cases

Variable	Value			
	Case 1	Case 2	Case 3	Case 4
Basin length in x-direction (meter)	100,000	5,000	100,000	5,000
Basin length in y-direction (meter)	5,000	100,000	5,000	100,000
Latitude (degrees)	45	45	-45	-45
Earth's rotation rate (rad/s)	7.2921159×10^{-5}			
Grid resolution (meter)	200			
Time step (minute)	2			
Implicit weighting factor	1.0			
Simulation duration (days)	4			
Water surface elevation tolerance (meter)	1×10^{-5}			
Volume tolerance (meter)	1×10^{-5}			
Steady-state upstream discharge (m^3/s)	500,000			
Downstream water level (meter)	100			
Initial water level (meter)	100			
Energy grade slope	2.15×10^{-7}			

Results and Discussion

The total computational time was approximately 2.5 minutes for each four-day simulation. In order to compare the computed results with the analytical solution, profiles of water levels were extracted in the transverse direction near the center of basin in the longitudinal direction. The gradient along each transect was then computed a linear regression. The results are summarized in the table below. The computed and analytical water level gradients agree at the transects that were extracted near the center of the basins. Table 4-20 details the HEC-RAS parameters and boundary conditions that were entered.

Table 4-20. General HEC-RAS Parameters and Boundary Conditions

Case	Latitude (degree)	WSEL Gradient	Analytical	Computed
1	45	y-direction	1.0512×10^{-5}	1.0507×10^{-5}
2	45	x-direction	1.0512×10^{-5}	1.0500×10^{-5}
3	-45	y-direction	1.0512×10^{-5}	1.0501×10^{-5}
4	-45	x-direction	1.0512×10^{-5}	1.051×10^{-5}

Example water level and current velocity fields are presented in Figure 4-28 for CoriolisTest Case 1. The results for the other three cases were essentially the same but either rotated or flipped in the transverse direction. There is a small gradient in the stream-wise direction due to bottom friction but the larger water level gradient is in the transverse direction and is due solely to the Coriolis effect. As expected, the current velocity magnitude is nearly constant except near the downstream water level boundary condition. The effects of using a constant water level boundary condition downstream are viewed in both the water level and current velocity fields about 3,000 to 5,00 m upstream from the boundary. This limitation could be easily addressed by adding an internal correction to stage time series at boundaries to account for Coriolis and even potentially wind stresses and atmospheric pressure gradients. The current velocity and water levels near and at the upstream flow boundary condition are consistent with the analytical solution. In addition, the flow and stage at each upstream boundary cell was verified to be consistent with the applied total flow and the Manning's equation.

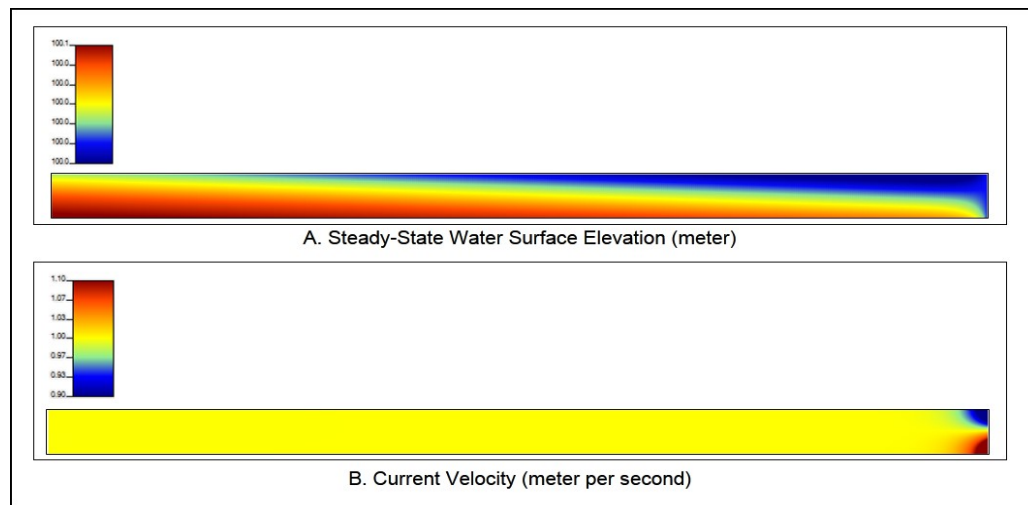


Figure 4-28. Steady-State Water Surface Elevation (A), and Current Velocity (B) Fields for Coriolis Test Case 1

References

1. Gill, (1982). Gill, Adrian E. *Atmosphere-Ocean Dynamics*. International Geophysics Series, 30, Academic Press (<http://www.academicpress.com>). 1982.
2. WBE, 1984. World Book Inc. *World Book Encyclopedia*, Volume 6. World Book Inc., Chicago Illinois.

4.3 Laboratory Datasets

4.3.1 Flow in a Compound Channel

Overview

The purpose of this test case is to validate HEC-RAS for simulating flow and velocity in a compound channel. The test case has a deep rectangular main channel and a shallow rectangular right overbank (floodplain). Model results are compared with measured velocities in the main channel, intersection with the floodplain, and the floodplain for a single steady flow rate.

Problem and Data Description

This is a flume experiment with a 1.19 meter flume with a 0.711 meter main channel and a 0.508 meter floodplain (Rajaratnam, 1981). The flume was 18.3 meters long and the bottom of the flume was smooth. One flow rate was run and velocity measurements were taken across the entire flume. Figure 4-29 displays a cross section of the flume.

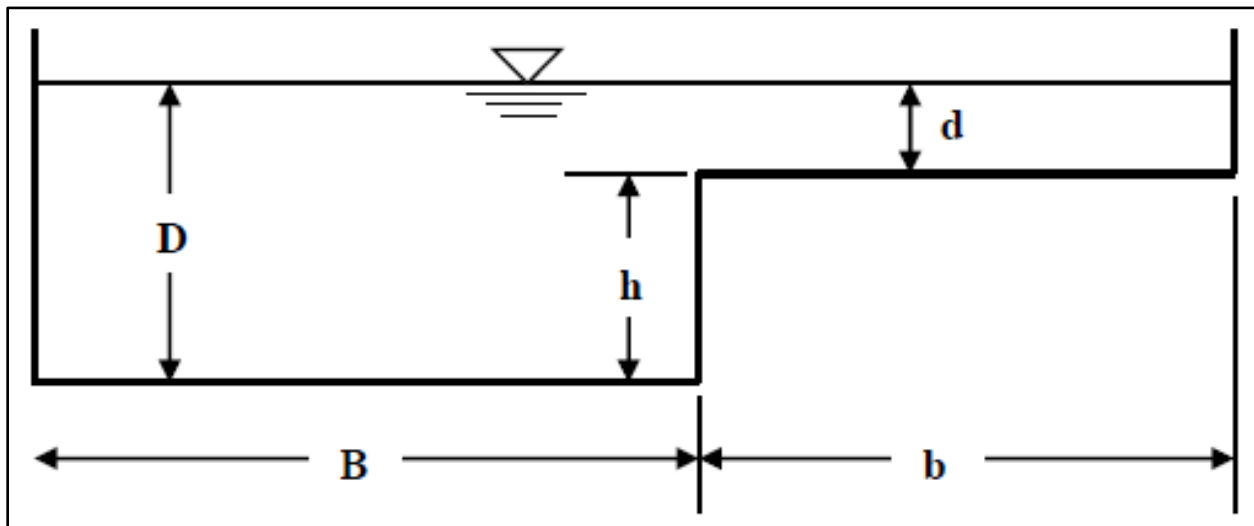


Figure 4-29. Cross Section of Flume for Compound Channel Test Case

Table 4-21 provides a listing of the data that describes this test case:

Table 4-21. Specification for Compound Channel Experiment

Item	Value
Bottom width (meter)	B= 0.711, b = 0.508
Main Channel Depth, h (meter)	0.0975
Bed slope, S	0.00045
Depth (meter)	D = .1128, d = .0152
Flow rate, Q (cms)	0.027
Down Stream Boundary Condition, WS (meter)	0.1128

Model Setup

A 2D model was developed for this dataset with a computational domain of 18.3 meters long and 1.19 meters wide. A constant grid resolution 0.05 x 0.05 meter cells and 0.025 x 0.025 meter cells was used (two separate meshes). A flow boundary condition was specified at the upstream end of the system and a stage boundary condition with a constant water level at the downstream end. A profile lines for extracting velocity was laid out in the lower half of the flume where the water surface and velocities settle down to constant values.

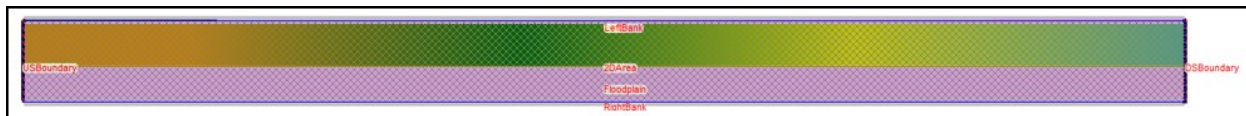


Figure 4-30. Computational Grid for the Compound Channel Experiments

Table 4-22 provides a list of the model specific values used for this test:

Table 4-22. Model Parameters for Compound Channel Experiment

Two mesh sizes (meter)	0.05 x .05 and 0.025 x 0.025
Main channel, n	0.009
Floodplain, n	0.012 (shallow depth)
Initial depth (meter)	0.1128
Time Step (second)	0.2 and 0.1
Theta	1.0
Eddie viscosity coefficient	0.50
Equation set	SWE

Results and Discussion

The results from the 2D computations analysis were compared to the measured velocities from the lab study. Figure 4-31 displays a spatial plot of the velocities associated with the higher flow rate ($Q = 0.027 \text{ m}^3/\text{s}$) and the location of where the velocity measurements were made.

The plot (Figure 4-32) displays the computed and measured velocities for the main channel and floodplain cross section. In general, the HEC-RAS computed velocities for the main channel, the intersection between main channel and floodplain, as well as the floodplain look reasonable compared to the observed data. The velocities at the intersection looked really good.

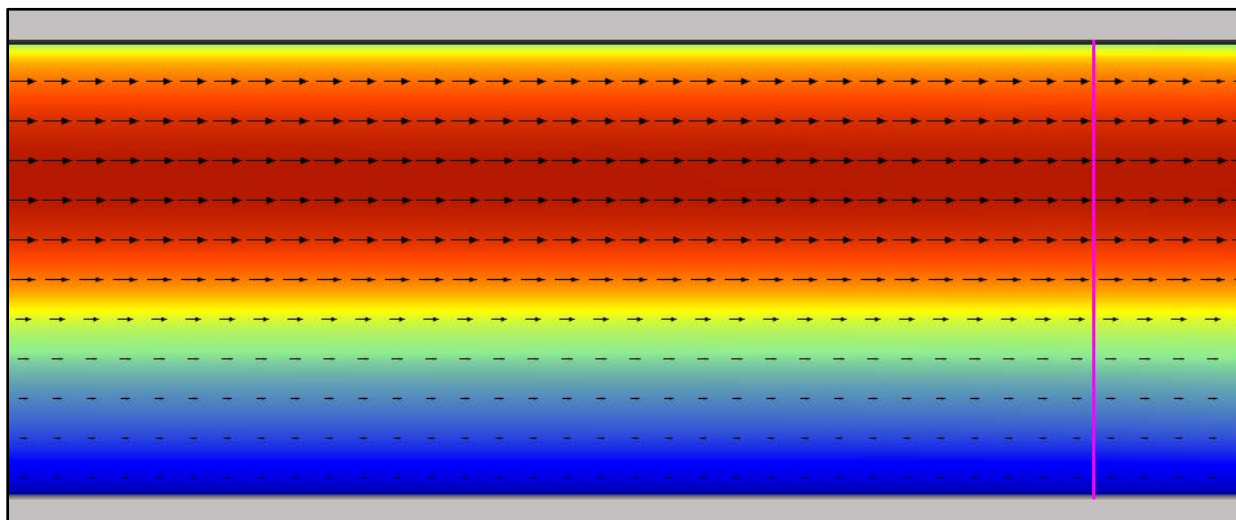


Figure 4-31. RAS Mapper Velocity Plot with Profile Line at Location of Velocity Measurements

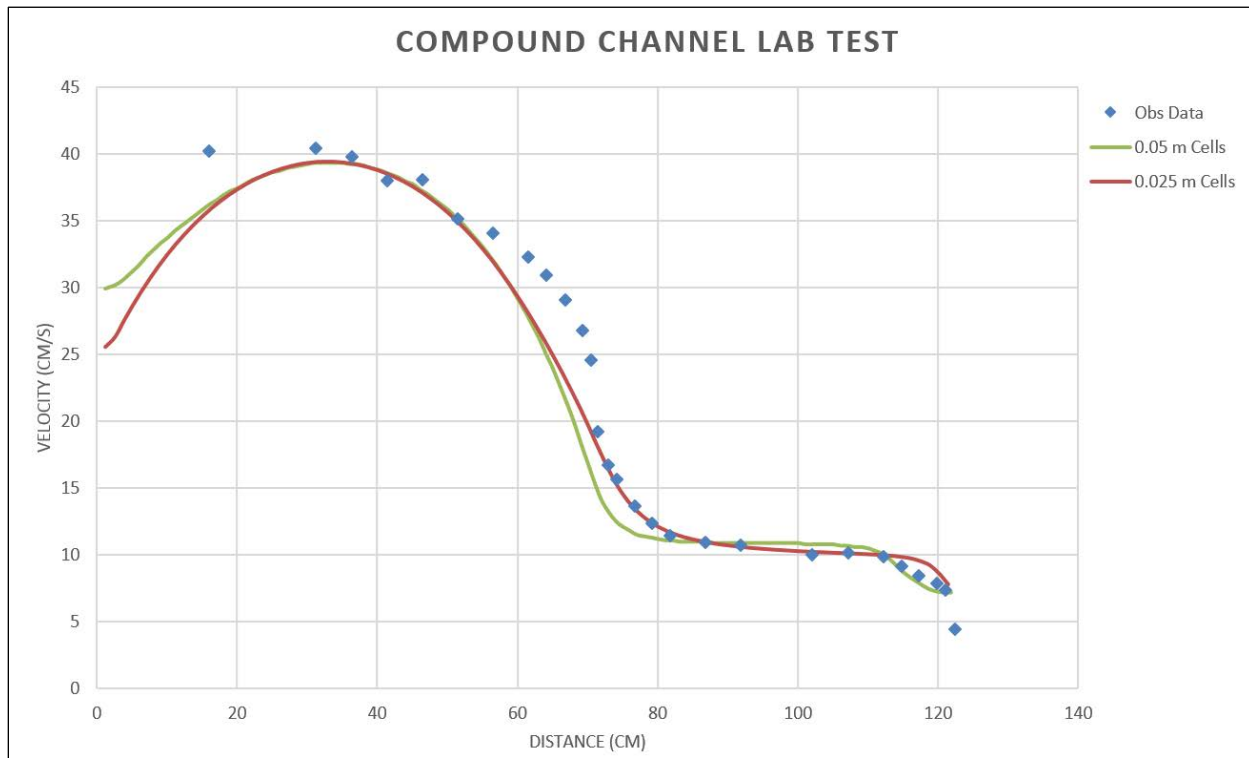


Figure 4-32. Observed and Computed Velocities for Compound Channel Test Case

References

1. Rajaratnam, 1981. Rajaratnam, N. and Ahmadai, R. *Hydraulics of channels with flood-plains*. Journal of Hydraulic Research, IAHR, Volume 19, Issue 1, pages 43-60. 1981.

4.3.2 Flow in a Rectangular Channel with a Sudden Expansion

Overview

The purpose of this test case is to validate HEC-RAS for simulating subcritical flow in a channel with a sudden expansion (in the aerodynamic literature, this classic test case is referred to as the "backward facing step"). The flow downstream of the expansion is complicated due to the presence of a shear layer resulting in large velocity gradients and the formation of an eddy zone (with reverse flow). In this case, the turbulent stresses (controlled by the Eddy Viscosity Mixing Coefficient, D_T) influence the computed results in the eddy zone. The HEC-RAS model results compare favorably with measured velocities through the eddy zone. Furthermore, the length of the eddy zone (i.e., reattachment or recirculation length) predicted by HEC-RAS compares well with the length measured in the experiment. The experimental data was obtained by Xie (1996) and later compared with numerical model results by Wu (2004), Song (2014), and Zhang (2007).

Problem and Data Description

This experiment was conducted in a concrete flume, 18 meters long and 1.2 meters wide. Half the flume width was blocked in the upper portion, resulting in an upper channel width of 0.6 meters. The channel expansion (from 0.6 meters to 1.2 meters) occurred 7.7 meters from the flume inlet. Table 4-23 describes the specifications of the experiment.

Table 4-23. Specifications of the Sudden Expansion Flume Experiment

Item	Value
Bottom width, B (meter)	0.6 (upstream); 1.2 (downstream)
Bed slope	$S_0 \approx 0$
Channel roughness, n	0.015 (bottom); 0.008 (wall, glass)
Upstream boundary condition, flow, Q (cms)	0.01815 and 0.03854
Downstream boundary condition, stage, h (meter)	0.11

Model Setup

The computational mesh for this test case is displayed in Figure 4-33. The mesh consisted of a 0.6 meter wide and five meter long upstream channel connected to an eight meter long and 1.2 meter wide downstream channel. The mesh cell size was 0.025 meters (with 24 cells across the upstream channel and 48 cells across the downstream channel). At the upstream inlet boundary, a constant flow of 0.01815 cms was specified. At the downstream outlet boundary, a constant depth of 0.11 meters was specified. The Manning's n value on the interior cells (associated with the channel bottom) was set to 0.015. To better approximate the velocity distribution in the channel just upstream of the expansion, the boundary cells (associated with the vertical channel sidewalls) were assigned a Manning's n value of 0.008. The Eddy Viscosity Mixing Coefficient (D_T), which influences the computed result in the eddy zone, was set to 1.4. A larger flow of 0.03854 cms was also simulated using the parameters listed above. Table 4-24 lists the model-specific values and parameters used for this test.

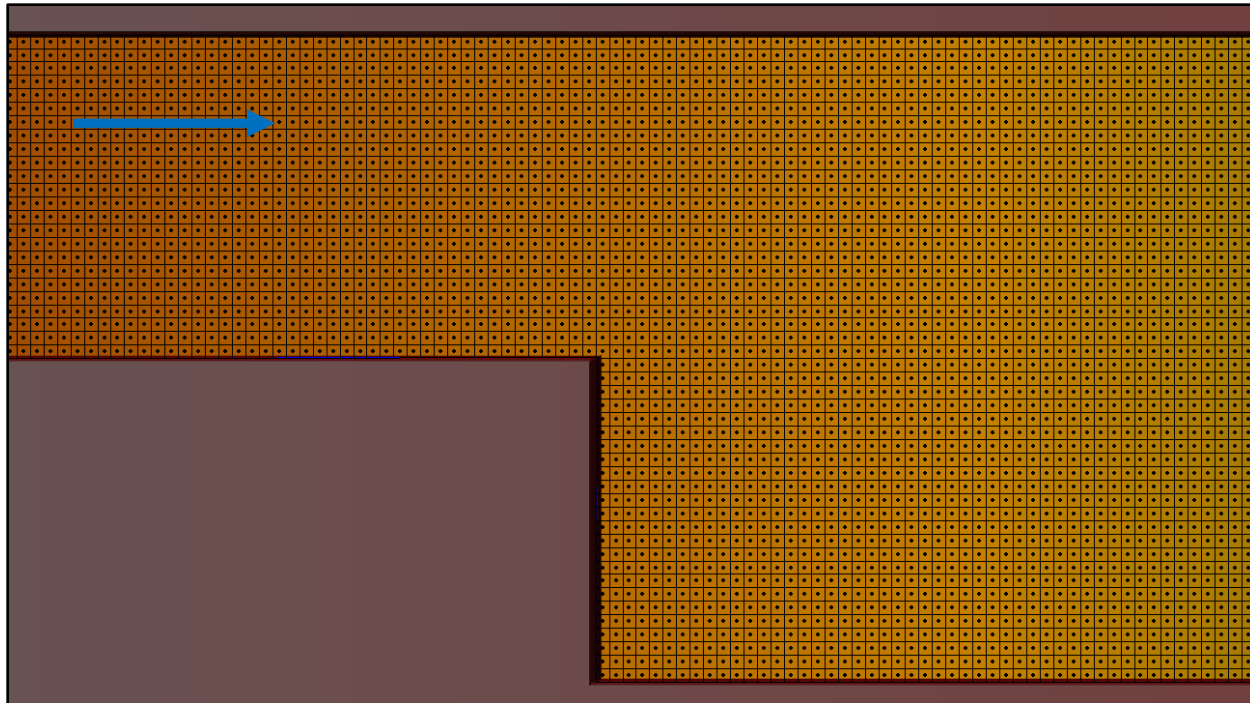


Figure 4-33. Computational Mesh for the Sudden Expansion Test Case (zoomed near the expansion)

Table 4-24. Model Specifications for the Sudden Expansion Test Case

Item	Value
Mesh cell size (meter)	0.025
Manning's n	0.015 and 0.008
Time step	0.05 s ($Cr_{max} \approx 1$), for $Q=0.01815$ cms 0.033 s ($Cr_{max} \approx 1$), for $Q=0.03854$ cms
Theta	1.0
Eddy viscosity coefficient	1.4
Equation set	Full momentum

Results and Discussion

The HEC-RAS 2D computed results were compared to the measured velocities and recirculation length from the laboratory study. Figure 4-34 is a velocity magnitude plot clearly showing the eddy zone with reverse flow (the low velocity blue region) downstream of the expansion for $Q = 0.01815$ cms. HEC-RAS computed eddy zone length (L_e) matches the experimentally observed value of 4.6 meters (L_e is influenced by the eddy viscosity coefficient, D_T) for $Q=0.01815$ cms. Figure 4-35 through Figure 4-40 display the velocity magnitude profile plots across the channel at the locations shown in Figure 4-34 ($X = 0, 1, 2, 3, 4$, and 5). Figure 4-41 through Figure 4-46 are velocity magnitude profile plots for the larger flow test case ($Q = 0.03854$ cms).

The HEC-RAS computed results compare well with the experimental data. The negative velocities in Figure 4-36 through Figure 4-39 and Figure 4-42 through Figure 4-45 ($X = 1, 2, 3$, and 4) indicate the reverse flow in the eddy zone.

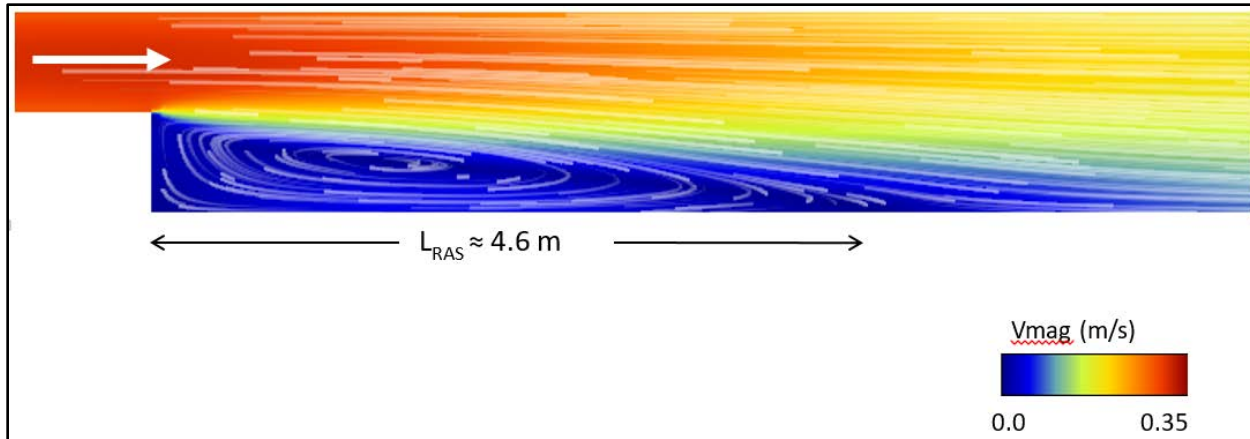


Figure 4-34. Computed Velocity Magnitude Plot with Particle Traces (for $Q=0.01815$ cms),
the Blue Shaded Eddy Zone is Clearly Evident Downstream of the Expansion

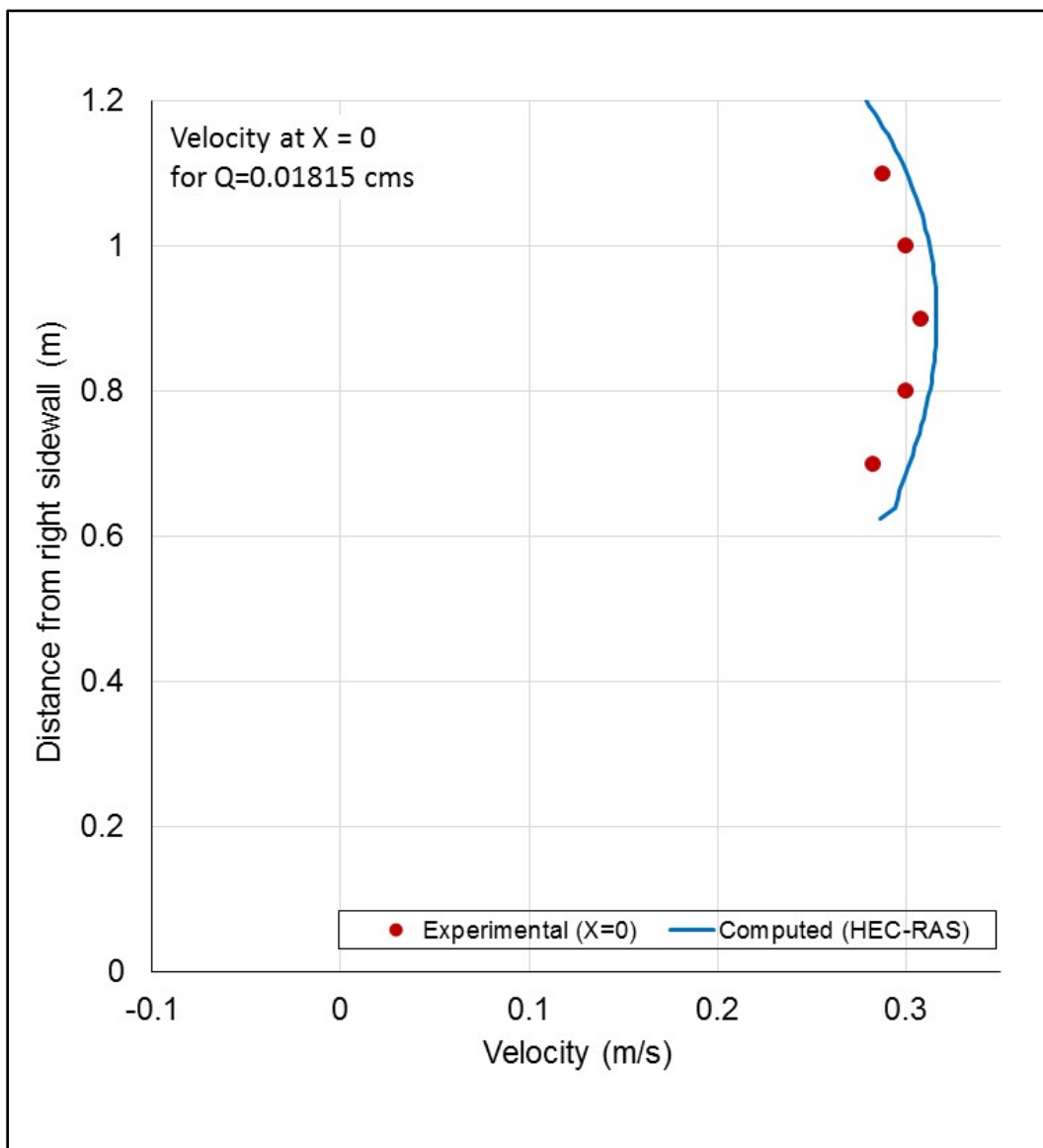


Figure 4-35. Velocity Profile (computed and experimental), at $X = 0$ in Figure 4-34
(just upstream of the expansion) for $Q = 0.01815 \text{ cms}$

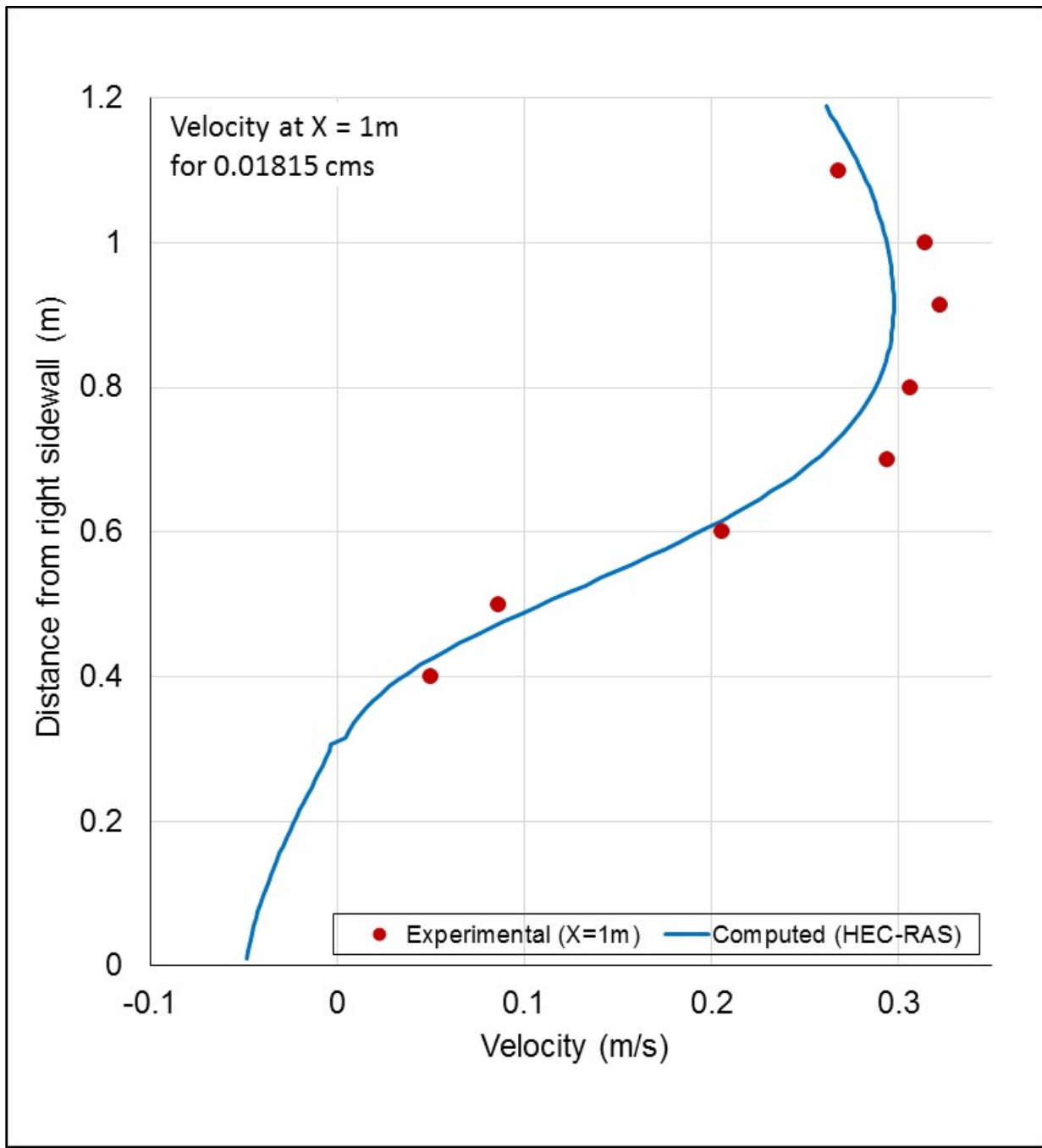


Figure 4-36. Velocity Profile (computed and experimental), at $X = 1$ in Figure 4-34 (one meter downstream of the expansion) for $Q = 0.01815 \text{ cms}$

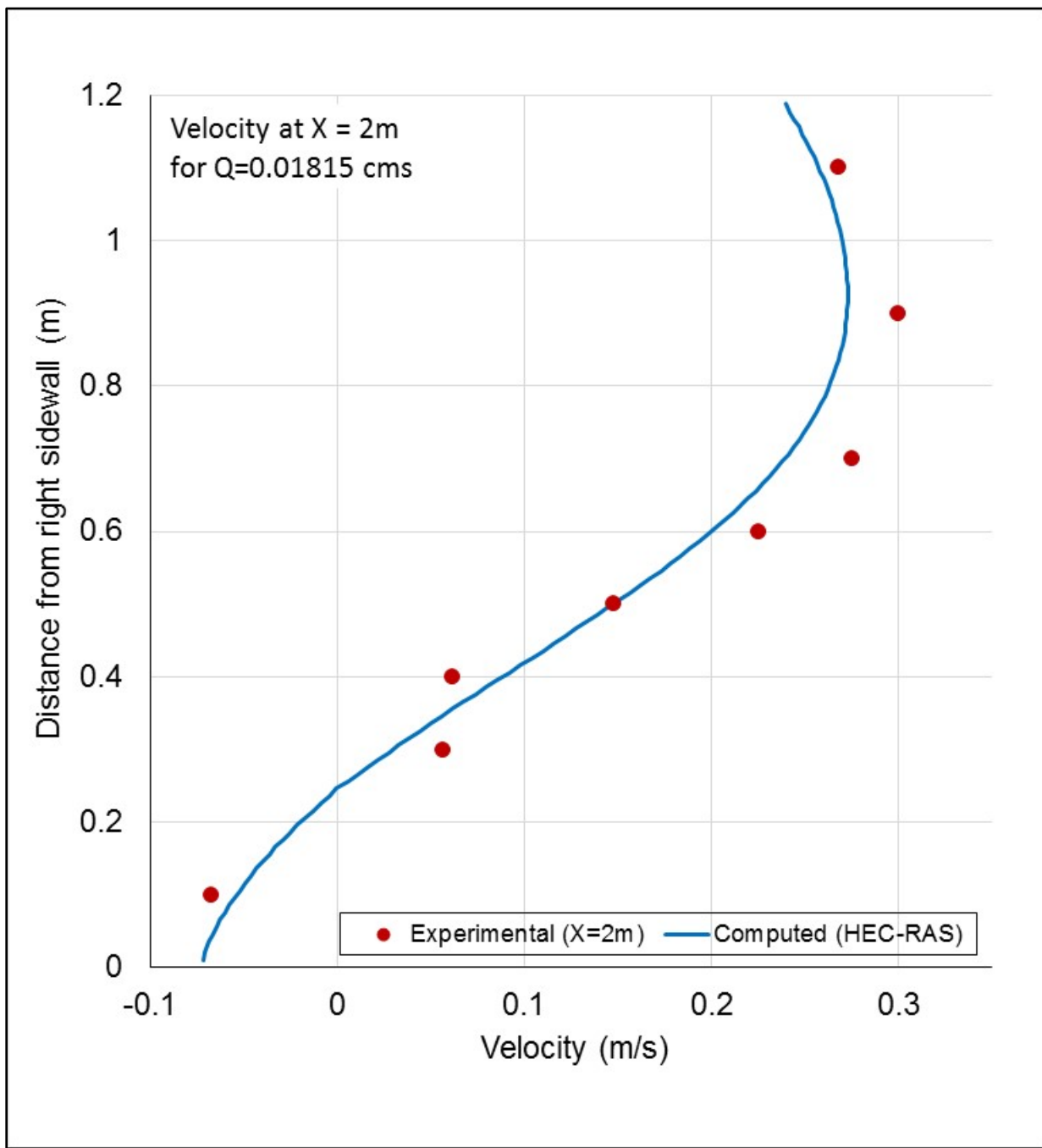


Figure 4-37. Velocity Profile (computed and experimental), at $X = 2$ in Figure 4-34 (two meters downstream of the expansion) for $Q = 0.01815 \text{ cms}$

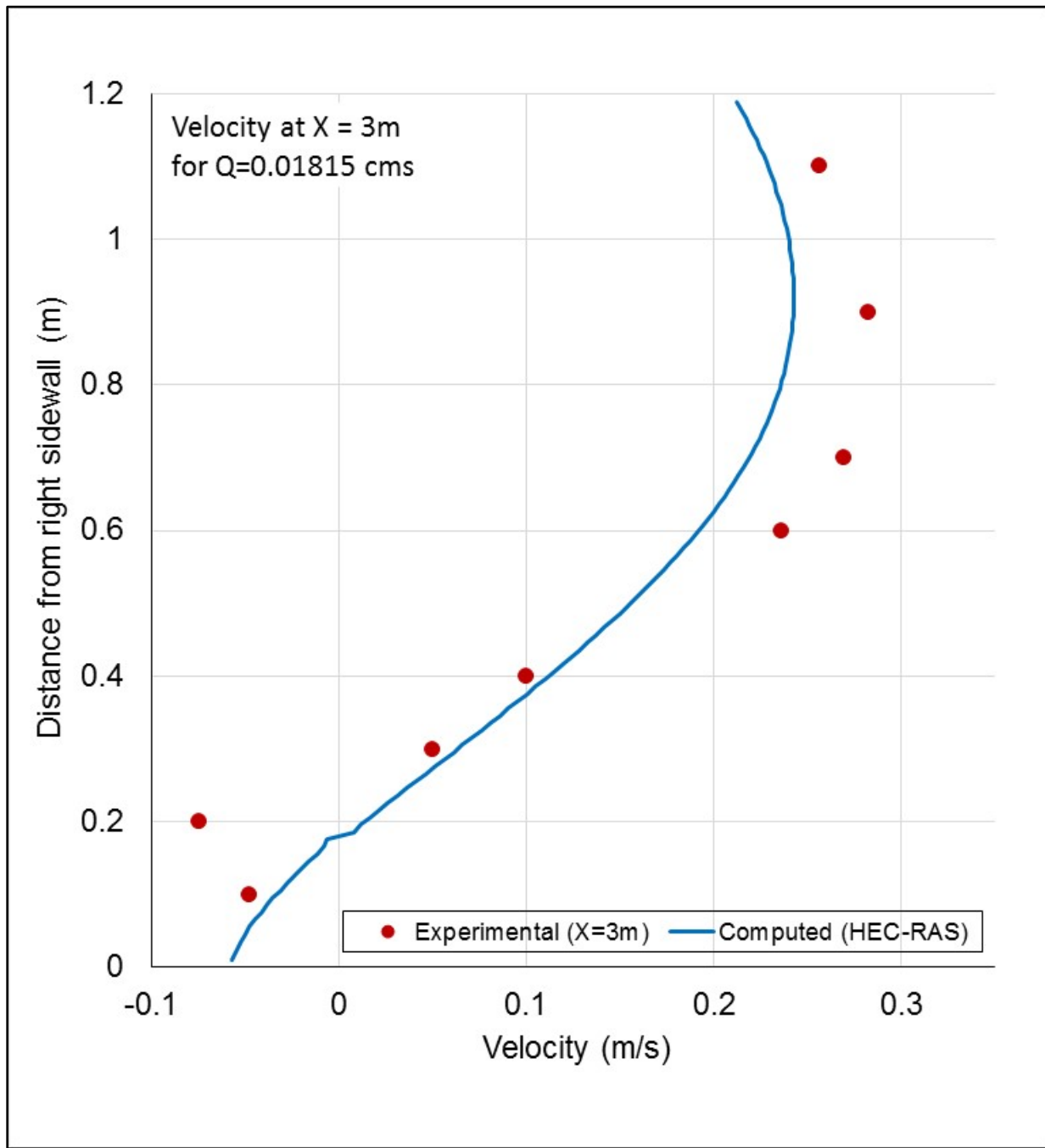


Figure 4-38. Velocity Profile (computed and experimental), at $X = 3$ in Figure 4-34 (three meters downstream of the expansion) for $Q = 0.01815$ cms

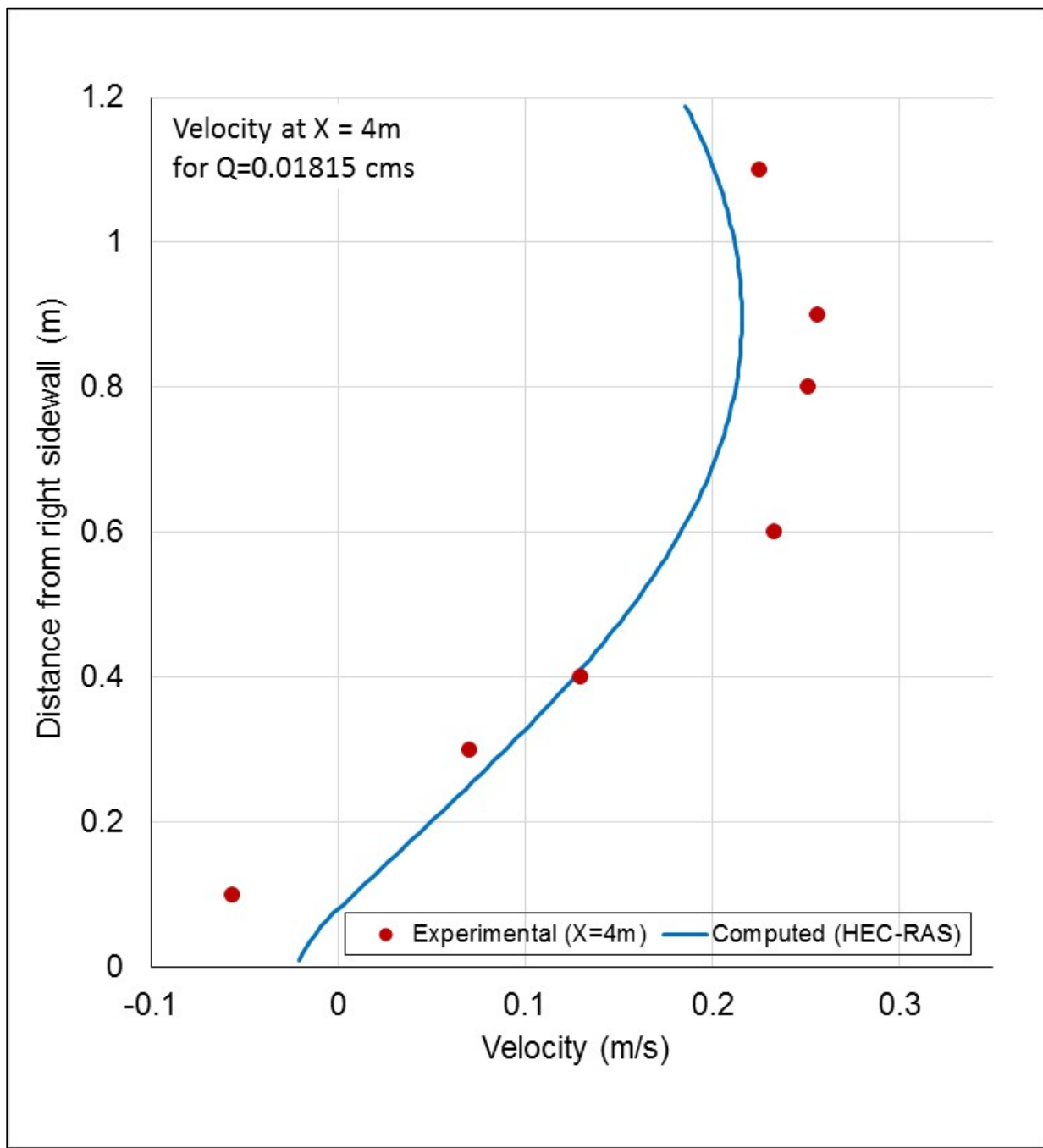


Figure 4-39. Velocity Profile (computed and experimental), at $X = 4$ in Figure 4-34 (four meters downstream of the expansion) for $Q = 0.01815 \text{ cms}$

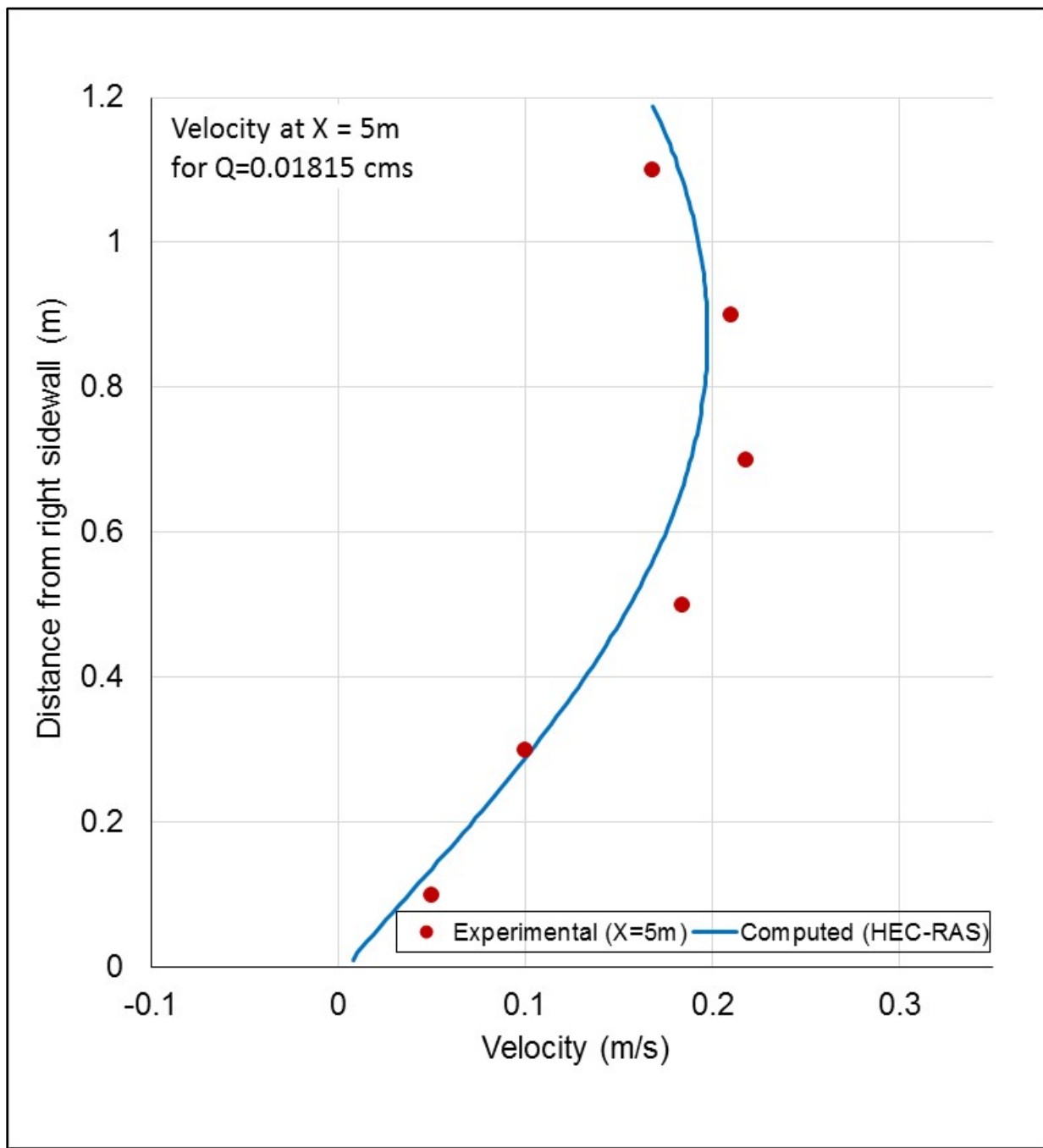


Figure 4-40. Velocity Profile (computed and experimental), at $X = 5$ in Figure 4-34 (five meters downstream of the expansion) for $Q = 0.01815 \text{ cms}$

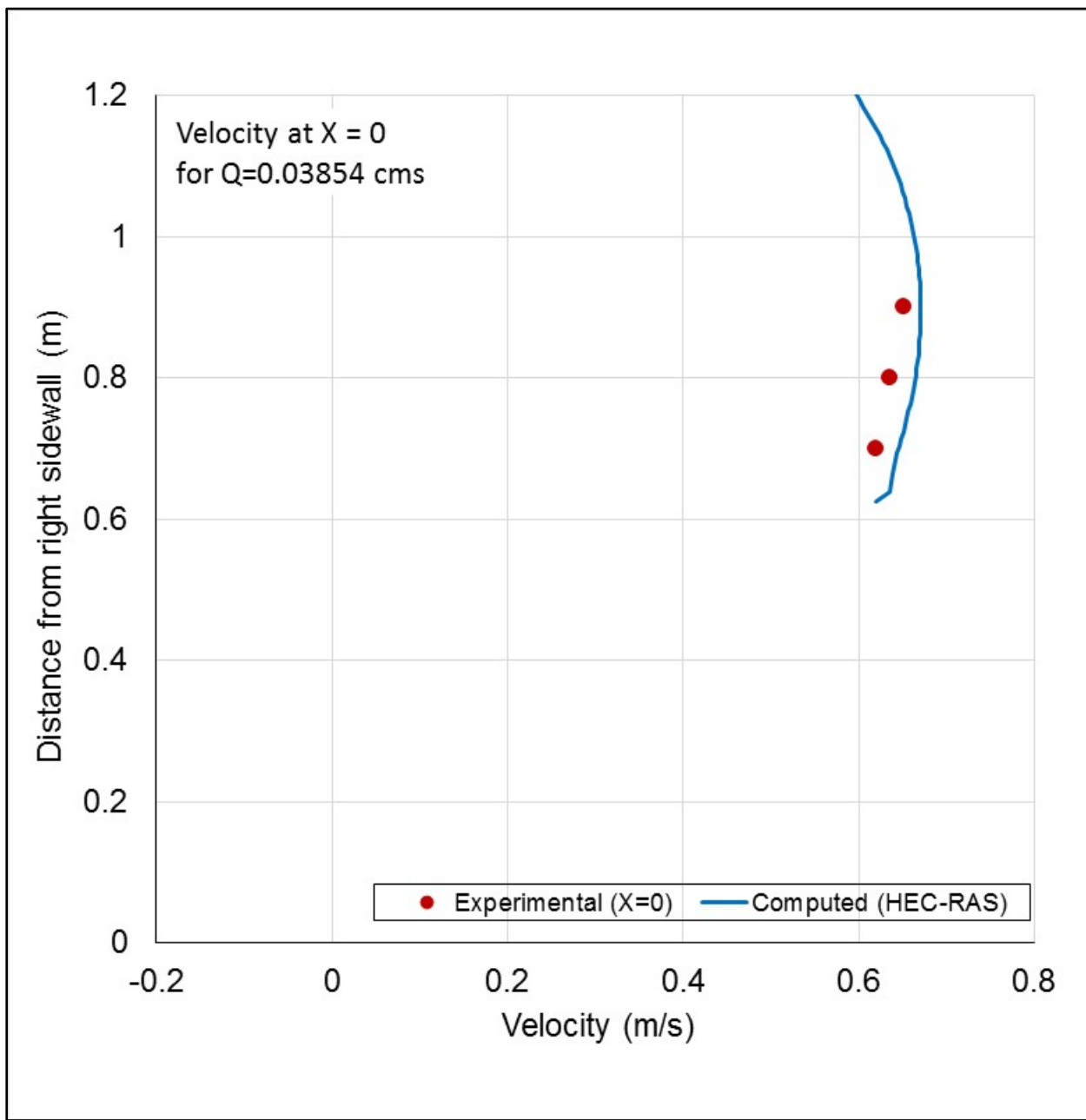


Figure 4-41. Velocity Profile (computed and experimental), at $X = 0$ (just upstream of the expansion) for $Q = 0.03854 \text{ cms}$

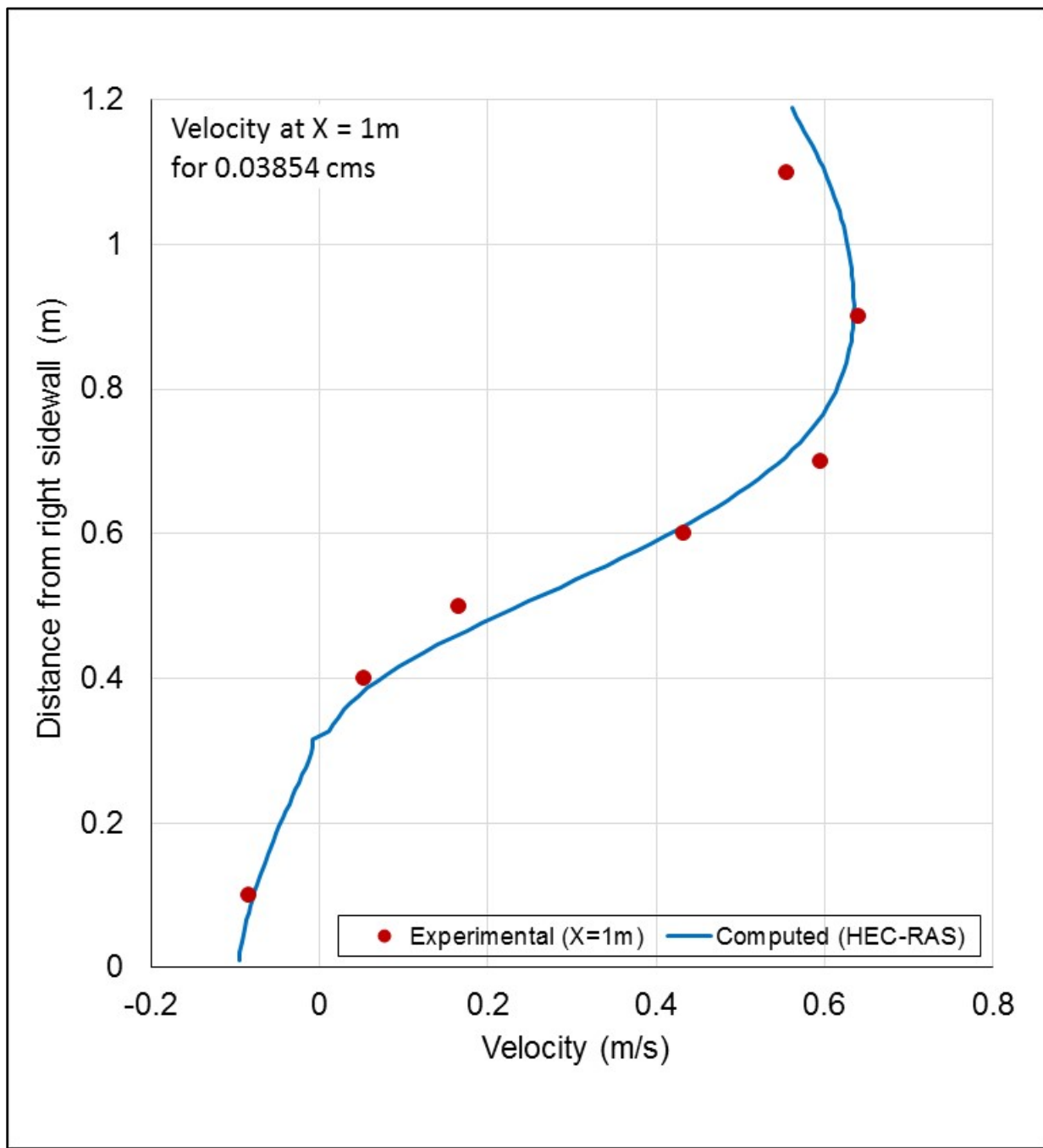


Figure 4-42. Velocity Profile (computed and experimental), at $X = 1$ (one meter downstream of the expansion) for $Q = 0.03854$ cms

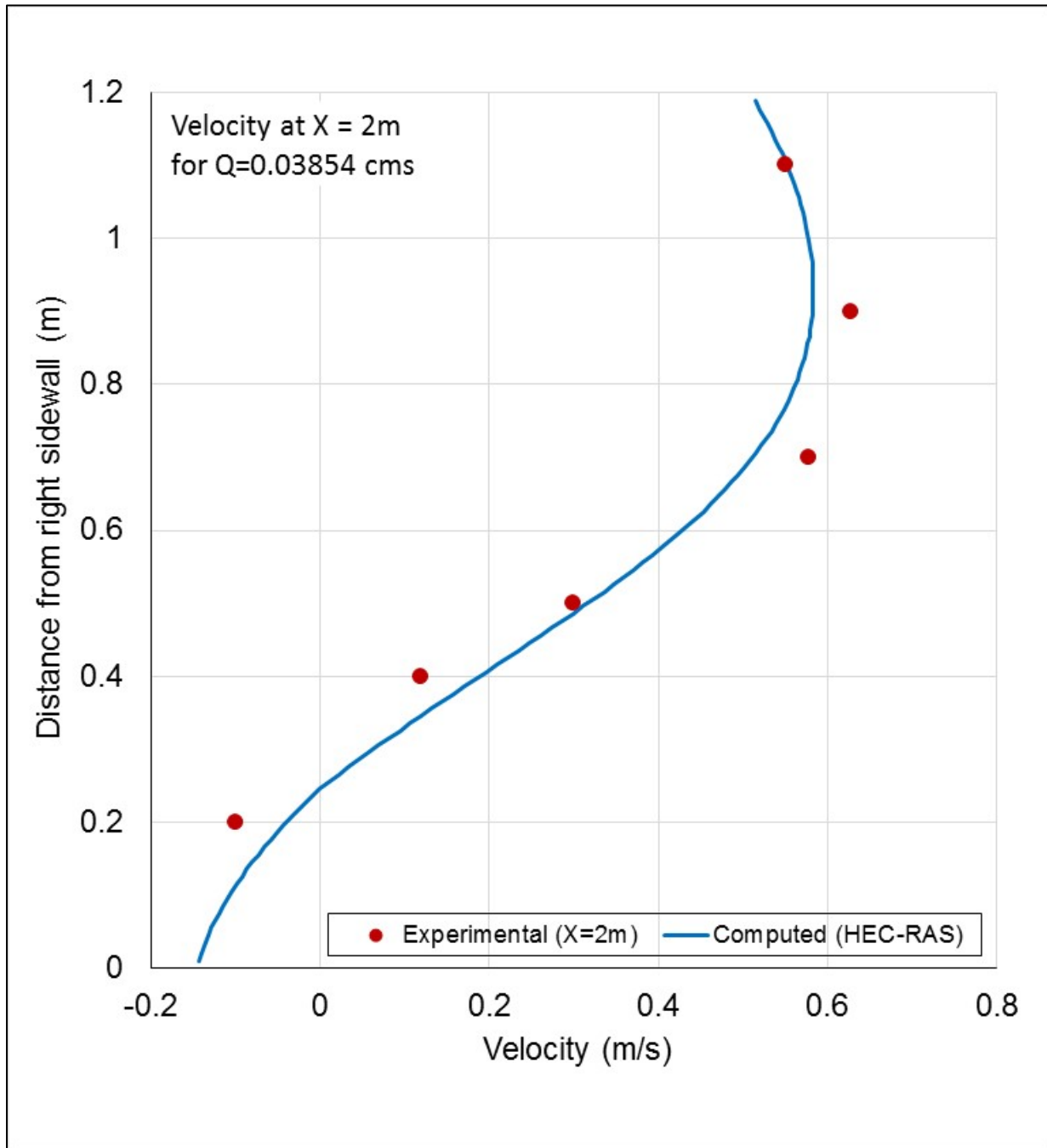


Figure 4-43. Velocity Profile (computed and experimental), at $X = 2$ (two meters downstream of the expansion) for $Q = 0.03854$ cms

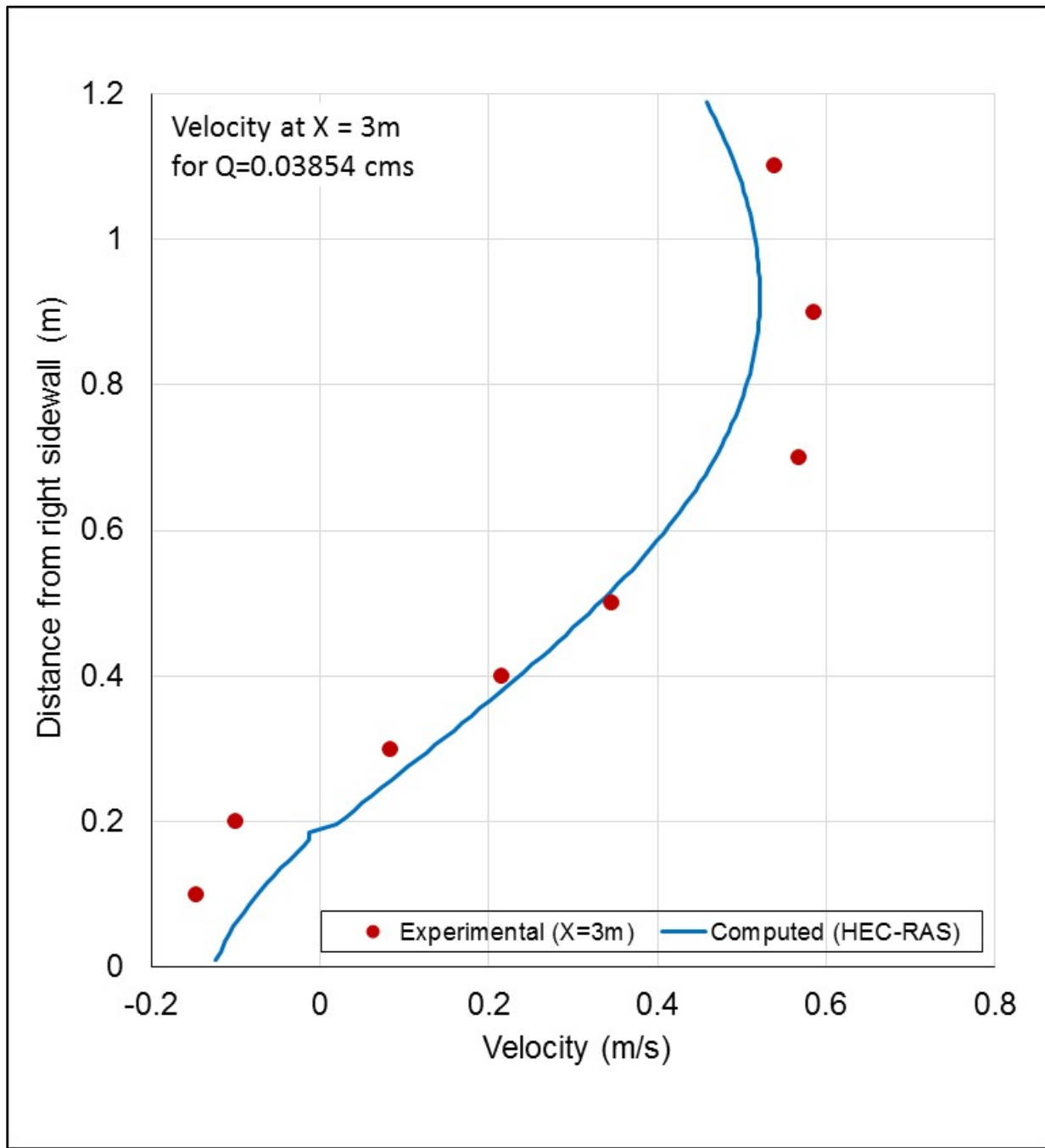


Figure 4-44. Velocity Profile (computed and experimental), at $X = 3$ (three meters downstream of the expansion) for $Q = 0.03854$ cms

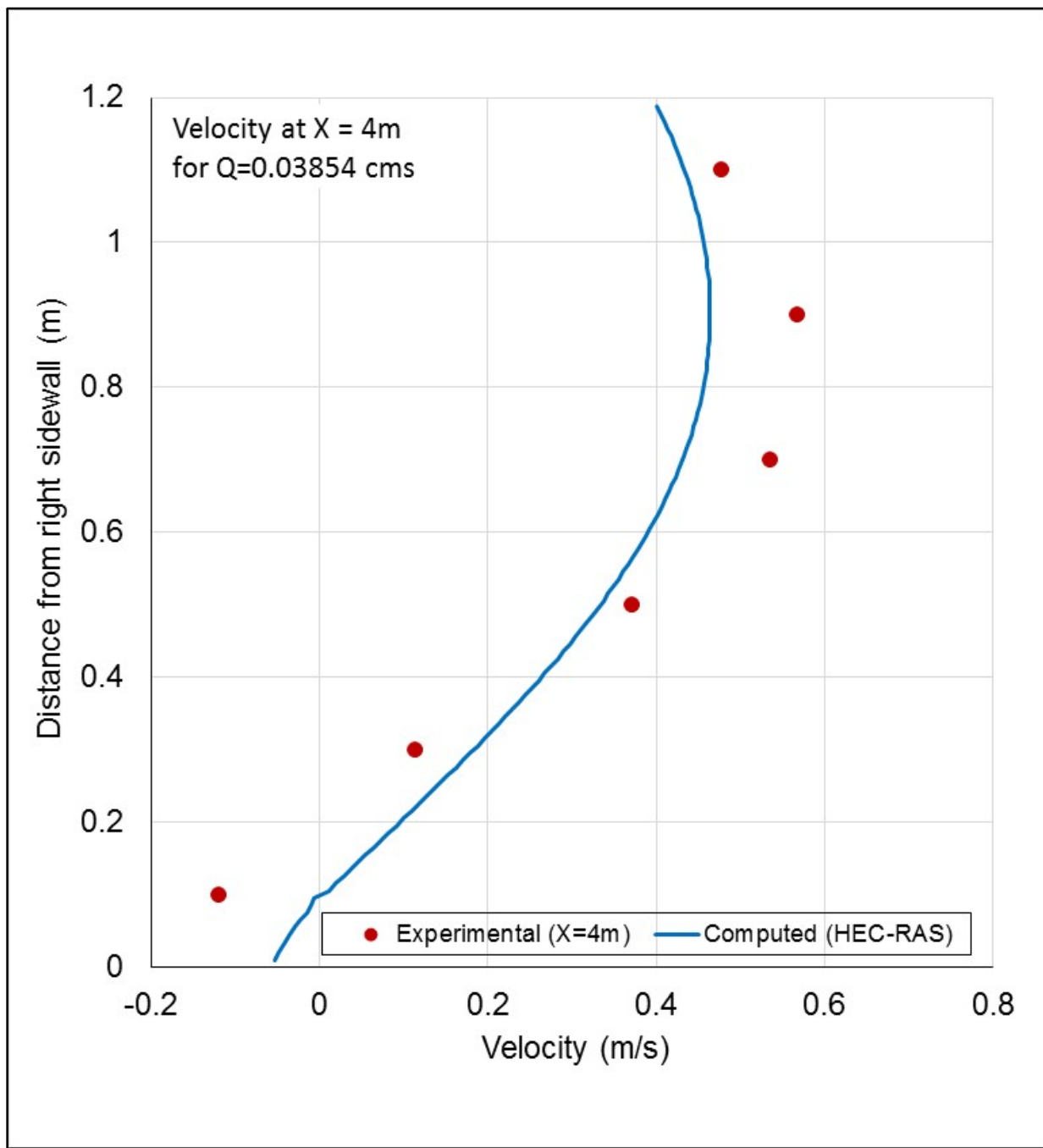


Figure 4-45. Velocity Profile (computed and experimental), at $X = 4$ (four meters downstream of the expansion) for $Q = 0.03854 \text{ cms}$

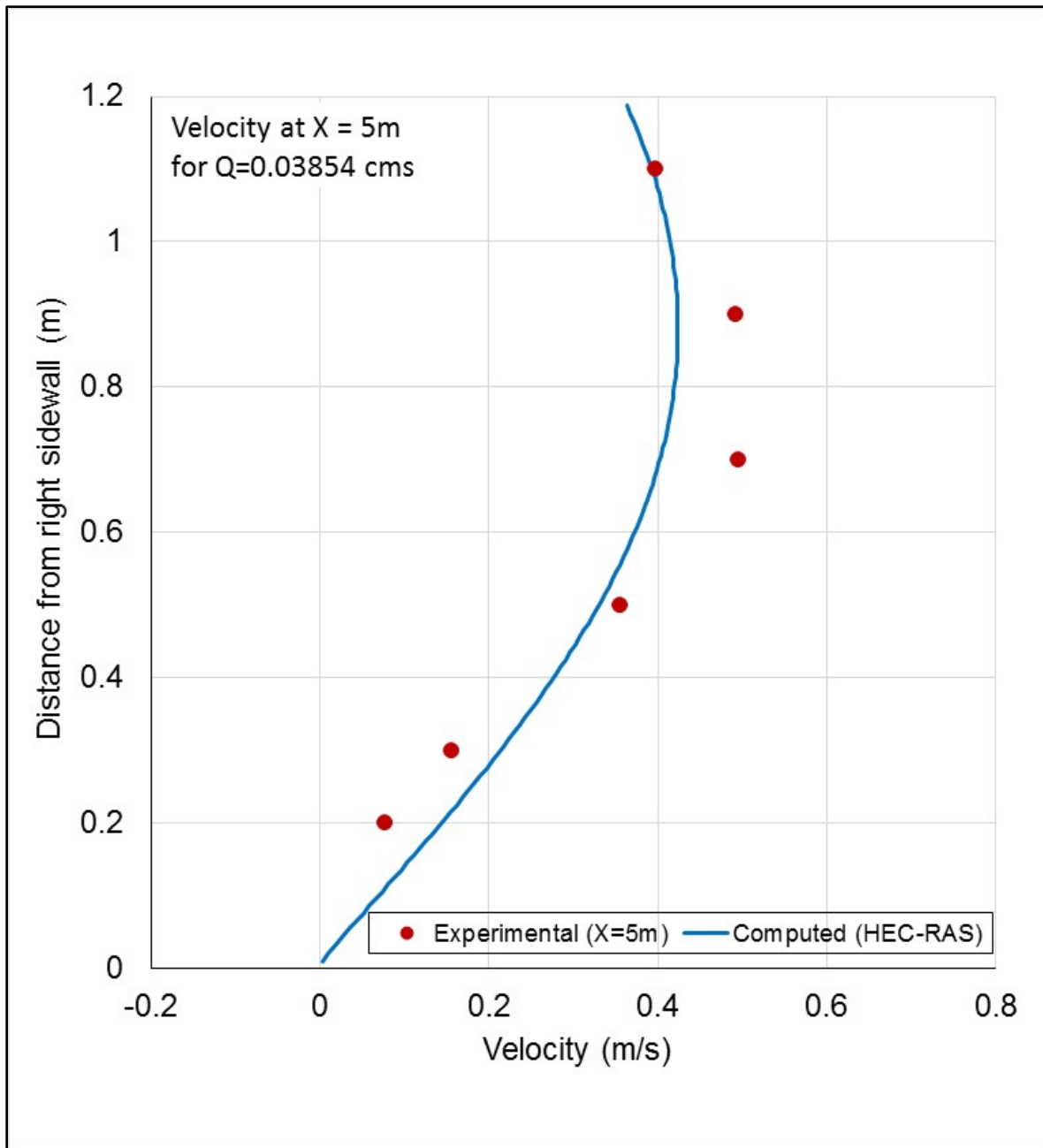


Figure 4-46. Velocity Profile (computed and experimental), at $X = 5$ (five meters downstream of the expansion) for $Q = 0.03854$ cms

References

1. Song, 2014. Song, Chang Geun, Seo, Il Won, Shin, Jae Hyun, and Park, In Hwan. *Development and Application of a Shallow Water Flow Model HDM-2D*. International Conference on Hydroinformatics, City of New York (CUNY), New York. Paper 262. August 2014.
2. Wu, 2004. Wu, Weiming, Wang, P., and Nobuyuki, C. *Comparison of Five Depth-Averaged 2-D Turbulence Models for RiverFlows*. Archives of Hydro-Engineering and Environmental Mechanics, Volume 51, No. 2, pages 183-200. 2004.

3. Xie, 1996. Xie, B.L. *Experiment on flow in sudden-expanded channel*. Technical Report, Wuhan University of Hydraulic and Electrical Engineering, China. 1996.
4. Zhang, 2007. Zhang, Yaoxin, Jia, Y., and Wang Sam S.Y. *Conservative Multi-block Algorithm for Two-dimensional Numerical Model*. World Academy of Science, Engineering and Technology, International Journal of Physical and Mathematical Sciences, Volume 1, No. 1, pages 43-55. January 2007.

4.3.3 Two-Dimensional Surface Runoff

Overview

The purpose of this test case is to validate HEC-RAS for simulating surface runoff. The test case has spatially uniform but unsteady rainfall and a two-dimensional geometry. Model results are compared with measured discharge data for three different unsteady precipitation events. The test case is best suited for the SWE solver, but the DWE solver is also applied for comparison. The model features which are verified are the precipitation time series (rainfall hyetograph), normal depth downstream boundary condition, and water volume conservation.

Problem and Data Description

The experiment consists of a 2 x 2.5 meter rectangular basin with a bed made of three stainless steel planes (Figure 4-47). The planes have a constant slope of five percent. Two walls are located with the basin which block the flow and increase the time of concentration for the basin. Rain is simulated with 100 nozzles arranged in on a uniform grid over the basin. Three cases were run with different rainfall intensities and durations. In Test Case C1 (Coe, 2008), the rainfall intensity is 317 mm/hour during 45 seconds, and then stops. In Test Case 2B (Coe, 2008), the rainfall has an intensity of 320 mm/hour for 25 seconds, then stops for 4 seconds, and starts again for another 25 seconds with the same intensity. Test Case 2C (Coe, 2008) is the same as Test Case 2B (Coe, 2008) but the rain stops for seven seconds, and the rain intensity is 328 mm/hr.

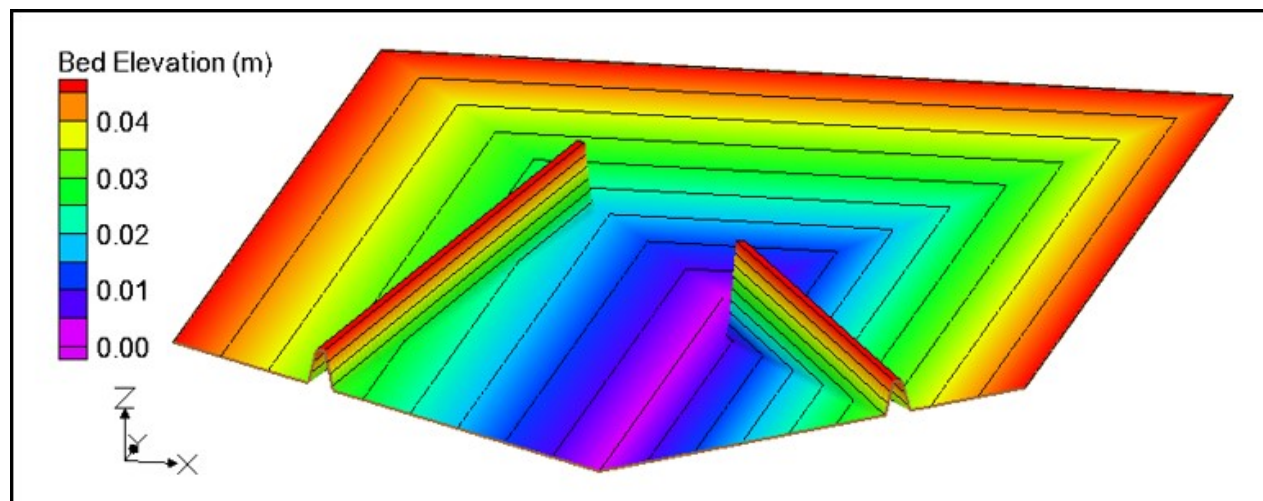


Figure 4-47. Physical Model Geometry for the Cea (2008) Test Cases

Model Setup

The basin was discretized using a constant grid resolution of two centimeters, except near the walls where the grid resolution varied slightly due to the boundary fitting (Figure 4-48). Table 4-25 provides the model parameters used for the Cea (2008) test cases.

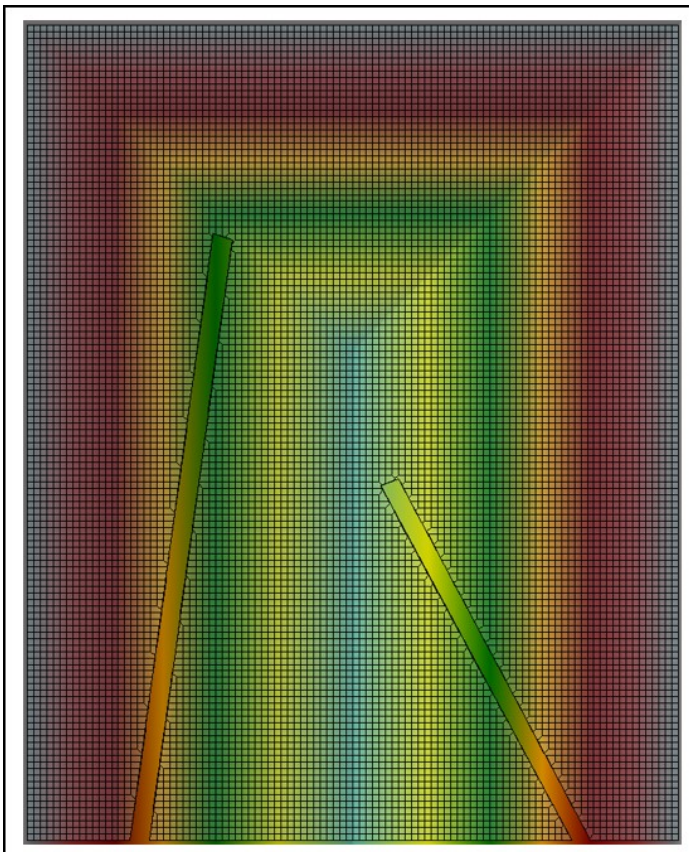


Figure 4-48. Computational Mesh and Terrain for the Cea (2008) Test Cases

Table 4-25. Model Setup Parameters for the Cea (2008) Test Cases

Parameter	Value
Manning's roughness coefficient ($s/m^{1/3}$)	0.01
Grid resolution (cm)	2
Initial water depth (cm)	0
Governing equations	SWE, DWE
Time step (second)	0.025
Implicit weighting factor	1.0
Water Surface Tolerance (meter)	1×10^{-5}
Volume Tolerance (meter)	1×10^{-5}
Mixing coefficient (SWE only)	0.5

Results and Discussion

A comparison of the computed and measured water discharge at the basin outlet for Test Cases C1, 2B, and 2C (Coe, 2008) are shown in Figure 4-49, Figure 4-50, and Figure 4-51, respectively. In all three cases, SWE model results agree well with measurements. The SWE

model is able to capture well the rise in the hydrograph and the timing and magnitude of the peak discharge. The DWE model over-predicts discharge values during the rise of the hydrograph and under-predicts during the fall of the hydrograph. The DWE model is not able to accurately capture the rise in the hydrograph and the peak discharge. The DWE model results show a time of concentration which is too early compared to the measurements. This is because the lack of inertial effects in the DWE. The experiment is very dynamic with sharp changes in fluid direction around the walls. Table 4-26 shows the goodness of fit statistics for both the DWE and SWE model results. Figure 4-52 shows the inundation and the current velocity field for Test Case 2C (Coe, 2008) at 55 seconds.

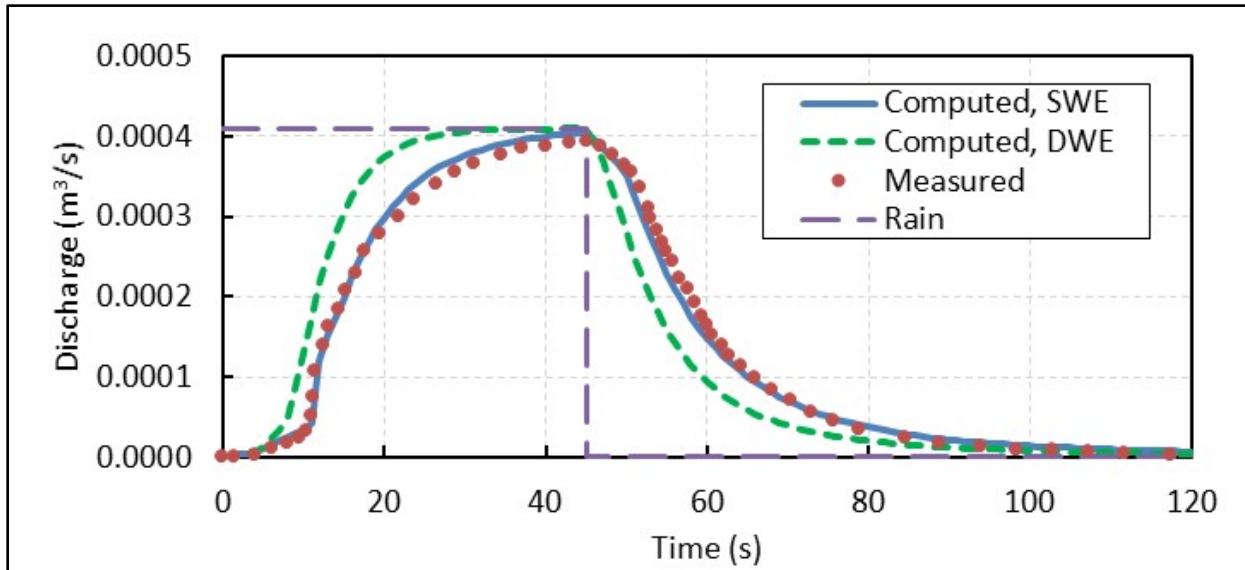


Figure 4-49. Comparison of Measured and Computed Discharge for Test Case C1 (Coe, 2008)

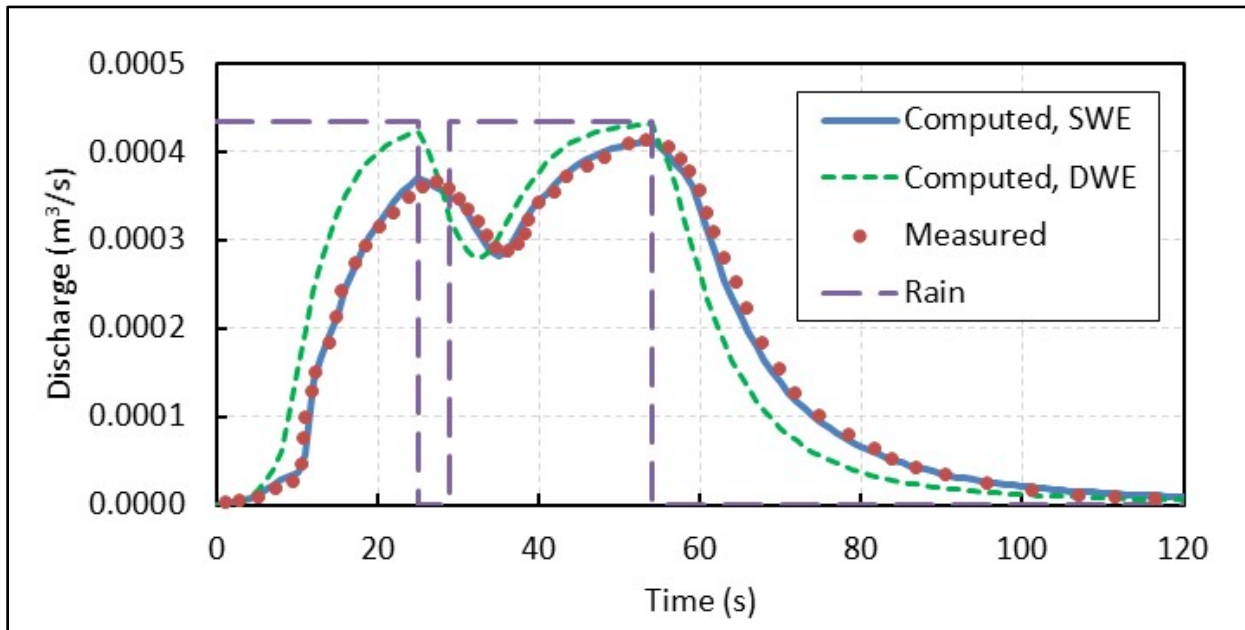


Figure 4-50. Comparison of Measured and Computed Discharge for Test Case 2B (Coe, 2008)

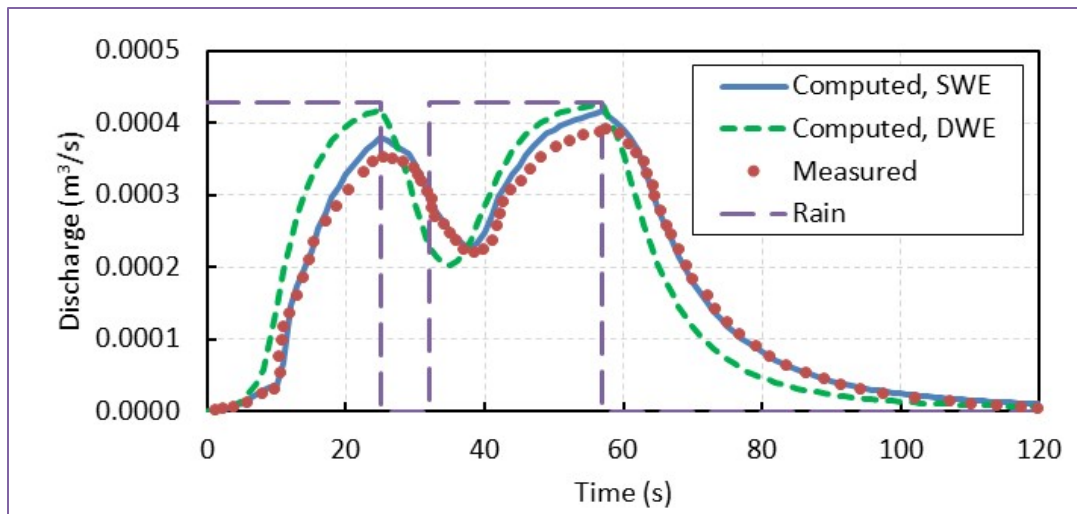


Figure 4-51. Comparison of Measured and Computed Discharge for Test Case 2C (Coe, 2008)

Table 4-26. Goodness-of-fit statistics for the Cea (2008) Test Cases

Parameter	Case C1		Case 2B		Case 2C	
	SWE	DWE	SWE	DWE	SWE	DWE
ME ($10^{-5} \text{ m}^3/\text{s}$)	-0.04	-0.02	-0.27	1.11	0.63	0.53
NME (percent)	-1.01	-0.49	-0.66	2.68	1.63	1.35
MAE ($10^{-5} \text{ m}^3/\text{s}$)	1.19	5.56	0.89	5.32	1.02	5.24
NMAE (percent)	3.02	14.14	2.16	12.88	3.06	13.39
RMSE ($10^{-5} \text{ m}^3/\text{s}$)	1.51	6.76	1.18	6.57	1.63	6.19
NRMSE (percent)	3.85	17.18	2.86	15.89	4.17	15.82
R ²	0.989	0.791	0.993	0.817	0.991	0.866
Volume Error (percent)	0.002	0.016	0.009	0.016	0.042	0.016

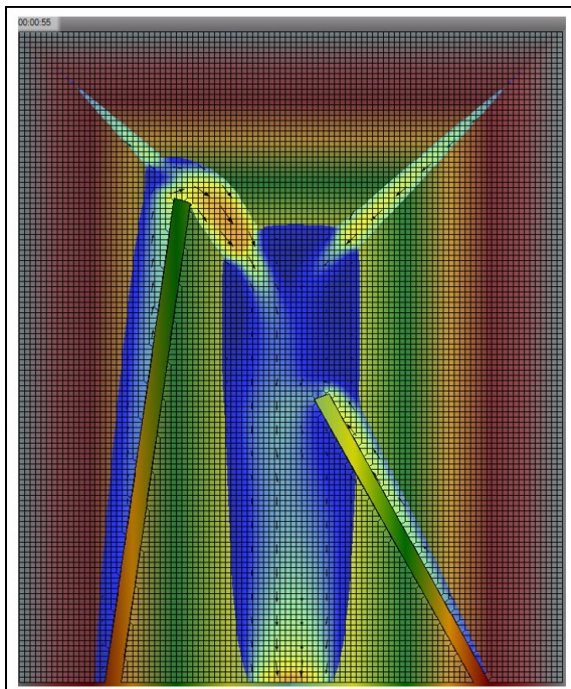


Figure 4-52. Example Current Velocity Field for Test Case 2C at 55 seconds

References

1. Cea, 2008. Cea, Lulia, Puertas, J., Pena, L., and Garrido, M. *Hydrologic forecasting of fast flood events in small catchments with a 2D-SWE model. Numerical model and experimental validation.* World Water Congress 2008, Montpellier, France. 1–4 September 2008.
2. Shirmーン, 2015. Shirmーン, T., Jia, Y., Locke, M.A., Lizotte, R.E., Jr. *Numerical modeling of rain induced overland flows.* World Environmental and Water Resources Congress 2015. Floods, Droughts, and Ecosystems. Pages 1532-1544.

4.3.4 Rectangular Channel with a 180-Degree Bend

Overview

The purpose of this test case is to validate HEC-RAS for simulating subcritical flow in a 180-degree channel bend. The flow around a 180-degree bend is complicated and exhibits super-elevation and velocity redistribution. Furthermore, this bend is tight (with a mean radius to width ratio of 1.0), amplifying the three-dimensional nature of the flow. Nevertheless, HEC-RAS model results compare favorably with measured velocities and depths throughout the bend (and with computed results from other 2D models). The experimental data was obtained by Rozovskii (1957) and later compared with numerical model results by Leschziner (1979), and Molls (1995).

Problem and Data Description

This is a flume experiment with a 180-degree bend, six meters long approach channel, and three meter long exit channel (Rozovskii, 1957). The flume is rectangular with a bottom width of 0.8 meters. The entire channel is set on a horizontal bed. The curve has an inner radius of 0.4 meters and a mean radius-to-width ratio of 1.0, resulting in a tight bend. The flume is shown in Figure 4-53. Table 4-27 describes the specifications of the experiment.

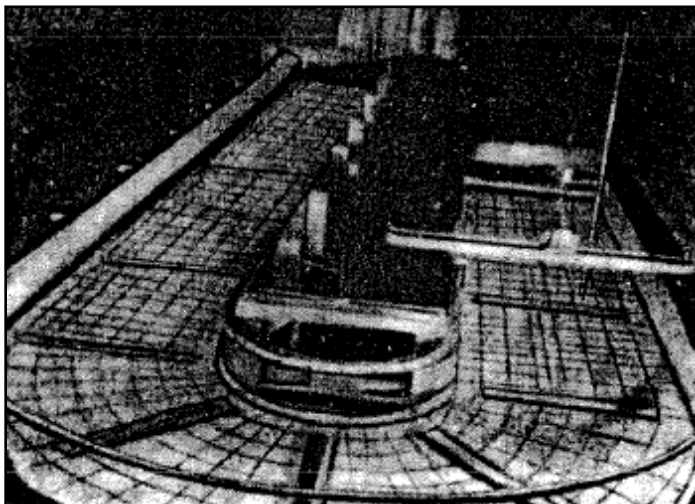


Figure 4-53. Rectangular Channel with a 180-degree Bend (Rozovskii, 1957)

Table 4-27. Specifications of the 180-degree Bend Flume Experiment

Item	Value
Bottom width (rectangular), B (meter)	0.8
Bed slope, S_0	0
Channel roughness (smooth), n	0.01
Bend mean radius-to-width ratio (tight bend)	1.0
Upstream boundary condition, low	$Q = 0.0123 \text{ cms}$ (subcritical flow) and $F=0.11$
Downstream boundary condition, stage, h (meter)	0.057

Model Setup

The computational mesh for this test case, shown in Figure 4-54, consisted of the 180-degree bend connected to 1 m upstream and downstream straight sections. The mesh cell size ranged between approximately 0.015 and 0.05 meters (with 40 cells across the channel and a mesh interval of approximately 2.5 degrees within the bend). This test case uses a curvilinear mesh (which can be constructed using breaklines or by creating the mesh cell center points "outside" HEC-RAS and manually inserting them into the geometry file). At the upstream inlet boundary, a constant flow of 0.0123 cms was specified. At the downstream outlet boundary, a constant depth of 0.057 meters was specified. The Manning's n value was 0.01. Table 4-28 lists the model-specific values and parameters used for this test.

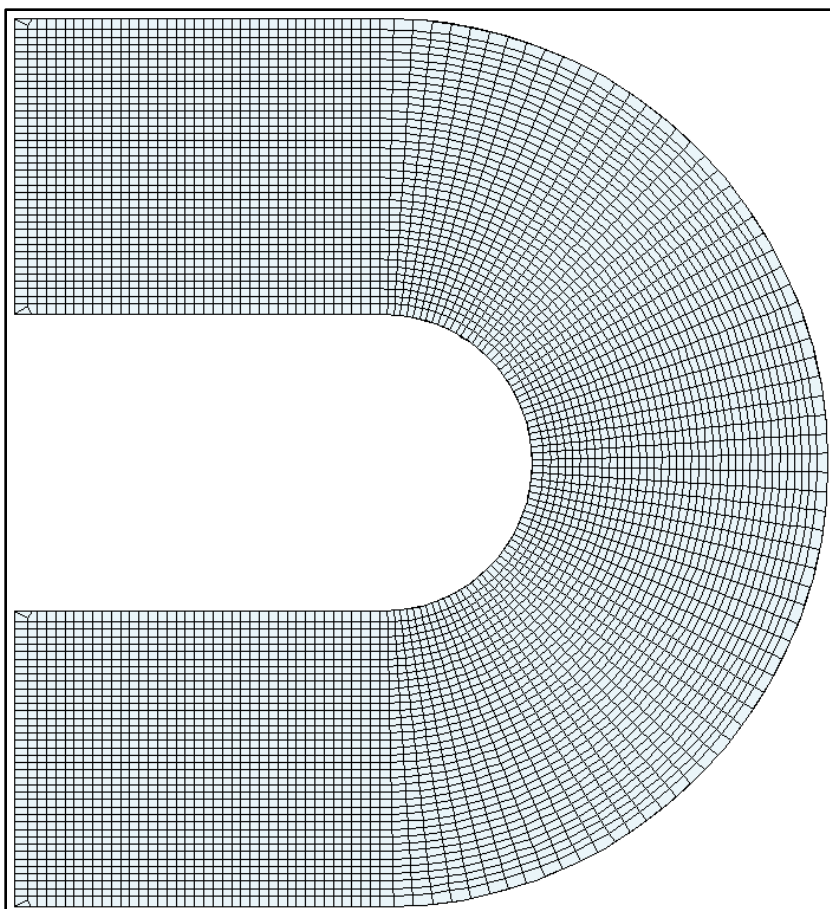


Figure 4-54. Curvilinear Computational Mesh for the 180-degree Bend Test Case

Table 4-28. Model Specifications for the 180-degree Bend Test Case

Item	Value
Curvilinear grid (meter)	$0.015 < \text{cell size} < 0.05$
Manning's n	0.01
Time step (seconds)	0.1 ($\text{Cr}_{\max} \approx 1$)
Theta	1.0
Eddy viscosity mixing coefficient	0.0
Equation set	Full momentum

Results and Discussion

The 2D computed results were compared to the measured velocities and depths from the laboratory study. Figure 4-55 is a velocity magnitude plot showing, as expected, faster velocities along the inner bend wall. Figure 4-56 through Figure 4-58 are velocity magnitude profile plots across the channel at the locations shown on Figure 4-55. (A-B, C-D, and E-F). The computed results in Figure 4-56 and Figure 4-57 compare well with the experimental data. Downstream of the bend, Figure 4-58 shows lower computed velocities along the outer wall. This velocity under-prediction is consistent with other 2D model results (Molls, 1995) and is likely due to limitations associated with the 2D Saint Venant Equations. Figure 4-59 is a depth plot showing, as expected, higher depths along the outer bend wall (super-elevation). Figure 4-60 shows the inner and outer wall depths (clearly indicating the super-elevation). Again, the HEC-RAS computed depths are consistent with other 2D model results (Molls, 1995).

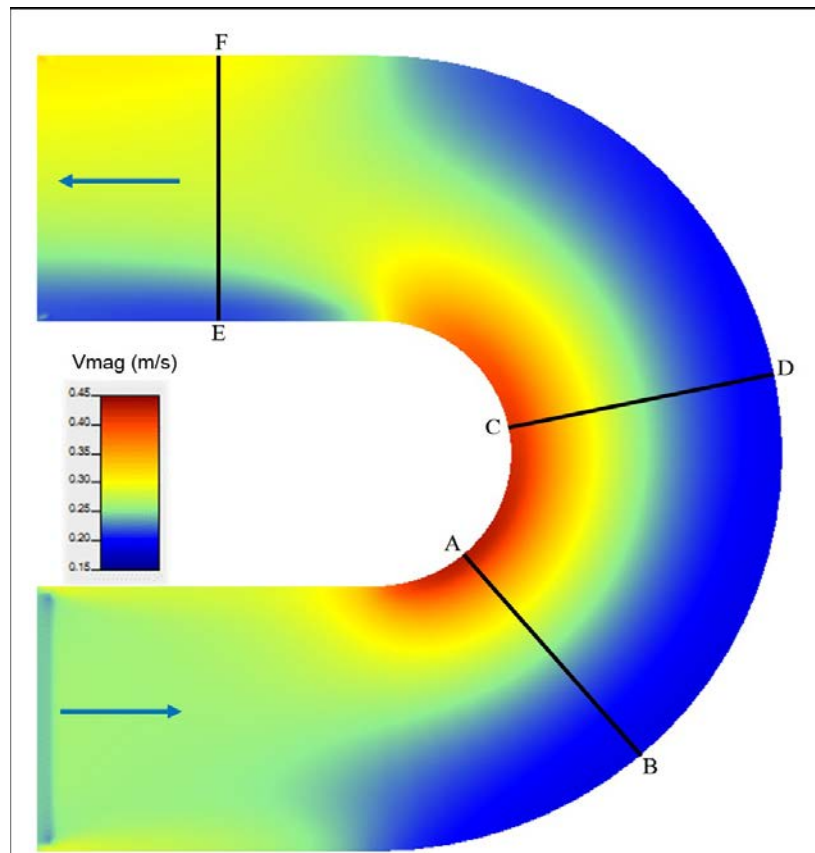


Figure 4-55. Velocity Magnitude (computed by HEC-RAS), with Faster Velocity along inside of Bend

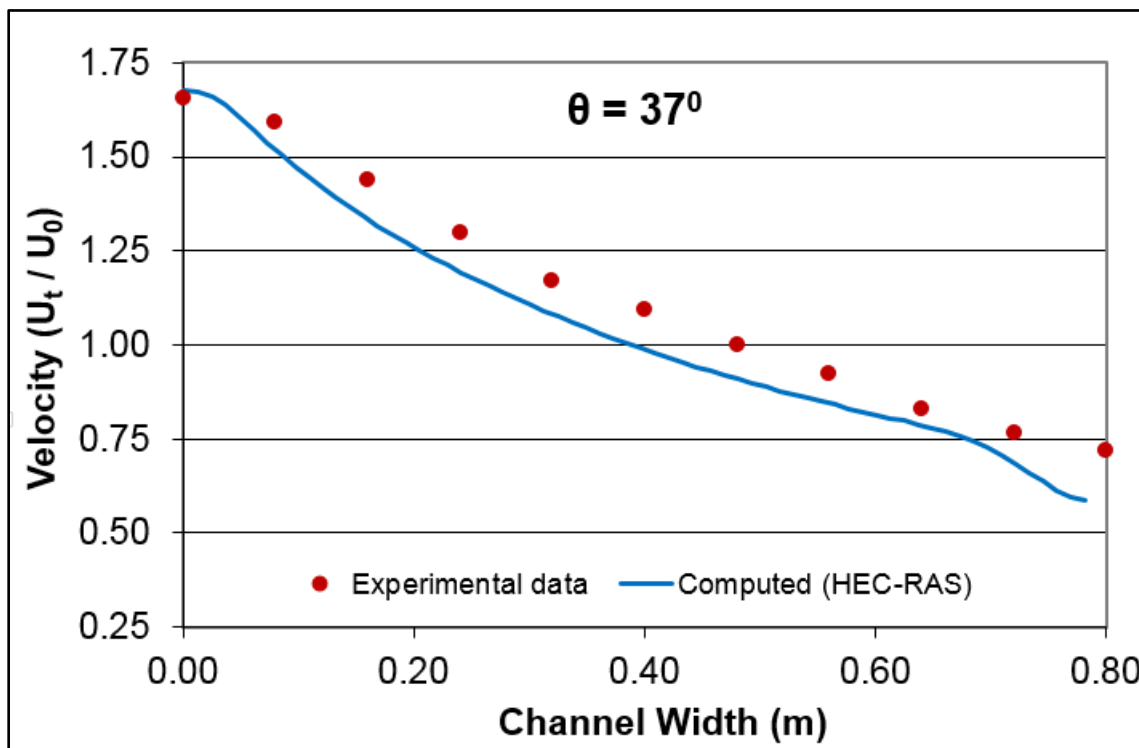


Figure 4-56. Velocity Profile (computed and experimental), at Section A-B in Figure 4-55
(with entrance velocity $U_0 = 0.265$ m/s)

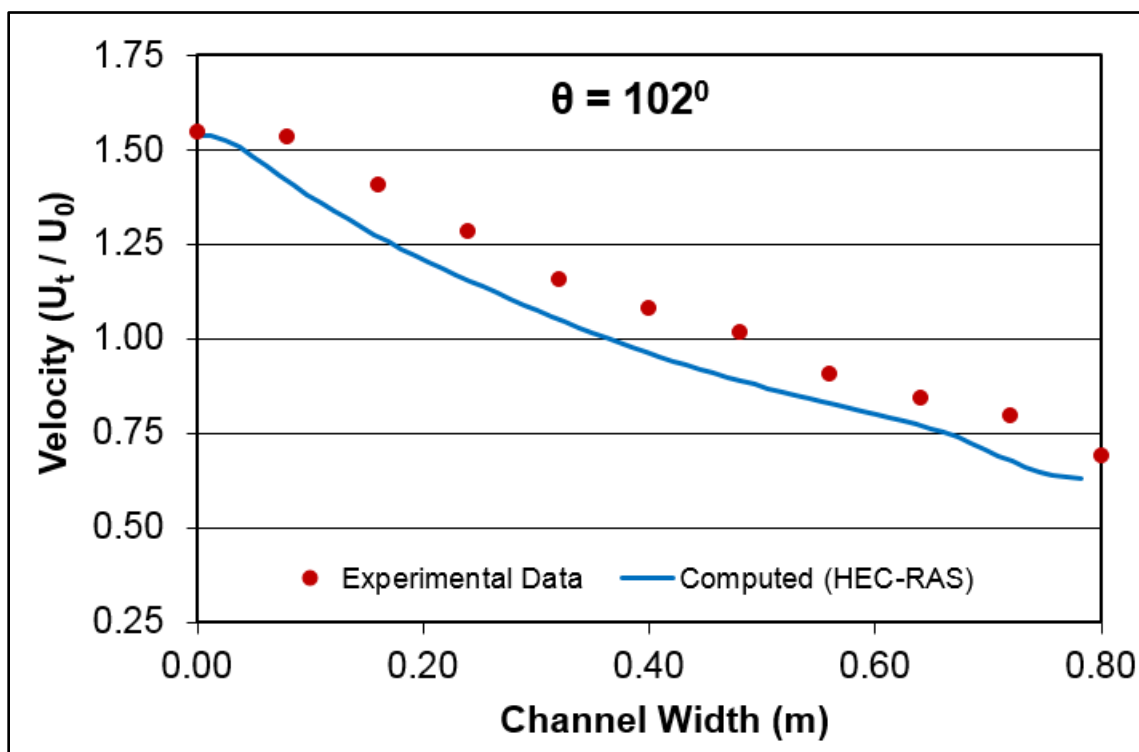


Figure 4-57. Velocity Profile (computed and experimental), at Section C-D in Figure 4-55
(with entrance velocity $U_0 = 0.265$ m/s)

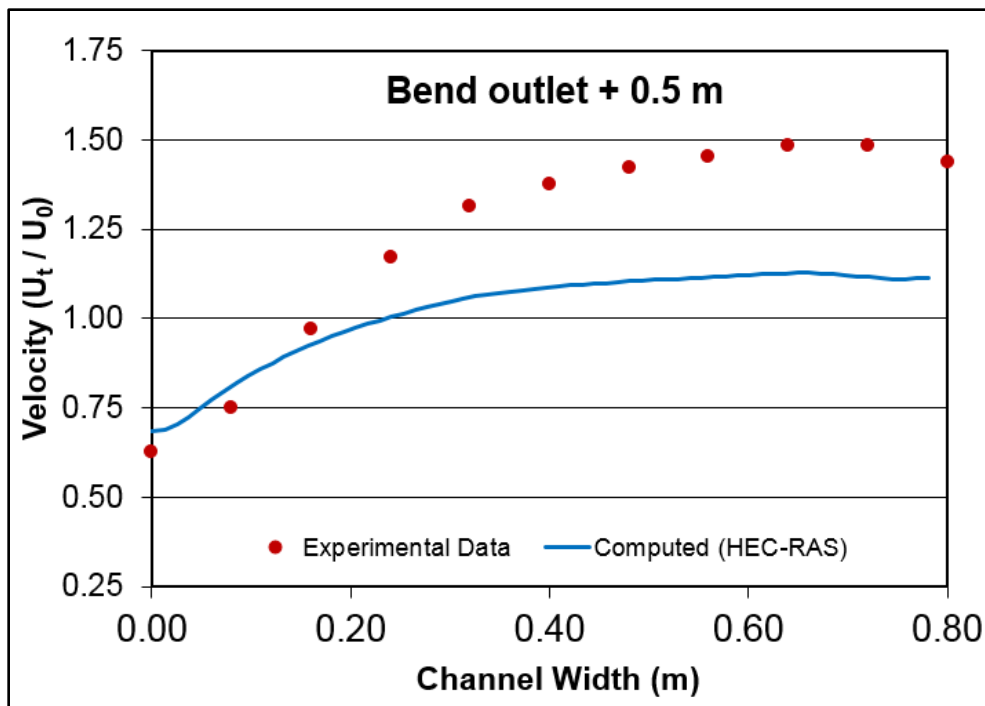


Figure 4-58. Velocity Profile (computed and experimental), at Section E-F in Figure 4-55
(with entrance velocity $U_0=0.265$ m/s)

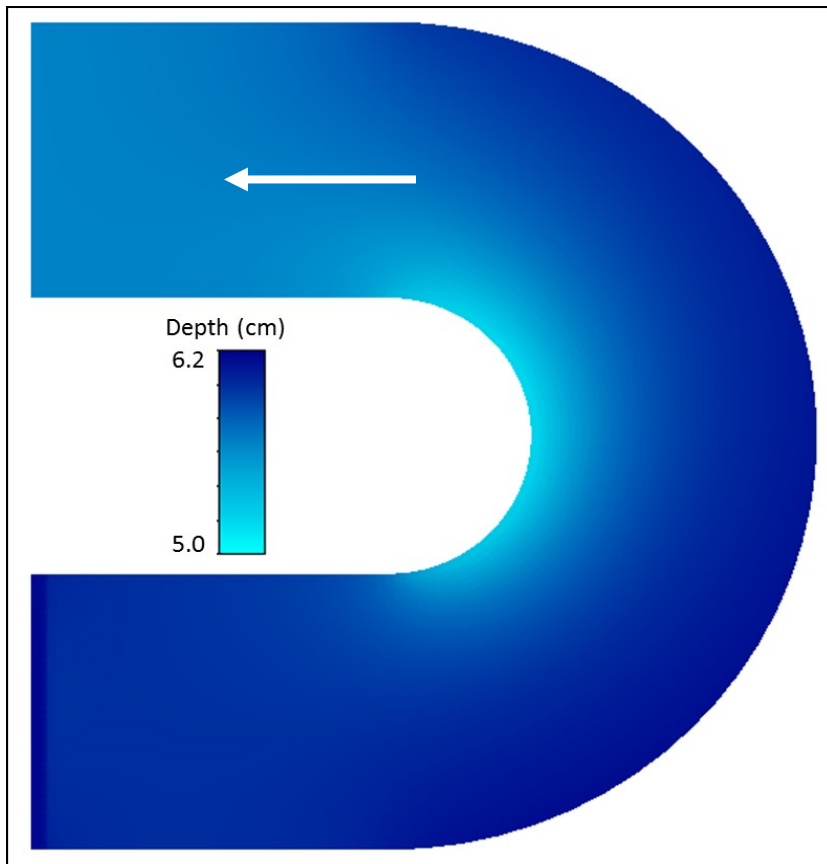


Figure 4-59. Depth (computed by HEC-RAS), with Deeper Depths along Outside of Bend (super-elevation)

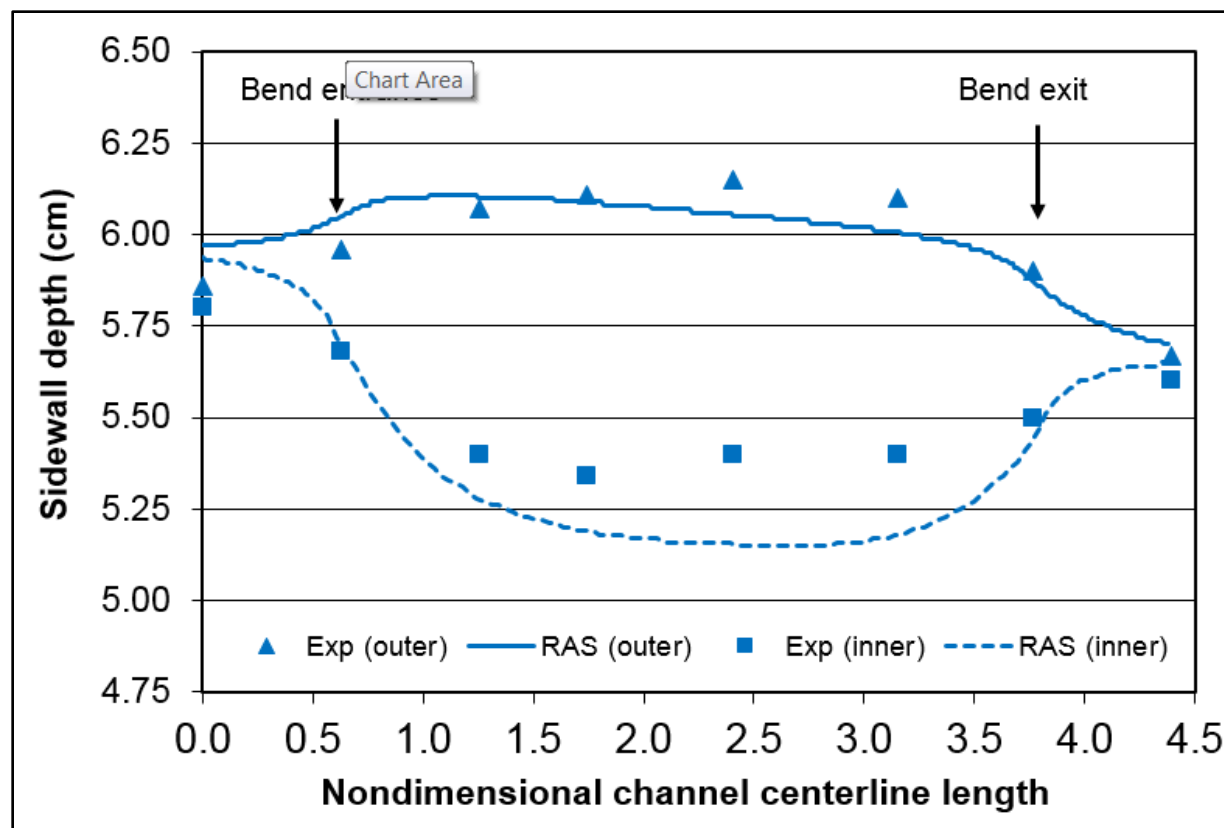


Figure 4-60. Sidewall Depth (computed and experimental) Showing Super-Elevation

References

1. Leschziner, 1979. Leschziner, Michael A. and Rodi, Wolfgang. *Calculation of strongly curved open channel flow*. Journal of the Hydraulics Division, ASCE, Volume 105, No. 10, pages 1297-1314. 1979.
2. Molls, 1995. Molls, Thomas R. and Chaudhry, M. Hanif. *Depth-averaged open-channel flow model*. Journal of Hydraulic Engineering, ASCE, Volume 121, Issue 6, pages 453-465. June 1995.
3. Rozovskii, 1957. Rozovskii, I.L. *Flow of water in bends of open channels*. Kiev, Academy of Sciences of the Ukrainian SSR, Israel Program for Scientific Translations. Available from the Office of Technical Services, U.S. Dept. of Commerce, Washington, DC. 1957.

4.3.5 Sudden Dam Break in a Rectangular Flume

Overview

The purpose of the test case is to validate HEC-RAS for simulating flow and stage from an extreme dam breach scenario. This test case is an almost instantaneous release of a wall of water in a rectangular flume on a slope. The downstream portion of the flume was dry, while the upstream was a reservoir full of water blocked by a gate. The gate was extracted from the flume

with a spring loaded arm, which made it an almost instantaneous release of the vertical wall of water. Model results are compared with measured depths of water in the flume, both downstream and upstream from the gate. Data is also measured at various time frames from the release of the gate.

Problem and Data Description

The experiments (WES, 1960) were conducted in a 4 foot wide wooden flume that was 400 feet long (Figure 4-61). The slope of the flume was set at 0.005. Water was impounded at Station 200 with a gate to a depth of 1.0 feet. Due to the material used to construct the experiment, low roughness values were used within the HEC-RAS model. The left wall of the flume was made of plastic coated wood. While the right wall of the flume, from Station 172 to 208, was fabricated out of glass panels. To simulate a near instantaneous dam breach, the dam was made from an aluminum panel, and was attached to a 100 pound weight by a pulley system. The 100 pound weight would be released and the gate would be released from the wall of water vertically in around 1/30 of a second.

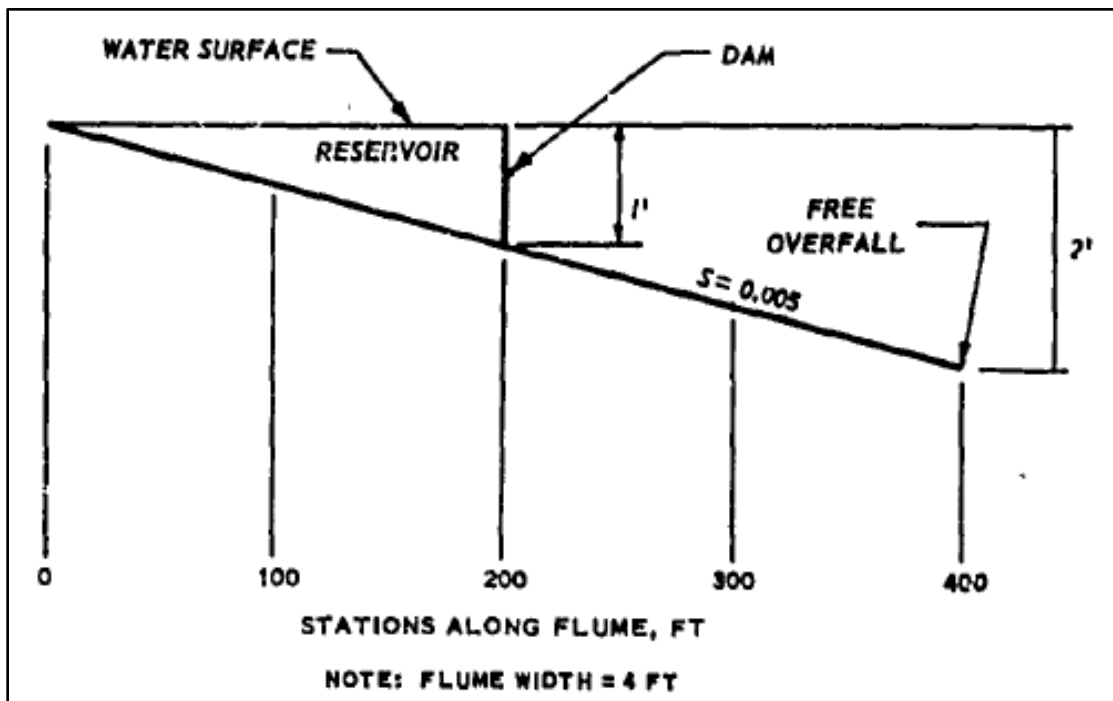


Figure 4-61. Schematic Diagram of the Test Flume

The following is a listing of the data to describe this problem:

- Bottom width, $B = 4.0$ feet
- Bed slope, $S = 0.005$
- Depth, $D = 1.0$ feet at Station 200

While twelve different experiments were performed under this research work, this test with HEC-RAS is a comparison of just one of the instantaneous breaches. The observed results measurements for Experiment 1.1, were used in this verification analysis and are shown in Figure 4-62.

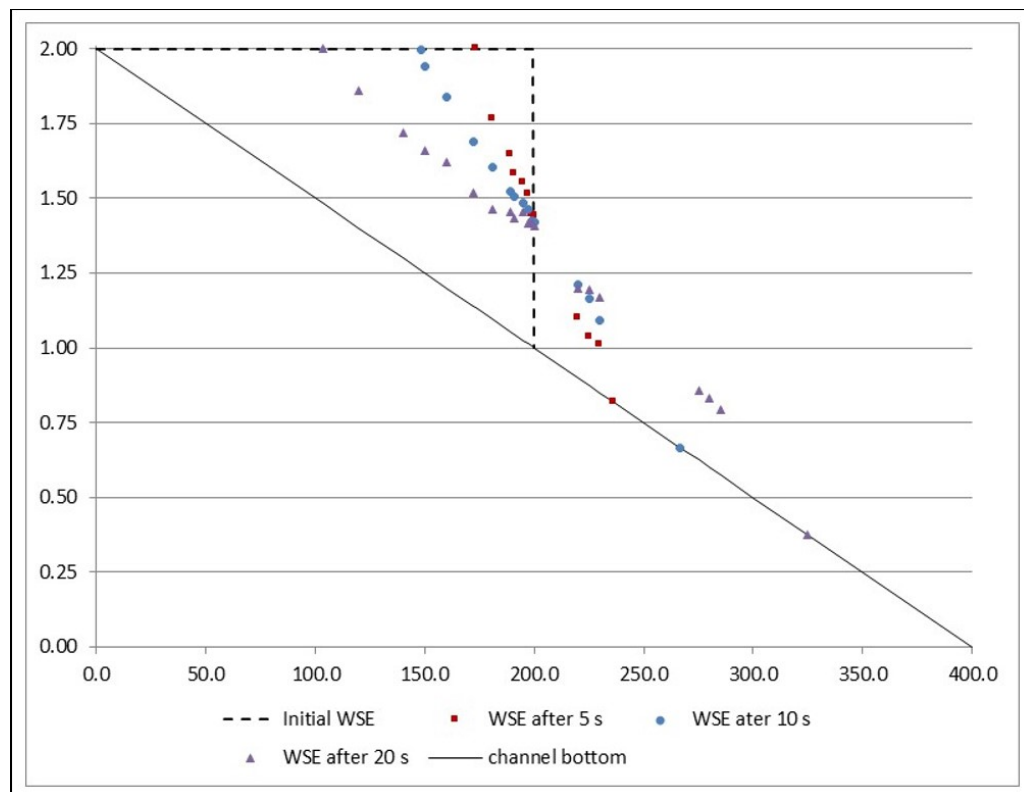


Figure 4-62. Measured Water Surface Elevations for the Instantaneous Dam Break Flume Experiment

Model Setup

An HEC-RAS 2D model was developed for this dataset with a computational domain of five feet wide (in order to fully capture flume walls) and 400 feet long. A constant grid resolution 0.2 x 0.2 foot cells was used in order to get approximately 20 cells across the flume (Figure 4-63). A flow boundary condition was specified at the upstream end of the system and a normal depth boundary condition with a constant energy slope of 0.005 was used at the downstream end. A profile line for extracting water surface elevations was laid out in the center of the flume for the entire length of the flume.

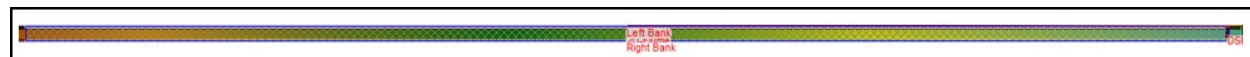


Figure 4-63. Computational Grid for the Instantaneous Dam Break Experiments

Table 4-29 provides a list of the model specific values used for this test:

Table 4-29. Model Data for Sudden Dam Break Flume Experiment

Two Mesh Sizes (feet)	0.2 x 0.2 cells
Main channel, n	0.009 for the bottom 0.008 for the sides.
Initial Depth (feet) at Station 200	1.0
Time Step (second)	0.025
Theta	1.0
Eddy Viscosity Coefficient	none
Equation Set	SWE

Results and Discussion

The results from the 2D computations analysis were compared to the measured water surface elevations from the lab study at times 5, 10, and 20 seconds. Figure 4-64 displays a spatial plot of the computed water surface elevations versus the measured data for each of these three locations in time.

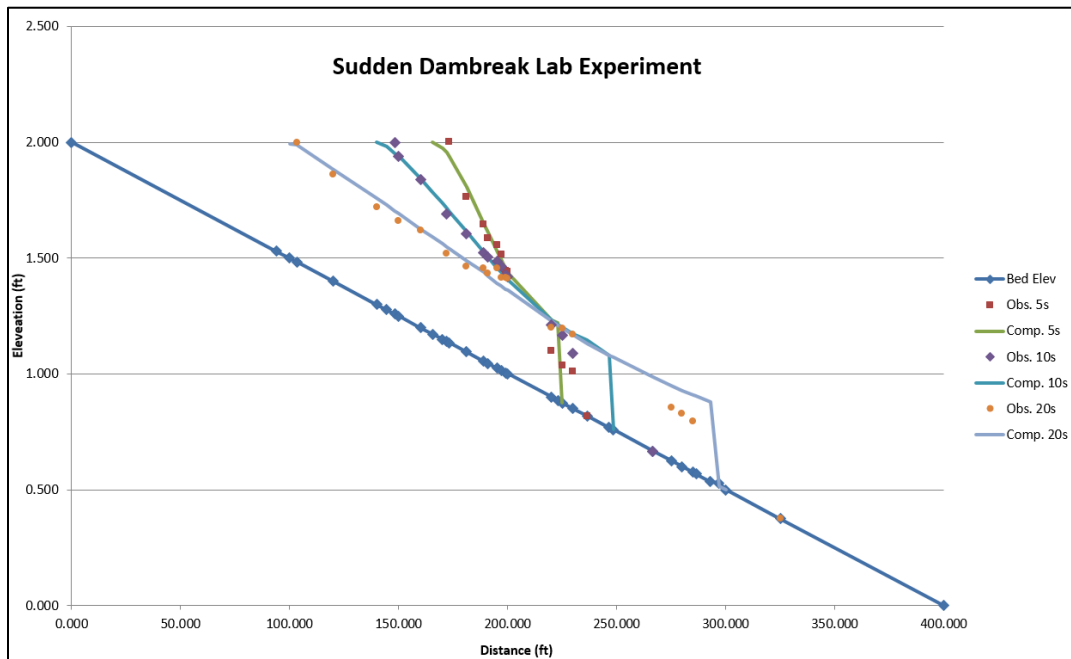


Figure 4-64. HEC-RAS Computed Results versus the Measured Water Surface Elevations

In general the HEC-RAS computed water surface elevations compare very well to the observed data. The upstream water surface elevations, and the tracking of the negative upstream wave are extremely accurate. The downstream water surface elevations track really well, except for the very front of the flood wave (wetting front). The measured wetting front moved downstream a little faster than what HEC-RAS computed.

References

1. WES, 1960. *Floods Resulting from Suddenly Breached Dams, Conditions of Minimum Resistance*. Paper No. 2-374, Report 1. U.S. Army Corps of Engineers, Waterways Experimentation Station, Vicksburg, Mississippi. February 1960.

4.3.6 Flow in a Channel Contraction

Overview

The purpose of this test case is to validate HEC-RAS for simulating subcritical flow in a channel with a straight-walled contraction. For a subcritical contraction, the flow accelerates through the contraction (and the velocity increases and depth decreases). In most HEC-RAS applications, inflow hydrographs are specified at upstream boundaries, however this case is simulated using

only stage boundary conditions. Thus, HEC-RAS must compute the channel flow from the upstream and downstream stage boundary conditions (the inflow is not directly specified). The HEC-RAS computed depths decrease through the contraction and compares favorably with the measured depths. The computed flow more closely matches the experimental value when the upstream stage boundary condition is slightly increased above the experimental depth. The experimental data was reported in Ippen (1951) and later compared with numerical model results by Molls (1995).

Problem and Data Description

This experiment was conducted in a concrete flume consisting of two straight rectangular upstream and downstream channel sections joined by a 4.75 foot long straight-walled contraction. The upstream section was two feet wide, while the downstream section was one foot wide. The contraction walls were angled in at six degrees. The experimental data reported by Ippen (1951) consisted of a water surface contour plot and the measured flow rate (velocities were not acquired). Table 4-30 describes the specifications of the experiment.

Table 4-30. Specifications of the Channel Contraction Flume Experiment

Item	Value
Bottom width, B (feet)	2 feet (upstream); 1 foot (downstream)
Bed slope, S_0	≈ 0
Channel roughness, n	0.01 (smooth)
Upstream boundary condition, stage, h (feet)	0.55
Downstream boundary condition, stage, h (feet)	0.36
Channel flow, Q (cfs)	1.45

Model Setup

The computational mesh for this test case, shown in Figure 4-65, consisted of a one foot long upstream and downstream rectangular channels connected with a 4.75 foot long straight-walled contraction. The upstream channel was two feet wide and the downstream channel was one foot wide. The contraction walls were angled in at six degrees. The mesh cell size was 0.1 feet (with twenty cells across the upstream channel and ten cells across the downstream channel). At the upstream inlet boundary, a constant depth of 0.55 feet was specified (resulting in subcritical flow). At the downstream outlet boundary, a constant depth of 0.36 feet was specified (resulting in slightly supercritical flow). The cells were assigned a Manning's n value of 0.01. Table 4-31 lists the model-specific values and parameters used for this test.

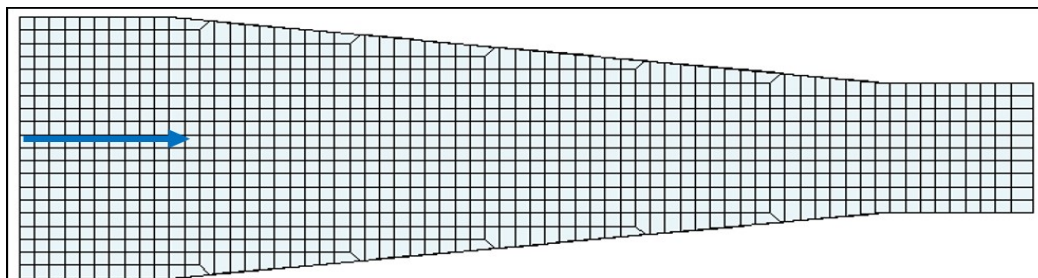


Figure 4-65. Computational Mesh for the Channel Contraction Test Case

Table 4-31. Model Specifications for the Channel Contraction Test Case

Item	Value
Mesh cell size (feet)	0.1
Manning's n	0.01
Time step (second)	0.025 ($Cr_{max} \approx 1$)
Theta	1.0
Eddy viscosity coefficient	0
Equation set	Full momentum

Results and Discussion

The HEC-RAS 2D computed results were compared to the measured depths and flow rate from the laboratory study. Figure 4-66 is a contour plot showing good agreement between the experimental and computed depth contours. Both experimental and computed contours show a relatively uniform depth across the channel with the depth decreasing through the contraction.

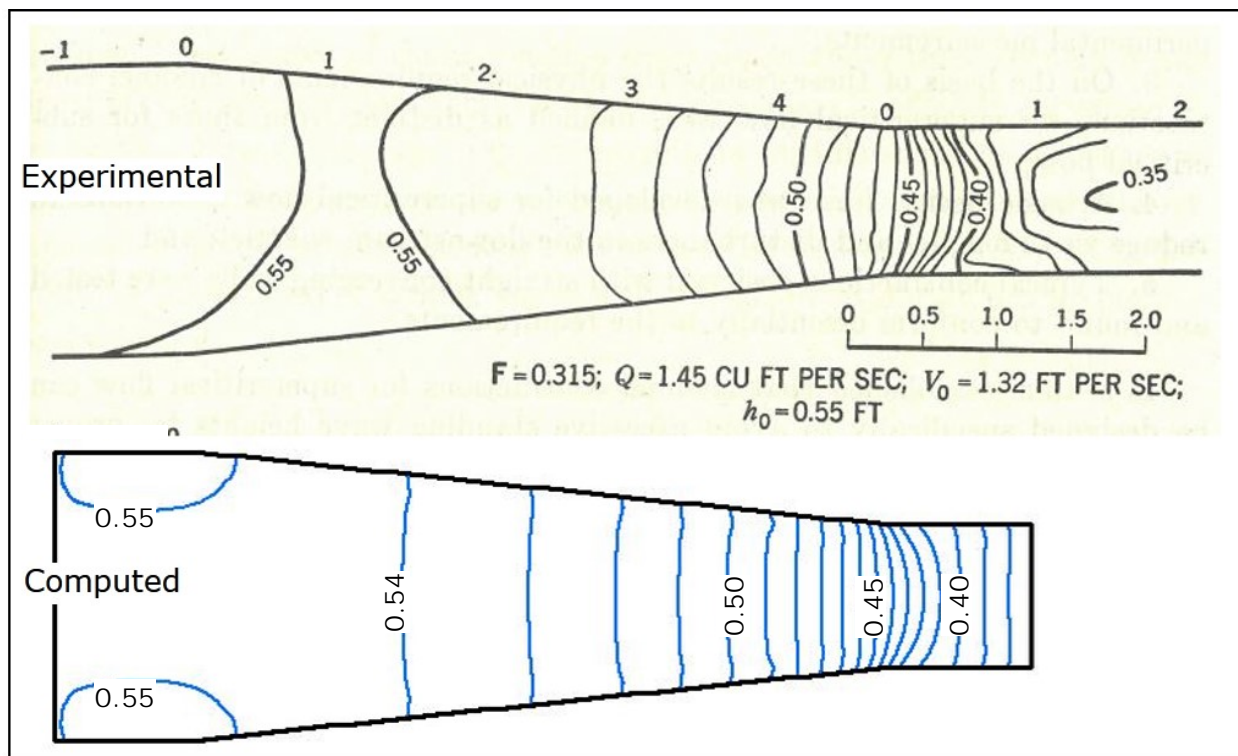


Figure 4-66. Depth Contour Plot (experimental and computed)

Furthermore, within the contraction the contours bow slightly toward the inlet boundary, while immediately downstream of the contraction the contours bow toward the outlet boundary. Figure 4-67 compares the experimental and computed channel centerline depth. The solid blue computed profile is based on the experimentally reported upstream depth of 0.55 feet and results in a computed flow rate of 1.34 cfs (slightly below the experimentally reported value of 1.45 cfs). Slightly increasing the upstream depth to 0.58 feet (the dashed blue line) generally improves the agreement between the computed and experimental depths through the contraction and results in a computed flow rate of 1.45 cfs (matching the experimentally reported value). Thus, the computed results through the contraction are sensitive to the upstream depth boundary condition (and increasing the upstream depth by 0.03 feet, or 0.36 in, improves the computed

solution). The accuracy of the upstream water surface at this location is a little suspect. So a difference of a few hundredths of a foot of measurement error is possible. 0.55 feet was used as the baseline upstream boundary condition because this is the depth associated with the most upstream experimental contour line. However, it should be noted that the inflow boundary of the HEC-RAS domain extends one foot upstream of the 0.55 feet contour (and the experimental depth was not reported at this location). The HEC-RAS computed depths shown in Figure 4-67 are consistent with other 2D model results (Molls, 1995).

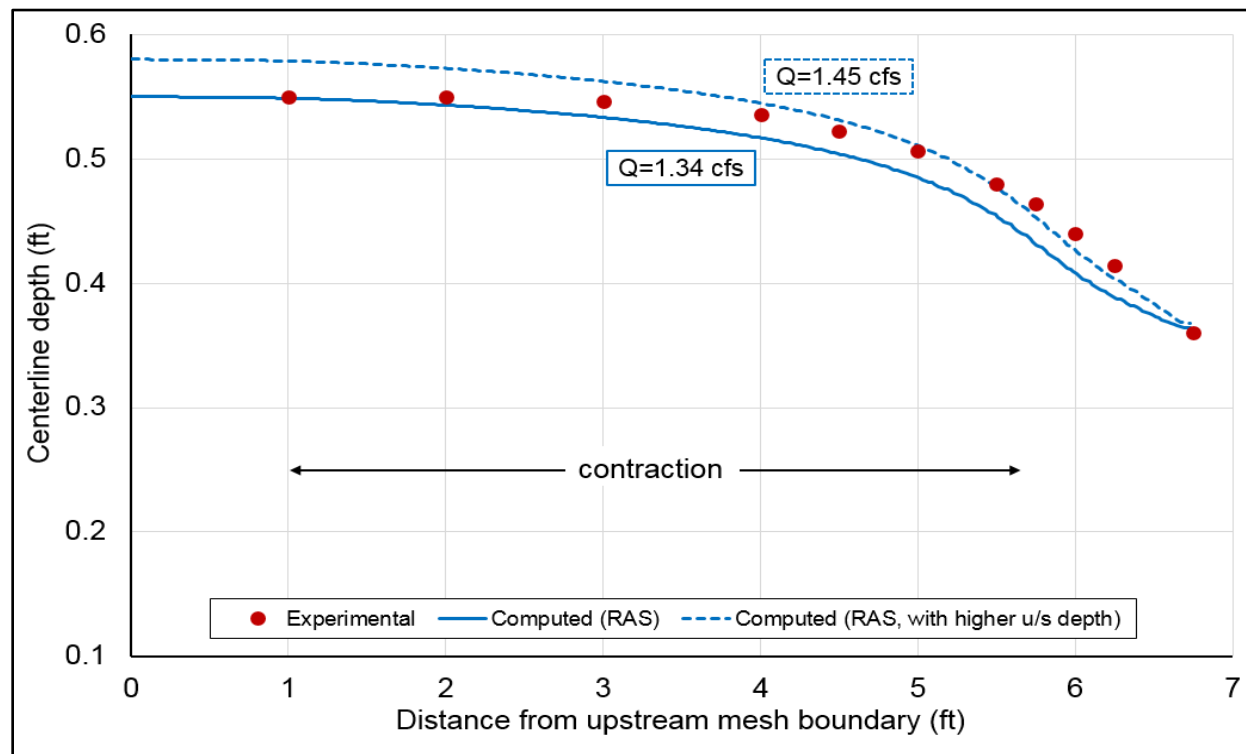


Figure 4-67. Channel centerline depth profile plot (experimental and computed), with computed flow rates shown in boxes. Solid and dashed lines are based on upstream depths of 0.55 and 0.58 feet, respectively.

References

1. Ippen, 1951. Ippen, A.T. and Dawson, J.H. *Design of channel contractions*. Transactions of the American Society of Civil Engineers, Volume 116, pages 326-346. 1951.
2. Molls, 1995. Molls, Thomas R. and Chaudhry, M. Hanif. *Depth-averaged open-channel flow model*. Journal of Hydraulic Engineering, ASCE, Volume 121, Issue 6, pages 453-465. June 1995.

4.3.7 Dam Break in a Channel with a 180-Degree Bend

Overview

The purpose of this test case is to validate HEC-RAS for simulating unsteady dam break flow. In this case, an instantaneous dam break creates a surge wave that travels through a rectangular

channel with a 180-degree bend. In most HEC-RAS applications, inflow hydrographs are specified at upstream boundaries and stages are specified at downstream boundaries. However, simulating this case only requires specifying the initial water surface elevation (higher in the upstream reservoir and lower in the channel). The water surface elevation difference between the reservoir and channel "drives" the flow (and upstream and downstream flow and stage boundary conditions are not required). Of importance in the analysis is the arrival time of the wave, the wave height, and the super-elevation as the wave proceeds around the bend. HEC-RAS computed results reproduce the wave height and super-elevation well (with higher depth along the outer wall). HEC-RAS also reproduces the movement of the wave down the channel. However, the computed wave arrival times are delayed by approximately 0.2 to 0.3 seconds when compared with the experimental data (the computed wave travels slightly slower than the experimental wave). The experimental data was reported in Bell (1989) and a subset of test cases were later published in Miller (1989) and Bell (1992).

Problem and Data Description

This experiment (Bell, 1989) was conducted in a laboratory facility that consisted of an upstream reservoir connected to a rectangular flume with a 180-degree bend. An instantaneous dam break failure was experimentally simulated by quickly removing a plate separating the reservoir from the flume. Movement of the flood wave was experimentally recorded using video cameras and presented as depth hydrograph and contour plots. The case considered here was referred to as Test 21 (with an initial reservoir depth of 1.167 feet, initial channel depth of 0.25 feet, and a Manning's n value of 0.0165). Table 4-32 describes the specifications of the experiment and Figure 4-68 displays a schematic of the test facility.

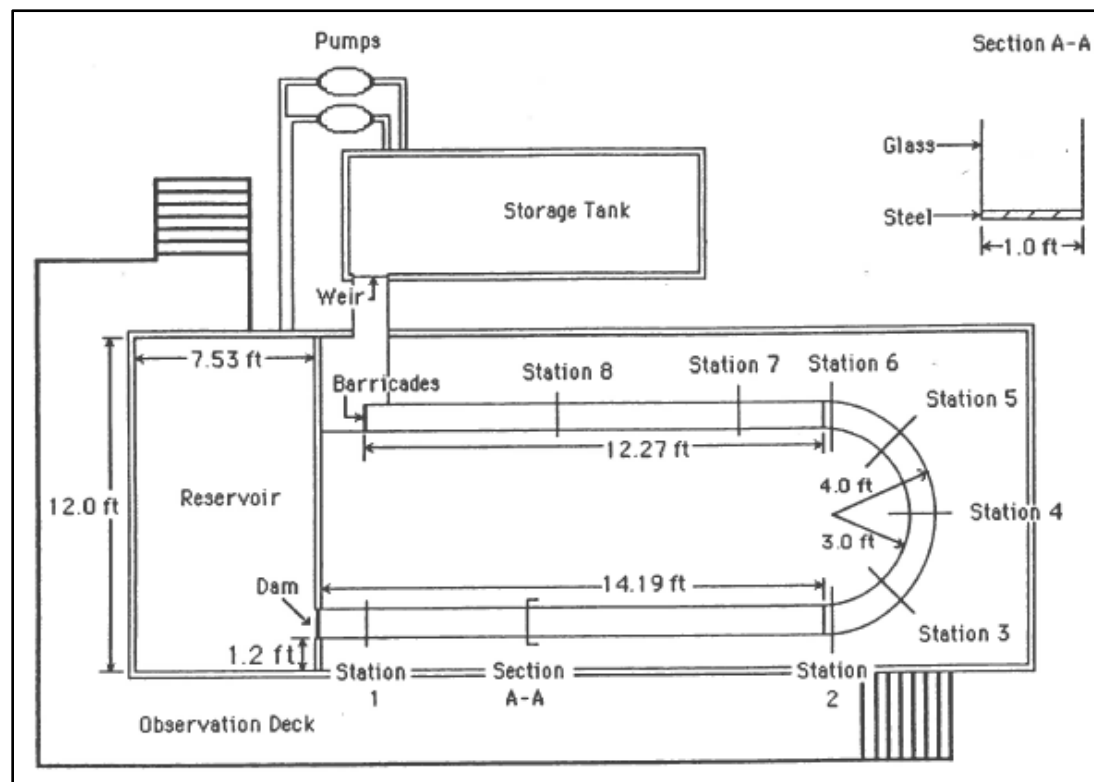


Figure 4-68. Test Facility Schematic: Dam Break in a Channel with a 180-degree Bend (Bell, 1989)

Table 4-32. Specifications of the Dam Break Experiment

Item	Value
Channel bottom width, B (feet)	1
Bed slope, S_0	≈ 0
Channel roughness, n	0.0165
Bend mean radius-to-width ratio	3.5 (moderately tight bend)
Initial reservoir depth, h_r (feet)	1.167
Initial channel depth, h_c (feet)	0.25

Model Setup

The computational mesh for this test case consisted of the reservoir and the downstream channel (represented as a single 2D flow area). The mesh cell size was 0.05 feet (with 20 cells across the channel). The initial reservoir water surface elevation was set to 1.167 feet, while the initial channel water surface elevation was 0.25 feet. For this test case, inflow and outflow boundary conditions were not utilized. The cells were assigned a Manning's n value of 0.0165. Table 4-33 lists the model-specific values and parameters used for this test.

Table 4-33. Model Specifications for the Dam Break Test Case

Item	Value
Mesh cell size (feet)	0.05
Manning's n	0.0165
Time step (second)	0.0143 ($Cr_{max} \approx 1$)
Theta	1.0
Eddy viscosity coefficient	0
Equation set	Full momentum

Results and Discussion

Once the plate representing the dam is removed, the dam break wave travels down the channel and reaches the downstream end of the channel in approximately eight seconds. The HEC-RAS 2D computed results were compared with measured wave heights and arrival times (depth hydrographs) at four locations in the channel (Stations 2, 4, 6, and 8 shown in Figure 4-68). In general, the computed and experimental depths compare favorably; however, the computed wave arrival times are delayed by approximately 0.2 to 0.3 seconds (the computed wave travels slightly slower than the experimental wave). This is believed to be due to numerical diffusion within the HEC-RAS 2D solution scheme. Station 2 is located at the bend entrance where the computed and experimental results are predominantly one-dimensional, with Figure 4-69 showing good agreement between the computed and experimental depth. Station 4 is located midway through the bend and exhibits super-elevation, with, Figure 4-70 showing good agreement between the computed and experimental inner and outer wall depths. Station 6 is located at the bend exit and also exhibits super-elevation; here, Figure 4-71 shows the computed inner wall depth is slightly higher than the experimental depth and the computed outer wall depth is slightly lower than the experimental depth. Station 8 is located 7.5 feet downstream of the bend exit where the flow is again predominantly one-dimensional, with Figure 4-72 showing the computed depth slightly higher than the experimental depth.

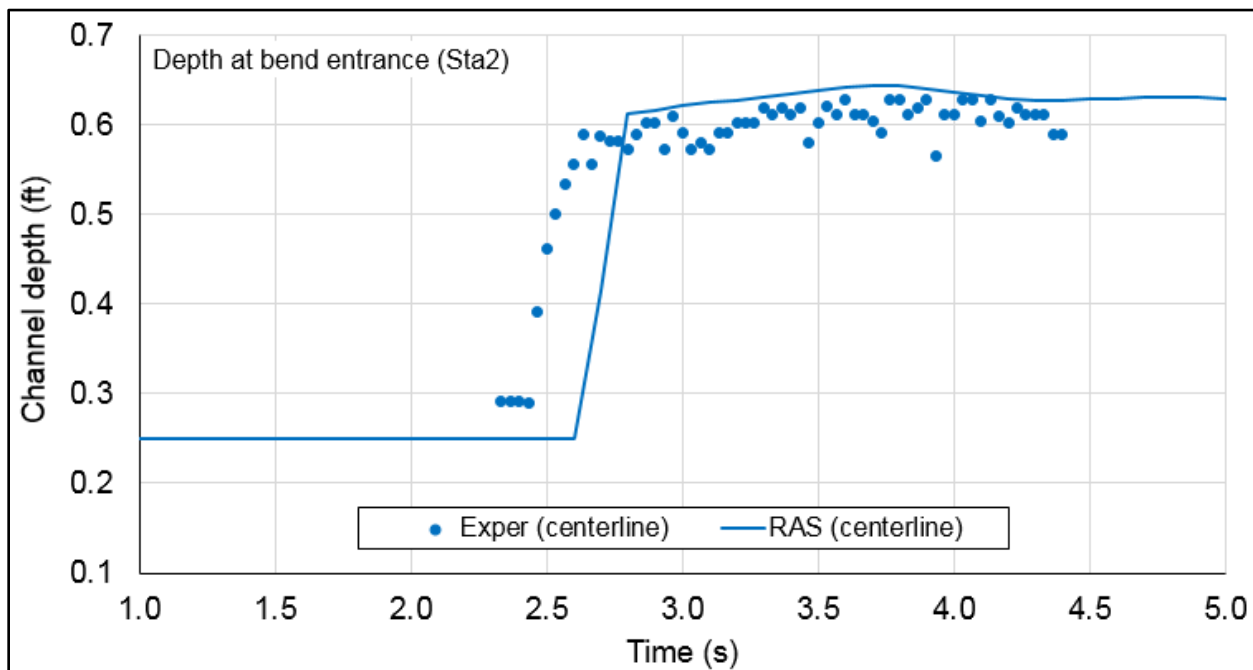


Figure 4-69. Depth Hydrograph (computed and experimental), at Station 2 in Figure 4-68 (bend entrance)

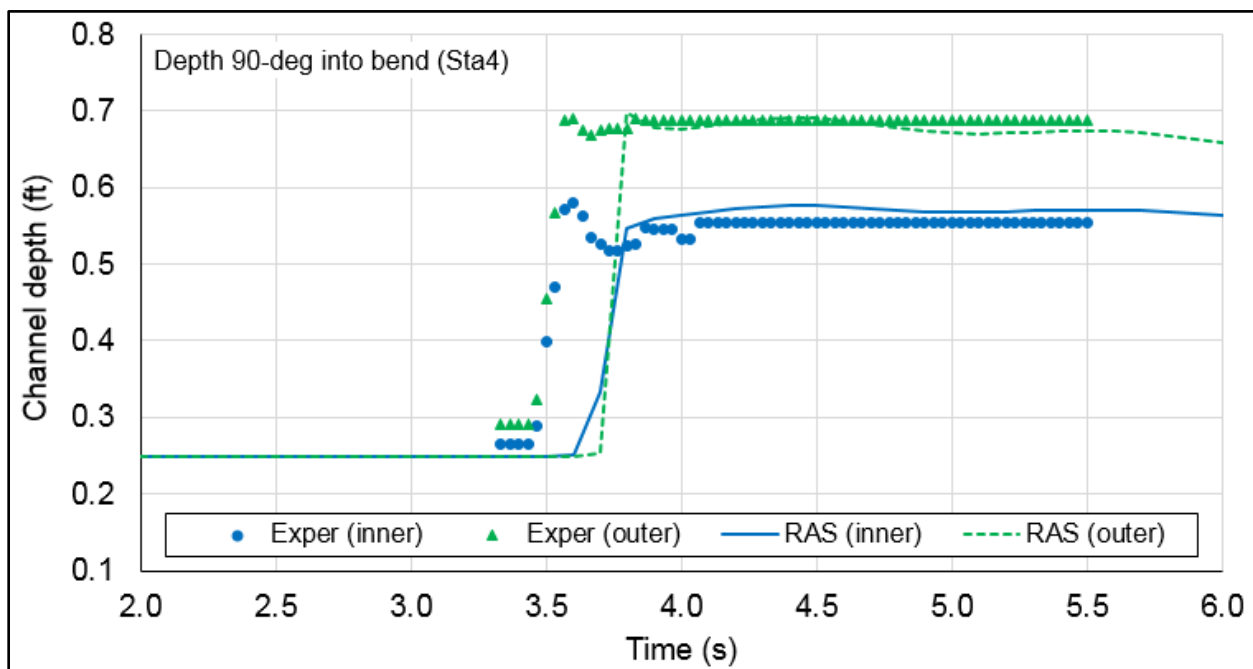


Figure 4-70. Depth Hydrograph (computed and experimental), at Station 4 in Figure 4-68 (midway through bend, 90-degrees)

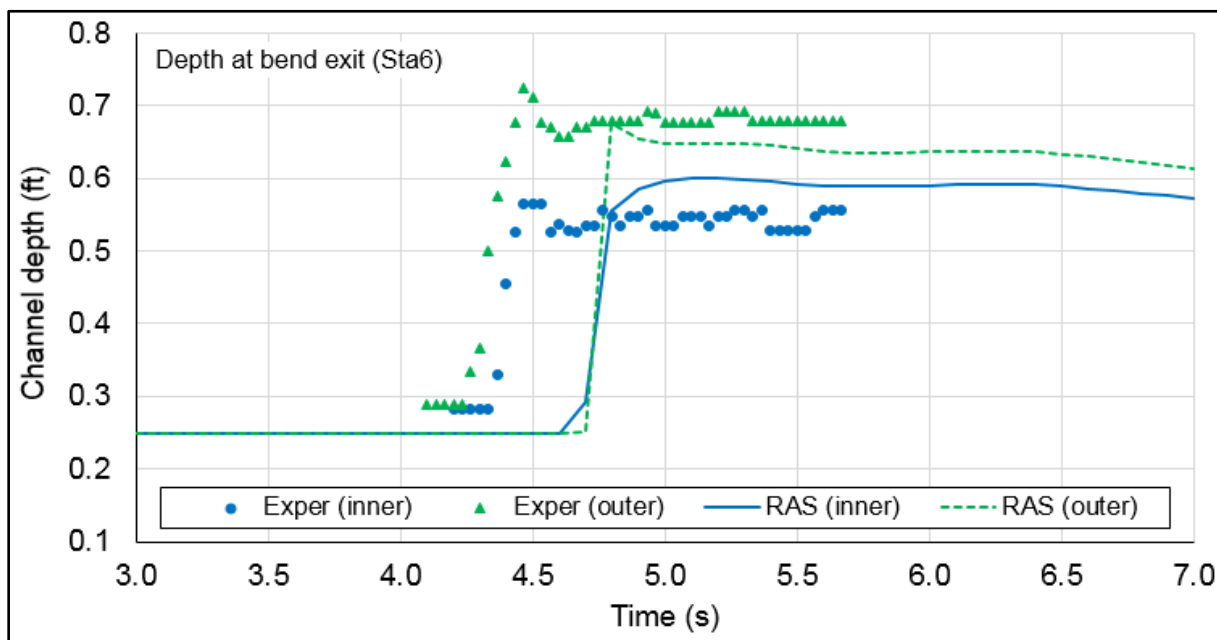


Figure 4-71. Depth Hydrograph (computed and experimental), at Station 6 in Figure 4-68 (bend exit)

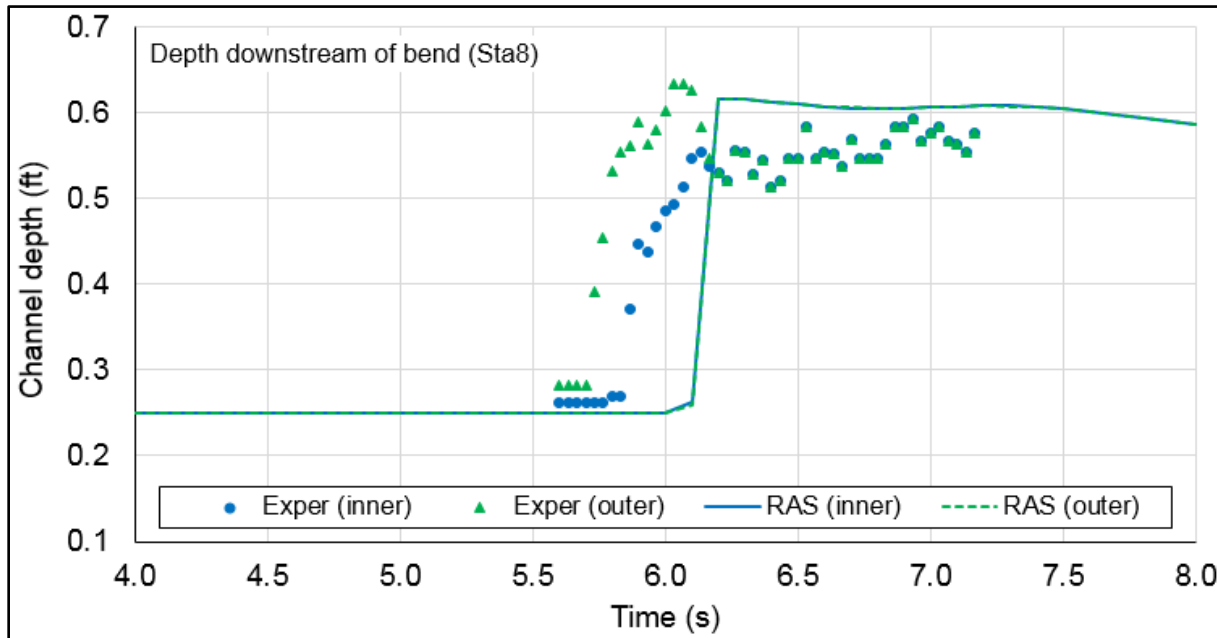


Figure 4-72. Depth Hydrograph (computed and experimental), at Station 8 in Figure 4-68 (7.5 feet downstream of bend exit)

References

1. Bell, 1989. Bell, S.W., Elliot, R.C., Chaudhry, M.H. *Experimental data on two-dimensional dam-break flows – Report*. Albrook Hydraulics Laboratory, Washington State University, Pullman, WA. 1989.

2. Bell, 1992. Bell, S.W., Elliot, R.C., Chaudhry, M.H. *Experimental results of two-dimensional dam-break flows*. Journal of Hydraulic Research, IAHR, Volume 30, Issue 2, pages 225-252. 1992.
3. Miller, 1989. Miller, Sky and Chaudhry, M. Hanif. *Dam-break flows in curved channel*. Journal of Hydraulic Engineering, ASCE, Volume 115, Issue 11, pages 1465-1478. November 1989.

4.3.8 Flow around a Spur-Dike

Overview

The purpose of this test case is to validate HEC-RAS for simulating subcritical flow in a channel with a spur-dike, or groin (a river-training structure with one end adjacent to the river bank and the other end projecting into the main flow). Spur-dikes are mainly used as bank protection structures because of the low-velocity eddy zone that is formed downstream of the spur. Thus, the flow downstream of the spur-dike is complicated due to the formation of the eddy zone (with reverse flow) and the presence of a shear layer resulting in large velocity gradients (between the main flow and the eddy zone). In this case, the turbulent stresses (controlled by the Eddy Viscosity Mixing Coefficient, D_T) influence the computed results in the eddy zone. The HEC-RAS model results compare favorably with measured velocities near the eddy zone. Furthermore, the length of the eddy zone (i.e., reattachment or recirculation length) predicted by HEC-RAS compares well with the length measured in the experiment. The experimental data was reported in Rajaratnam (1983) and later compared with numerical results by Tingsanchali (1990) and Molls (1995).

Problem and Data Description

This experiment was conducted in a smooth rectangular flume, 37 meters long and 0.915 meters wide. The spur-dike consisted of an aluminum plate, 3 mm thick and 150 mm long ($b = 150$ mm is used to denote the spur-dike length), projecting normally from the flume sidewall into the main flow path and extending above the water surface. Velocities and water surface profiles were measured at various locations near the spur-dike. The test case considered here was referred to as Experiment A1. Table 4-34 describes the specifications of the experiment.

Table 4-34. Specifications of the Spur-Dike Experiment

Item	Value
Bottom width, B (meter)	0.915
Spur (or groin), b (mm)	150 mm long x 3 mm thick
Bed slope, S_0	≈ 0
Channel roughness, n	0.01 (smooth)
Upstream boundary condition, flow, Q (cms)	0.043 with $U_0 \approx 0.252$ m/s
Downstream Boundary, stage, h (meter)	0.189

Model Setup

The computational mesh for this test case, shown in Figure 4-73, consisted of a 0.915 meter wide and 5.4 meter long channel with the spur-dike located 1.8 meters from the channel inlet. The mesh cell size was 0.015×0.015 meter. At the upstream inlet boundary, a constant flow of 0.043 cms was specified (resulting in an upstream channel velocity of $U_0 \approx 0.252$ m/s and $Fr_0 \approx 0.2$). At the downstream outlet boundary, a constant depth of 0.189 meters was specified. The Manning's n value was set to 0.01. The Eddy Viscosity Mixing Coefficient (D_T), which influences the computed result in the eddy zone, was adjusted to 2.0. Table 4-35 lists the model-specific values and parameters used for this test.

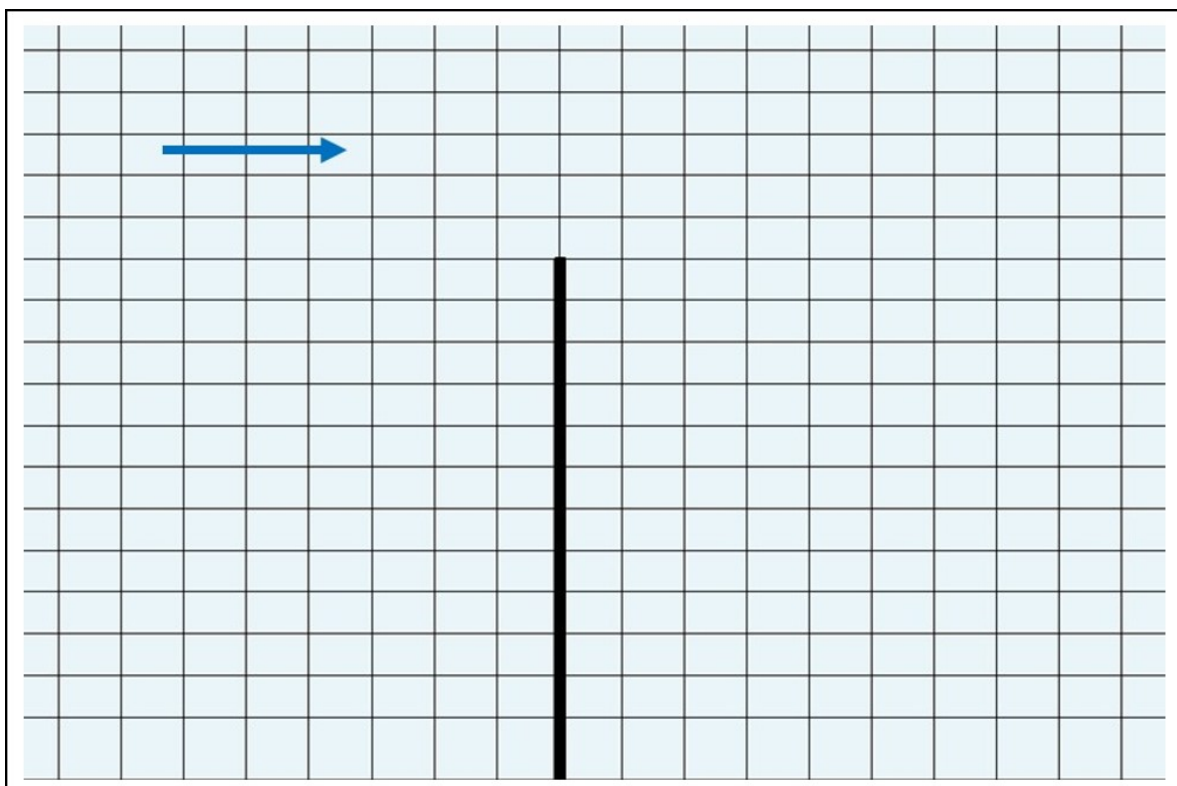


Figure 4-73. Computational Mesh for the Spur-Dike (zoomed-in near the spur-dike)

Table 4-35. Model Specifications for the Spur-Dike Test Case

Item	Value
Mesh cell size (meter)	0.015×0.015 m
Manning's n	0.01
Time step (second)	0.01 ($Cr_{max} \approx 1$)
Theta	1.0
Eddy viscosity coefficient	2.0
Equation set	Full momentum

Results and Discussion

The HEC-RAS 2D computed results are compared to the measured velocities and recirculation length from the laboratory study. Figure 4-74 is a velocity magnitude plot clearly showing the eddy zone with reverse flow (the low velocity blue region) downstream of the spur-dike. The

HEC-RAS computed eddy zone length (L_e) matches the experimentally observed value of 1.8 meters (L_e is influenced by D_T and the Manning's n value) very well, with a length slightly longer. Figure 4-74 also shows a low velocity region immediately upstream of the spur-dike and increased velocities over the spur, as the flow is deflected toward the opposite channel side wall. Figure 4-75 through Figure 4-78 are longitudinal velocity magnitude profile plots at the locations shown in Figure 4-75 ($y/b=1.5, 2, 3$, and 4). Upstream of, and immediately over, the spur the HEC-RAS computed velocities compare well with the experimental data. However, downstream of the spur-dike, the computed velocities are lower than the experimental velocities for location $y/b=2$, and slightly lower at $y/b=3$. Location $y/b = 1.5$ and 4 looks very good. The HEC-RAS lower computed velocities shown in Figure 4-76 (at $y/b=2$) are consistent with other 2D model results (Molls, 1995).

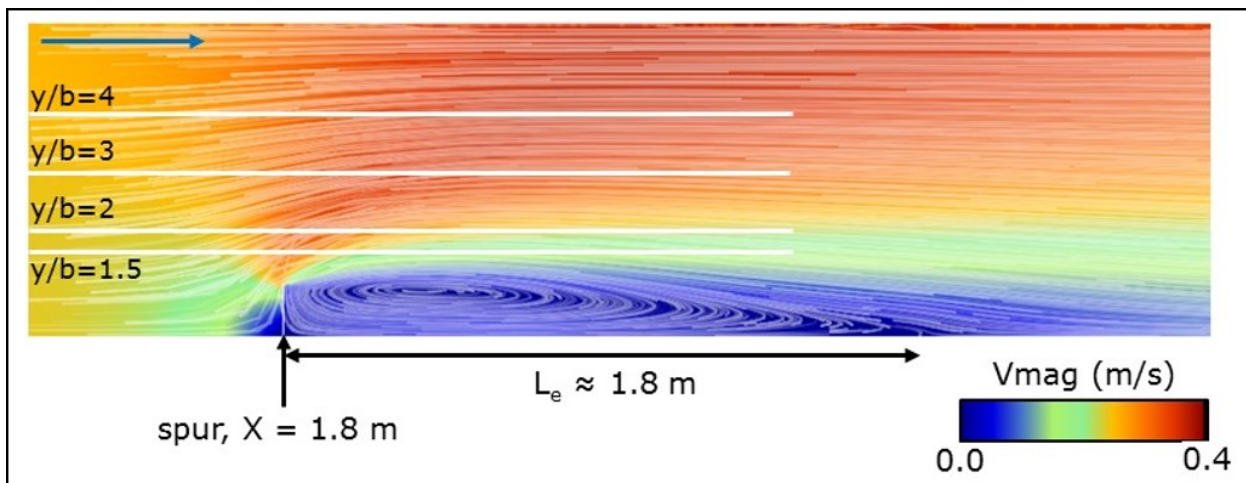


Figure 4-74. Computed Velocity Magnitude Plot with Particle Traces, the Blue Shaded Eddy Zone is Clearly Evident Downstream of the Spur-Dike

References

1. Molls, 1995. Molls, Thomas R. and Chaudhry, M. Hanif. *Depth-averaged open-channel flow model*. Journal of Hydraulic Engineering, ASCE, Volume 121, Issue 6, pages 453-465. June 1995.
2. Rajaratnam, 1983. Rajaratnam, Nallamuthu and Nwachukwu, Benjamin A. *Flow near groin-like structures*. Journal of Hydraulic Engineering, ASCE, Volume 109, Issue 3, pages 463-480. January 1983.
3. Tingsanchali, 1990. Tingsanchali, Tawatchai and Maheswaran, Selvaratnam. *2-D Depth-Averaged Flow Computation near Groyne*. Journal of Hydraulic Engineering, ASCE, Volume 116, Issue 1, pages 71-86. January 1990.

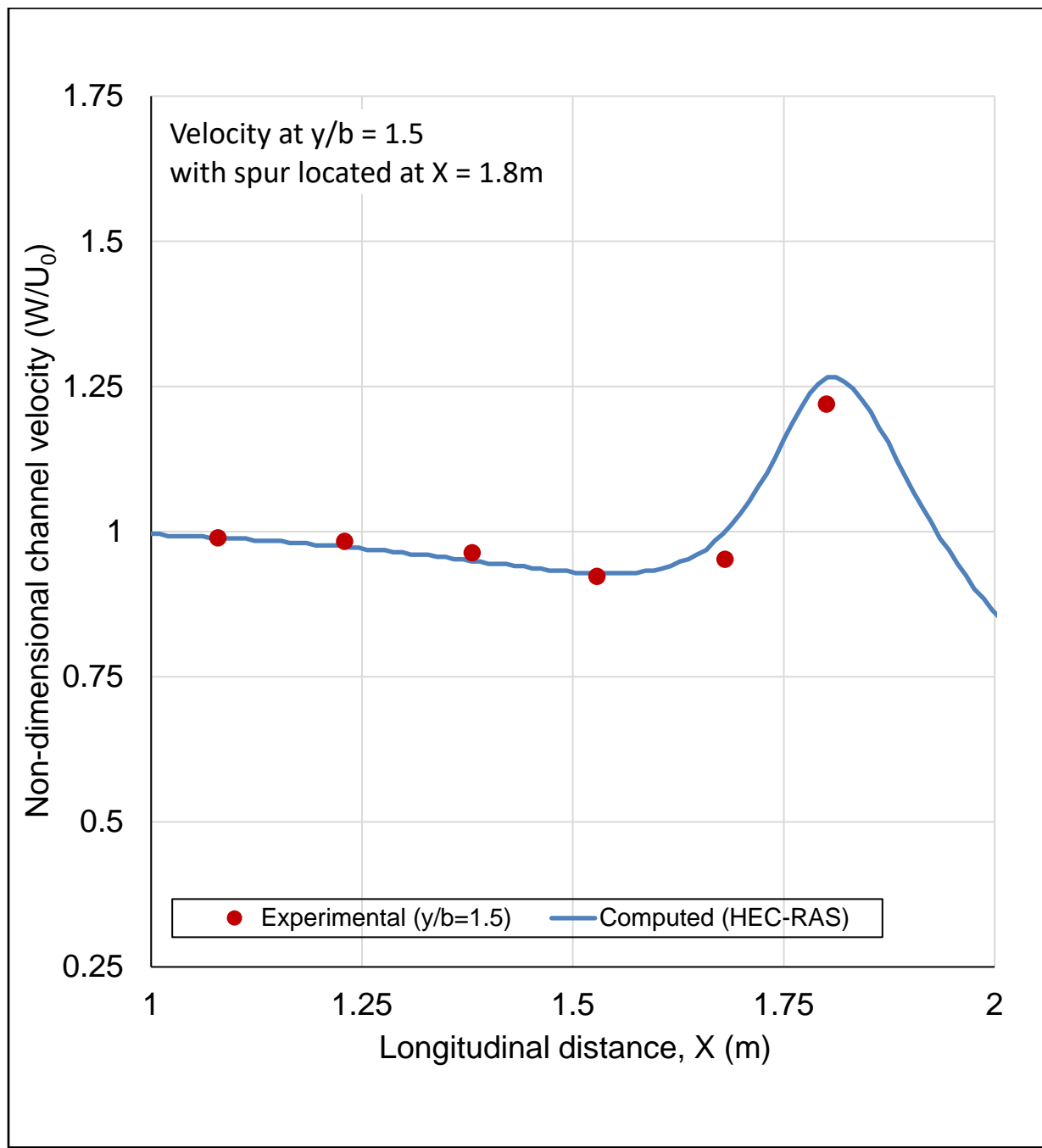


Figure 4-75. Longitudinal Velocity Profile (computed and experimental), at $y/b=1.5$ in Figure 4-74
(where $U_0=0.242$ m/s is the average upstream channel velocity)

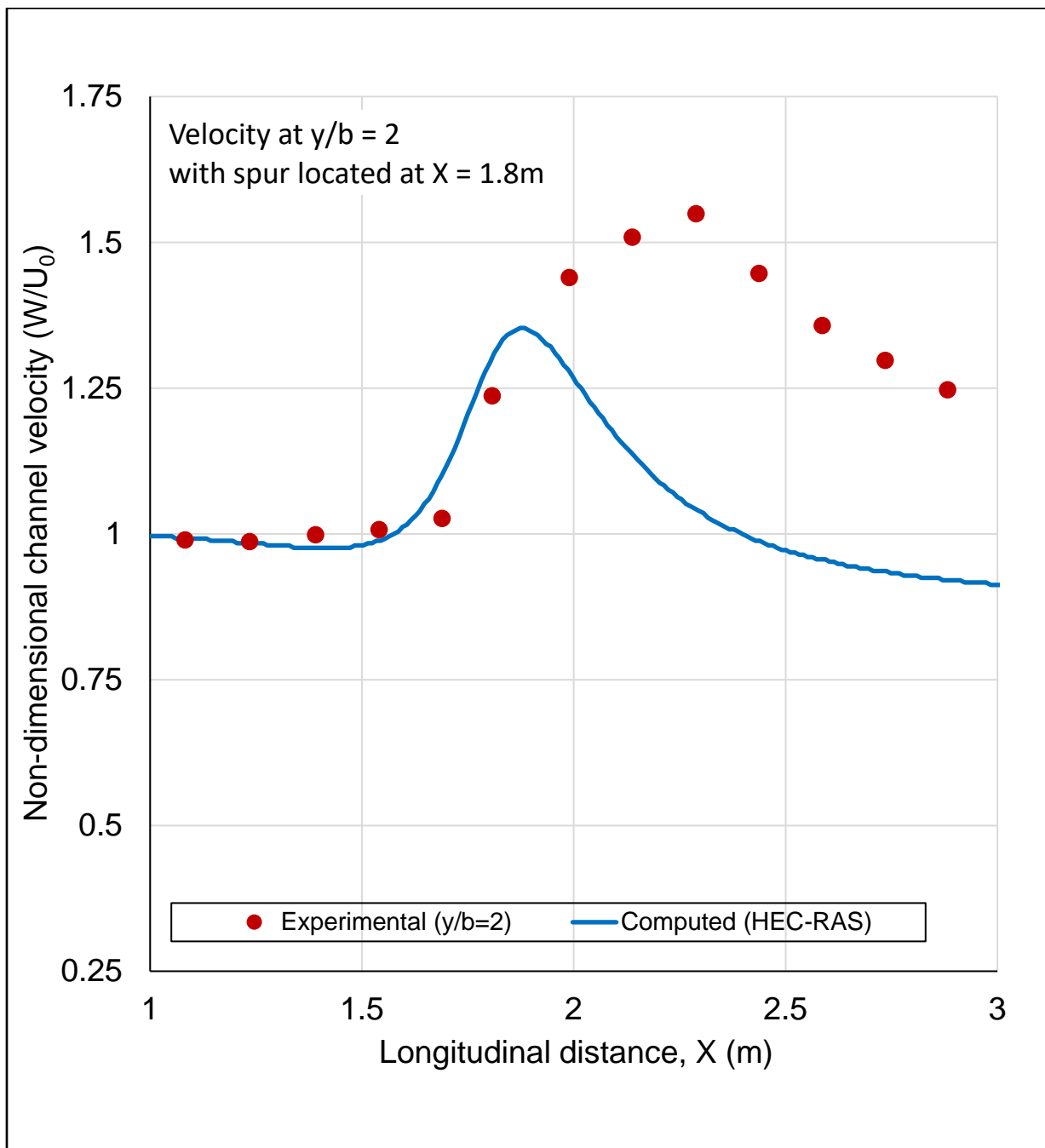


Figure 4-76. Longitudinal Velocity Profile (computed and experimental), at $y/b=2$ in Figure 4-74 (where $U_0=0.242$ m/s is the average upstream channel velocity)

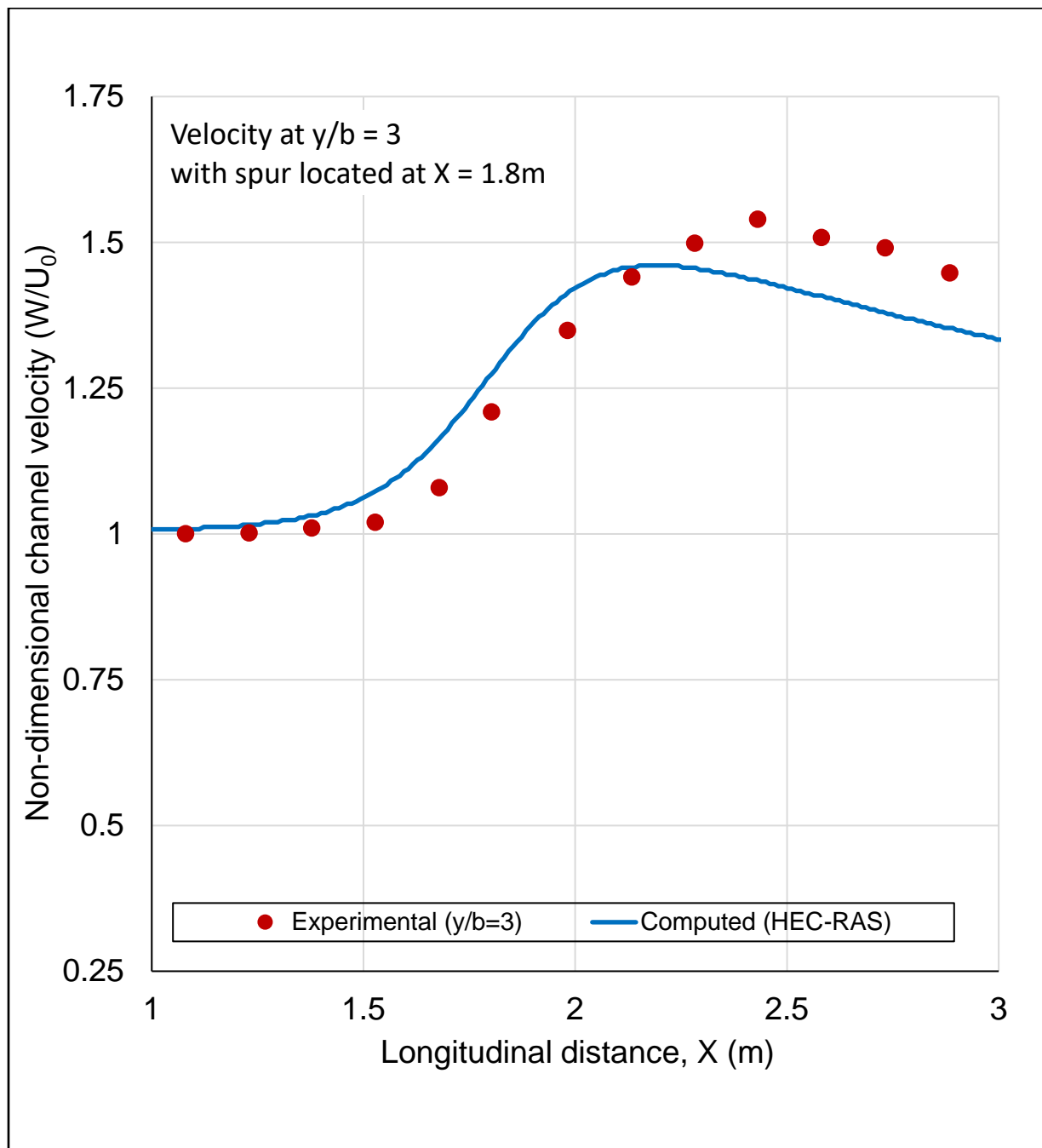


Figure 4-77. Longitudinal Velocity Profile (computed and experimental), at $y/b=3$ in Figure 4-74 (where $U_0=0.242 \text{ m/s}$ is the average upstream channel velocity).

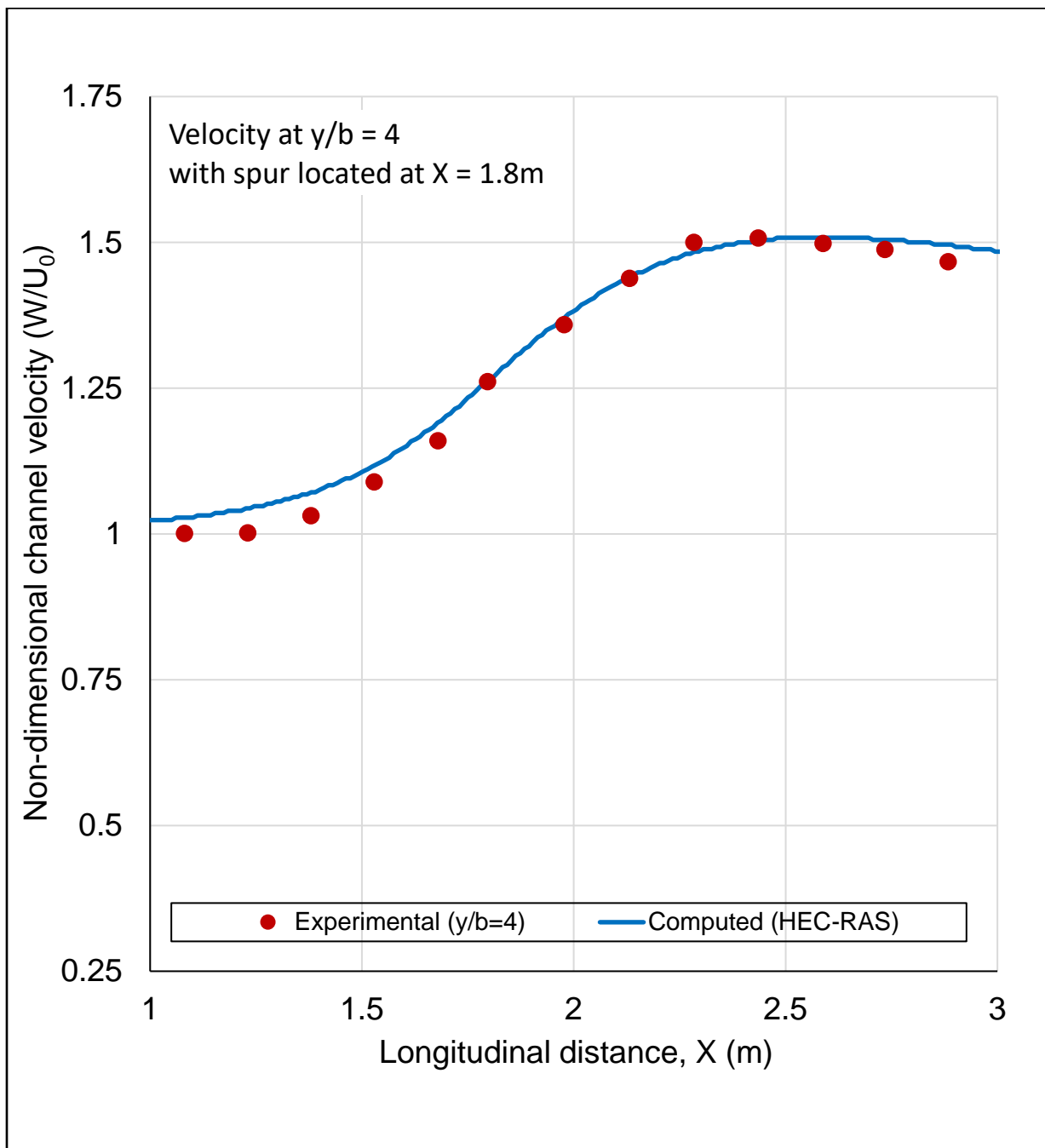


Figure 4-78. Longitudinal Velocity Profile (computed and experimental), at $y/b=4$ in Figure 4-74 (where $U_0=0.242$ m/s is the average upstream channel velocity).

4.3.9 Flow through a Bridge

Overview

The purpose of the test case is to validate HEC-RAS 2D for simulating flow through a bridge opening. The laboratory flume had left and right rectangular overbanks and a trapezoidal main channel. Abutments and bridge piers were located in the middle of the test reach. HEC-RAS 2D model results are compared to measured laboratory piezometer readings. The HEC-RAS model was developed assuming a 20-scale undistorted representation of the laboratory flume.

Problem and Data Description

The experimental flume was constructed in the Robert L. Smith Water Resources Laboratory at the University of Kansas (KU). The flume shown in Figure 4-79 had a 24-foot-long test region with the middle 7.5 feet containing piezometers located in the left sidewall of the trapezoidal main channel. The 20-scale HEC-RAS model dimensions are also shown in parenthesis. The bed was horizontal and constructed of marine grade plywood. The abutments were concrete and the four bridge piers (not shown in Figure 4-79) were 5/8-inch wood dowels. A bridge deck was also constructed of wood. All wooden surfaces were epoxy painted. The piezometer locations are shown in Figure 4-80 which shows both laboratory and 20-scale HEC-RAS model stations. Figure 4-81 shows the measured hydraulic grade line (HGL) for one of the experiments. The measured n-value of the flume was 0.0141. Froude number similarity gives an n-value of 0.0233 for the 20-scale HEC-RAS model as shown in Figure 4-79.

$$n_{model} = 20^{1/6} n_{lab} \rightarrow n_{model} = 1.648(0.0141) = 0.0233 \quad (4-25)$$

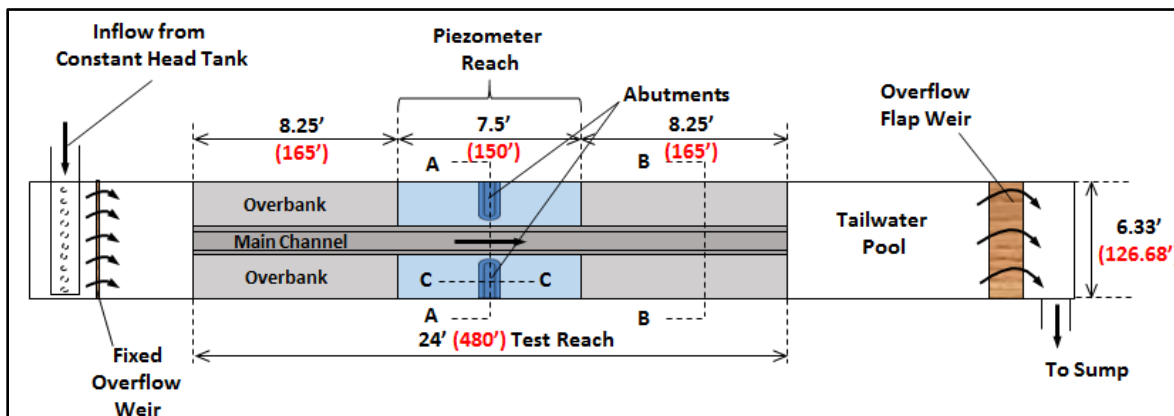


Figure 4-79. Plan View of Laboratory Flume (20-scale HEC-RAS model Dimensions in parenthesis)

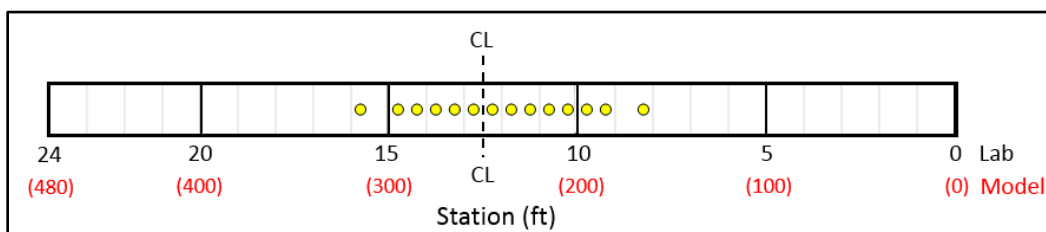


Figure 4-80. Piezometer Locations

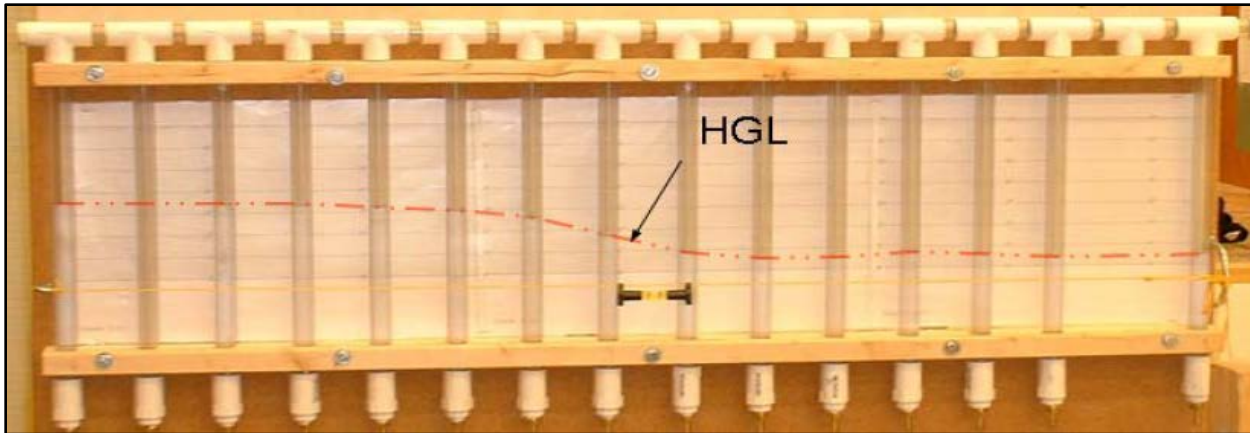


Figure 4-81. Piezometer Surface for an Experiment

Section A-A from Figure 4-79 is shown in Figure 4-82a in 20-scale model dimensions for the laboratory as a plot from a 1D HEC-RAS model. Figure 4-82b shows the bridge cross section used in the HEC-RAS model. Sections B-B and C-C from Figure 4-79 are shown in Figure 4-83 and Figure 4-84, respectively. The 2D HEC-RAS model does not use the bridge deck in Figure 4-82a since the water did not reach the low steel elevation for any of the experiments. Table 4-36 gives the cross section and bridge values needed to construct a 1D HEC-RAS geometry file. Such a model was developed and tested as reported by Parr (2010).

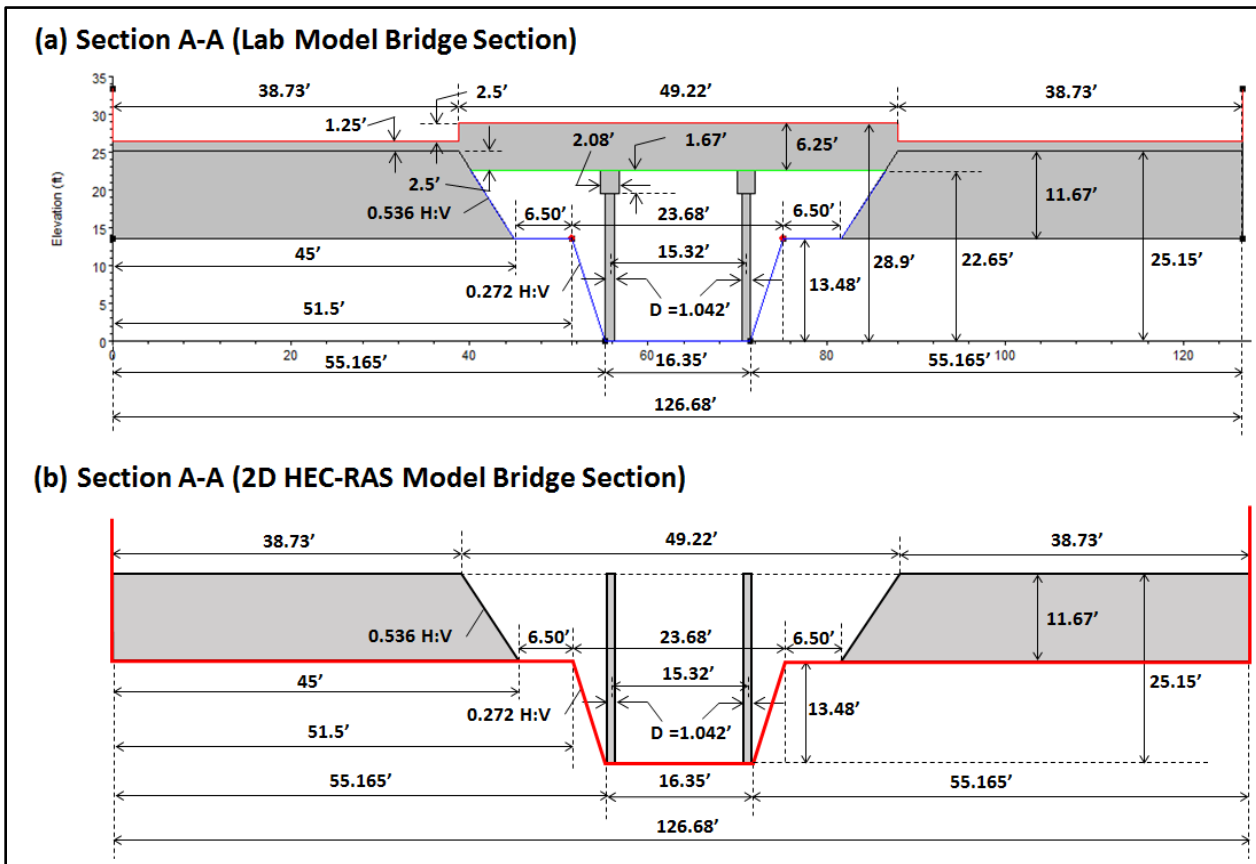


Figure 4-82. Section A-A in 20-scale Model Dimensions

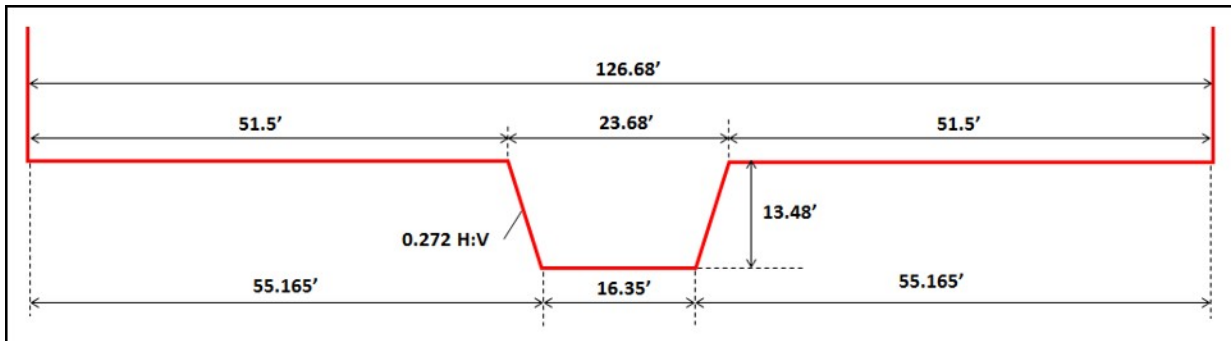


Figure 4-83. Section B-B in 20-scale Model Dimensions for Labatory and Model

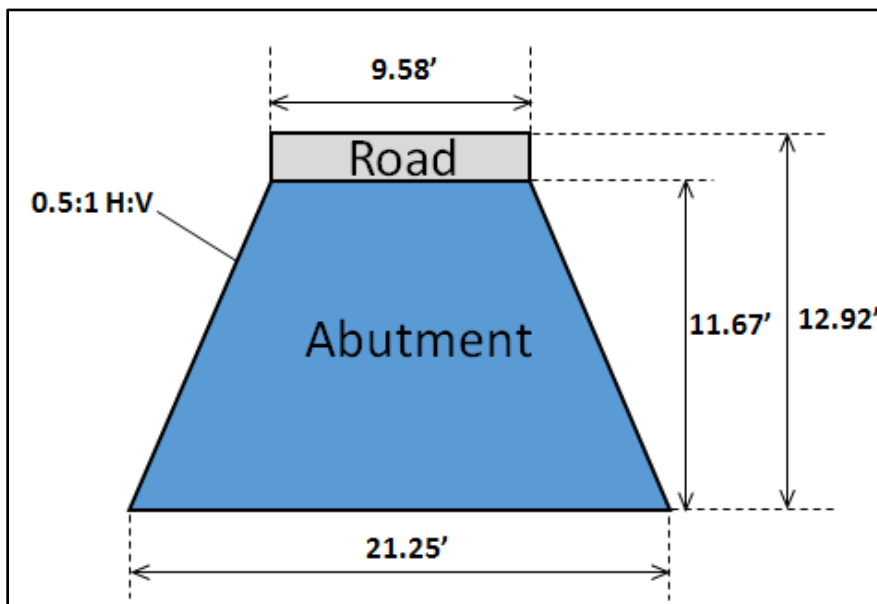


Figure 4-84. Section C-C in 20-scale Model Dimensions

Table 4-36. Cross Section and Bridge Station-Elevation Data for Sections A-A and B-B

Section A-A Bound Cross Sections				Section B-B Channel Cross Sections			
Lab Model		Prototype		Lab Model		Prototype	
Sta (inches)	Elev (feet)	Sta (inches)	Elev (inches)	Sta (inches)	Elev (feet)	Sta (inches)	Elev (inches)
0.00	20.00	0.00	33.33	0.00	20.00	0.00	33.33
0.00	8.09	0.00	13.48	0.00	8.09	0.00	13.48
30.90	8.09	51.50	13.48	30.90	8.09	51.50	13.48
33.10	0.00	55.17	0.00	33.10	0.00	55.17	0.00
42.91	0.00	71.52	0.00	42.91	0.00	71.52	0.00
45.11	8.09	75.18	13.48	45.11	8.09	75.18	13.48
76.01	8.09	126.68	13.48	76.01	8.09	126.68	13.48
76.01	20.00	126.68	33.33	76.01	20.00	126.68	33.33

Section A-A Abutments				Section B-B			
Lab Model		Prototype		Lab Model		Prototype	
Left		Right		Left		Right	
Sta (feet)	Elev (feet)	Sta (feet)	Elev (feet)	Sta (feet)	Elev (feet)	Sta (feet)	Elev (feet)
0.00	15.09	49.01	8.09	0.00	25.15	81.68	13.48
23.24	15.09	52.77	15.09	38.73	25.15	87.95	25.15
27.00	8.09	76.01	15.09	45.00	13.48	126.68	25.15

**Section A-A
Bridge Deck**

Lab Model			Prototype		
Sta (inch)	HS (inch)	L (inch)	Sta (inch)	HS (inch)	L (inch)
0.0	15.84	0.00	0.00	26.40	
23.24	15.84	0.00	38.73	26.40	
23.24	17.34	13.59	38.73	28.90	22.65
52.77	17.34	13.59	87.95	28.90	22.65
52.77	15.84	0.00	87.95	26.40	
76.01	15.84	0.00	126.68	26.40	

**Section A-A
Pier Locations and Size**

D	Model		Prototype	
	1.25 inch	1 inch	2.08 feet	1.67 feet
Cap (b, h)	1.25 inch	1 inch	2.08 feet	1.67 feet
Pier	Sta (inch)	Elev (inch)	Sta feet)	Elev (feet)
Left	33.41	15.09	55.69	25.15
Right	75.70	15.09	126.16	25.15

Laboratory Results

The laboratory results are summarized in Table 4-37. Nine experiments were performed using three discharges with three tailwater conditions. The discharges shown are for the flume experiments and the 20-scale HEC-RAS model.

Table 4-37. Laboratory Results

1D Model Station (feet)	2D Model Station (feet)	Laboratory Results			Laboratory Results			Laboratory Results		
		Run 1 (feet)	Run 2 (feet)	Run 3 (feet)	Run 4 (feet)	Run 5 (feet)	Run 6* (feet)	Run 7 (feet)	Run 8 (feet)	Run 9 (feet)
		1	2	3	4	5	6	7	8	9
150	315	20.08	19.36	18.18	19.49	18.77	17.91	21.33	21.00	19.45
130	295	20.08	19.36	18.18	19.49	18.77	17.91	21.24	20.91	19.37
120	285	20.08	19.27	18.09	19.40	18.60	17.83	21.16	20.83	19.28
110	275	20.00	19.19	18.01	19.32	18.52	17.66	20.99	20.75	19.20
100	265	19.91	19.11	17.84	19.24	18.27	17.41	20.83	20.50	18.87
90	255	19.66	18.86	17.51	18.82	17.77	16.66	20.49	20.16	18.45
80	245	19.33	18.52	16.93	17.99	16.77	15.41	19.83	19.33	17.45
70	235	19.00	18.11	16.34	17.32	15.93	14.16	19.33	18.75	16.53
60	225	18.91	18.02	16.34	17.24	15.85	13.91	19.16	18.66	16.45
50	215	18.83	17.94	16.18	17.07	15.77	13.91	18.99	18.50	16.28
40	205	18.83	17.86	16.18	17.07	15.60	13.75	18.99	18.50	16.20
30	195	18.83	17.86	16.18	17.07	15.68	13.58	19.08	18.58	16.20
20	185	18.83	17.86	16.18	17.02	15.60	13.75	19.08	18.58	16.28
0	165	18.83	17.86	16.09	16.90	15.43	13.58	19.08	18.50	16.03

*DS piezometer reading too low at just 0.1 feet above overbank elevation in model dimensions.

The following equation based on Froude number similarity was used to determine the HEC-RAS model discharges.

$$\text{Undistorted } Q_p = L_r^{5/2} Q_m \quad (4-26)$$

Where L_r is the scale for undistorted models.

Note that the piezometer readings were only for the middle 7.5 foot region shown in Figure 4-85. Run 6 was discounted since the tailwater elevation in the lab model was only 0.167 inches deep in the overbanks. This converts to 0.1 feet in the model. Neither the HEC-RAS 1D nor 2D models were able to replicate the Run 6 laboratory data. This was likely due to flow conditions on the downstream side from the bridge that did not adhere well to either 1D or 2D flow assumptions. Essentially this flow resembled jet flow with side to side oscillations.

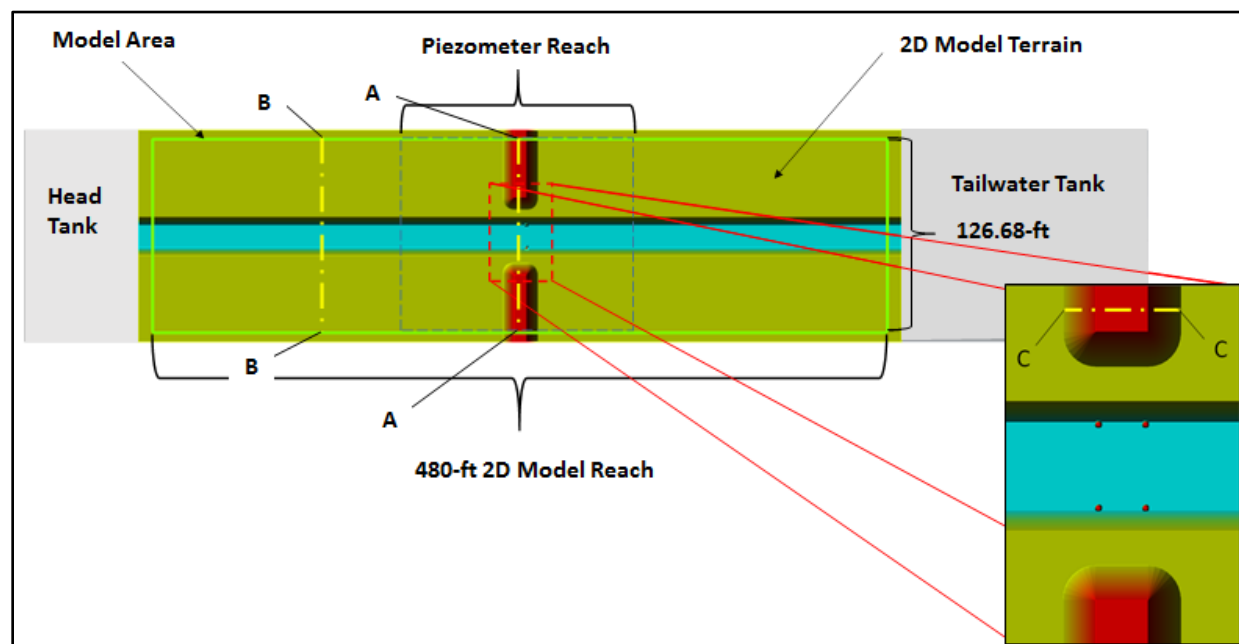


Figure 4-85. Plan View Showing the HEC-RAS 2D Model Domain

Model Setup

A model simulating the entire 24-foot lab test reach was created as a 480-foot long, 126.68-foot wide 2D model. Figure 4-85 shows the plan view of the terrain created in HEC-RAS and used to assign the pertinent ground characteristics to the HEC-RAS 2D grid cells. The terrain was created in HEC-RAS by inputting two raster surfaces: one for the piers at a grid-cell size of 0.01 feet (pier raster) and the other for the model surface including the overbanks, channel and abutments (land raster).

The land raster was created from the Z polylines shown in Figure 4-86. This was accomplished by first creating a TIN in ArcGIS from the polylines in Figure 4-86 and then creating the 0.1-foot raster. The extent of the land raster was beyond the edges of the model area to avoid errors that can occur during grid development in HEC-RAS 2D. The land raster was 500-foot long and 140-foot wide.

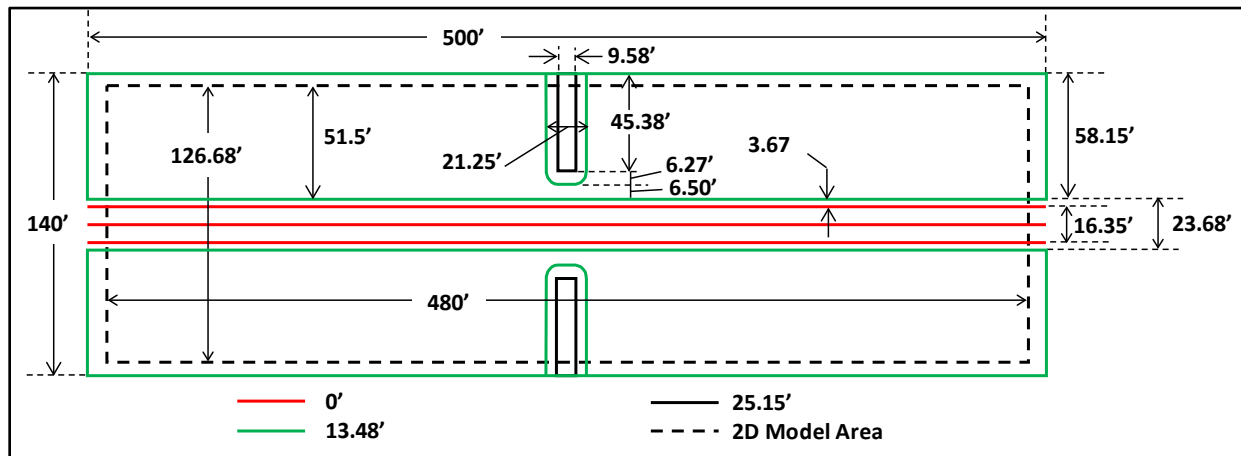


Figure 4-86. Three-Dimensional Shapefiles used to create 0.1-foot Land Raster

The pier raster was created by using the Mosaic function in ArcGIS® to combine a 0.01-foot pier top raster that has a diameter somewhat larger than the actual pier and a 0.01-foot land disk raster larger in diameter than the pier top raster. The process is illustrated in Figure 4-87, where the size of the land disk raster is greatly exaggerated. Figure 4-88 shows the pier raster used in this study. The bright inner circle is the outline of the 1.042-foot diameter pier.

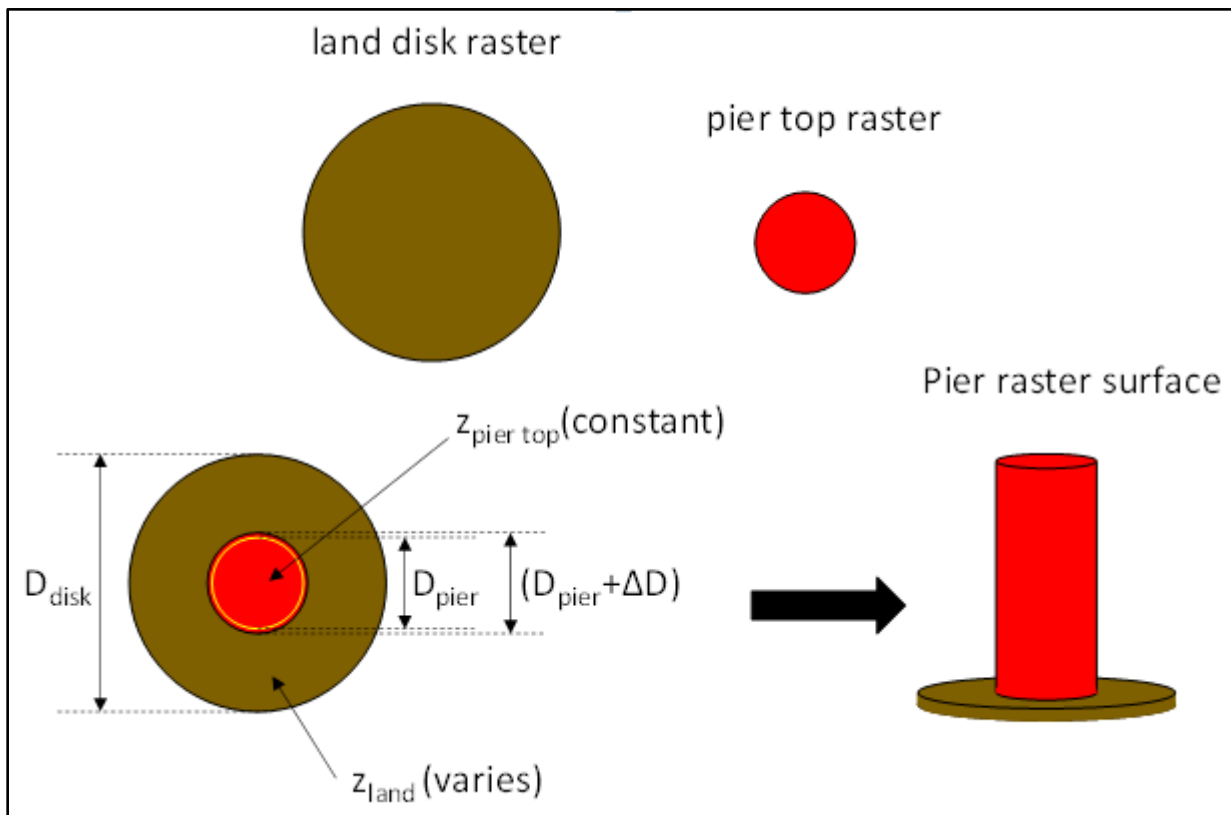


Figure 4-87. Creating a Pier Raster

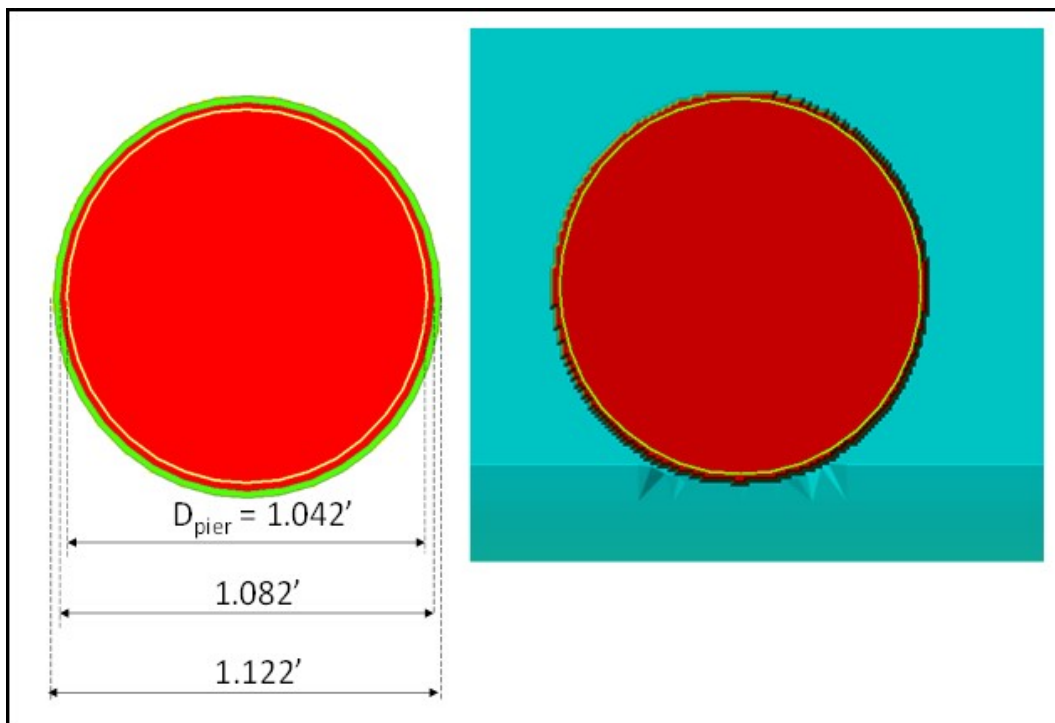


Figure 4-88. Pier 0.1-foot Raster used in this Study

Figure 4-89 illustrates merging the land raster and the pier raster within HEC-RAS 2D to create the requisite terrain.

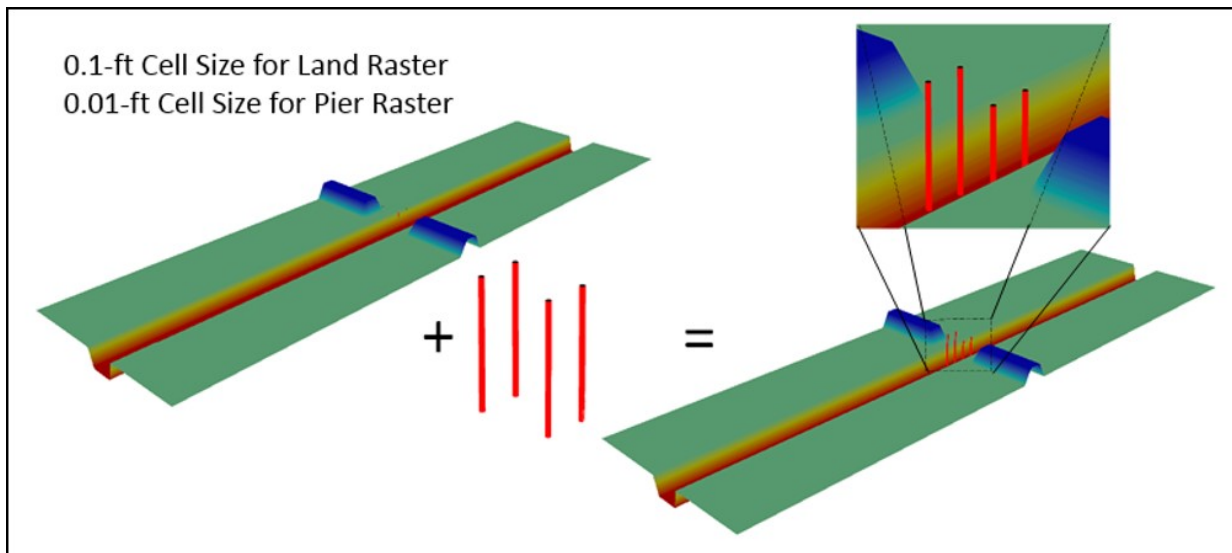


Figure 4-89. ArcScene® Illustration of Combining Land and Pier Rasters to Create the HEC-RAS Two-Dimensional Terrain

The original KU 2D HEC-RAS models were developed with a mesh that used a two foot nominal grid size, and 1.0 foot cells along all break lines (20,578 cells). The piers and the area around the piers were modelled in great detail. After running the KU lab datasets with HEC-RAS, it was deemed that a simpler version of the mesh world work just as well, given that the lab results were only comparing the changes in the water surface elevations, and not the velocity profiles. For detailed velocity profiles around the piers and abutments, as well as through the

bridge, the KU mesh is the best approach. However, for computing change in water surface elevations through the bridge, that level of detail is not really required. Because of the sub-grid terrain technologies that HEC-RAS employs, the details of the terrain can still be picked up with much larger and fewer cells. A new mesh was developed in which the nominal cell size was set to 4.0 feet (the KU models used 2.0 feet). Far fewer break lines were used, and the cell size along the break lines was set to 2.0 feet instead of 1.0 feet as they were in the KU models. The new mesh is shown in Figure 4-90 (entire mesh) and Figure 4-91 (zoomed in view around bridge opening).

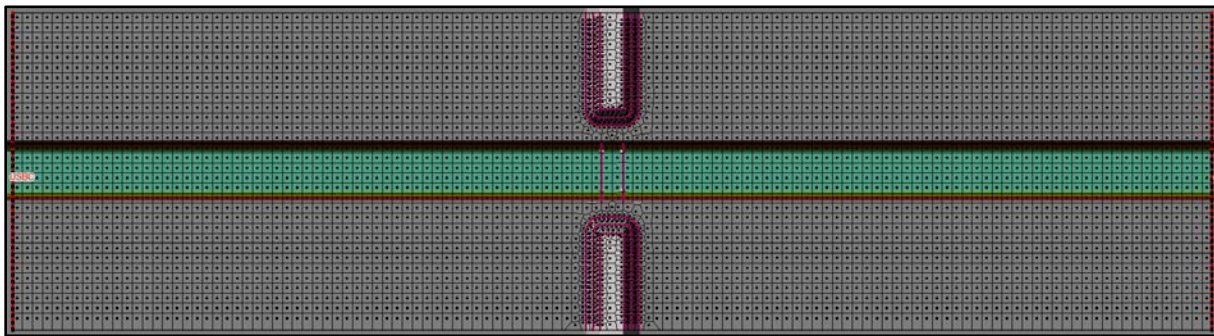


Figure 4-90. Plan View of the Entire HEC-RAS 2D Mesh and Terrain

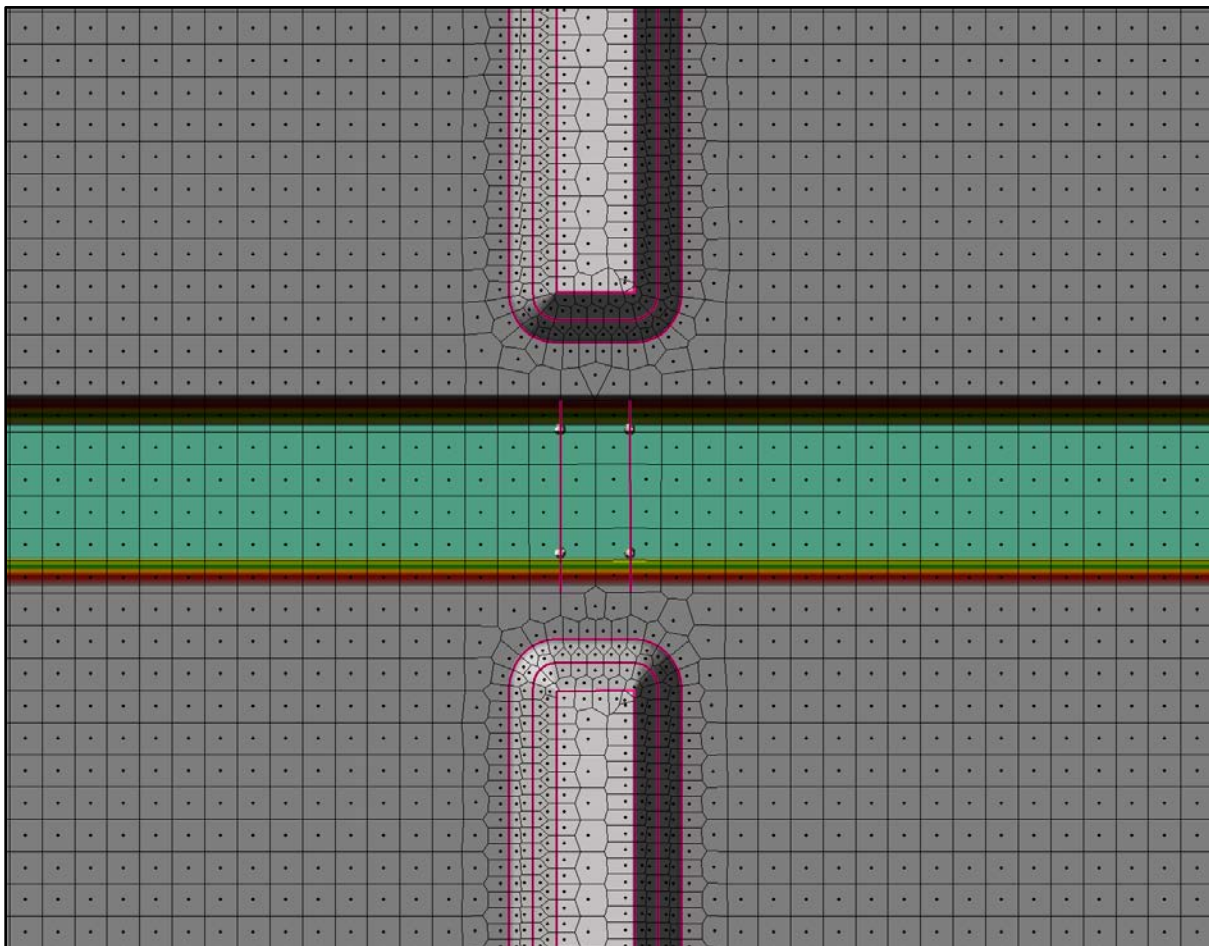


Figure 4-91. Zoomed in View of the HEC-RAS Two-Dimensional Mesh near Bridge Piers and Abutments

The computational HEC-RAS grid cell size was four-feet except near break lines where the minimum cell spacing was set at two-feet.

As shown in Figure 4-90 and Figure 4-91, break lines were used to capture the curvature of the spill through abutments and to ensure that faces went right through the center of the piers. This type of mesh will still capture the details of the channel and abutments extremely well. The piers are being modelled in a much simpler manner, in which the full pier width is captured in a face, and additionally the wetted perimeter along the sides of the piers are captured. As stated earlier, this type of mesh will not produce detailed velocity distributions around the piers, but is still a very good approach for capturing the water surface profiles through the bridge with far fewer cells than the KU mesh approach. The KU model had 20,578 cells, while this mesh has only 4,171 cells. This is a much more computationally efficient approach, while still capturing all the major features that will affect the water surface elevations.

In addition to the changes made to the mesh, turbulence modeling was turned on for all of the runs. In order to capture the numerical diffusion, it is necessary to turn on turbulence in model applications like this bridge example, where there is a great amount of physical diffusion that occurs as the water surface jet comes out of the bridge opening and expands into the overbank areas. Additionally there are two larger Eddy recirculation zones on the downstream side of the bridge. The Eddy Viscosity Transverse Mixing coefficient was set to 2.0 for all of the runs. This produced good results across all of the lab runs for the range of flows and tail waters.

Computational time steps for this model were based on having a Courant number around 1.0 or less for the cells with the highest velocities. Additionally, when the Turbulence modeling is turned on, there is a second computational criteria that should be checked in order to ensure model stability when running the model. This criteria is documented in the HEC-RAS Hydraulic Reference Manual under Chapter 2, under the section labeled "Robustness and Stability", which is at the end of the section on the 2D equations. For this mesh, with turbulence turned on, the computational time steps were set to 0.1 seconds for Runs 1 through 5, and 0.05 seconds for Runs 7 through 9 (higher flow and velocities).

The upstream boundary conditions were based on starting with a minimum flow of 200 cfs, then ramping the flow up to the maximum for each run. A slope is required for the upstream flow boundary condition in order to distribute the flow across the boundary. The slope was set to a value of $S=0.0001$. The hydrograph shown in Figure 4-92 reaches the peak flow at 25 minutes. The downstream boundary conditions were stage hydrographs with a constant depth. In order to reproduce the stages at the most downstream piezometer location, an iterative procedure was used for each run to determine the downstream boundary condition for the 2D model that produced a good WSEL at Station 165 (which corresponds to the downstream piezometer).

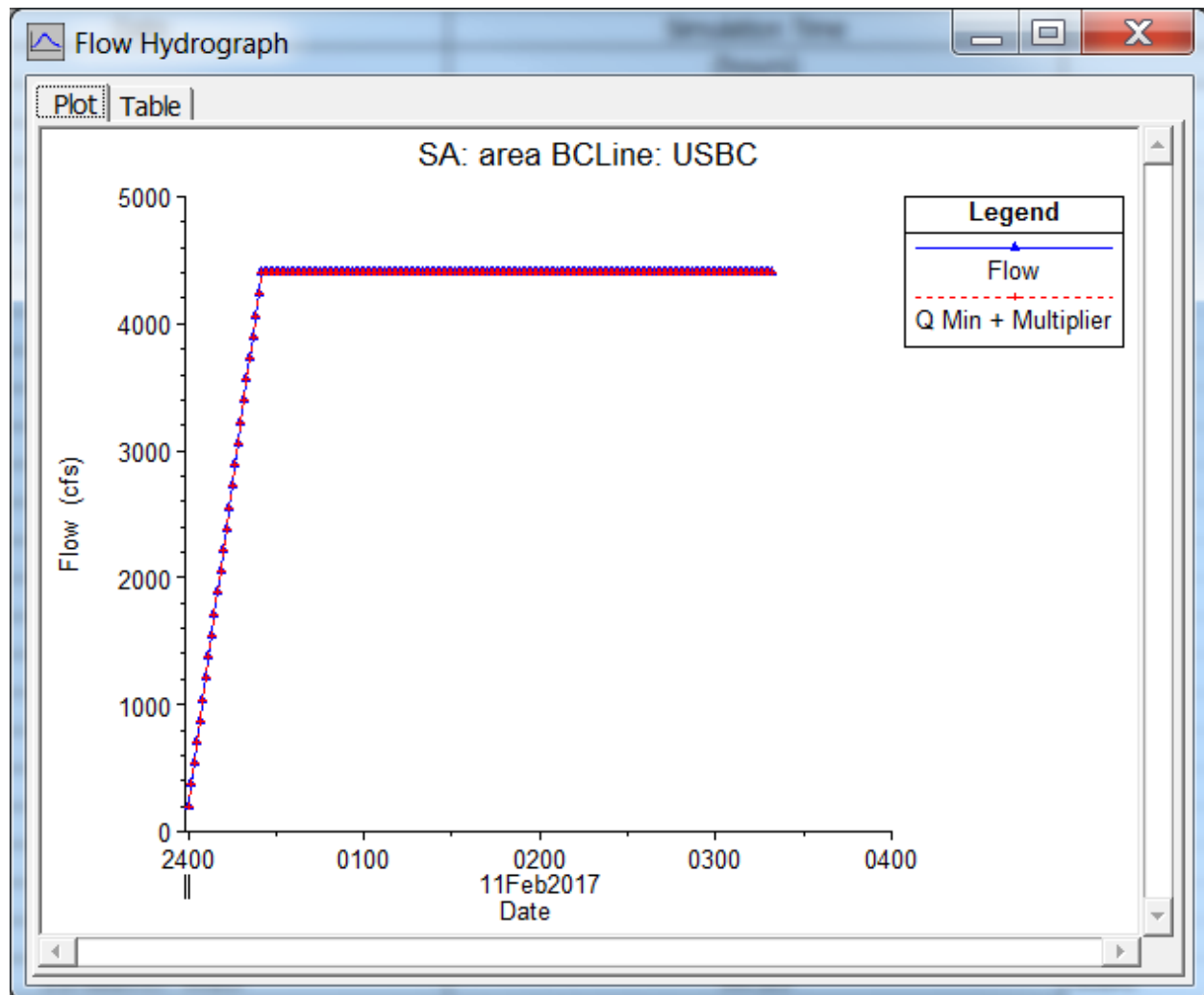


Figure 4-92. Example Upstream Boundary Condition Flow Hydrograph

Results and Discussion

The simulation were all run with the Full Momentum equation set. The centerline maximum WSEL profiles for Runs 1 through 3, are shown in Figure 4-93. Runs 4 and 5 are shown in Figure 4-94, and Runs 7 through 9 are shown in Figure 4-95.

The results of this study are very encouraging. As shown in Figure 4-93 through Figure 4-95, the HEC-RAS 2D model did very well in matching the laboratory data. Also, it should be noted that the results are very similar to the models run from the more detailed mesh (20,000 plus cells), with the simpler mesh producing slightly higher upstream water surface elevations.

These results are very good for lab Runs 1 through 5, good for Runs 7 and 8, and not too bad for Run 9. Run 9 was the laboratory run with the highest flow rate and lowest tail water elevation. This model run produced the highest velocities through the bridge opening. Run 9 was highly three-dimensional (3D), in that the flow was basically a jet of water coming through the bridge opening, then expanding both horizontally and vertically downstream of the bridge. This made it very difficult for a 2D model to pick up the level of necessary detail required.

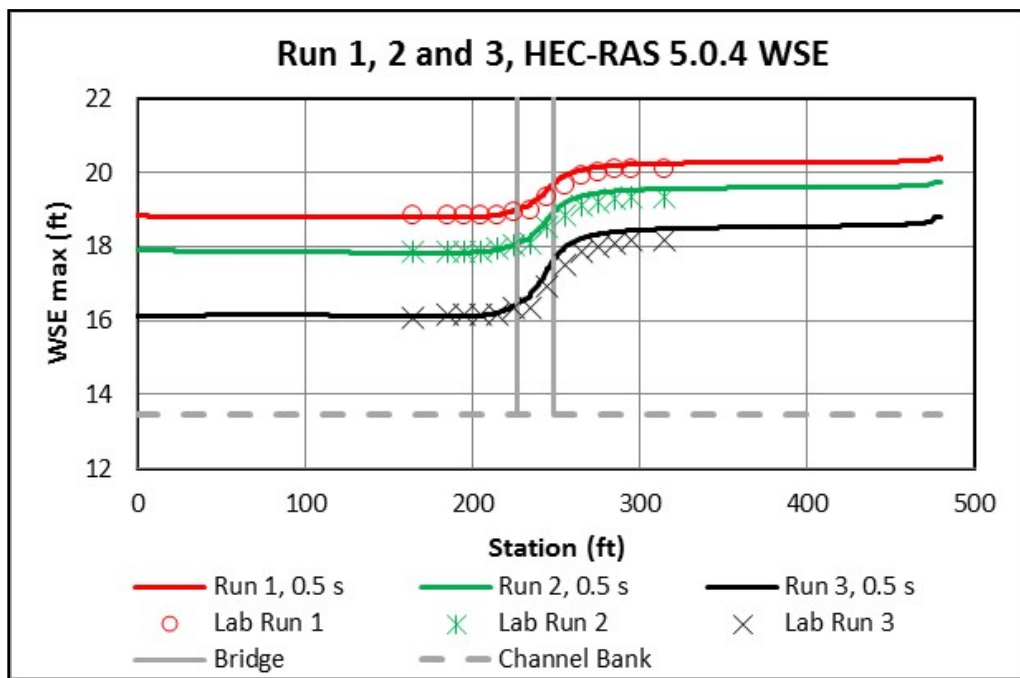


Figure 4-93. Computed and Observed Profiles for Runs 1 to 3

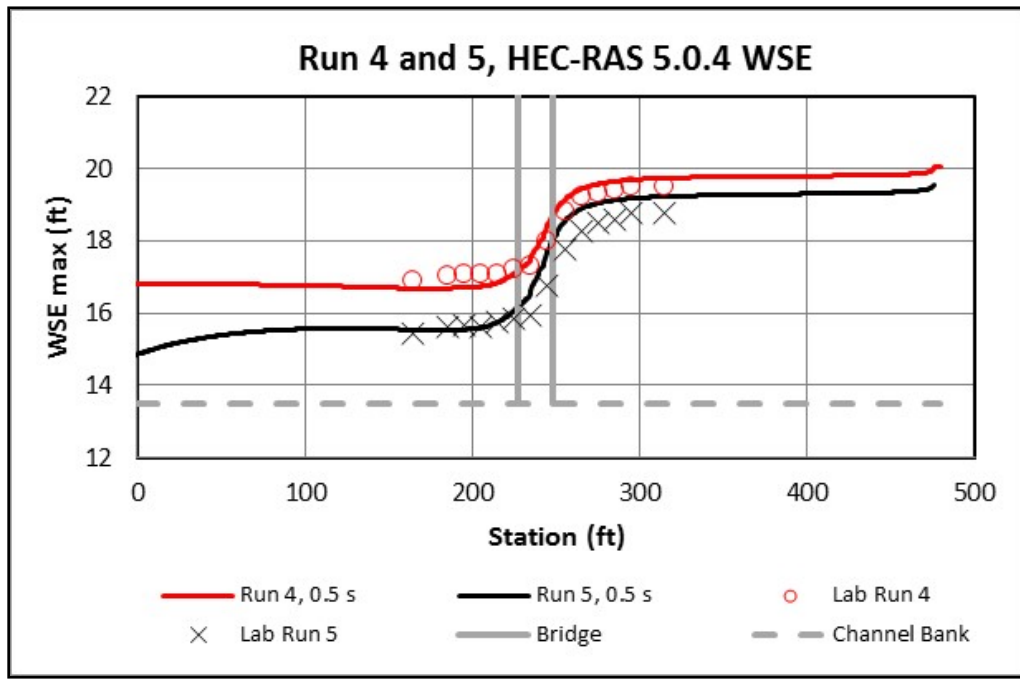


Figure 4-94. Computed and Observed Profiles for Runs 4 and 5

These runs also show the utility of the HEC-RAS sub-grid technology, in that larger cell sizes could be used and still retain all the details of the terrain (channel, abutments, and piers). Additionally, the model run times were dramatically reduced when increasing the cell size in the 2D mesh, and thus reducing the number of cells. Typical run times for the more detailed mesh were around 20 to 25 minutes, and 4 to 6 minutes for the less detailed mesh.

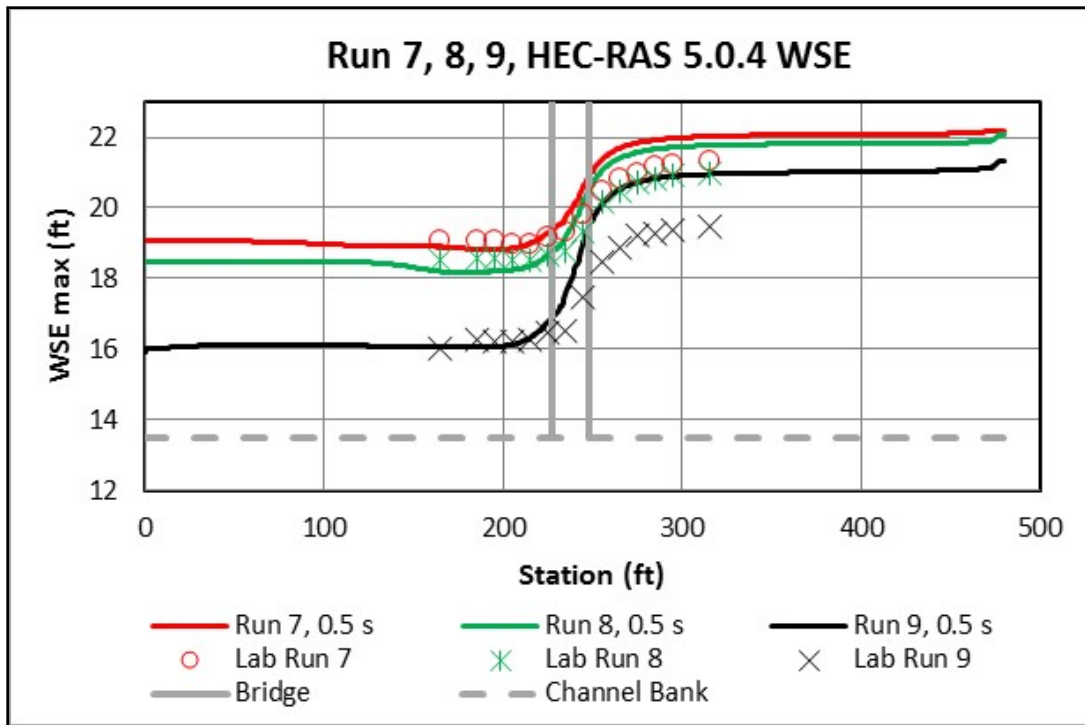


Figure 4-95. Computed and Observed Profiles for Runs 7 to 9

References

1. Parr, 2010. Parr, A. David, Milburn, Shannon, Malone, Travis, and Bender, Theodore. *A Model Study of Bridge Hydraulics*, Edition 2. Report No. K-TRAN: KU-03-4R. Cooperative research program between Kansas Department of Transportation, Kansas State University, and University of Kansas. August 2010.
https://ntl.bts.gov/lib/34000/34000/34019/KU034R_Final.pdf

4.4 Field Datasets

4.4.1 Malpasset Dam Break

Overview

The performance of HEC-RAS in simulating a real life dam break is evaluated using the Malpasset dataset. The test case is useful for comparing HEC-RAS 2D results to real world data.

Problem and Data Description

The Malpasset Dam was located in a narrow gorge on the Reyran River about 7 km north of Fréjus on the South West Coast of France. The arch dam was 66.5-meters tall and 223-meters wide at the crest (Figure 4-96). The capacity of the reservoir behind the dam was 55 million m³. Construction on the dam began in 1952 and was completed in 1954. The dam had an emergency spillway and a low flow gate near the bottom. The dam was only 6.7 meters wide at the base and 1.5 meters wide at the crest. Between 19 November and 2 December 1959, there was

approximately 20 inches of rainfall in 24-hours, raising the water level to within twelve inches of the spillway. On 2 December 1959, at 18:00 hours the water release valves were opened with a discharge rate of $40 \text{ m}^3/\text{s}$. Unfortunately, this was not enough to empty the reservoir in time and at 21:14 hours, the dam failed, explosively releasing 48 million m^3 of water and flooding the towns of Malpasset, Bozon, and Frejus, France.

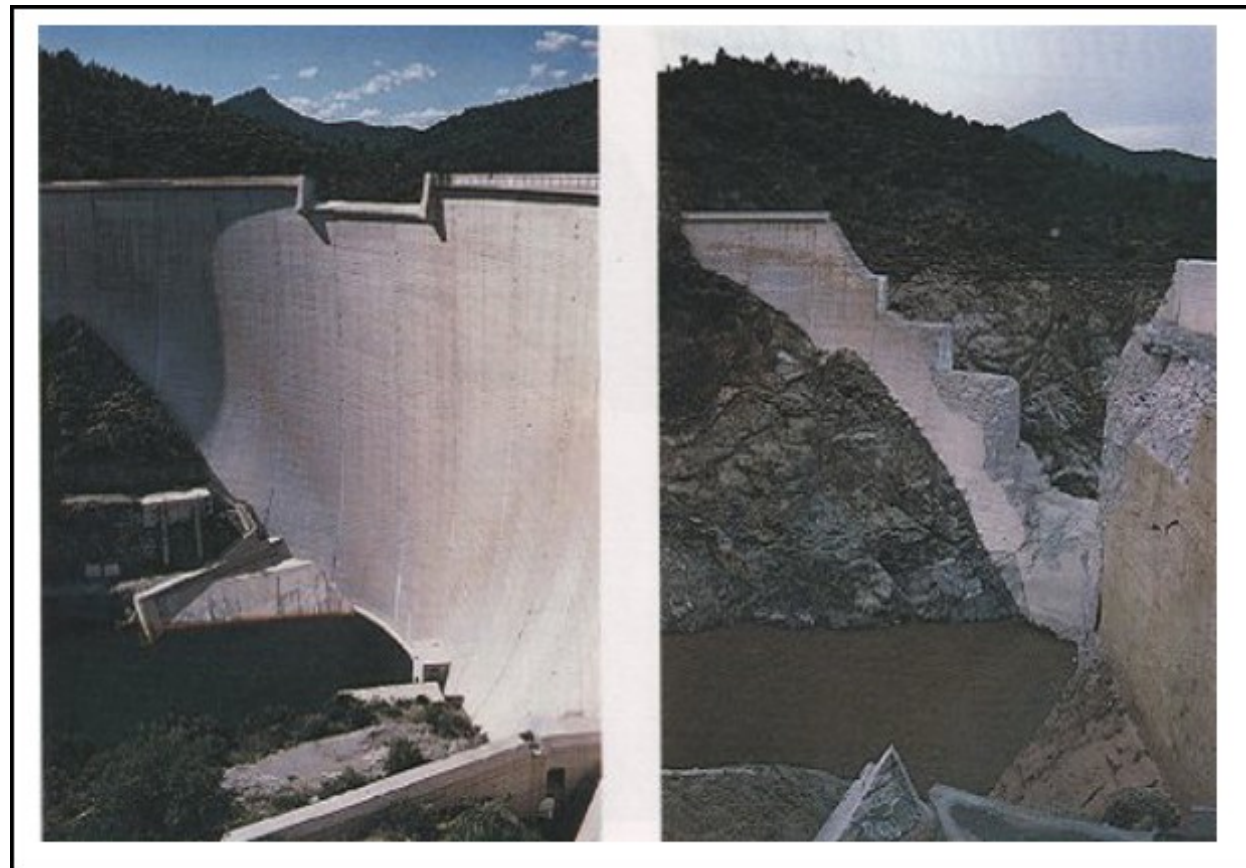


Figure 4-96. Malpasset Dam, France after having Failed on 2 December 1959 (source http://ecolo.org/documents/documents_in_french/malpasset/malpasset.htm)

Figure 4-97 shows a map with the terrain and the location of measurement stations. The terrain was obtained from a previous existing mesh for the area from the study of Savant (2011). The terrain outside of the bounding polygon is not real since it is a result of spatial interpolations and therefore can be ignored. The terrain outside of the bounding polygon it is not used in the HEC-RAS model. The original terrain was digitized from an Institute Géographique national 1:20,000 map of Saint-Tropez n 3 from 1931. Stations A, B, and C (Figure 4-97) represent destroyed electric transformers which were used to estimate the flood wave arrival times. Stations beginning with a letter P (Figure 4-97) indicate maximum water level survey locations by the police after the event. Stations beginning with a letter S (Figure 4-97) indicate experimental measurement stations from a scaled physical model built at the Laboratoire National d'Hydraulique in 1964. The scale factor of the undistorted model was 1:400 (Soares Frazão, 2000).

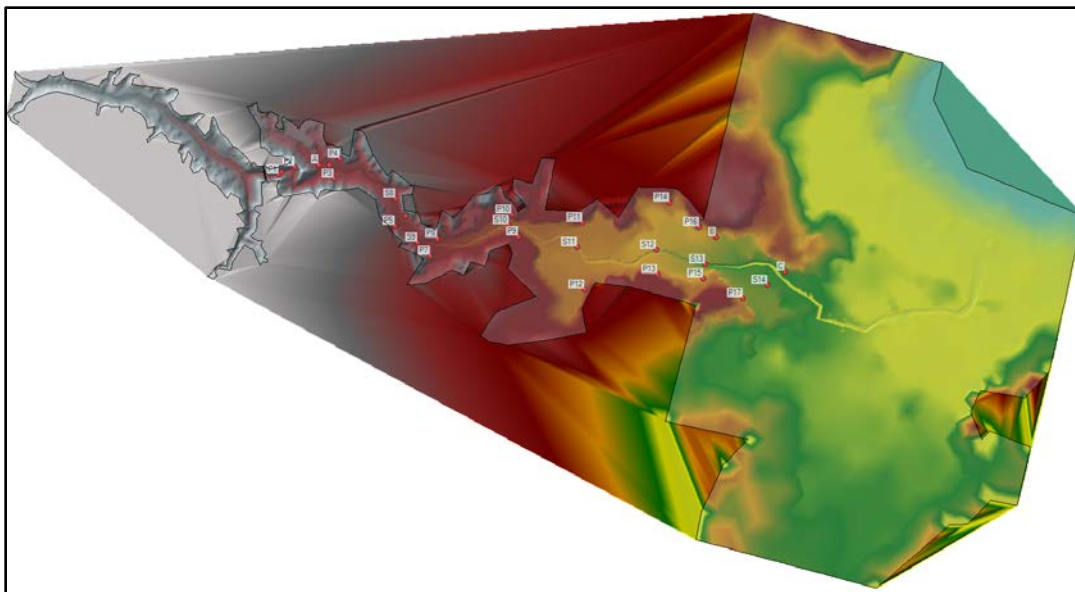


Figure 4-97. Malpasset Dam Area Showing Location of Measurement Stations and Terrain

Model Setup

Two model setups were created; one representing the real life breach and another representing the laboratory experiment. Both setups utilized the same terrain and computational mesh but varied in the simulation of the breach. The polygonal mesh has a variable grid resolution ranging from about ten meters near the dam to about 300 meters near the ocean. The computational mesh has approximately 12,800 cells (Figure 4-98). An HEC-RAS Storage Area/2D Area Connection was utilized to simulate the dam structure.

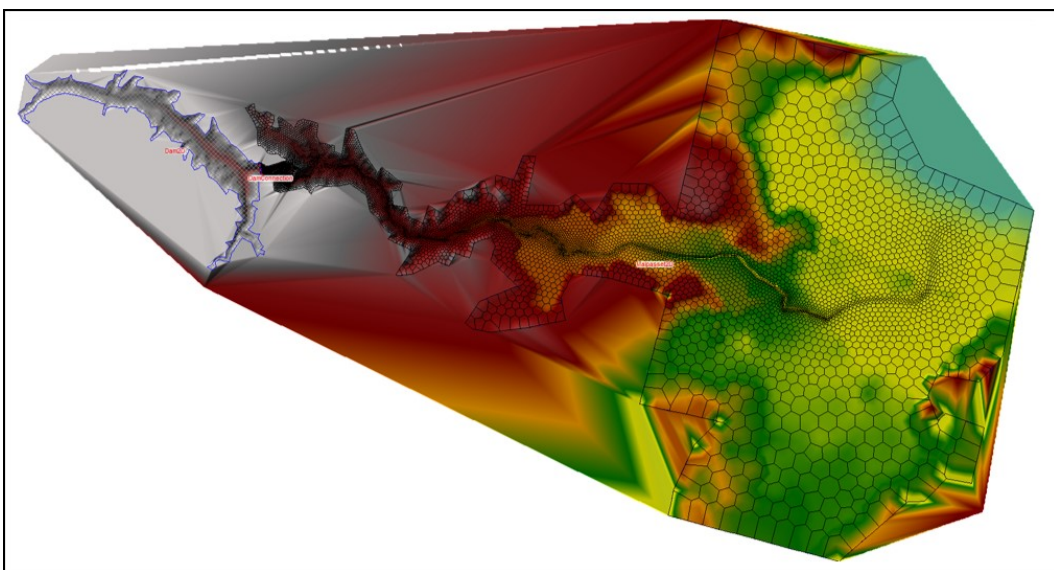


Figure 4-98. Computation Domain and Model Terrain

A summary of the important model input parameters is presented in Table 4-38. For the real-life breach simulation the breach parameters were based on images of the dam after the breach and accounts of the event. The gate was opened at 18:00 such that the discharge was equal to the reported $40 \text{ m}^3/\text{s}$. The dam breach was initiated at 21:14. A breach formation time of about 7 s

was specified. For simplicity, a constant Manning's roughness coefficient of 0.035 s/m^{1/3} was used for the whole modeling domain. In addition, the eddy viscosity coefficient was set to 1.0. The model setup representing the physical model experiment was similar except no gate was utilized, and the Manning's and mixing coefficient were lowered to 0.025 s/m^{1/3} and 0.6 respectively. In addition the simulation start time was set to the start of the dam breach at 21:14. The initial water level in the reservoir was set to 100 meters following previous numerical studies (Valiani, 2002; Schwanenberg, 2004; Savant, 2011; and, Ying, 2004). A variable time step was used based on a maximum courant number of one.

Table 4-38. Model Parameters for the Malpasset Dam Break Validation Test Case

Parameter	Real Life Setup	Laboratory Model Setup
Governing Equations	SWE	SWE
Time step (second) - Variable	0.15625, 0.3125, 0.625, 1.25, and 2.5	0.15625, 0.3125, 0.625, 1.25, and 2.5
Maximum Courant	1	1
Implicit Weighting Factor	1	1
Manning's n roughness coefficient (s/m ^{1/3})	0.035	0.025
Eddy viscosity coefficient	1	0.6
Initial Reservoir Water Level (meter)	100	100
Breach formation time (second)	7	7
Breach bottom width (meter)	20	20
Breach left slope	2.1	2.1
Breach right slope	2.7	2.7
Gate discharge (m ³ /s)	40	0

Results and Discussion

A comparison of the measured and computed maximum WSEL at the seventeen high-water mark stations collected by the police are shown in Figure 4-99. In general, the model reproduced well the maximum water levels at the stations. The maximum differences were located near the dam where the model tends to under-predict the water levels. The mean maximum water level different is -0.77 meters.

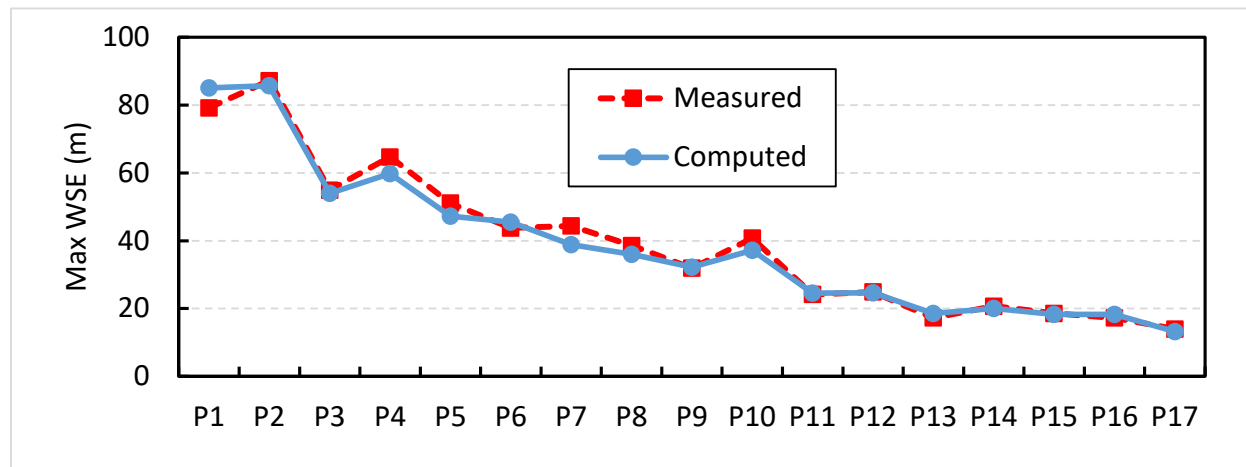


Figure 4-99. Measured and Computed Maximum Water Surface Elevations (WSEL) for the High-Water Marks Collected by the Police after the Malpasset Dam Break

Figure 4-100 shows a comparison of the computed and measured arrival times at the three electric transformers which were destroyed during the flood. The computed value show

excellent agreement with the estimated values from the field. The largest difference is at the transformer furthest downstream. A series of snap shots of the water depths for the real-life dam breach are presented in Figure 101.

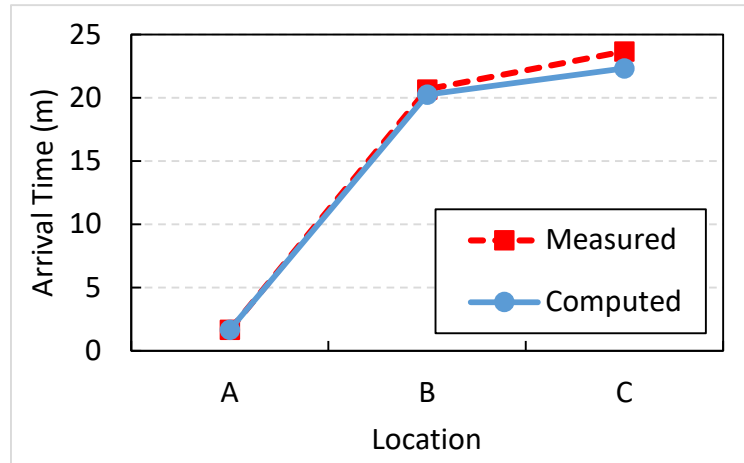


Figure 4-100. Measured and Computed Flood Wave Arrival Times for the Malpasset Dam Break at Three Locations where Electric Transformers were Damaged

The results for the model setup of the laboratory study are presented in Figure 4-102 and Figure 4-103. Figure 4-102 shows a comparison of the measured and computed maximum water surface elevations. In general the computed maximum water levels agree well with the laboratory measurements. The mean maximum water level is 1.18 meters.

Figure 4-03 shows a comparison of the measured and computed arrival times for the laboratory experiment simulation. The agreement between the measured and computed values is reasonable. The arrival times at Stations S8 through S10 are slightly late, while the arrival time at S13 is slightly early.

In general the computed and measured results for both the real-life and laboratory study were reasonable and similar to those obtained in previous studies (i.e., Valiani, 2002; Schwanenberg, 2004; Savant, 2011; Ying et al. 2009).

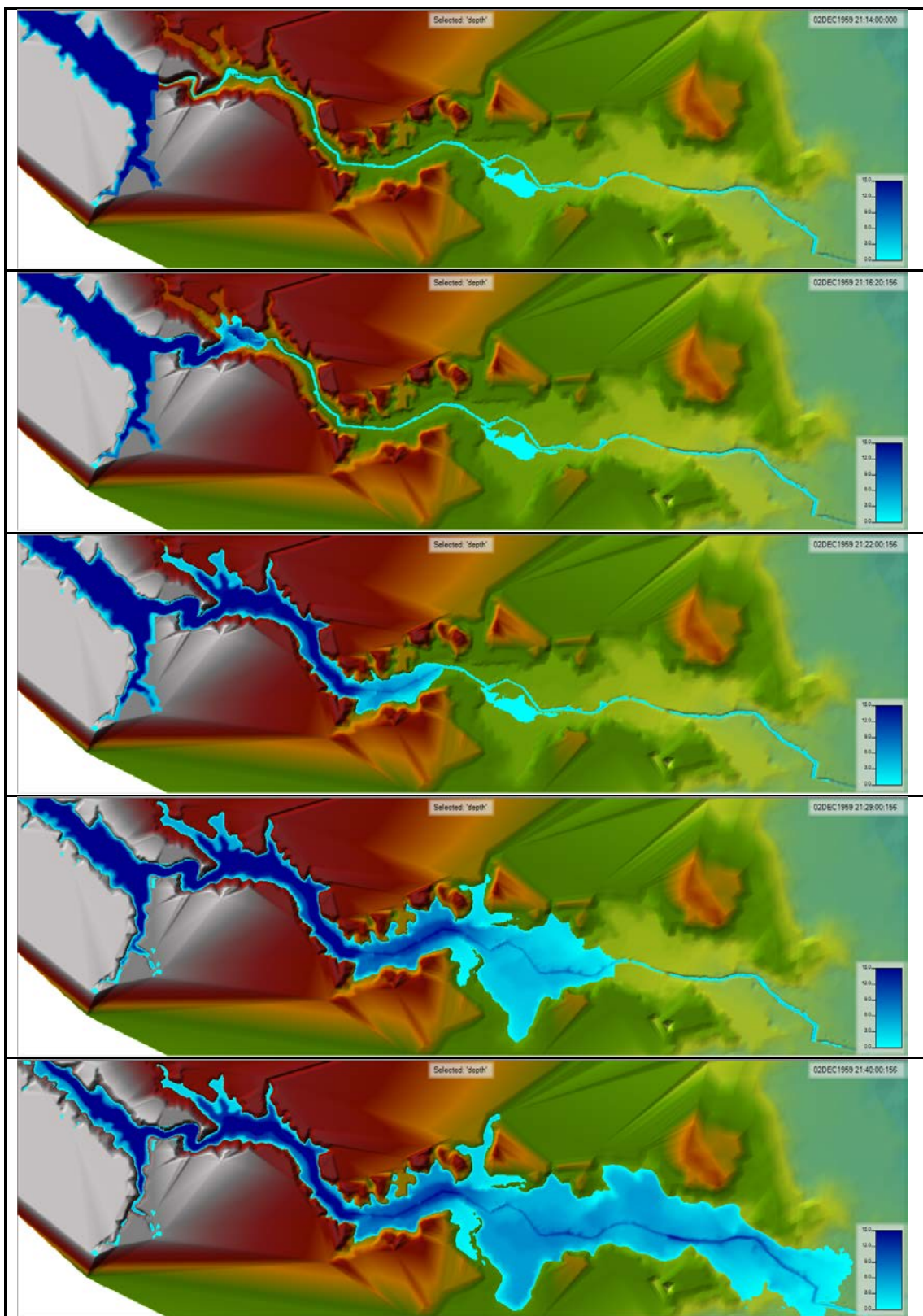


Figure 4-101. Computed Water Surface Elevation Maps for the real-life Malpasset Dam Break Simulation

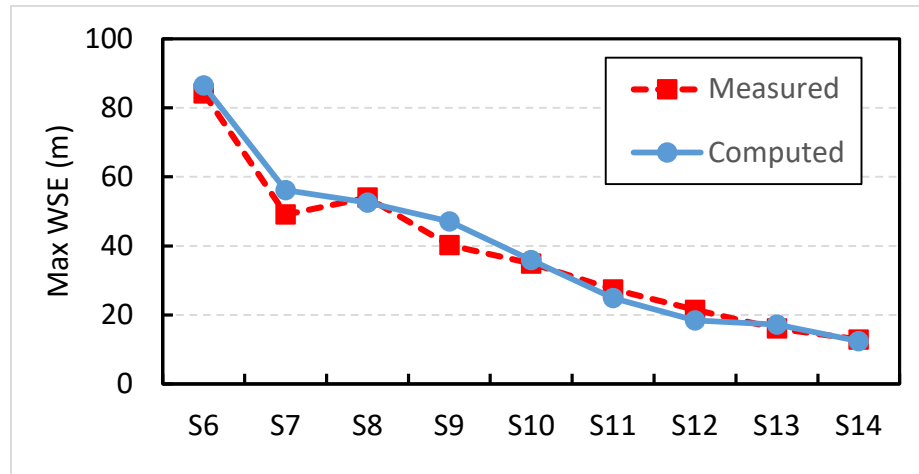


Figure 4-102. Measured and Computed Maximum Water Surface Elevations (WSEL) as Estimated by a Physical Model of the Malpasset Dam Break

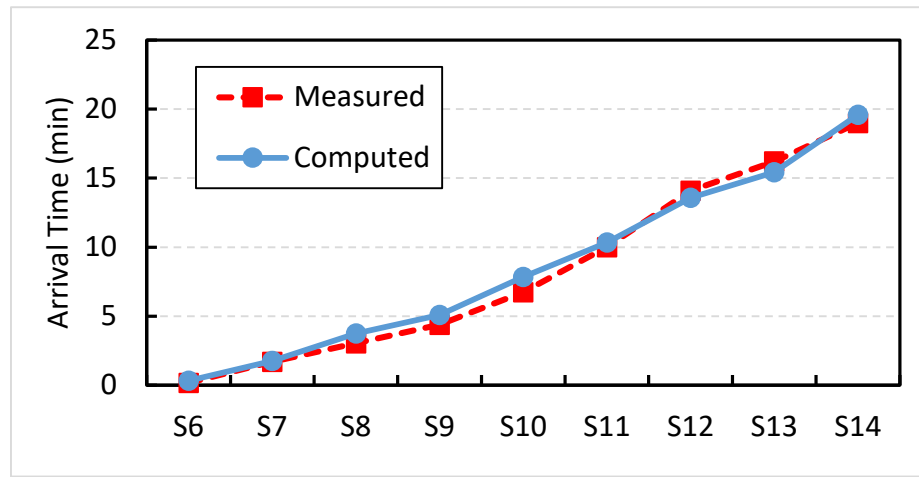


Figure 4-103. Measured and Computed Arrival Times (minutes) as Estimated by a Physical Model of the Malpasset Dam Break.

References

1. Bruel, F. Malpasset The Disaster in 1959. http://ecolo.org/documents/documents_in_french/malpasset/malpasset.htm. (Accessed July 2016).
2. Savant, 2011. Savant, G., Berger, C., McAlpin, T.O., and Tate, J.N. *Efficient implicit finite-element hydrodynamic model for dam and levee breach*. Journal of Hydraulic Engineering, ASCE, Volume 137, Issue 9, pages 1005-1018. September 2011.
3. Schwanenberg, 2004. Schwanenberg, Dirk and Harms, M. *Discontinuous Galerkin finite element method for transcritical two-dimensional shallow water flows*. Journal of Hydraulic Engineering, ASCE, Volume 130, Issue 5, pages 412–421. May 2004.
4. Soares-Frazão, 2000. Soares-Frazão, Sandra, Morris, M. and Zech, Y. *Concerted Action on Dam Break Modelling: Objectives, Project report, Test cases, Proceedings*. UCL, Belgium, CDRom. 2000.

5. Valiani, 2002. Valiani, A., Caleffi, V., and Zanni, A. *Case study: Malpasset dam-break simulation using a two-dimensional finite volume method.* Journal of Hydraulic Engineering, ASCE, Volume 128, Issue 5, pages 460–472. May 2002.
6. Ying et al. 2009. Ying, X., Jorgeson, J., and Wang, S.S.Y. 2009. *Modeling dam-break flows using finite volume method on unstructured grid.* Engineering Applications of Computational Fluid Mechanics, Volume 3, Issue 2, pages 184–194.

4.4.2 New Madrid Floodway Levee Breaching

Overview

The performance of HEC-RAS in simulating a real life levee breach and interior flooding is demonstrated with the New Madrid Floodway dataset. During the May 2011 flood in the Mississippi and Ohio Rivers, the New Madrid Floodway was activated by blowing up the levee in three locations, in order to reduce flooding along the Mississippi and Ohio Rivers. Before the levee was activated, the U.S. Geological Survey (USGS) went out and placed 38 pressure transducers within the floodway, in order to measure the water levels during the event. The levee system was activated by USACE on 2 May 2011. The measured water surface elevations inside the floodway are used to compare against the computed values from an HEC-RAS model of the New Madrid Floodway. This test case is useful for comparing HEC-RAS 2D results to real world data.

Problem and Data Description

The New Madrid Floodway is located just below the confluence of the Ohio and Mississippi Rivers. This floodway is surrounded by a levee system, which is designed to be activated during major floods. Approximately 9,400 feet of the upper levee was activated on 2 May 2011 just after 2200 hours. Later, two lower sections of the levee were also activated to allow water to drain out more efficiently. Shown in Figure 4-104 is the New Madrid Floodway along the Mississippi River, as well as the levee system. The three locations in which the levee system was breached are shown in red.

Detailed terrain data was obtained for the area inside of the floodway. The grid cell size for this terrain area is five feet. Outside of the floodway the terrain data varied from twenty to thirty foot cell sizes. Surveyed cross section data was obtained from several Corps District offices for the Upper and Lower Mississippi Rivers, as well as the Ohio River. Levee locations (X, Y coordinates), and elevation data were obtained from the Corps' National Levee Database.

Flow data was obtained for the upstream boundaries from USGS gaged locations. A rating curve was used for the downstream boundary condition of the lower Mississippi River 1D reach. Breaching information was obtained from USACEs.

Model Setup

The HEC-RAS model developed for this analysis is a combined 1D/2D model. All of the river systems were modeled as 1D river reaches. The levee systems, including the new Madrid floodway levees were modelled with lateral structures within HEC-RAS. Most of the areas behind the levee system were modelled with either single storage areas, or interconnected storage

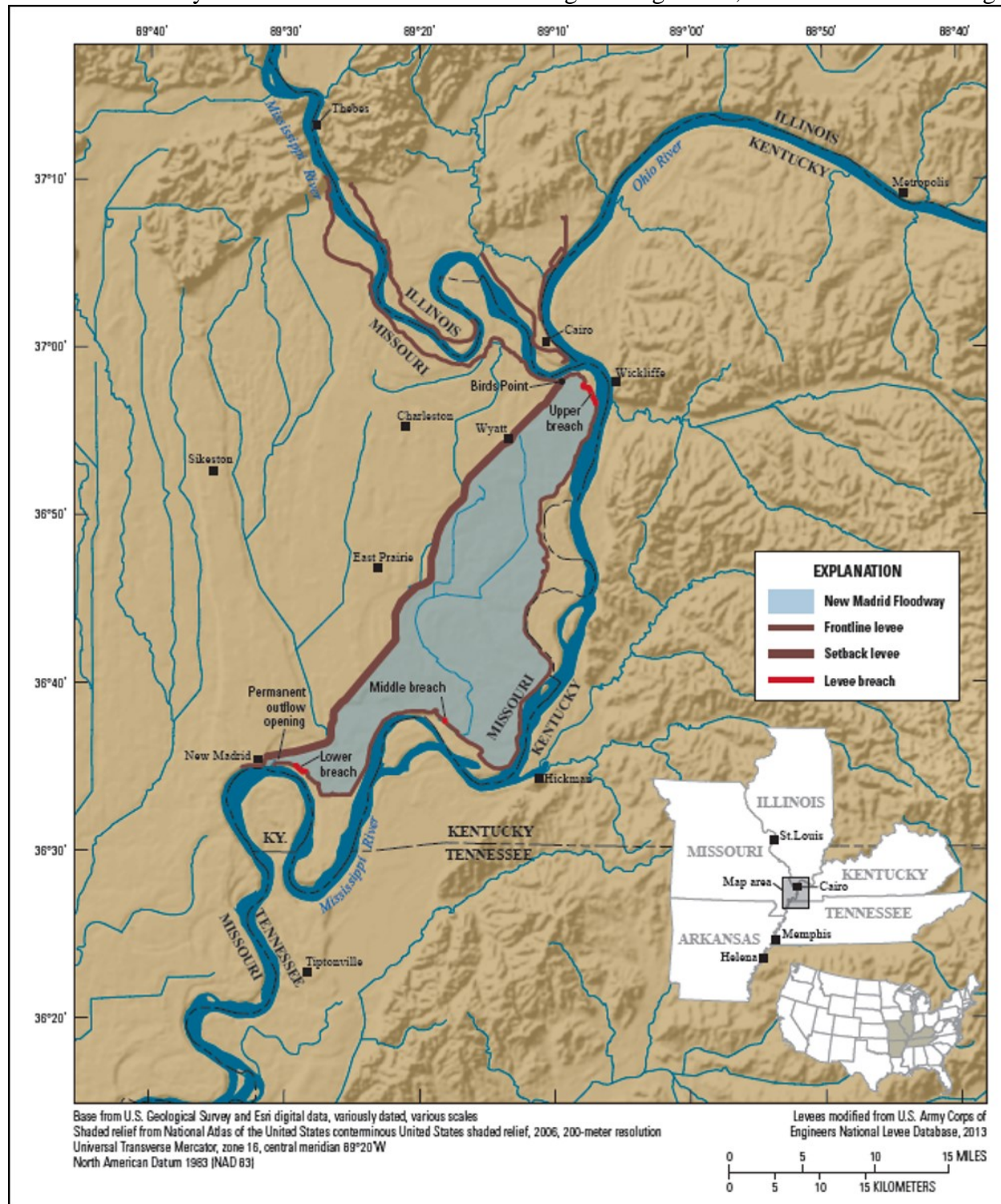


Figure 4-104. Location Map of the New Madrid Floodway and Levee Breach Locations (USGS, 2013)

areas. However, the entire area inside of the New Madrid floodway was modelled as a single 2D flow area, connected to the 1D river system with the lateral structures. Figure 4-105 is a zoomed in piece of the model around the 2D flow area (New Madrid Floodway). Also, in Figure 4-105 is the 37 locations in which the USGS took water surface elevation measurements during the event, labeled H1 – H37.



Figure 4-105. Combined One- and Two-Dimensional HEC-RAS Model of the Mississippi, Ohio, and New Madrid Floodway

The 2D flow area was setup by importing a shapefile of the outer boundary of the New Madrid floodway. This is a very larger area, approximately 40 miles long and over ten miles wide in

some areas of the floodway. The 2D cell size was set at 500 x 500 feet. A land cover dataset was obtained for this area, and Manning's n values were established for each land cover type. Shown Figure 4-106 the final Manning's n values that were used within the New Madrid floodway area for each of the land cover types.

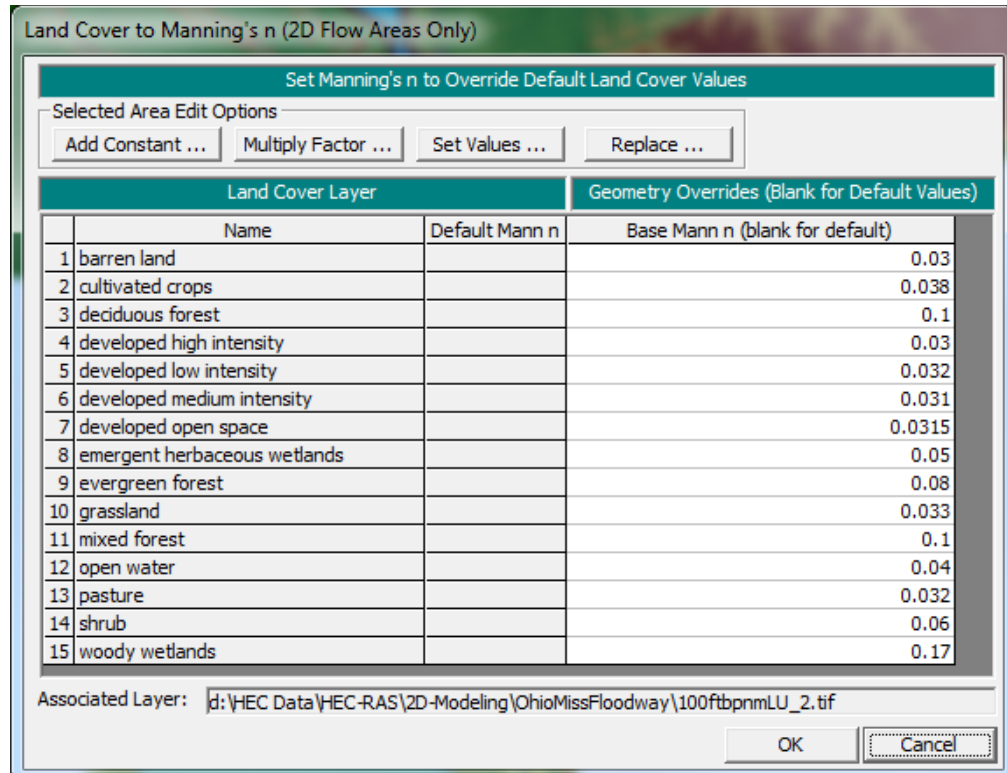


Figure 4-106. Manning's n versus Land Cover Data for the New Madrid Floodway Area

A summary of the other relevant model input parameters is presented in Table 4-39.

Table 4-39. Model parameters for the New Madrid Floodway Breaching Validation Test Case

Parameter	Value
Time step (minute)	2
Governing Equations	SWE
Implicit Weighting Factor	1
Manning's roughness 1D rivers	0.021 – 0.033 main channel 0.080 – 0.200 overbank areas
Upper Levee Breach width (feet)	9,400
Middle Levee Breach width (feet)	690
Lower Levee Breach width (feet)	4,100

Results and Discussion

The results from within the 2D flow area of the New Madrid floodway were compared to the measured water surface elevations from the USGS. Shown in Table 4-40 are the measured and computed peak water surface elevations, along with the difference between the model simulation results and the observed data. The maximum difference at all locations was 0.68 feet, the minimum difference was 0.0 feet, and the average difference was 0.15 feet. Shown in Figure 4-

107 through Figure 4-116 are the computed water surface elevations versus the measured data for ten of the locations within the floodway. In general, the HEC-RAS computed water surface elevations compare very well to the observed data. The results shown in the figures are for ten locations that are scattered throughout the entire length of the floodway, going from the upstream end to the downstream end.

Table 4-40. Measured and Computed Peak Water Surface Elevations (WSEL)

Location	Computed WSEL (feet)	Observed WSEL (feet)	Difference (feet)
H1	324.47	324.10	0.37
H2	324.51	324.24	0.27
H3	324.64	324.17	0.47
H4	324.65	324.24	0.41
H5	324.46	324.24	0.22
H6	324.48	324.16	0.32
H7	324.57	325.01	-0.44
H8	323.83	323.69	0.14
H9	324.21	323.76	0.45
H10	323.93	323.86	0.07
H11	323.94	323.78	0.16
H12	322.56	322.52	0.04
H13	321.71	321.89	-0.18
H14	323.17	323.09	0.08
H15	323.69	323.14	0.55
H16	322.70	322.70	0.00
H17	321.09	321.63	-0.54
H18	315.00	314.64	0.36
H19	321.44	321.79	-0.35
H20	312.79	313.20	-0.41
H21	313.17	313.45	-0.28
H22	311.90	311.93	-0.03
H23	312.46	312.63	-0.17
H24	311.65	311.60	0.05
H25	311.31	311.36	-0.05
H26	310.97	311.06	-0.09
H27	310.74	310.84	-0.10
H29	310.24	310.24	0.00
H30	310.24	309.80	0.44
H31	309.97	309.74	0.23
H32	310.21	309.71	0.50
H33	309.55	309.00	0.55
H34	309.21	308.84	0.37
H35	310.13	309.47	0.66
H36	310.20	309.52	0.68
H37	306.82	306.40	0.42
H38	310.20	309.68	0.52
		Ave ABS Diff	0.29

References

1. USGS, 2013. Koeing, Todd A. and Holmes, Robert R., Jr. *Documenting the Stages and Streamflows Associated with the 2011 Activation of the New Madrid Floodway, Missouri*. U.S. Department of the Interior, U.S. Geological Survey, Reston, Virginia. Professional Paper 1798-E (Chapter E of 2011 Floods of the Central United States). 2013.
<https://pubs.usgs.gov/pp/1798e/pdf/pp1798e.pdf>

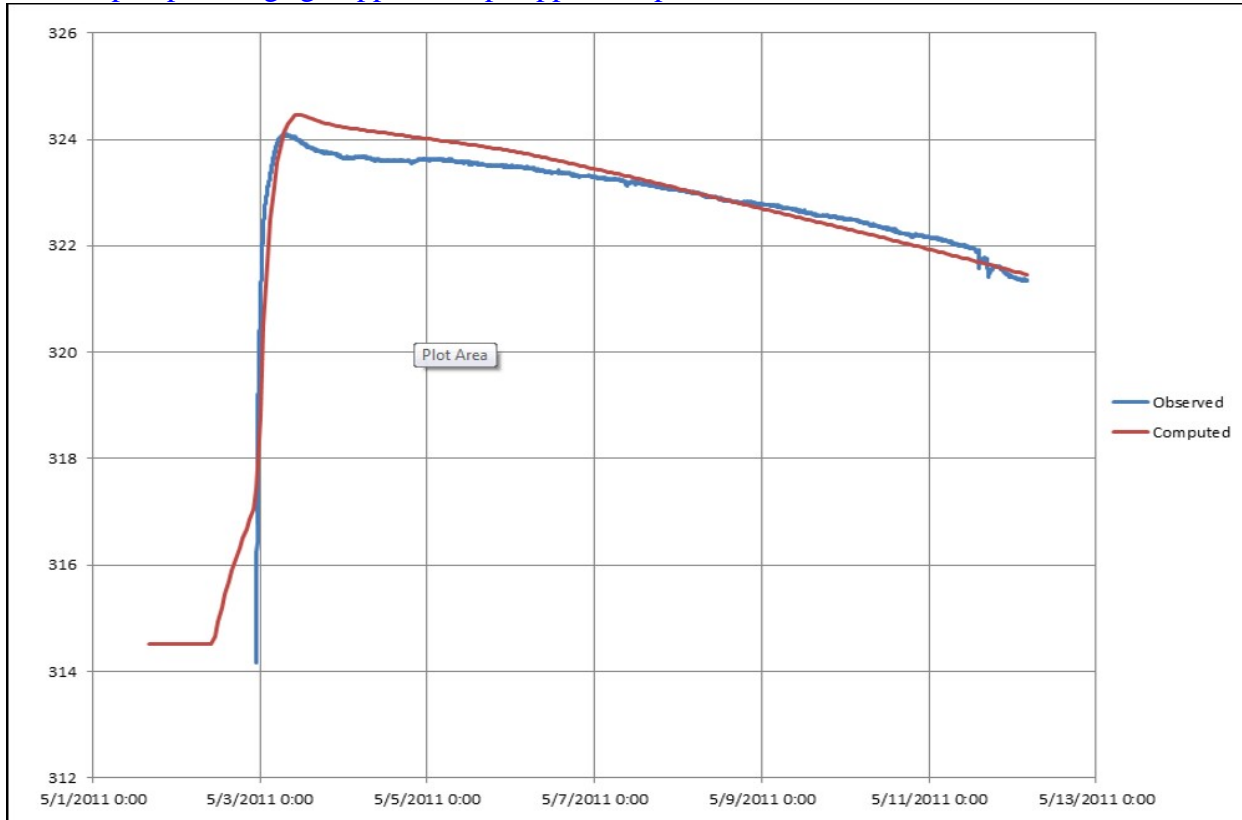


Figure 4-107. Computed versus Observed Water Surface Elevations for Location H1

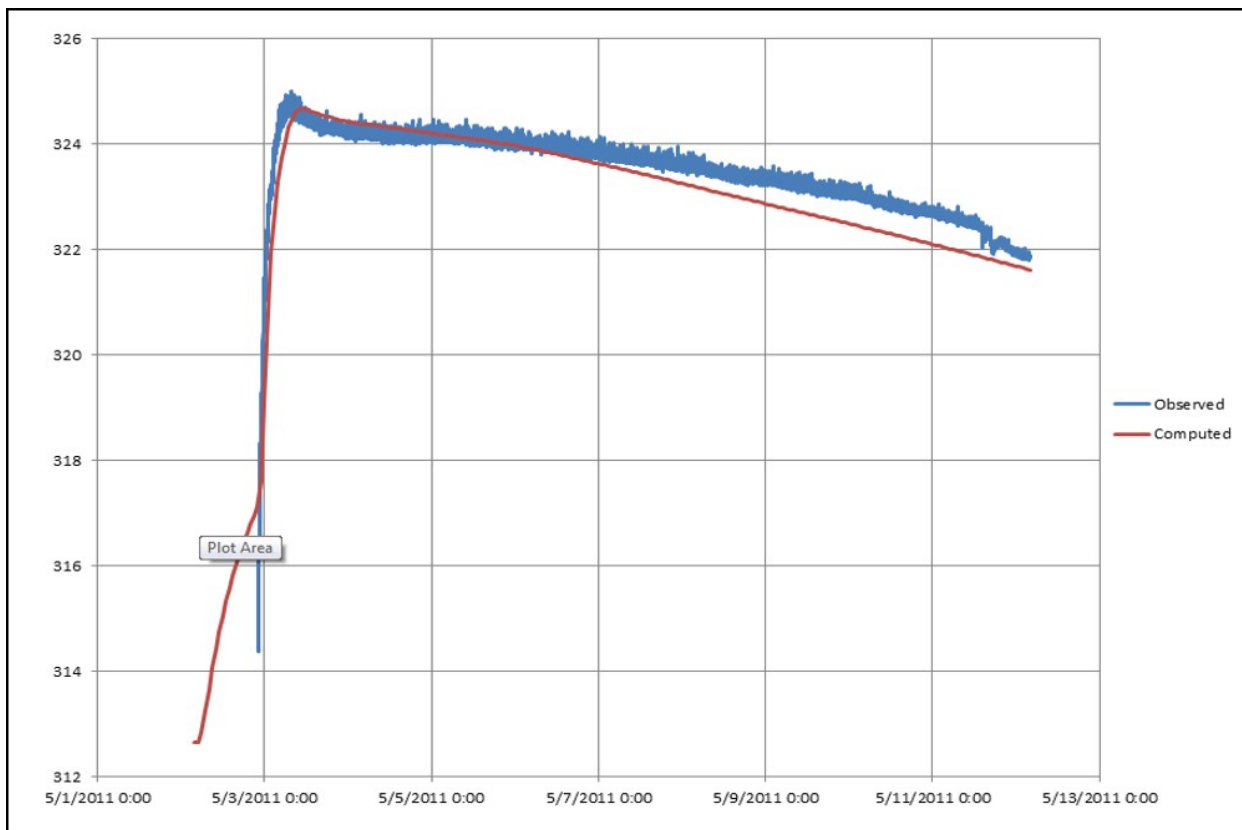


Figure 4-108. Computed versus Observed Water Surface Elevations for Location H7

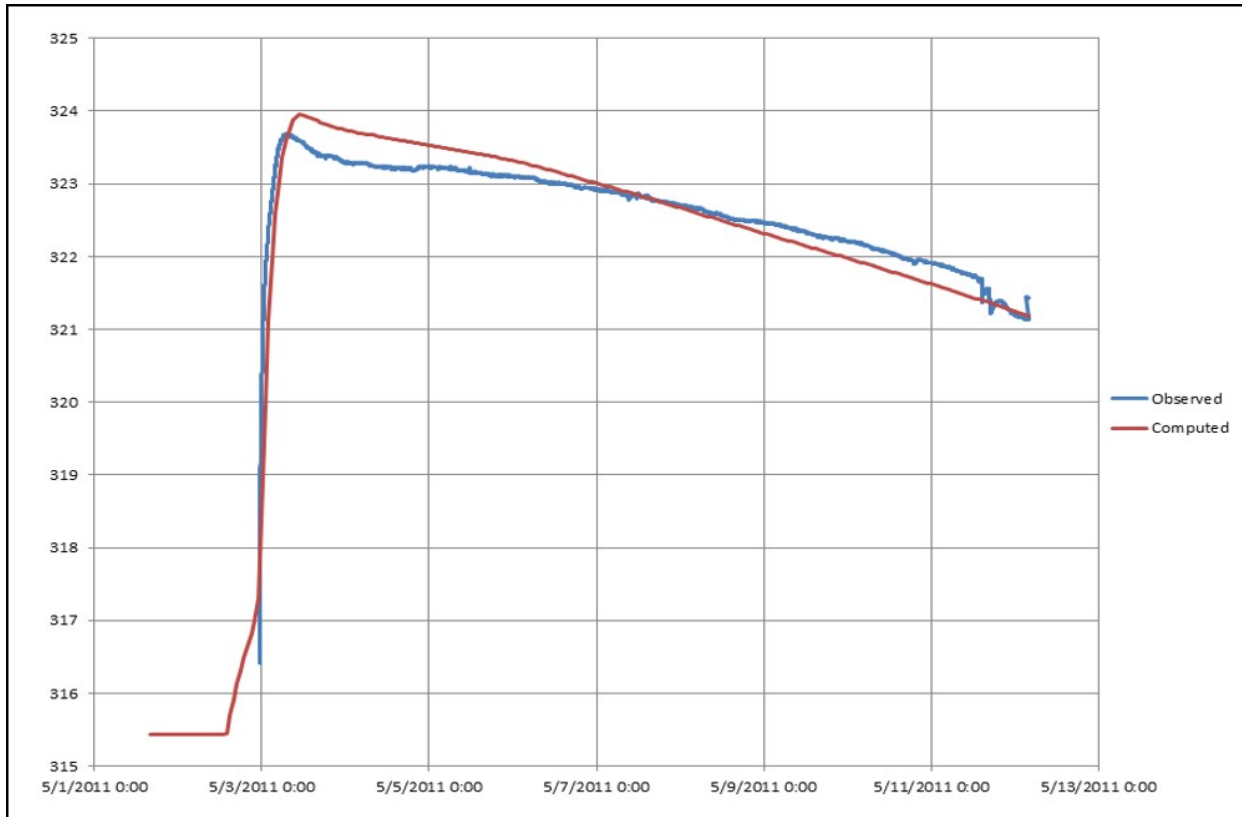


Figure 4-109. Computed versus Observed Water Surface Elevations for Location H8

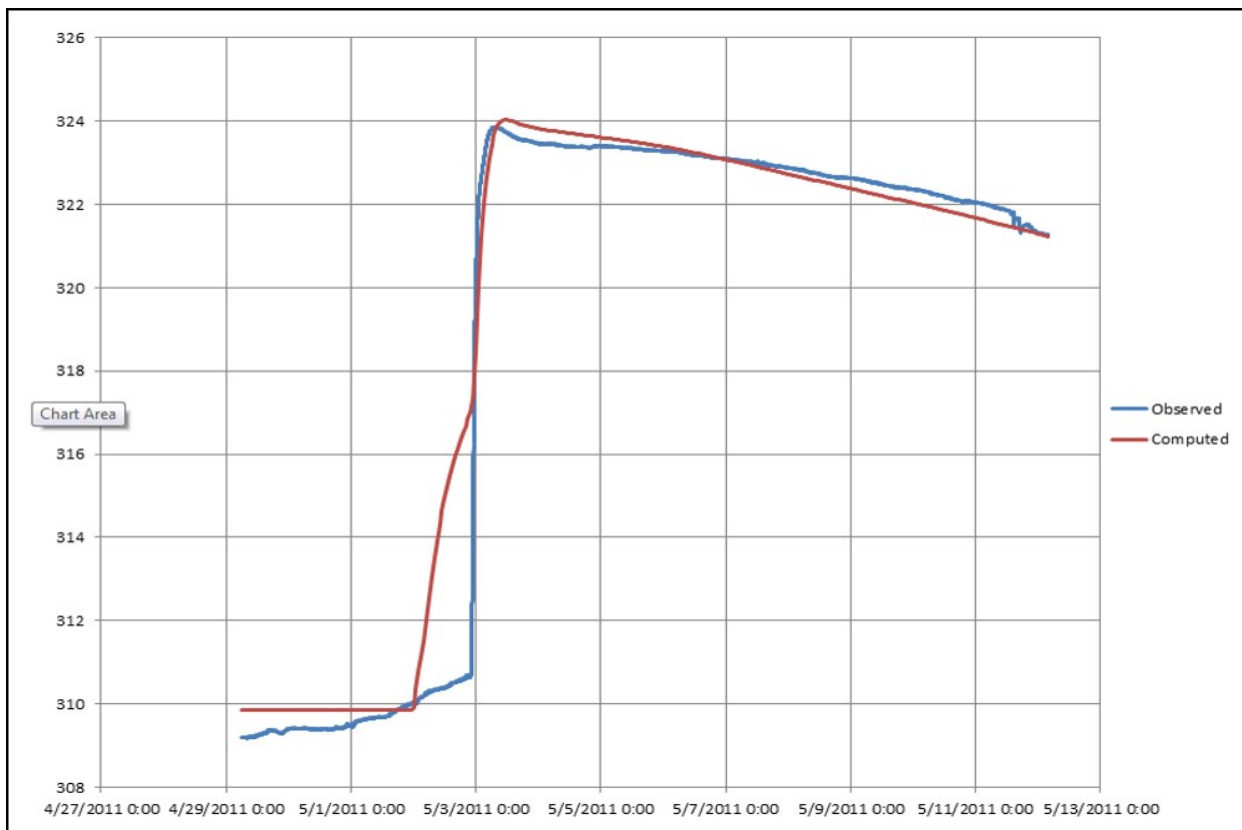


Figure 4-110. Computed versus Observed Water Surface Elevations for Location H10

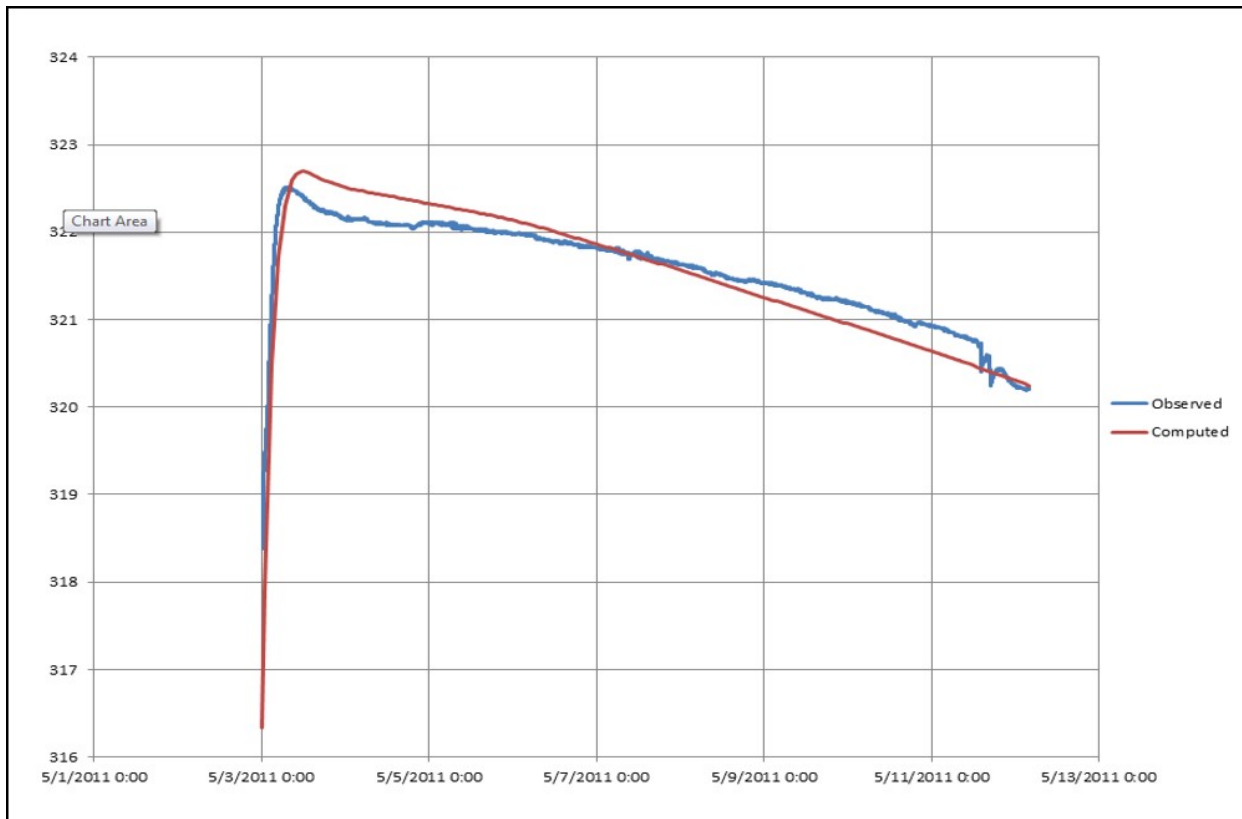


Figure 4-111. Computed versus Observed Water Surface Elevations for Location H12

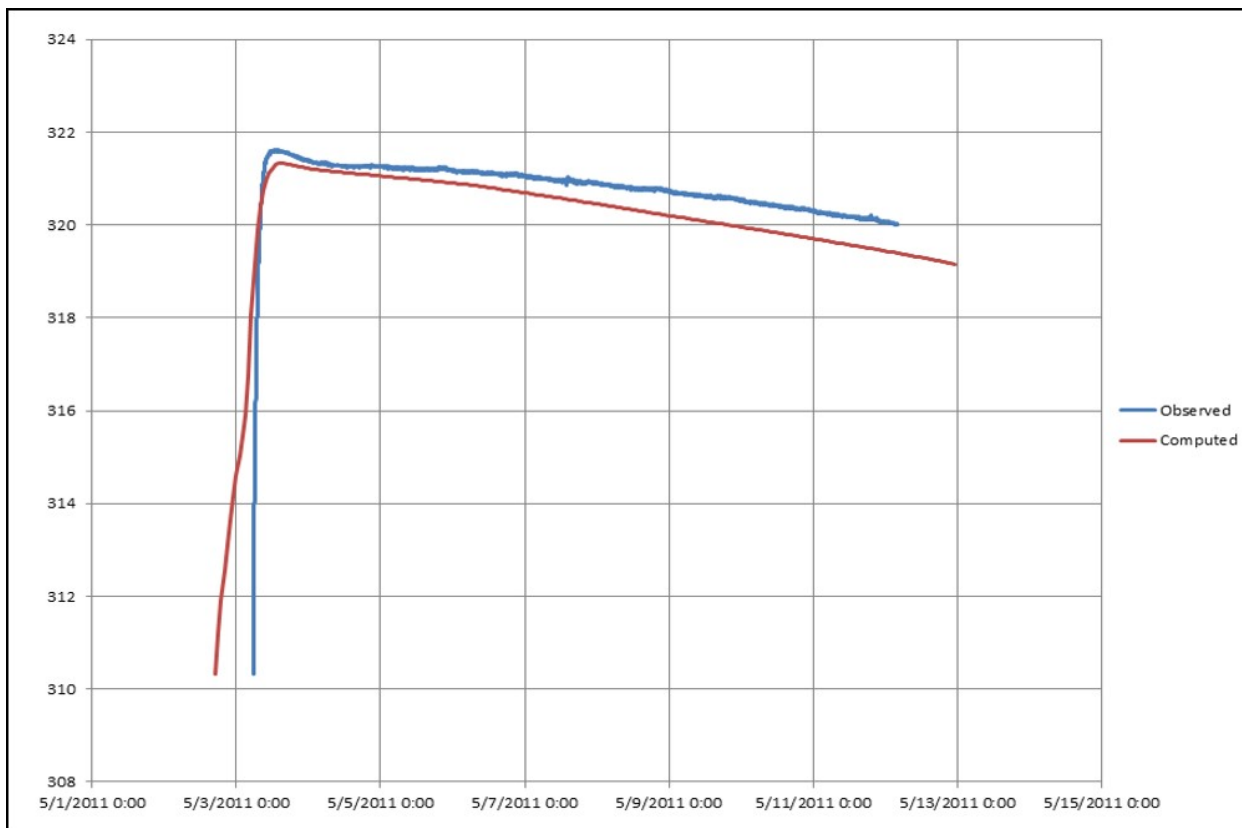


Figure 4-112. Computed versus Observed Water Surface Elevations for Location H17

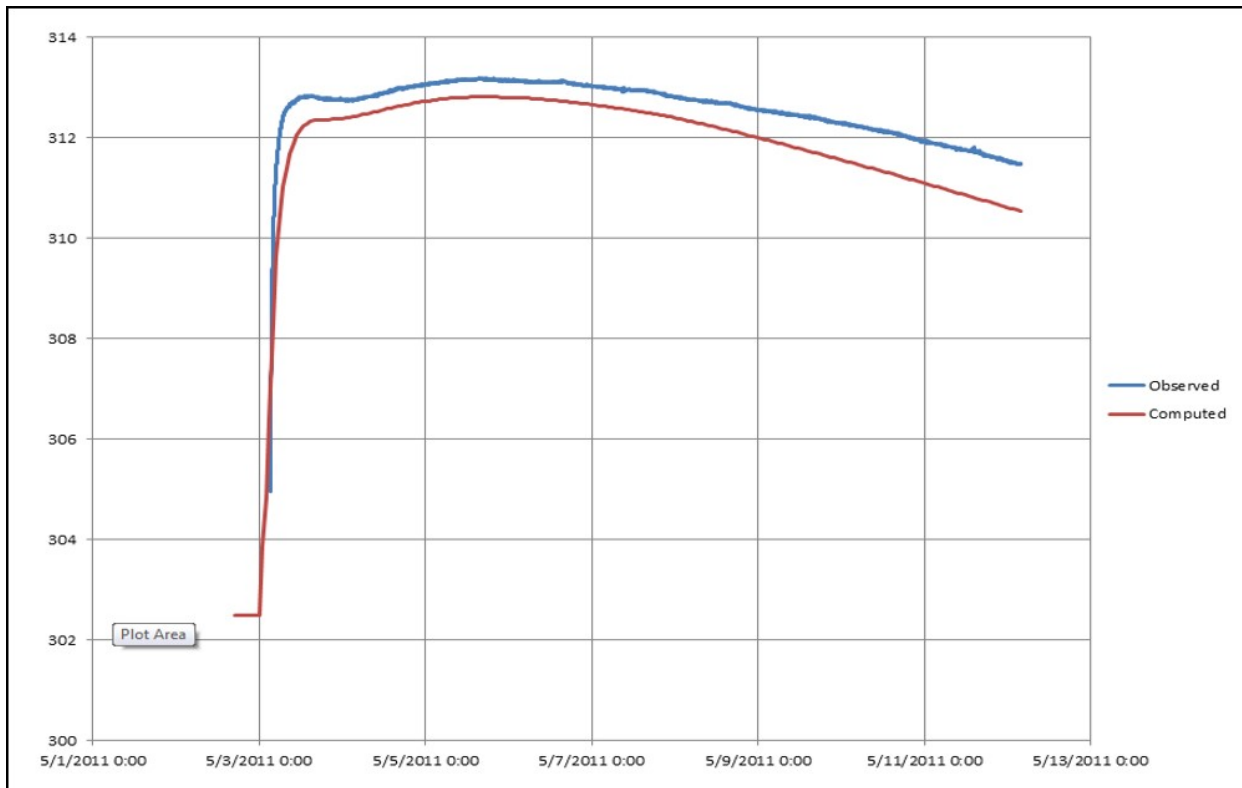


Figure 4-113. Computed versus Observed Water Surface Elevations for Location H20

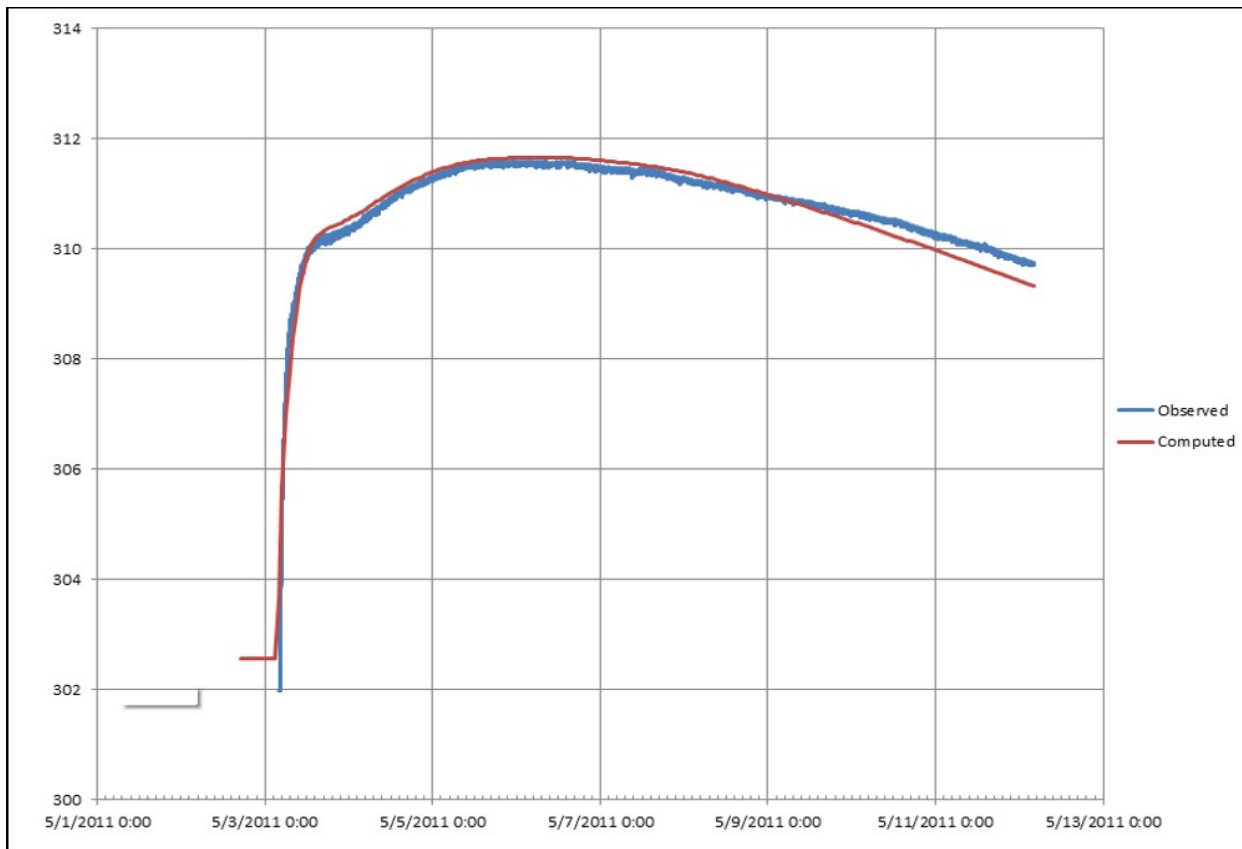


Figure 4-114. Computed versus Observed Water Surface Elevations for Location H24

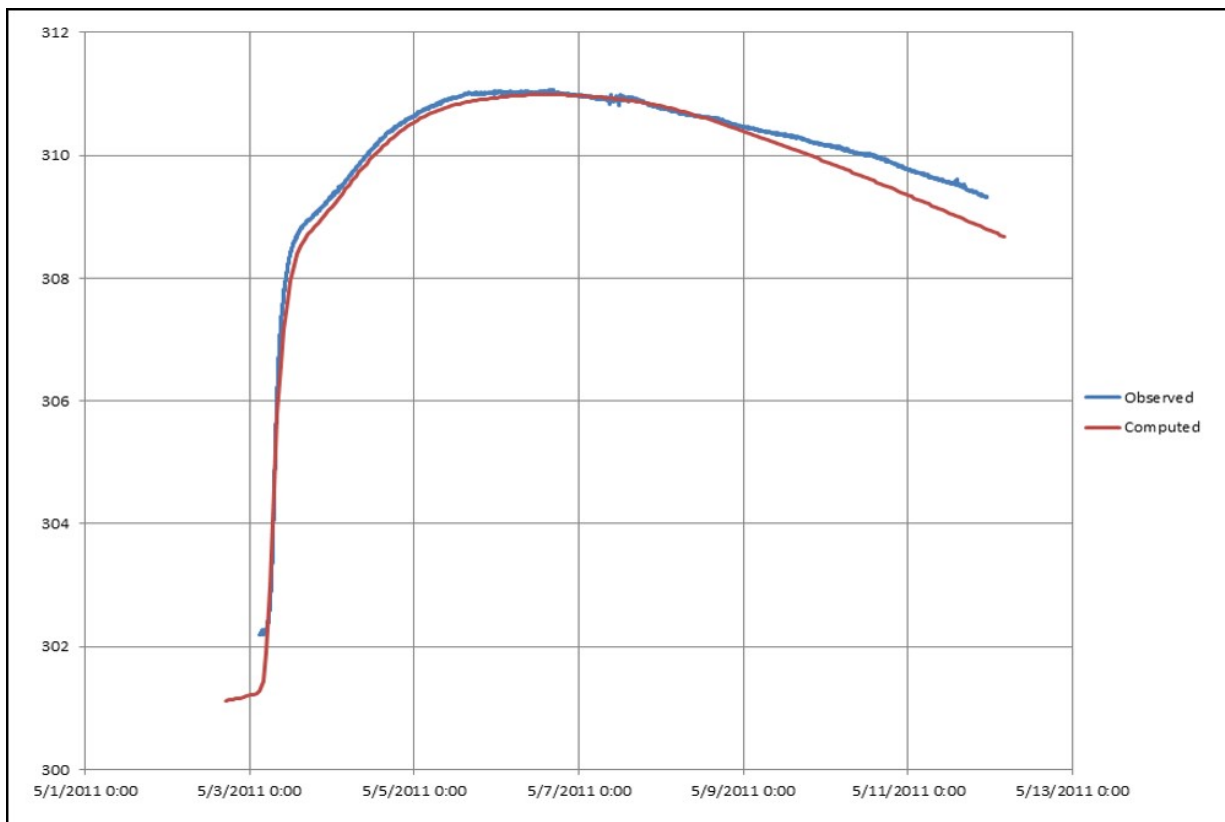


Figure 4-115. Computed versus Observed Water Surface Elevations for Location H26

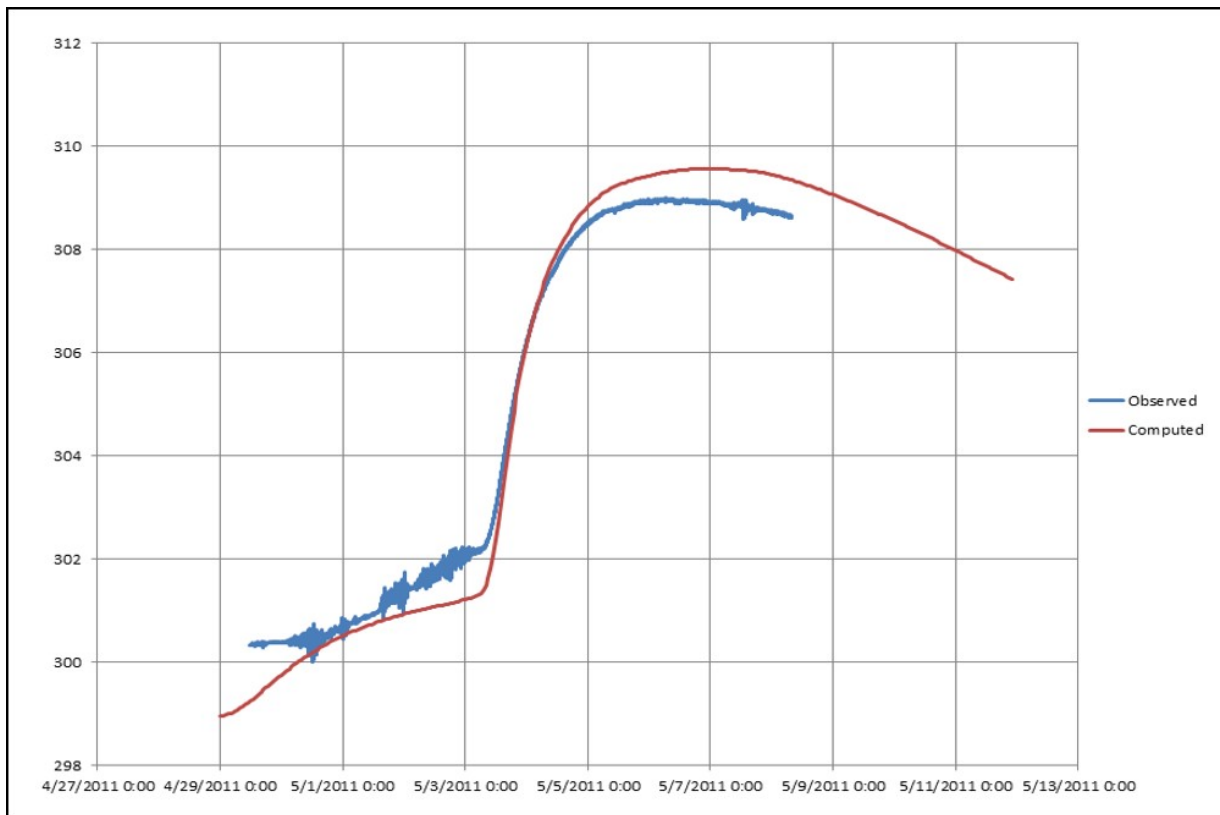


Figure 4-116. Computed versus Observed Water Surface Elevations for Location H33

Appendix A

Goodness-of-Fit Statistics

A.1 Overview

The goodness-of-fit statistics are utilized to compare model results to measured data or analytical solutions and evaluate model performance. The goodness-of-fit statistics utilized throughout this verification and validation document are defined below. In all of the equations, x_c indicates a computed model result, x_m is a measured or analytic solution, and $\langle \quad \rangle$ indicates the expectancy operator.

A.2 Goodness of Fit Statistics

A.2.1 Mean Error (ME) or Bias (B)

The mean error (ME), also referred to as bias (B) is given by:

$$ME = B = \langle x_c - x_m \rangle = \langle x_c \rangle - \langle x_m \rangle \quad (\text{A-1})$$

Smaller absolute ME values indicate better agreement between measured and calculated values. Positive values indicate positively biased computed values (over-prediction) while negative values indicate negatively biased computed values (under-prediction).

A.2.2 Mean Absolute Error (MAE)

The mean absolute error is given by:

$$ME = \langle |x_c - x_m| \rangle \quad (\text{A-2})$$

Similarly to the $RMSE$, smaller MAE values indicate better agreement between measured and calculated values.

A.2.3 Root Mean Squared Error (RMSE)

The Root-Mean-Squared Error ($RMSE$) also referred to as Root Mean Squared Deviation ($RMSD$) is defined as:

$$RMSE = \sqrt{\langle (x_c - x_m)^2 \rangle} \quad (\text{A-3})$$

The $RMSE$ has the same units as the measured and calculated data. Smaller values indicate better agreement between measured and calculated values.

A.2.4 Standard Deviation of Residuals (SDR)

The Standard Deviation of Residuals (*SDR*) is calculated as:

$$SDR = \sqrt{[(x_c - x_m) - (\langle x_c \rangle - \langle x_m \rangle)]^2} \quad (A-4)$$

SDR is a measure of the dynamical correspondence. Smaller values indicate better agreement. The *RMSE*, *ME*, and *SDR* are related by the following formula:

$$RMSE^2 = ME^2 + SDR^2 \quad (A-5)$$

A.2.5 Normalization

The dimensional statistics above, namely *RMSE*, *MAE*, and *ME*; can be normalized to produce a non-dimensional statistic. When the variable is normalized the statistic is commonly prefixed by a letter *N* for normalized or *R* for relative (e.g. *NRMSE*, *NMAE*, and *NME*). This also facilitates the comparison between different datasets or models which have different scales. For example, when comparing models to laboratory data, the dimensional statistics will produce relatively smaller dimensional goodness-of-fit statistics compared to field data comparisons. One drawback of normalization is that there is no consistent means of normalization. Different types of data or normalized differently literature. For example, water levels are commonly normalized by the tidal range, while wave heights may be normalized by the offshore wave height. In some cases, the range of the measured data is a good choice. The range is defined as the maximum value minus the minimum value.

$$x_N = \text{range}(x_m) - \min(x_m) \quad (A-6)$$

When the *RMSE* value is normalized by the mean measured value, is sometimes referred to as the scatter index (*SI*) (Zambresky, 1989). When the RMS value is normalized by a specific measured value used to drive a model, it is sometimes referred to as the Operational Performance Index (*OPI*) (Ris, 1999). The *OPI* can be used for example to give an estimate of the performance of a nearshore wave height transformation model based on the offshore measured wave height. More important than the choice of normalization variable is to properly describe how the statistics have been normalized.

A.2.6 Performance Scores (PS)

There are several goodness-of-fit statistics in literature of the form:

$$PS = 1 - \frac{\langle (x_c - x_m)^2 \rangle}{\langle (x_m - x_R)^2 \rangle} \quad (A-7)$$

where x_R is a reference value(s). When the reference value is equal to the base or initial measurements (i.e., $x_R = x_0$), the Performance Score (PS) is referred to as the Brier Skill Score (*BSS*) or Brier Skill Index (*BSI*). When the reference value is equal to the mean measured value (i.e., $x_R = \langle x_m \rangle$) the Performance Score is referred to the Nash-Sutcliffe Coefficient (*E*) or Nash-Sutcliffe Score (*ES*) (Nash, 1970). When the reference value is a specific measured value such

as a model forcing value, then it is referred to as the Model Performance Index (*MPI*) or Model Performance Score (*MPS*).

The various PS ranges between negative infinity and one. A PS of 1 indicates a perfect agreement between measured and calculated values. Scores equal to or less than zero indicates that the reference value is as or more accurate than the calculated values. Recommended qualifications for different *BSS* ranges are provided in Table 1.

Table A-1. Performance Score (PS) Quantifications.

Range	Quantification
0.8 < PS < 1	Excellent
0.6 < PS < 0.8	Good
0.3 < PS < 0.6	Reasonable
0 < PS < 0.3	Poor
PS < 0	Bad

A.2.7 Index of Agreement (IA)

The index of agreement (*IA* or *d*) is given by (Willmott, 1985):

$$IA = 1 - \frac{\langle (x_c - x_m)^2 \rangle}{\langle (|x_c - \langle x_c \rangle| + |x_m - \langle x_m \rangle|)^2 \rangle} \quad (\text{A-8})$$

The IA is a standardized measure of the degree of model prediction error and varies between zero and one. A value of one indicates a perfect match, and zero indicates no agreement at all (Willmott, 1981). The denominator in the above equation is referred to as the potential error. The non-dimensional statistics *IA* varies between zero and one. Values closer to one indicate better agreement.

A.2.8 Correlation Coefficient (R)

The correlation is a measure of the strength and direction of a linear relationship between two variables. The correlation coefficient (*R*) is defined as:

$$R = \frac{\langle x_c x_m \rangle - \langle x_c \rangle \langle x_m \rangle}{\sqrt{\langle x_c^2 \rangle - \langle x_c \rangle^2} \sqrt{\langle x_m^2 \rangle - \langle x_m \rangle^2}} \quad (\text{A-9})$$

A correlation of 1 indicates a perfect one-to-one linear relationship and -1 indicates a negative relationship. The square of the correlation coefficient describes how much of the variance between two variables is described by a linear fit.

A.3 References

1. Nash, 1970. Nash, J.E. and Sutcliffe, J.V. *River flow forecasting through conceptual models Part I - A discussion of principles*. Journal of Hydrology, Volume 10, Issue 3, pages 282–290. <https://hydrology.agu.org/wp-content/uploads/sites/19/2016/04/NashSutcliffe1.pdf>

2. Ris, 1999. Ris, R.C., Holthuijsen, L.H., and Booij, N. *A third-generation wave model for coastal regions 2, verification.* Journal of Geophysical Research, Volume 104, Issue C4, pages 7667-7681. April 1999.
3. Willmott, 1985. Willmott, C.J., Ackleson, S.G., Davis, R.E., Feddema, J.J., Klink, K.M., Legates, D.R., O'Donnell, J., and Rowe, C.M. *Statistics for the evaluation and comparison of models.* Journal of Geophysical Research, Volume 90, Issue C5, pages 8995–9005. 1985.
4. Zambreskey, 1988. Zambreskey, Liana. *A verification study of the global WAM model, December 1987 – November 1988.* Research Department, Technical Report No. 63. GKSS, Forschungszentrum Geesthacht, GMBH Report GKSS 89/E/37.